# Promotion & Inspection Cubic Satellite

*Designing a femto-satellite for inspection and promotion purposes*


| | | | |
|---|---|---|---|
| R.M.Colijn | 4284909 | L.Schreiber | 4297350 |
| M.Geng | 4003780 | V.J.H.Trees | 4115937 |
| J.Mollinga | 4233263 | B.Wang | 4132262 |
| R.P.Rikken | 4206738 | R.H.H.Wolfs | 4017536 |
| B.G.T.Schoemaker | 4298624 | | |


Final Report

Design Synthesis Excercise

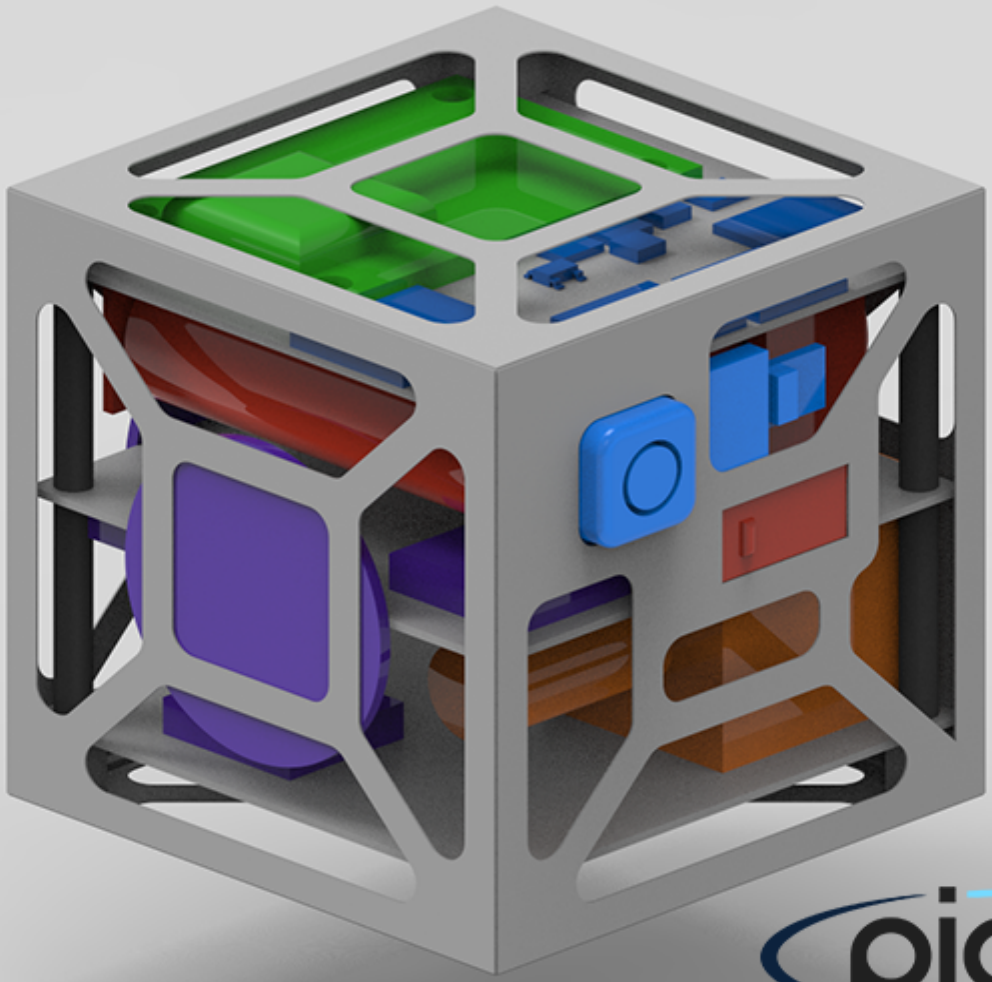

pics


TU Delft Delft University of Technology

Aerospace Engineering


June 28, 2016

INTENTIONALLY BLANK

# Preface

Dear reader,

This report is the fourth and final progress report of group 13 for the Spring 2016 Design Synthesis Exercise (DSE). The DSE is a 11 week full-time design assignment in the last quarter of the third year which concludes the Bachelor program of Aerospace Engineering at Delft University of Technology. The objective of this DSE was to design a femto-satellite with a mass less than $100g$ for technology demonstration. This report was preceded by a Project Plan, a Baseline Report and a Mid-Term Report. In the Mid-Term Report it was decided to design an inspection and promotion satellite that can be used to inspect and promote a host spacecraft. It will be referred to as the PICS: Promotion and Inspection Cubic Satellite.

This report focuses on the design of the inspection and promotion satellite up to subsystem level, presented in Part 2 of the report, from Chapter 7 to 17. Furthermore the report includes, among other aspects, a market analysis, a sustainable development strategy, a technical risk assessment and verification and validation procedures. A future vision on femto-satellites and their role in the space industry is given in Chapter 27. It is written primarily for the project supervisor, principal tutors, DSE committee and students of Aerospace Engineering and therefore assumes undergraduate aerospace engineering knowledge. The report functions as a preliminary stage to the detailed design, although this is not part of the DSE.

Special thanks goes out to project supervisor ir. Prem Sundaramoorthy and principal tutors ir. Bart Root and ir. Christophe de Wagter for their support and feedback during the weekly meetings. We would like to thank the following staff members from the Faculty of Aerospace Engineering: dr. ir. Erwin Mooij, ir. Barry Zandbergen, ir. Jasper Bouwmeester, dr. Daphne Stam, dr. ir. Ernst Schrama, ir. Stefano Speretta, dr. ir. Chris Verhoeven, dr. Alessandra Menicucci, ir. Ron Noomen, dr. ir. Wim Verhagen, dr. ir. Angelo Cervone and master student Victor Moreno Villa for their help and input in various stages of the DSE. We would also like to thank the companies Innovative Solutions In Space (ISIS), GSM Berkel and Global Aerospace Corporation for their support. This report would have been of much lesser quality without their help.

Delft, 28th of June 2016

R.M. Colijn
M. Geng
J. Mollinga
R.P. Rikken
B.G.T. Schoemaker
L. Schreiber
V.J.H. Trees
B. Wang
R.H.H. Wolfs

# Summary

This report documents the development process of the PICS (Promotion Inspection Cubic Satellite). This summary will only elaborate upon the final design of the spacecraft. For information behind the organisation of the project see *Part I* of the report.

The final result is a satellite that is 5×5×5 $cm$ large and that weighs 72 $g$ in its current design iteration. This satellite consists of the following subsystems: a complementary metal–oxide–semiconductor (CMOS) sensor camera as payload, a full 3-axis momentum-wheel controlled attitude determination & control system (ADCS), a non-rechargeable battery for power, a commercial off-the-shelf (COTS) WiFi module for communication, a command & data handling (C&DH) system and a de-orbit device. The satellite will be deployed from the Terra Bella SkySat C12 in 2017, after which it will take images of the SkySat for 442 seconds, transmit this data to the host spacecraft over 6250 seconds and then de-orbit itself within roughly 11 days.

The femto-satellite will be deployed from the host spacecraft by a deployment system which weighs 798 $g$. This deployment system will give the femto-satellite a $\Delta$V of 1.3 $cm/s$ which will make it slowly drift away from the host spacecraft. During this drift the femto-satellite will start with taking pictures at 38.8 $cm$ until 5.61 $m$ from the host spacecraft. This will result in 442 seconds of taking pictures. After which it will go into transmission mode. This will take 6250 seconds until a distance of 85 $m$ from the host spacecraft. This deployment action can occur every orbit, with a deployment window of 29 minutes. The payload is capable of taking 16 MP images and the C&DH subsystem allows it to take 30 pictures every 10 seconds. These images are stored on internal storage and are transferred to the host spacecraft at a speed of 54 Mb/s. After approximately 13 000 seconds the femto-satellite will have drifted too far for communication.

The satellite is thermally proofed with Kapton foil so that all the components operate within their operational temperature ranges. The thermal range of all the subsystems combined is 5 to 40 °C when the camera is turned on and -10 to 50 °C when it is disabled. The structure consists of three PCBs that are layered on pins and surrounded by a support structure. A structural analysis is performed to see if it will survive the launch loads. Models are made of the femto-satellite in CATIA. The system design has been verified and a mission validation plan is set-up. The cost of a single satellite is equal to €7,649. The entire mission will cost €131,625, which includes one femto-satellite.

The femto-satellite will be assembled and integrated in the period after the DSE. All the operations and logistics are set-up so that the satellite can be assembled and launched on time. The result from the RAMS analysis is that the system will be very reliable, available for a long time after launch. However, in-orbit maintenance will not be possible. Also, safety precautions need to be taken during assembly.

# Contents

**Preface** i
**Summary** ii
**List of Figures** vi
**List of Tables** viii
**List of Abbreviations** x
**List of Symbols** xi
**1 Introduction** 1

**I Project Analysis** 2
**2 Mission Determination & Description** 3
2.1 Mission Trade-Off . . . 3
2.2 Concept Trade-Off . . . 4
2.3 Inspection Satellite Potential . . . 5
2.4 Promotion Satellite Potential . . . 8
2.5 Mission Description . . . 8
**3 Market Analysis** 10
3.1 Market Needs and Trends . . . 10
3.2 Competition . . . 10
3.3 Barriers to Market Entry . . . 11
3.4 Regulations . . . 11
3.5 Marketing Strategy . . . 11
3.6 SWOT Analysis . . . 12
**4 Sustainable Development Strategy** 13
4.1 Regulatory Sustainability . . . 13
4.2 Future Sustainability . . . 14
4.3 Environmental Sustainability . . . 14
4.4 Conclusion on Sustainable Development . . . 14
**5 Design Prerequisites** 15
5.1 System Interface Definition . . . 15
5.2 Functional Flow Diagram . . . 16
5.3 Functional Breakdown Structure . . . 16
5.4 Contingencies and Margins . . . 17
**6 Requirements** 18
6.1 Mission and Stakeholder Requirements . . . 18
6.2 System Requirements . . . 18
6.3 Subsystem Requirements . . . 19
6.4 Requirement Iterations . . . 21
6.5 Requirements Categorisation . . . 23

**II Design** 24
**7 Astrodynamics** 25
7.1 Relative Motion . . . 25
7.2 Orbit Perturbations . . . 26
7.3 Orbit Determination . . . 27
7.4 Probability of Collision . . . 29
7.5 Eclipses and De-orbiting . . . 29
**8 Payload** 30
8.1 Requirements . . . 30
8.2 Imaging Geometry . . . 30
8.3 Image Quality . . . 31
8.4 Camera Selection . . . 32
8.5 Post-Processing Techniques . . . 33
8.6 Data Size Determination . . . 34
8.7 Number of Pictures . . . 34
**9 Communication System** 35
9.1 Subsystem Requirements . . . 35
9.2 Communication Flow Design . . . 35
9.3 Communication Methods . . . 37
9.4 Subsystem Design Trade-off . . . 38
9.5 Data Transmitting . . . 39

**10 Attitude Determination & Control System** **40**
10.1 Control Modes . . . 40
10.2 Subsystem Requirements . . . 40
10.3 Type of Attitude Determination & Control . . . 40
10.4 Hardware Sizing . . . 43
10.5 Subsystem Overview . . . 46
**11 De-orbit Device** **47**
11.1 Subsystem Requirements . . . 47
11.2 Investigation Into De-orbit Devices . . . 47
11.3 Spherical Inflatable De-orbit Device . . . 48
**12 Command & Data Handling System** **50**
12.1 Subsystem Requirements . . . 50
12.2 System Architecture . . . 50
12.3 Data Processing . . . 51
12.4 Payload Data Acquisition . . . 52
12.5 Mass Storage . . . 52
12.6 Subsystem Overview . . . 53
**13 Power System** **55**
13.1 Subsystem Requirements . . . 55
13.2 Power Budget . . . 55
13.3 Non-Rechargeable Power Solution . . . 55
13.4 Power Architecture . . . 57
13.5 Subsystem Overview . . . 57
**14 Thermal Control System** **58**
14.1 Thermodynamic Model . . . 58
14.2 Subsystem Requirements . . . 59
14.3 Mission Profile . . . 60
14.4 Thermal Design . . . 60
**15 Deployment System** **62**
15.1 Subsystem Requirements . . . 62
15.2 Design Justification . . . 62
15.3 Spring Design . . . 64
15.4 Deployment Interface Design . . . 68
15.5 Integral Design Strategy . . . 70
**16 Structural and Vibrational Analysis** **74**
16.1 Requirements . . . 74
16.2 Vibrational Analysis . . . 74
16.3 Structural Analysis . . . 77
**17 Configuration and Structure** **79**
17.1 Shape of the Femto-Satellite . . . 79
17.2 Components of the Structures Subsystem . . . 79
17.3 Configuration of Femto-Satellite . . . 80
17.4 Resource Allocation . . . 82
17.5 Hardware and Software Diagrams . . . 84
**18 Design Iterations** **87**
18.1 Iteration 0 on 26-05-2016 . . . 87
18.2 Iteration 1 on 02-06-2016 . . . 87
18.3 Iteration 2 on 08-06-2016 . . . 88
18.4 Iteration 3 on 16-06-2016 . . . 88
18.5 Iteration 4 on 27-06-2016 . . . 88
**19 Risk Management** **89**
19.1 General Process Risks . . . 89
19.2 Development and Operation Risks . . . 90
19.3 Risk Iteration . . . 90
19.4 Risk Analysis . . . 91
19.5 Risk Mitigation . . . 91
19.6 Conclusion on Risk Management . . . 93
**20 Verification and Validation** **94**
20.1 Requirements Verification . . . 94
20.2 System Validation . . . 98
20.3 Model Verification and Validation . . . 98
20.4 Compliance Matrix . . . 100
20.5 Feasibility Analysis . . . 102
**21 Performance Analysis** **103**
21.1 Hardware Performance . . . 103
21.2 Mission Performance . . . 103
21.3 Sensitivity Analysis . . . 104

**III Post-Design Activities & Recommendations** **106**
**22 Assembly & Integration Plan** **107**
22.1 Facilities . . . 107
22.2 Assembly . . . 108
**23 Operations and Logistics** **109**
23.1 Operations . . . 109
23.2 Logistics . . . 110
**24 Reliability, Availability, Maintainability & Safety** **111**
24.1 Reliability . . . 111
24.2 Availability . . . 112
24.3 Maintainability . . . 112
24.4 Safety . . . 112
**25 Project Design & Development Logic** **113**
25.1 Post-DSE Design and Development . . . 113
25.2 Post-DSE Gantt Chart . . . 114
**26 Cost Estimation** **115**
26.1 Cost Breakdown Structure . . . 115
26.2 Final Mission Cost Estimation . . . 116
26.3 Return on Investment . . . 116
**27 Vision on Femto-Satellites** **118**
27.1 Technological Challenges . . . 118
27.2 The Future of Femto-Satellites . . . 119
**28 Conclusion** **120**
**29 Recommendations** **121**
29.1 Astrodynamics . . . 121
29.2 Payload . . . 121
29.3 Communication . . . 121
29.4 Attitude Determination & Control . . . 121
29.5 De-orbit Device . . . 121
29.6 Power . . . 122
29.7 Thermal Analysis . . . 122
29.8 Deployment system . . . 122
29.9 Structural and Vibrational Analysis . . . I
**A Trajectory estimation** **II**
**B Absolute ADCS Sensors** **III**
**C Propulsion** **V**
C.1 Selection Propulsion System . . . V
C.2 Cold Gas Propulsion System . . . V
C.3 MEMS Based Solid Propulsion System . . . VII
C.4 Conclusion on Propulsion System . . . VIII
**D Rechargeable power solution** **IX**
D.1 Rechargeable Power Solution . . . IX
D.2 Power Solution Selection . . . XI
**Bibliography** **XII**

# List of Figures


2.1 Flux density versus crater size for HST and EuReCa . . . 7
2.2 Impact crater dimensions . . . 7
2.3 Flux densities according to various micro-meteoroid and space debris models[1] . . . 7
2.4 3D render of the SkySat C1 . . . 9

3.1 PICS logo . . . 11

5.1 $N^2$ chart for the detailed design phase . . . 15
5.2 Functional flow block diagram . . . 16
5.3 Functional breakdown structure . . . 17

7.1 Football orbit inertial view [1] . . . 26
7.2 Football orbit LVLH view [1] . . . 26
7.3 Oscillating orbit inertial view [1] . . . 26
7.4 Oscillating orbit LVLH view [1] . . . 26
7.5 Distance between the host spacecraft and femto-satellite at an altitude of $450km$ . . . 27
7.6 Stages during the orbit of the host spacecraft and femto-satellite . . . 28
7.7 Distance from the host spacecraft. $\Delta V = 1.3cm/s$, TA = 45° . . . 29
7.8 Activities during the first stage of the mission . . . 29

8.1 Horizontal, vertical and diagonal FOV . . . 30
8.2 Imaging geometry . . . 30
8.3 Image sharpness breakdown structure . . . 31

9.1 Communication flow diagram . . . 37

10.1 Gyroscope Bias vs Time . . . 42
10.2 Gyroscope Drift vs Time . . . 42
10.3 Edge detection algorithm example with an image of the Hubble telescope . . . 42

12.1 Three command and data handling architectures [2] . . . 51
12.2 The mass storage architecture . . . 53
12.3 Command and Data Handling diagram . . . 54

13.1 The electrical block diagram specifying the voltages of different parts . . . 57

14.1 Temperature development over mission lifetime plotted against the requirements, hot case. . . . 61
14.2 Temperature development over mission lifetime plotted against the requirements, cold case. . . . 61

15.1 The nichrome wire cutter deployment mechanism designed by A. Thurn, Naval Research Laboratory 63
15.2 The process of deployment in the nichrome wire cutter release concept . . . 63
15.3 Schematic representation of the deployment mechanism before release . . . 64
15.4 Schematic representation of the deployment mechanism after release . . . 64
15.5 Axial load applied on the spring . . . 65
15.6 Free Body Diagram of the spring . . . 65
15.7 3D Catia drawing of the Deployment Interface . . . 69
15.8 Technical Drawing Deployment Interfact: Topview . . . 69
15.9 Technical Drawing Deployment Inerface: Sideview . . . 69

16.1 FEM-analysis of PCB1 . . . 78

17.1 Configuration drawing of the PICS femto-satellite . . . 81
17.2 The evolution of the mass budget the detailed design duration. . . . 84
17.3 Hardware diagram of the femto-satellite . . . 85

17.4 Software diagram for the femto-satellite throughout the mission . . . . . 86

18.1 Motion of the femto-satellite in a non-rotating reference frame centred at the host spacecraft in 24 hours. Delta-Vs are applied to keep the distance between the two satellites within 3.38 $m$. The red ball in the centre symbolises a host spacecraft with a diameter of 1 $m$. The axis scale is kilometres. . . 87

20.1 Designing according to the V-diagram . . . . . 94
20.2 Temperature envelope with different surface finishes . . . . . 99
20.3 Telemetry of FUNcube-1 over the duration of one orbit. Temperatures are in $^{\circ}C$, currents in $dA$ and voltages in $V$. . . . . 100
20.4 Thermal simulation of FUNcube over one orbit after model stabilisation . . . . . 100

22.1 Assembly & Integration Plan . . . . . 107

23.1 Operational flow block diagram . . . . . 109

25.1 Project design & development diagram . . . . . 113
25.2 Project Gantt chart for post DSE activities . . . . . 114

26.1 Cost breakdown structure . . . . . 115

B.1 Using image processing to obtain spacecraft attitude [3] . . . . . IV

D.1 Orientation of solar panels on the satellite with option 1 . . . . . IX
D.2 Orientation of solar panels on the satellite with option 2 . . . . . X

# List of Tables


2.1 Trade-ff table for all the proposed missions. Factors are weighted out of 10. . . . . 4
2.2 Concept Trade-Off table . . . . . 5
2.3 Facts of the SkySat C1 . . . . . 9

6.1 Flow down of system requirements from the mission and stakeholder requirements . . . . . 19
6.2 The dependency between subsystem requirements . . . . . 21
6.3 The dependency between subsystem requirements . . . . . 21

7.1 Satellite characteristics . . . . . 26
7.2 Orbit parameters . . . . . 26

8.1 Camera specifications . . . . . 32
8.2 Final imaging specifications using the Samsung S6 camera . . . . . 33

9.1 Wifi versus Bluetooth trade-off . . . . . 37
9.2 WiFi modules trade-off . . . . . 38

10.1 Gyroscope specifications . . . . . 41
10.2 Flywheel material properties . . . . . 45
10.3 Wheel parameters of different materials . . . . . 46

11.1 Different de-orbit systems. For small satellites with an mass-over-area $\beta$ less than $100 kg/m^2$ at an altitude of $450 km$. Normal de-orbit time is $0.4 yr - 2.7 yr$ (based on solar radiation levels) [2]. . . . . 48
11.2 Amount of days till de-orbit ($130 km$) and the mass-over-area $\beta$ for each SIDD configuration. † indicates simulated with GMAT, ‡ indicates taken from SMAD. . . . . 48

12.1 Microprocessor candidates *Mass estimated using density of silicon . . . . . 52
12.2 Mass storage component summary *Mass estimated using density of silicon . . . . . 53

13.1 The amount of power consumption of each operational phase (*is only for the secondary battery) . . 55
13.2 Non-rechargeable battery selection . . . . . 56
13.3 Operational phases with their corresponding time and power usage . . . . . 56

14.1 Heat radiation environment around Earth [2] [p.455] . . . . . 58
14.2 Temperature ranges of various components . . . . . 59
14.3 Main components of the femto-satellite . . . . . 61
14.4 Sensitivity analysis: maximum (hot case) and minimum (cold case) temperatures for varying absorptivity and emissivity . . . . . 61

15.1 Properties of common spring materials . . . . . 68
15.2 A selection of spring designs options . . . . . 73

16.1 Launch system accelerations and vibrations. (+ = tension; – = compression) . . . . . 74
16.2 Fundamental frequencies for critical parts and total structure. * indicates matching lateral direction. 76
16.3 Vibration analysis of Soyuz harmonic and random vibrations. Based on the femto-satellite's natural frequency of $207 Hz$. . . . . 77
16.4 Data on structural analysis. . . . . 77
16.5 Maximum stress and displacement of PCBs under 8.3 $g$ launch load . . . . . 78

17.1 Comparison of different shapes . . . . . 79
17.2 Component masses of the structures subsystem . . . . . 80
17.3 Resource allocation . . . . . 82
17.4 Resource allocation (ctd.) . . . . . 83
17.5 Mass and Volume budget for the orbiting spacecraft . . . . . 84

19.1 The potential risks faced during the design process with their respective ID . . . 89
19.2 The potential risks faced during mission development (D) and operation (O) with their respective ID 90
19.3 Risk map . . . 92
19.4 Posterior risk map . . . 93

20.1 Verification values for the thermal model . . . 99
20.2 Compliance matrix of mission, stakeholder and system requirements, ✓ means it complies, × means it does not . . . 100

21.1 Operational limits with different orbital altitudes . . . 104
21.2 Operational limits with different ballistic coefficient of host-satellite . . . 105
21.3 Hibernation time with payload operational duration due to degradation of main battery . . . 105

26.1 Total mission cost . . . 116

A.1 SMA = 6828 km, ECC = 0.002, INCL = 97 deg, RAAN = 0 deg, AOP = 0 deg, TA = 0 deg . . . II
A.2 SMA = 6828 km, ECC = 0.002, INCL = 97 deg, RAAN = 0 deg, AOP = 0 deg, TA = 45 deg . . . II
A.3 SMA = 6828 km, ECC = 0.002, INCL = 97 deg, RAAN = 0 deg, AOP = 0 deg, TA = 90 deg . . . II

B.1 Elmos integrated solar angle sensor specifications . . . III
B.2 Two GPS Systems . . . III
B.3 The OmniVision OVM7695-RAEA camera specifications . . . IV

C.1 Different considered propulsion systems [2] . . . V
C.2 Ranges of parameters for micro valves . . . VI
C.3 Cold gas propulsion systems configurations for $\Delta V$ and different $F_T$ needed. Tank skin stress has a safety factor of 4. . . . VII
C.4 Different amount of thruster needed for a needed $\Delta V$, based on $100g$ total initial satellite mass. . . . VIII

D.1 Orbit parameters with eclipse period . . . X
D.2 Solar panel selection . . . X
D.3 Rechargeable battery selection . . . X
D.4 Power solution trade-off . . . XI

# List of Abbreviations

| Abbreviation | Definition |
|---|---|
| ADC | Attitude Determination and Control |
| ADCS | Attitude Determination and Control System |
| AOP | Argument Of Periapsis |
| ATOX | Atomix oxygen |
| CCD | Charge-coupled device |
| CMOS | Complementary metal-oxide- semiconductor |
| COTS | Commercial off-the-shelf |
| CSI-2 | Camera Serial Interface 2 |
| CW | Clohessy-Wiltshire |
| C&DH | Command and Data Handling |
| CGG | Cold Gas generator |
| DET | Direct Energy Transfer |
| DOF | Depth of Field |
| ECEF | Earth Centered Earth Fixed |
| ECI | Earth Centered Inertial |
| ERSA | Electric rod-style actuator |
| ESA | European Space Agency |
| ESC | Electronic Speed Controller |
| ESD | Electrostatic discharge |
| EuReCa | European Retrievable Carrier |
| FBS | Functional Breakdown Structure |
| FFD | Functional Flow Diagram |
| FEM | Finite element method |
| FOV | Field of View |
| fps | Frames per second |
| FR4 | Flame retardant, glass-reinforced epoxy laminate |
| GaAs | Gallium Arsenide |
| Gbps | Giga-bits per second |
| GEO | Geostationary Earth orbit |
| GMAT | General Mission Analysis Tool |
| GOLD | Gossamer Orbit Lowering Device |
| GPIO | General Purpose Input & Output |
| IDOD | Inflatable de-orbit device |
| IFOV | Instantaneous Field of View |
| IR | Infrared |
| $I^2C$ | Inter-Integrated Circuit |
| ISIS | Innovative Solutions In Space |
| ISS | International Space Station |
| KISS | Keep it simple stupid |
| KLOC | Thousands of Lines Of Code |
| LEO | Low Earth orbit |
| LVLH | Local Vertical Local Horizontal |
| Mb/s | Mega-bits per second |
| MB/s | Mega-bytes per second |
| Mb/s | Mega-bits per second |
| MB/s | Mega-bytes per second |
| MEMS | Micro-Electro-Mechanical Systems |
| MLI | Multi Layer Insulation |
| MP | Mega Pixels |
| NASA | National Aeronautics and Space Administration |
| NRCSD | NanoRacks CubeSat Deployer |
| OFDM | Orthogonal frequency-division multiplexing |
| PCB | Printed Cicruit Board |
| P-POD | Picosatellite Orbital Deployer |
| PSD | Power Spectral Density |
| PWM | Pulse Width Modulation |
| RAAN | Right Ascension of the Ascending Node |
| RF | Radio frequency |
| SMA | Semi-Major Axis |
| SMA | Shape Metal Actuator |
| SPI | Serial Peripheral Interface |
| SR | multi-frame image Super-Resolution method |
| SRP | Solar Radiation Pressure |
| SIDD | Spherical Inflatable De-orbit Device |
| TA | True Anomaly |
| TNO | Netherlands National Organisation for Research into Applied Natural Sciences |
| UAV | Unmanned Aerial Vehicle |
| UHF | Ultra High Frequency |
| UTS | Ultimate tensile strength |
| VHF | Very High Frequency |

# List of Symbols

| Symbol | Name | Units |
|---|---|---|
| $a$ | Semi-major axis | $[m]$ |
| $a$ | side length of the satellite | $[m]$ |
| $A$ | Area | $[m^2]$ |
| $A$ | Amplitude | $[m]$ |
| $A$ | Spring ultimate yield strength intercept value | $[MPa \cdot mm^m]$ |
| $A^*$ | Throat area | $[m^2]$ |
| $A_p$ | Projected area | $[m^2]$ |
| $A_S$ | Surface area | $[m^2]$ |
| $b_r$ | Body reflectance | [-] |
| $B$ | Magnetic field strength | $[T]$ |
| $c$ | Speed of light | $[m/s]$ |
| $C$ | Specific heat | $[J/(kgK)]$ |
| $C$ | Spring index | $[-]$ |
| $C_{CP}-C_{CG}$ | distance between centre of pressure and centre of gravity | $[m]$ |
| $C_D$ | Drag coefficient | [-] |
| $C_{spring}$ | Energy storage capacity | $[J]$ |
| $C_1'$ | First elastic constant, spring | $[-]$ |
| $C_2'$ | Second elastic constant, spring | $[-]$ |
| $d$ | Diameter | $[m]$ |
| $d$ | Spring wire diameter | $[m]$ |
| $d^*$ | Throat diameter | $[m]$ |
| $a_D$ | acceleration due to drag | $[m/s^2]$ |
| $d_{full}$ | Full frame sensor size | $[m]$ |
| $D$ | Amount of data | $[bits]$ |
| $D$ | Spring outer diameter | $[m]$ |
| $D$ | Dipole of the spacecraft | $[Am^2]$ |
| $E$ | Young's modulus | $[Pa]$ |
| $f$ | Frequency | $[Hz]$ |
| $f_b$ | Base excitation frequency | $[Hz]$ |
| $f_{eq}$ | Equivalent focal length | $[m]$ |
| $f_n$ | Natural frequency | $[Hz]$ |
| $f_{real}$ | Physical focal length | $[m]$ |
| $F$ | Force | $[N]$ |
| $F_{crit}$ | Critical force | $[N]$ |
| $F_{albedo}$ | View factor for albedo | [-] |
| $F_{EarthIR}$ | View factor for Earth IR | [-] |
| $F_T$ | Thrust | $[N]$ |
| $F_{Tavg}$ | Average thrust | $[N]$ |
| $g_0$ | Standard gravity | $\left[m/s^2\right]$ |
| $g$ | Gravitational acceleration | $\left[m/s^2\right]$ |
| $G$ | Shear modulus | $[Pa]$ |

| Symbol | Name | Units |
|---|---|---|
| $H_E$ | Equator value of horizontal magnetic field component | $[T]$ |
| $i$ | Angle of incidence | [rad] |
| $I$ | Impulse | $[Ns]$ |
| $I$ | Mass moment of inertia | $\left[kgm^2\right]$ |
| $I$ | Area moment of inertia | $[m^4]$ |
| $I_{EarthIR}$ | Intensity of Earth IR flux | $[W/m^2]$ |
| $I_{solar}$ | Intensity of the solar flux | $[W/m^2]$ |
| $I_{SC}$ | Spacecraft moment of inertia | $[kgm^2]$ |
| $I_{wh}$ | Momentum wheel moment of inertia | $[kgm^2]$ |
| $I_{sp}$ | Specific impulse | $[s]$ |
| $J$ | Polar moment of inertia | $[m^4]$ |
| $k$ | Spring stiffness | $[N/m]$ |
| $k_a$ | Axial spring stiffness | $[N/m]$ |
| $k_l$ | Lateral spring stiffness | $[N/m]$ |
| $K_B$ | Bergsträsser factor | [-] |
| $L$ | Length | $[m]$ |
| $L_s$ | Solid length, spring | $[m]$ |
| $L_0$ | Free length, spring | $[m]$ |
| $m$ | Mass | $[kg]$ |
| $m$ | Spring ultimate tensile strength exponent | $[-]$ |
| $\dot{m}$ | Mass flow | $[kg/s]$ |
| $m_0$ | Mass at point 0 in time | $[kg]$ |
| $m_1$ | Mass at point 1 in time | $[kg]$ |
| $m_f$ | Fuel mass | $[kg]$ |
| $m_f$ | Femto-satellite mass | $[kg]$ |
| $m_h$ | Host spacecraft mass | $[kg]$ |
| $m_T$ | Mass of empty fuel tank | $[kg]$ |
| $M$ | Earth dipole | $\left[Am^2\right]$ |
| $M$ | Moment | $[Nm]$ |
| $M_W$ | Molecular mass | $[kg/mol]$ |
| $n$ | Amount of substance | $[moles]$ |
| $n_b$ | Number of bits per pixel | [-] |
| $N_a$ | Number of active spring coils | [-] |
| $N_e$ | Number of end spring coils | [-] |
| $N_t$ | Number of total spring coils | [-] |
| $p$ | Spring pitch | $[m]$ |
| $p$ | Pixel size | $[m]$ |
| $p$ | Momentum | $[Ns]$ |
| $p_p$ | Amount of pixels | [-] |
| $P$ | Pressure | $[Pa]$ |
| $P$ | Power | $[W]$ |

| Symbol | Name | Units |
|---|---|---|
| $P_a$ | Ambient pressure | $[Pa]$ |
| $P_C$ | Chamber pressure | $[Pa]$ |
| $P_e$ | Exit pressure | $[Pa]$ |
| $Q_{albedo}$ | Heat load due to albedo | $[W]$ |
| $Q_{EarthIR}$ | Earth IR heat load | $[W]$ |
| $Q_{solar}$ | Solar heat load | $[W]$ |
| $r$ | Radius of the orbit | $[m]$ |
| $r$ | Moment arm | $[m]$ |
| $r$ | Coverage of one pixel | $[m]$ |
| $r$ | Ratio base excitation and natural frequency | $[-]$ |
| $r^*$ | Throat radius | $[m]$ |
| $rpm$ | Rounds per minute | $[\frac{rad}{2\pi}/min]$ |
| $r_T$ | Radius of tank | $[m]$ |
| $R$ | Radius | $[m]$ |
| $R^2$ | Coefficient of determination | $[-]$ |
| $R_A$ | Gas constant | $[\frac{J}{Kmol}]$ |
| $R_E$ | Earth Radius | $[m]$ |
| $s$ | Number of samples per pixel | [-] |
| $s$ | Spring deflection | $[m]$ |
| $S_0$ | Solar energy flux near Earth | $[W/m^2]$ |
| $s_{max}$ | Maximum spring deflection | $[m]$ |
| $S_{ut}$ | Spring ultimate tensile strength | $[Pa]$ |
| $S_{yield}$ | Spring yield strength | $[Pa]$ |
| $t$ | Time | $[s]$ |
| $t$ | Thickness | $[m]$ |
| $t_T$ | Thickness of tank | $[m]$ |
| $T$ | Temperature | $[K]$ |
| $T$ | Torsion | $[N \cdot m]$ |
| $T_C$ | Chamber temperature | $[K]$ |
| $T_m$ | Residual dipole torque | $[Nm]$ |
| $T_{min}$ | Lower end of temperature range | $[K]$ |
| $T_{max}$ | Upper end of temperature range | $[K]$ |
| $T_s$ | Slew torque | $[Nm]$ |
| $T_{sp}$ | Solar radiation torque | $[Nm]$ |
| $v$ | Velocity | $[m/s]$ |
| $v_a$ | velocity relative to the atmosphere | $[m/s]$ |
| $v_e$ | Exit velocity | $[m/s]$ |
| $v_f$ | Velocity femto-satellite | $[m/s]$ |
| $v_h$ | Velocity host spacecraft | $[m/s]$ |
| $V$ | Volume | $[m^3]$ |
| $w_i$ | Dimension square hole of supporting plate in deployment system | $[m]$ |
| $w_o$ | Outer dimension of supporting plate in deployment system | |
| $x$ | Distance | $[m]$ |

| Symbol | Name | Units |
|---|---|---|
| $\dot{x}$ | Velocity | $[m/s]$ |
| $\ddot{x}$ | Acceleration | $[m/s^2]$ |
| $X$ | Magnitude of object motion | $[m]$ |
| $y$ | Spring deflection | $[m]$ |
| $y_{cr}$ | Critical spring deflection for buckling | $[m]$ |
| $y_{max}$ | Maximum spring deflection | $[m]$ |
| $Y$ | Magnitude of base motion | $[m]$ |
| $\alpha$ | Coefficient of reflectivity | [-] |
| $\alpha$ | Coefficient of absorptivity | [-] |
| $\alpha$ | Spring end constant | [-] |
| $\beta$ | Mass-over-area ratio | $[kg/m^2]$ |
| $\gamma$ | Specific heat ratio | [-] |
| $\Gamma$ | Vandenkerckhove parameter | [-] |
| $\delta$ | Displacement | $[m]$ |
| $\delta_a$ | Axial displacement | $[m]$ |
| $\delta_l$ | Lateral displacement | $[m]$ |
| $\Delta t$ | Time step | $[s]$ |
| $\Delta T$ | Temperature change | $[K]$ |
| $\Delta V$ | Velocity increment | $[m/s]$ |
| $\epsilon$ | Orbital energy | |
| $\epsilon$ | Coefficient of emissivity | [-] |
| $\zeta$ | Damping ratio | [-] |
| $\eta_s$ | Efficiency of solar cells | [-] |
| $\theta$ | Angle for slew manoeuvre | $[rad]$ |
| $\theta$ | Angle relative to north-pointing axis | $[rad]$ |
| $\mu_0$ | Vacuum magnetic permeability constant | $[H/m]$ |
| $\lambda_{eff}$ | Effective slenderness ratio, spring | [-] |
| $\rho$ | density | $[kg/m^3]$ |
| $\rho_{albedo}$ | Albedo | [-] |
| $\rho_{body}$ | Body Reflectance | [-] |
| $\sigma$ | Stress | $[Pa]$ |
| $\sigma$ | Stefan-Boltzmann constant | $[W/(m^2K^4)]$ |
| $\sigma_y$ | Yield stress | $[Pa]$ |
| $\tau$ | Shear stress | $[Pa]$ |
| $\omega_{n-a}$ | Axial angular natural frequency | $[rad/s]$ |
| $\omega_{n-l}$ | Lateral angular natural frequency | $[rad/s]$ |
| $\omega_{wh}$ | angular velocity of momentum wheel | $[rad/s]$ |
| $\omega_{SC}$ | angular velocity of spacecraft | $[rad/s]$ |
| $\omega_n$ | Angular natural frequency | $[rad/s]$ |

# 1

# Introduction

Since the launch of the first satellite in 1957 the mass of satellites increased tremendously, leading up to the 17 000 $kg$ Compton Gamma Ray Observatory. Due to innovations in consumer electronics industry the size and mass of satellites have decreased significantly over the last few years [4]. Recently CubeSats have established their presence within the space industry, but the miniaturisation still continues. The next step in the trend is for satellites to reach the sub-100$g$ mass. Satellites that fall into this next class of satellites are called femto-satellites. These satellites allow for new markets to be opened by allowing for cheaper and faster launches of satellites. Universities and other institutions are making use of these small satellites to motivate and support the learning of their students for a price that is within their budget. This high level of miniaturisation includes many challenges but also opens up many possibilities that were previously not feasible. The challenge is finding these possibilities and making clear to users why femto-satellites are such a good alternative to larger satellites. That is why a mission needs to be performed that can show this potential and explain why femto-satellites have a place in the satellite market. DSE group S13 has been given the assignment to:

*Design a femto-satellite for technology demonstration*

In previous design stages it has been established that showing the femto-satellite potential is best achieved them for inspection and promotion purposes, which can be achieved by having the satellite take images of a host spacecraft. These features have been combined in the PICS (Promotion and Inspection Cubic Satellite) mission. The images taken during the mission will provide the engineering team of the host spacecraft with data concerning impact damage and will help the marketing team with promoting their spacecraft to the greater public. The PICS mission will focus on inspecting the effect of micro-meteoroids and space debris impact on the solar arrays and the spacecraft bus. Very little knowledge exists about these subjects and existing models are only based on obsolete statistical data. The pictures taken by the PICS mission will contribute to updating these models and will help with the mapping of space debris objects on a sub-millimetre level.

A very important aspect in designing a satellite is space debris. The probability of creating additional space debris should be mitigated as much as possible. This is especially important for femto-satellites because, due to their small size, they are on the edge of what is possible to track using radar. That is why the PICS will have its own active de-orbit device in the form of an inflatable balloon.

This report has a different structure compared to the group's *Midterm Report* [5] and *Baseline Report* [6]. It is divided into three parts. The first part contains the topics that are important prerequisites for the design process, like the mission description in Chapter 2, the sustainable development strategy in Chapter 4 and the design requirements in Chapter 6. The second part focuses on the design of the femto-satellites and related topics. First, the mission astrodynamics are discussed in Chapter 7. Then, the designs of the subsystems are presented in Chapter 8 to 14. In Chapter 15 the deployment system is discussed. The structural and vibrational analysis is outlined in Chapter 16. In Chapter 17 the integral configuration and structure of the femto-satellite is discussed. Different iterations of the design are discussed in Chapter 18. A risk analysis is performed in Chapter 19. The verification and validation procedures of the models and the design are presented in Chapter 20. *Part 3* focuses on the post-design activities. The assembly & integrations plan is discussed in Chapter 22, followed by the operations and logistics plan. A future vision on femto-satellites is outlined in Chapter 27 and the recommendations are discussed in Chapter 29.

# I

# Project Analysis

# 2

# Mission Determination & Description

In this chapter the mission selection is elaborated upon and a description of the mission is given. In the midterm phase of the project [5] the mission statement was determined to be:

*DSE group S13 at the Faculty of Aerospace Engineering at TU Delft will design a femto-satellite to demonstrate its inspection and promotion potential.*

This means that a mission shall be set up in which this potential can be demonstrated. First in Section 2.1 the reasoning behind the selection of this mission is presented by performing a trade-off between a list of suggested mission. Second in Section 2.2 three concepts for the previously selected mission are traded off, resulting in a final mission concept. In Section 2.3 the potential of femto-satellites with regard to inspection of a host spacecraft is elaborated upon by building on past spacecraft failures and performing a study into impact damage inspection. In Section 2.4 the reasoning behind using femto-satellites for promotion purposes is motivated. Lastly in Section 2.5 a full description of the mission is given.

## 2.1. Mission Trade-Off

First a short summary of each of the missions will be presented. Afterwards that the trade-off and weights for the trade off are shown.

**Scientific experiment** is a mission where a scientific experiment is performed on board of a femto-satellite which will be launched in space. The advantages of using a femto-satellite is that it is light-weight and cheap, which lowers the barrier for research groups and universities to do such experiments.
**Telescope TinySat constellation** is a mission inspired by LOFAR[1]. The mission entails building a radio telescope in space to detect wavelengths longer than 10 meters. This is done by putting multiple femto-satellites in a grid to create a large synthetic aperture. With this method a much larger aperture can be obtained with respect to one large satellite. Another advantage is the absence of losses due to the influence of the atmosphere.
**Earth observation TinySat** is a mission where a grid of femto-satellites is used to observe the Earth. This grid will have a larger and continuous coverage of the Earth compared to a single satellite.
**Modular satellite system** is a femto-satellite where the subsystems are interchangeable. In this manner the customer is able to build his femto-satellite according to his personal scientific or commercial goals. Hence, components can be mass-produced to provide a large variety of different satellites.
**Space debris removal TinySat** is a mission focused on reducing space debris. The femto-satellite shall attract space debris by deploying a long charged electrodynamic tether, causing it to de-orbit along with the collected space debris. The advantage of this design is that a lot of femto-satellites can be launched for a relatively low cost, thus covering a larger area.
**Inspection TinySat** is a mission where a femto-satellite is deployed to inspect a bigger satellite. The inspection can help determining why the ground lost contact with a satellite. Also the femto-satellite could inspect the current attitude stability of the satellite. This can help improve future design of satellites.
**Exploration aid femto-satellite** is a mission where the femto-satellite is deployed from a exploration mission. The femto-satellite can then be employed to take pictures or as an additional payload for performing scientific measurements.
**Planetary Navigation System** is a cheap and light weight solution for a navigation system. A grid of femto-satellites will be deployed around a planet which functions as a navigation system for that planet. This mission is useful in light of future human colonisation of other planets.
**Space debris detection femto-satellite** is a mission focused on mapping space debris. This can be a good alternative for the larger satellites which are currently used to detect space debris. With the information from this satellite a more accurate model of space debris can be made.
**Space advertisement TinySat constellation** is an innovative mission. The idea is that a grid of femto-satellites will be deployed in space with a high-power light source on it. The satellites will charge its batteries during the sunlit phase. During eclipse the lights will switch on and each satellite will form one pixel of an advertisement image in space which will be visible from the Earth.

[1] LOFAR,http://www.lofar.org/about-lofar/general-information/introduction,14-06-2016

Next a trade-off between these missions are needed. The different criteria for the trade-off are given below with there specific weights.

1. **Technical Feasibility (TF)** **Weight: 25**
   The mission must be evaluated based on whether it is technically feasible to perform. If the mission is not technically feasible it will be impossible to use it for demonstration purposes.
2. **Demonstrability (D)** **Weight: 25**
   It is very important to draft a mission that can be demonstrated well. If a mission can only be successful with a full scale test where a large project needs to be set-up or the mission results are hard or even impossible to validate the mission can not be used to demonstrate femto-satellite capabilities.
3. **Need(N)** **Weight: 20**
   Need is taken as a criterion because the mission is to *demonstrate* femto-satellite technology, which implies that a mission should be selected which is considered useful by the space community in order to guarantee that future missions will feature femto-satellites.
4. **Risk (R)** **Weight: 15**
   Risk is a very important parameter when considering the mission. If the proposed mission has a high probability of failing or there are high consequences when the mission fails the risk will be too high.
5. **Cost (C)** **Weight: 10**
   Cost is important because the mission is only to provide a demonstration which means that the femto-satellite design itself will not be able to sell anything other than its idea. This is why the costs need to remain low while still achieving the goal of demonstration.
6. **Sustainability (S)** **Weight: 5**
   The mission must be as sustainable as possible, meaning that the amount of debris generated and the environmental impact of the mission must be minimised.

The trade-off is shown in Table 2.1. Here it is shown that the *Inspection TinySat* has the highest score. After the trade-off a sensitivity analysis is performed and it is concluded that the *Inspection TinySat* is the best candidate to show the potential of femto-satellites with the technology of today.

Table 2.1: Trade-ff table for all the proposed missions. Factors are weighted out of 10.

| Mission Proposal | TF | D | N | R | C | S | Weighted Average |
|---|---|---|---|---|---|---|---|
| Scientific experiment femto-satellite | 9 | 8 | 7 | 7 | 5 | 3 | 7.35 |
| Telescope TinySat constellation | 2 | 8 | 7 | 4 | 2 | 4 | 4.90 |
| Earth observation TinySat | 8 | 9 | 5 | 5 | 3 | 6 | 6.60 |
| Modular satellite system | 7 | 7 | 5 | 3 | 3 | 7 | 5.60 |
| Space debris removal TinySat | 1 | 4 | 9 | 2 | 3 | 7 | 4.00 |
| Inspection TinySat | 9 | 9 | 6 | 6 | 8 | 6 | 7.70 |
| Exploration aid femto-satellite | 6 | 4 | 3 | 2 | 6 | 5 | 4.25 |
| Planetary Navigation System | 2 | 7 | 0 | 2 | 1 | 3 | 2.80 |
| Space debris detection femto-satellite | 4 | 6 | 8 | 5 | 6 | 6 | 5.75 |
| Space advertisement TinySat constellation | 5 | 10 | 7 | 4 | 9 | 2 | 6.75 |

## 2.2. Concept Trade-Off

After the mission selection three design concepts needed to be traded off. First these concepts are presented after which one of them will be selected based on a trade-off.

**Orbiting:** This concept comprises a femto-satellite which will be installed on the host spacecraft during launch. At a certain time the femto-satellite will be released from the host spacecraft. The femto-satellite will be deployed in such a way that it can inspect the host spacecraft. This orbit can be found in Section 7.1.1. In this concept the femto-satellite will be self-sustained in its orbit.

**Docking:** This concept also consist of a femto-satellite which will be attached to the host spacecraft during launch. After launch the femto-satellite can be released, perform a mission for half an orbit and re-dock with the host. More information about this orbit can be found in Section 7.1.2. During docking the femto-satellite can refuel, recharge and send the data to the host.

**Pick & Place:** This concept is specially designed for the International Space Station (ISS). Here a femto-satellite is deployed from the ISS to inspect the damage on the ISS. Also the femto-satellite can assist with human space

operations. The femto-satellite can be deployed and re-dock using the robotic arm on board of the ISS. During docking the femto-satellite can be recharged. These three concepts are traded according to the criteria presented below. It should be noted that the midterm estimates were used for the input of the trade-off, so not the values presented in this report. For more information on midterm estimates see Chapter 17.4.

- **Mass** **Weight: 15**
  In order to grade the concepts on mass the estimates were taken and a scale was devised. This scale was from 60 to 100 $g$ where 60 $g$ was a ten and 100 $g$ a zero.
- **Power** **Weight: 15**
  In order to grade the concepts on power the maximum and minimum power estimate in the *active* condition of the femto-satellite are taken, these are then used to determine a scale, where a power consumption of $0.925W$ is a ten and a power consumption of 4.40 is a zero.
- **Sustainability** **Weight: 20**
  The sustainability will be graded based on the three types of sustainability. Below the three types are defined and their relative values are defined.
  1. Regulatory sustainability **4**
  2. Future sustainability **2**
  3. Environmental sustainability **1**

  Regulatory sustainability is the most important type of sustainability since if the spacecraft does not comply with the regulations it is not in line with the goals set by the international space community. Second the future sustainability is considered, which takes into account the amount of data the spacecraft can gather and the value of this data for future research. Lastly the environmental sustainability is considered. This aspect obtained the lowest value because of the extreme space environment it will be near impossible to create a spacecraft without using materials that are harmful to the Earth's environment.
- **Technical Performance** **Weight: 20**
  In order to assess the femto-satellite's technical performance three criteria will be applied.
  1. The coverage of the host spacecraft the femto-satellite is capable of achieving **1**
  2. What range of host spacecraft the concept is applicable for **1**
  3. The operational independence of the femto-satellite with regard to the host spacecraft **1**
- **Risk** **Weight: 20**
  Three criteria will be used for the risk assessment, which are listed below.
  1. The risk of collision with the host spacecraft **1**
  2. The risk of not being able to properly insert into the orbit **1**
  3. The risk of subsystem failure **1**
- **Cost** **Weight: 10**
  The cost will be graded based on three criteria.
  1. Operational costs 1
  2. Costs related to additional operations of the host spacecraft required to facilitate the femto-satellite 1
  3. Development costs 1

Based on these criteria a trade-off is performed. The results of the trade-off are presented in Table 2.2. From this table it can be concluded that the orbiting concept obtained the highest score. After performing a sensitivity analysis it was safe to say that the orbiting concept is the best design concept in order for the femto-satellite to fulfil the inspection mission.

Table 2.2: Concept Trade-Off table

| Criteria | **Mass** | **Power** | **Sustainability** | **Technical Performance** | **Risk** | **Cost** | **Weighted Average** |
|---|---|---|---|---|---|---|---|
| **Orbiting** | 8.5 | 5.75 | 2.9 | 8.3 | 6.6 | 8.3 | 6.3 |
| **Docking** | 8.5 | 5 | 7.1 | 1.6 | 1.6 | 5 | 4.7 |
| **Pick & Place** | 10 | 4.25 | 6.4 | 3.3 | 5 | 3.3 | 5.4 |

## 2.3. Inspection Satellite Potential

From the requirement **TS-MIS-IMG-INS-01-A** the requirements on the inspection aspect of the femto-satellite can be derived. These requirements pose the question what inspection is exactly, in this section a literature study is presented that shows what types of inspection exist and what inspection can be applied to. Inspection on satellites

can be performed using five different methods:[7]

1. Infrared (IR) camera
2. Radio frequency (RF) probe
3. Electrostatic discharge (ESD) sensor
4. Radiation sensor
5. Visual camera

A literature study was performed into IR cameras, however these are very often very limited in resolution for small scale cameras and are not feasible on the femto-satellites. RF probes and ESD sensors require physical contact with the host spacecraft which is also not possible. Lastly, radiation sensors are discarded since they have a very limited applicability. The *visual camera* is able to diagnose the highest number of potential problems occurring on a host spacecraft. These potential problems are given below (adapted from Jacobovits [7]).

- Damaged solar arrays
- Failed deployment (solar arrays, antenna reflectors, etc.)
- Separation failure
- Micro-meteoroid and space debris strikes
- Damaged optics
- Damaged antenna
- Frayed or cut wiring
- Erroneous spin rate
- Pointing inaccuracies
- Propellant leak
- ESD arcing
- Blanket damage

With this list of possible failures that can be detected the employment of the femto-satellite as an inspection satellite is justified. However, a concrete mission still needs to be set up. In the next section the potential for *Inspection of impact damage due to micro-meteoroid and space debris* will be treated.

### 2.3.1. Impact Damage Inspection

In this section it is explored whether micro-meteoroid and space debris impact damage detection can be part of the femto-satellite's mission. First a few papers are summarised that describe the impact damage inspection of structures retrieved from space. The imaging accuracy of the femto-satellite's camera is investigated in Section 8.4 and finally it is concluded whether impact monitoring can be a viable part of the femto-satellite's mission. From Earth only space debris and micro-meteoroids larger than a few millimetres in Low-Earth Orbit (LEO) can be tracked by optical or radar techniques. There are only two options to investigate objects smaller than a few millimetres. One is putting a particle detector in space. The other option is to inspect structures retrieved from space. The micro-meteoroids and Space Debris Department of ESA states on its website MADWEB[2]:

*'Impact pits observed on various materials (not purposely designed as particle detectors) that have been exposed to the space environment provide a wealth of useful data about the micro debris environment. [...] In the field of space debris, post-flight analysis of hardware is the only way to gain information on the 10 - 1000 micron size range to compare debris models, hyper-velocity impact testing and damage equations to actual impacts in space.'*

Extensive post-flight studies were conducted on impacts at NASA's Long Duration Exposure Facility (LDEF) which orbited in LEO from 1984 to 1990 [8, 9]. Later, ESA conducted studies into impact damage on solar panels of the Hubble Space Telescope returned to Earth in 2002 after 8.24 years in space and of solar panels and MLI blankets of the European Retrievable Carrier (EuReCa) satellite which was retrieved in 1993. On EuReCa impact craters were found ranging in diameter from 100 $\mu m$ to 6.4 $mm$. The distribution of impact crater sizes is shown in Figure 2.1[3]. Several thousands of them could be seen with the naked eye. Residue analysis was used to discriminate between space debris and micro-meteoroids. It was found that most (especially smaller) impacts were caused by space debris. In the range of medium impacts, micro-meteoroids dominated but space debris impacts were still significant. However, no failure on EuReCa could be related to an impact event. [10, 11]

Several models of the micro-meteoroid and space debris environment exist. For top impacts, crater diameters are about ten times the size of the particles that caused the impacts[4]. The flux densities that these models predict are

[2]MADWEB Archive, `http://space-env.esa.int/madweb/`, retrieved on 02-06-2016
[3]MADWEB, `http://space-env.esa.int/madweb/hdamage.php`, retrieved on 30-05-2016
[4]MADWEB, `http://space-env.esa.int/madweb/images/fig5.jpg`, retrieved on 30-05-2016

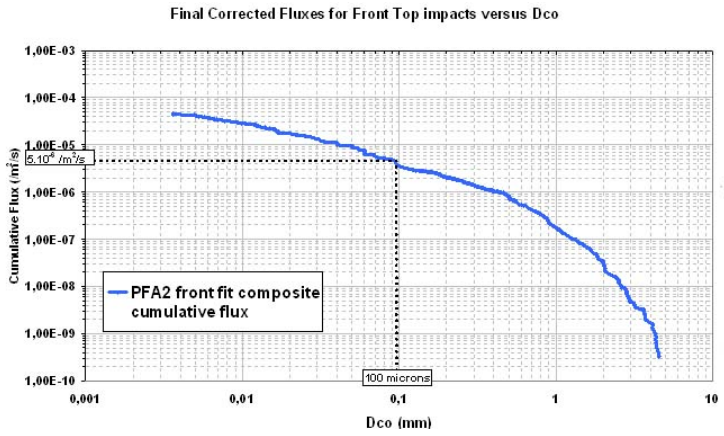


Figure 2.1: Flux density versus crater size for HST and EuReCa

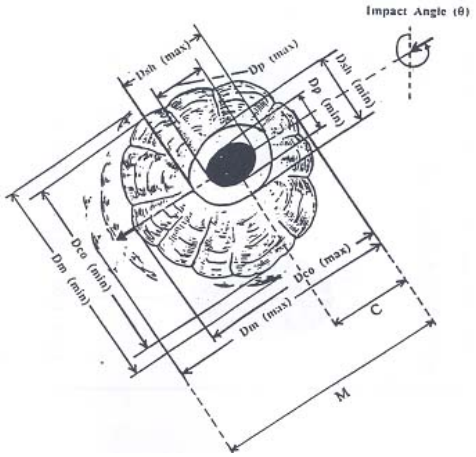


Figure 2.2: Impact crater dimensions

shown in Figure 2.3 as function of particle size, which shows that the particle flux density increases with decreasing particle size.

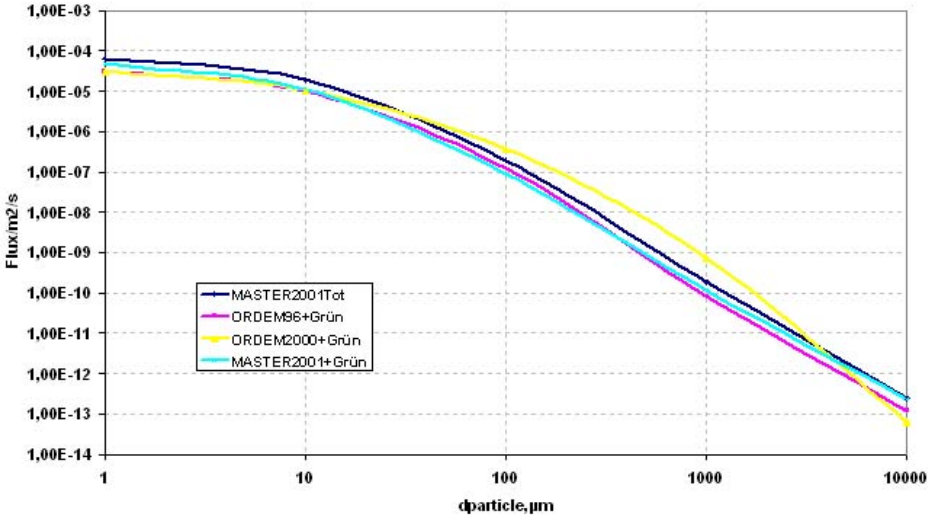


Figure 2.3: Flux densities according to various micro-meteoroid and space debris models[5]

The femto-satellite can contribute to the following functions [6]:

- Recording the impact features
- Analyzing the impacts and assessing the damage caused by space debris and micro-meteoroids
- Validating and improving current models of micro-meteoroid and space debris populations in LEO

ESA and NASA are planning to do more impact studies as more hardware is returned from space. However since the retirement of the Space Shuttle it is unlikely that substantial amounts of flight hardware are returned in the near to medium future. Therefore it becomes interesting to monitor impact damage directly from space instead. In Chapter 8 it will be investigated whether and how this can be done using a camera installed on the femto-satellite.

### 2.3.2. Resurs-P3 Solar Panel Deployment Failure

The *Resurs-P3* is a Russian Earth observation satellite that was launched on 13-03-2016. [7] The satellite was brought into an orbit at an altitude of 470–483 kilometres with an inclination 97.29°. After launch it was discovered that

[5] MADWEB, `http://space-env.esa.int/madweb/hmodels.php`, retrieved on 30-05-2016

[6] Micrometeorites and Space Debris - The Eureca Post-Flight Analysis, `http://www.esa.int/esapub/bulletin/bullet80/ace80.htm`, retrieved on 02-06-2016

[7] Resurs-P3 information, `https://www.wmo-sat.info/oscar/satellites/view/640`, retrieved on 27-05-2016

one of the satellite solar arrays did not deploy correctly, resulting in lower power generation, leaving the spacecraft permanently impaired. [8]

The mission officials are hoping that vibrations caused by the main engine during orbit corrections will shake the solar panel loose and allow the satellite to fulfil its mission. [8] This leaves great uncertainty about the future of the mission. The mission cost for Roskosmos (the Russian federal space agency) was around 40 million USD. [9] Given the fact that the satellite is currently unable to perform at peak efficiency the return on this investment, monetary by selling the images or intellectually by sharing the gained knowledge, will be lower. Also given the fact that it is currently not fully known what went wrong during the deployment of the solar panels, no advances can be made in the future to fix possible problems with the release mechanism.

For the Resurs-P3 it would have been desirable to have an inspection satellite to visualise the deployment mechanism and see which part of it failed. There are currently two options to inspect the mechanism on the satellite:

1. Launch a servicing/inspection satellite into the same orbit to inspect.
2. Carry a satellite that is launched on-board of the host into orbit and deploy it when needed.

The first option is very expensive and requires many resources like for example a launcher to bring it into orbit. The second option requires the engineering team to think ahead, but will be much cheaper since it is launched with the host spacecraft. Carrying a large external satellite however would add substantial weight to the host due to the increased launch loads and would have a very high development cost.

This is why a small femto-satellite would be the ideal solution, the low weight means that no large modifications need to be made to the host spacecraft to accommodate the inspection spacecraft. This femto-satellite would be able to visualise the hinge, transmit the images to the host spacecraft and give the engineers on the ground valuable information.

## 2.4. Promotion Satellite Potential

The space industry is currently unable to provide the general public with real in-orbit images of their spacecraft. This is due to the fact that their satellites to not come equipped with camera equipment that can take images from a distance. As a substitute 3D renders are often used, but these renders will always be underlined with the words: *Artists Impression*, which takes away the ability of the general public to grasp the work of space organisations.

The general public has no method of verifying the work that is being done by space organisations. In order to provide a solution to this issue a femto-satellite can be used that will take the pictures and transmit them back to the host spacecraft. This way space organisations are enabled to share real, in-operation images of their spacecraft, causing the public to get a real grasp of space travel.

## 2.5. Mission Description

In this section a full mission description is given, this is split up into two sections:

1. Host Spacecraft
2. Inspection mission description

### 2.5.1. Host Spacecraft

In 2016 and 2017 the Google/Alphabet owned company *Terra Bella* will launch a large series of Earth Observation satellites in the *SkySat C* series. These satellites are used for high resolution panchromatic and multispectral Earth observation.[10]

The femto-satellite demonstration mission will be centred around this spacecraft, of which a 3D render can be seen in Figure 2.4. This mission will be used as a demonstration of the capabilities of femto-satellites as a promotion and inspection tool and will thus be a test mission. If the mission is successful femto-satellite can be adapted to perform the same tasks on other host spacecraft. In Table 2.3 key data of the SkySat C1[11,12,13] are given, which will be used throughout the report for the mission design. The reasons that the SkySat forms a good host for the demonstration of femto-satellite potential are listed below:

1. **Spacecraft Dimensions**
   The SkySat C series of satellites are all relatively small, cubic-shaped satellites with no large extendeding

[8] Resurs-P3, `http://www.russianspaceweb.com/resurs-p3.html`, retrieved on 27-05-2016
[9] Resurs-P, `http://www.russianspaceweb.com/resurs_p.html`, retrieved on 27-05-2016
[10] Gunters space page SkySat C1, `http://space.skyrocket.de/doc_sdat/skysat-3.htm`, retrieved on 30-05-2016
[11] Satellitetoday SkySat C1, `http://www.satellitetoday.com/launch/2016/04/06/terra-bella-evaluating-launches-for-eight-skysats-by-2017/`, retrieved on 30-05-2016
[12] Gunters space page SkySat C1, `http://space.skyrocket.de/doc_sdat/skysat-3.htm`, retrieved on 30-05-2016
[13] eoPortal SkySat C1, `https://directory.eoportal.org/web/eoportal/satellite-missions/t/terra-bella`

components. This means that the inspection satellite can orbit relatively close to the host spacecraft without risk of collision, meaning that smaller features can be detected on the surface of the solar panels.

2. **Quantity**
   Due to the fact that a large series of them is planned (13 guaranteed) they benefit greatly from inspection since defects found on the earlier models can be fixed on the later models.
3. **Orbit**
   The spacecraft orbits in a low Earth orbit at 450 $km$, meaning that it is possible to quickly de-orbit the femto-satellite and thus no contribution to space debris will be made.
4. **Google**
   Given that the femto-satellite concept is a relatively new concept it is required to find a corporation that is willing to invest the money to demonstrate the femto-satellite potential. Under the name of *Google Ventures* Google has spent a large amount of money on new technology start-ups and ideas [14] so it is not unimaginable that they will fund a project like PICS.

Table 2.3: Facts of the SkySat C1

| **Property** | **Value** |
|---|---|
| Spacecraft mass | 120 [$kg$] |
| Spacecraft dimensions | $60 \times 60 \times 95$ [$cm$] |
| Orbit altitude | 450 [$km$] |
| Orbit shape | Circular, polar inclined |

### 2.5.2. Mission Timeline

As part of the SkySat C series, the SkySat C12 will launch somewhere in the year 2017. After development of the PICS satellite is finished the satellite will be integrated into the host spacecraft and will piggyback with the spacecraft. The femto-satellite will remain in storage on the SkySat C12 for at least one year so that the host spacecraft will contract impact damage that can be studied by the femto-satellite. The femto-satellite will then deploy and start its operational lifetime.

Figure 2.4: 3D render of the SkySat C1

During the operational lifetime of the femto-satellite it will have the first 30 seconds for attitude correction and detumbling. After these 30 seconds the femto-satellite will be continuously taking images for 442 seconds. During this period the femto-satellite will store all the images in its on-board storage. The first 300 seconds will feature inspection pictures and the last 142 seconds are reserved for promotion pictures. It should be noted that these types of images can be interchanged, however after the first 300 seconds the spacecraft is at a sufficient distance so it can take images of the entire host spacecraft.

When these 442 seconds are over the spacecraft attitude determination and control system will turn off and the communications system is started up. The communications system will be transmitting data for the next 6250 seconds, after which all the images are transferred to the SkySat C12. The SkySat C12 has a powerful down-link which will then transfer all these images to the ground station over a longer period of time which is to be determined by the the spacecraft's operators.

[14] Google Ventures portofolio, `http://www.gv.com/portfolio/`, retrieved 30-05-2016

# 3

# Market Analysis

Since the launch of the first satellite, the Spoetnik 1, in 1957, the number of satellites had increased exponentially. As of now, there have been approximately 8000 launches of man made objects in space[1]. Of those satellites, approximately 1000 are still operational. The budgets in the space sector are enormous, individual satellites easily cost over €250 million[2]. In case of a failure it is often hard to find out what went wrong because inspection is almost impossible.

Nearly all satellites are dependent on their solar panels for power. Once the solar panels fail, the mission will most certainly fail entirely due to the lack of power. Solar panels are a vulnerable subsystem, radiation, temperature fluctuations, micro meteoroids and space debris could all jeopardise their performance. A lot of research has been conducted into solar panel degradation, but the exact influence of these threats is unknown. Up to now, only the solar panels of two satellites have been brought back to Earth, from the EURECA and Hubble Space Telescope[2] [12], both in 1993. In the 23 years after that the amount of space debris has increased drastically. The exact influence of small pieces of space debris on solar panels over time is unknown, only statistical models exists which are hard to validate. Everyone with an interest in launching satellites into space will benefit from better predictions of solar panel degradation. The mission designed in this report will help with improving the existing models of solar panel degradation.

Another development in the space industry that has gained momentum the past decade is the use of photographs for promotional purposes. Space organisations invest a lot of money to enthuse the public for their project. For governmental space organisations this is important because they are dependent on tax payers while companies want to promote their product. Combined with the possibility of space tourism, space is becoming popular and accessible! The PICS mission designed in this report is specifically designed for inspection and promotion purposes.

## 3.1. Market Needs and Trends

As of now, conducting real time research into the effects of micro meteoroids or space debris on solar panel performance is nearly impossible. Statistical models are hard to develop because only particles bigger than $2cm$ can be seen from Earth [13]. While the numbers of particles bigger than $2cm$ is approximately known, it is hard to estimate the number of particles smaller than $2cm$ and calculating the probability of collision is even harder. This is where this mission comes in: since the femto-satellite is released from the host spacecraft, the distance is initially very small, allowing for very detailed pictures of the solar panels. These kinds of pictures are impossible to take otherwise, giving the operator of the host spacecraft a distinct advantage. It is likely that as missions will become more complicated in the next few decades and demand for better inspection methods will rise. The PICS can, at various moments during the lifetime of a mission, provide valuable information to the engineers.

Over the previous decade space organisations have discovered the importance of popularising their goals. All organisations involved in space have Facebook, LinkedIn and Twitter pages on which they share their progress, beautiful pictures and updates. Even individual missions have their own pages and website to explain what is going on. Selfies of astronauts are very common. The only thing that is hard to make a picture of is the satellite itself. The ISS does this with its robotic arm but most pictures of satellites are computer generated. When Rosetta made a selfie last year[3] this caused quite a stir. It is likely that the demand for such pictures will only increase the next few decades as missions increase in complexity. The PICS is specifically designed for promotional purposes.

## 3.2. Competition

In terms of in orbit inspection by a satellite there is no competition, PICS is the first to open up this market. In orbit inspection is possible if the host spacecraft has a robotic arm, but they are not common on satellites. A lot of time

[1] Quora.com, `https://www.quora.com/How-many-artificial-satellites-have-been-launched-and-are-in-orbit-around-the-Earth`, retrieved on 9-6-2016

[2] Flight impact studies, `http://space-env.esa.int/R_and_D/eureca/eureca.html`, retrieved on 9-6-2016

[3] Images in Space, `http://www.esa.int/spaceinimages/Images/2014/10/Rosetta_mission_selfie_at_16_km`, retrieved on 10-6-2016

and effort is spent on testing the design on Earth and the benefit from an inspection satellite is not immediately clear, but some situations are impossible to simulate and would benefit from in-orbit inspection.

Competition for promotional purposes mainly comes from the increased quality of computer generated imagery (CGI). Techniques to generate pictures are improving each year and are nearly indistinguishable from real pictures. However, the real picture will add significant value.

## 3.3. Barriers to Market Entry

The threshold to enter the in-orbit inspection market is high. Since satellites are expensive pieces of equipment having a smaller satellite orbit closely a bigger satellite seems risky, to say the least. Formation flying in space has almost never been done, and certainly not by satellites with a different $A/m$ ratio (see Chapter 7). The probability of collision is especially hard to calculate due to the uncertainties in factors like atmospheric drag and the effects on performance due to a long storage period. To come up with better estimates for the probability of collision, and to lower it, more research should be conducted in close formation flying. This research takes times and money and needs to be tested, but would result in convincing a potential customer that the chances of collision are negligible. Once a willing host spacecraft operator is found, and the PICS can show its full potential, more customers are expected to follow soon.

## 3.4. Regulations

One of the driving requirements of PICS are the de-orbit regulations. A satellite is required to de-orbit within 25 years of its end-of-life or put in a graveyard orbit [14]. To guarantee this requirement is fulfilled a de-orbit device is put on the PICS. This device also allows for higher orbits. Furthermore, having pressurised containers on a piggybacking satellite is undesirable, but no regulations could be found to back this up.

## 3.5. Marketing Strategy

It should be easy to convince potential customers of the advantages of the PICS. There is a demand for such photographic material. In order to convince potential customers of the safety of their satellite, emphasis should be put on the low probability of collision from the start. Only when it is clear that collision is not realistic a customer will consider the PICS. A lot of people associate femto-satellite with space debris. This is a logical assumption since a $5 \times 5 \times 5$ centimetre cube is difficult to track from Earth. The active de-orbiting procedure will guaranty the quick de-orbiting of the femto-satellite. Lastly, it is necessary to show that the system is safe, that the de-orbiting balloon will not blow up while it is still constained inside the host spacecraft for instance.

The first thing that many people will see from the product is the logo which will be present in presentations, banners, pamphlets, official documents and stands. This is why the logo forms an integral part of the design process. The target audience for any efforts made on promoting the concept will be engineers of various ages. The logo is shown in Figure 3.1.


Figure 3.1: PICS logo

## 3.6. SWOT Analysis

The SWOT analysis is one of the most popular methods used to complement a market analysis. SWOT analysis focuses on strengths, weaknesses, opportunities and threats of the analysed product.[4]

### 3.6.1. Strengths of PICS

The main strength and selling point of PICS is that is provides data that is otherwise impossible to obtain. There exists little knowledge on the effects of space debris and micro meteoroids on solar panels, so the data gathered by PICS can help improve existing models. Secondly, PICS can be used for promotional purposes, which can help popularise space travel, especially since governments are increasingly required to enhance the transparency on their expenditures, which may raise criticism on the relevance and high costs of space exploration during times of economic depression. Compared to other satellites, femto-satellites can be built fast and their material costs are low, which yields an overall low market price. This implies that the consumer market for satellites can be expanded beyond large organisations like ESA, Google and universities to smaller organisations, such as government institutions, high schools and small companies and research institutions. Another strength of PICS is its applicability to a wide range of host spacecraft in various orbits.

### 3.6.2. Weaknesses of PICS

The main weakness of PICS is the risk of collision, and that potential customers will always associate the femto-satellite with a collision even though this risk can well be mitigated. A second weakness is the femto-satellite's limited number of applications due to the fact that its small size puts a constraint of the usage of certain dedicated components. Moreover, although in many components a large degree of miniaturisation has been achieved, for other components this miniature technology is not fully mature, for example for COTS electronics which are featured by low reliability [15]. Lastly, another weakness is related to the small size of PICS since its dimensions are on the edge of what can be detected by currently existing space debris detection technology.[5]

### 3.6.3. Opportunities for PICS

Opportunities for PICS lie in the advancement of miniaturisation. It is expected that current developments in miniaturisation will continue in the future. Hence, femto-satellite technology that is not yet mature is likely to become more reliable in the future. As a result, the development costs for miniaturised components are also expected to decrease, which in turn decreases the market price of femto-satellites. This means the consumer market will expand and femto-satellites will become accessible for various applications like Earth observation with femto-satellite constellations and small-scale space-based research to serve educational purposes. If technology indeed advances in the expected way, PICS will lay the groundwork for a broader scope of femto-satellite applications. Moreover, since more satellites are launched every year [16] PICS could serve the needs of their owners to show their mission and spacecraft to the public in order to promote their business. Also, since commercial spaceflight (in the form of companies like SpaceX) and even space tourism (Virgin Galactic, XCOR Aerospace) is developing rapidly [6] PICS may be employed to aid this development by attracting investors and enthusing the public for space travel and exploration.

### 3.6.4. Threats to PICS

A threat to PICS lies in the fact that developments in miniaturisation do not progress according to current expectations. As the technology of certain components is yet immature, this increase development efforts and thus corresponding costs, which makes the business case for PICS less attractive. Secondly, there exists certain regulatory uncertainties since PICS might require a lengthy time for obtaining a Space Activity license and a costly liability insurance issued by a third party [15].

[4] Community Toolbox, SWOT Analysis`http://ctb.ku.edu/en/table-of-contents/assessment/assessing-community-needs-and-resources/swot-analysis/main`, retrieved on 20-06-2016

[5] Space Debris and Human Spacecraft, `http://www.nasa.gov/mission_pages/station/news/orbital_debris.html`, retrieved on 20-06-2016

[6] The Future of Commercial Space Travel According to Jeff Greason: Interview, `http://www.space.com/31224-commercial-spaceflight-future-jeff-greason.html`, retrieved on 20-06-2016

# 4

## Sustainable Development Strategy

The amount of space debris in Low Earth Orbit (LEO) has increased rapidly over the last twenty years, resulting in 500,000 debris pieces currently orbiting the Earth. These objects travel at speeds up to 7800 $m/s$. Hence, very small pieces like a sliver of paint can already cause severe damage. [1] Since it becomes obvious that space debris therefore poses an increasing threat to future space missions and also more satellites are launched into orbit every year, active means of mitigating the risk of space debris formation is of dire importance. In order to emphasise the relation between space debris and sustainable development, the definition of sustainable development from the World Commission on Environment and Development is: *Sustainable development is development that meets the needs of the present without compromising the ability of future generations to meet their own needs* [17]. This definition implies that everything done today serving to meet humanity's needs or scientific goals should not hinder the ability of future generations to do the same. Hence, it becomes clear that space debris should be mitigated in order to avoid that future generations are prevented from launching objects into space. Beside the threat of creating space debris, the launch of a new spacecraft in space implies it will occupy a certain frequency band for communication. Hence, with an increasing number of spacecraft frequency becomes a scarce resource. Therefore, frequency bands should be dealt with consciously.
Lastly, the design of every spacecraft involves the exploitation of the Earth's resources and thus impacts the environment. In this aspect too the compromising of the needs of future generations should be minimised.
Related to the aspects discussed above, the sustainable development approach is divided into subcategories, namely regulatory sustainability, future sustainability and environmental sustainability. Regulatory sustainability mainly relates to the mitigation of space debris. Future sustainability looks at the impact the mission has on the launch of future spacecraft. Environmental sustainability concerns the materials used, the manufacturing techniques and their impact on the environment. The following sections take a look at the three subcategories.

## 4.1. Regulatory Sustainability

As required the femto-satellite shall be de-orbited in 25 years after it stops operating by requirement **TS-STH-SUS-01-A** [14]. Space debris in general is seen as an increasing threat by the space community since it occupies the space of potential orbits for future missions, which increases the risk of collision with space debris. Therefore the mentioned regulation tries to mitigate the amount of space debris by setting a limit for the amount of time a defunct satellite or launcher is allowed to remain in an orbit around the Earth. Assuming a typical cubic femto-satellite configuration with an mass-over-area ratio of $28.8 kg/m^2$, the femto-satellite can never de-orbit naturally within 25 years at an altitude above $680 km$ [18]. In light of an adequate sustainable development approach this raises the question whether or not 25 years is still suitable for today's space industry since this regulation dates from 1997 and about $1,400$ new satellites are scheduled for launch until 2024. [2] Moreover, the trend of the development of micro-satellites and nano-satellites is rapidly acquiring momentum [4]. Also femto-satellites are relatively small and can be launched in large numbers, potentially generating much additional space debris in case no stricter regulations are posed, which may force the space community to ban femto-satellites entirely. To make femto-satellites more attractive and ensuring it will not contribute to future space debris outside the natural decay limit measurements for their de-orbiting should be made. Because the majority of space debris is in the band of 700 to 1000 $km$[3] future femto-satellite missions should still be able to adhere to regulations. The majority of satellites present in LEO is below an altitude of 1000 $km$ [4]. A requirement has been set up to increase the applicable range of femto-satellite while limiting the impact.

**TS-SYS-POD-DOD-01-A** The femto-satellite shall be able to de-orbit within 25 years up to an orbital altitude of 1000 $km$.

This means that PICS will have an active de-orbit device to increase its orbital decay rate. This can also ensure that the femto-satellite is detectable from Earth in order for it to be classified as trackable space debris, an aspect which

[1] Space Debris and Human Spacecraft, http://www.nasa.gov/mission_pages/station/news/orbital_debris.html, retrieved on 21-04-2016
[2] Euroconsult Satellite Manufacturing & Launch, `http://www.euroconsult-ec.com/sat-manuf-launch`, retrieved on 19-5-2016
[3] Space debris presentation, `http://www.unoosa.org/pdf/pres/lsc2012/tech-02E.pdf`, retrieved on 28-06-2016
[4] UCS satellite database, `http://www.ucsusa.org/nuclear-weapons/space-weapons/satellite-database.V3JKLrh96Uk`, retrieved on 28-06-2016

was previously identified as one of the weaknesses of PICS in the SWOT Analysis (see Section 3.6). This leads to the following requirement:

**TS-SYS-POD-DOD-02** The femto-satellite shall be made detectable from Earth after its operational lifetime.

## 4.2. Future Sustainability

A factor that is going to play a significant role parallel to the space debris accumulation is the saturation of the available frequency bands[5]. This aspect concerns the fact that if the number of satellite launches increases and the trend in small satellites progresses even further, the number of available frequencies for the satellites to be launched in the future will be less. However, communication via the host spacecraft implies that no additional frequency bands will be occupied and thus would be advantageous in this aspect.

## 4.3. Environmental Sustainability

Since the femto-satellite will be launched along with the SkySat which is launched on the DNEPR and Soyuz, the propellants of those rockets will be evaluated. The DNEPR uses $N_2O_4$/UDMH (liquid nitrogen tetroxide and hydrazine) which is very toxic [6]. Hydrazine is harmful only in the uncombusted state, so is only allowed when no leakage of the propellant is guaranteed. The combustion products of UDMH with $N_2O_4$ are nitrogen $N_2$ and water $H_2O$. The Soyuz uses RP-1 with liquid oxygen which is not as toxic as JP-8[7] [19], but is harmful to humans and is not found in nature[8]. The combustion products of RP-1 and liquid oxygen are carbon dioxide ($CO_2$) and water ($H_2O$); one $kg$ of kerosene emits about 3kg of $CO_2$ [20]. From this can be concluded that RP-1 is harmful to the environment both before and after combustion. The ADCS momentum wheels will be made of beryllium which is highly toxic to humans[9]. However, considering a burn-up in the atmosphere the small amount beryllium will not have a direct effect on the environment. The femto-satellite will employ aluminium in its design, which are non-toxic. However the production of aluminium is not considered sustainable as it is extracted from bauxite which is mostly found (90%) in tropical areas[10]. Titanium is the fourth abundant metal found on Earth an therefore not rare. Titanium is also not toxic[11]. To get the titanium out of the ores the Kroll Process or FFC Cambridge Process are used. The latter one has a lower environmental impact than the first. FR4 PCBs will be used on the femto-satellite, which is a glass fibre epoxy laminate. The glass fibre is made of silica $SiO_2$, which is a natural element found in quartz, hence not harmful to the environment[12]. Epoxy is made of epichlorohydrin, which is highly toxic [13], and Bisphenol A, which is not as toxic as Epichlorohydrin but exposure will lead to complications for humans[14]. Therefore production of FR4 PCBs can be dangerous for humans and might do damage to the environment in the process. The femto-satellite will use a lithium-manganese-dioxide battery which are considered non-toxic and non-expensive [21].

## 4.4. Conclusion on Sustainable Development

Concluding from the analysis for sustainable development the definition of that can not be met in its completeness. Mainly the manufacturing is hazardous and decreases the sustainability of the project because a lot of materials used in the manufacturing are toxic and most processes emit a substantial amount of $CO_2$ or use a lot of energy. The burn-up of the satellite when it de-orbits mainly puts some $CO_2$ and metals in the atmosphere, but these are of such small concentrations that it will have a negligible impact. Although environmental impact can thus barely be accounted for, regulatory and future sustainability are taking into account in the design indeed. Firstly, an active de-orbit device will be installed on the femto-satellite in order to ensure that it will not contribute to the formation of space debris. Secondly, communication via the host spacecraft would imply that no frequency bands are occupied and thus maintains the availability of frequency bands for future missions.

[5] US Frequency Allocation, `http://www.nasa.gov/sites/default/files/spectrum_wall_chart_aug2011.jpg`, retrieved on 20-5-2016
[6] Hydrazine, `http://www.toxipedia.org/display/toxipedia/Hydrazine`, retrieved on 18-5-2016
[7] Encyclopedia Astronautica Lox/Kerosene, `http://www.astronautix.com/props/loxosene.htm`, retrieved on 18-5-2016
[8] Compendium of Chemical Hazards: Kerosene (Fuel Oil), `http://www.who.int/ipcs/emergencies/kerosene.pdf`, retrieved on 18-5-2016
[9] Beryllium Instruction Sheet, `http://www.atsdr.cdc.gov/csem/csem.asp?csem=5&po=15`, retrieved on 19-5-2016
[10] How aluminium is produced, `http://www.aluminiumleader.com/production/aluminum_production/`, retrieved on 19-5-2016
[11] Risks of Titanium, `http://www.globalhealingcenter.com/natural-health/health-risks-of-titanium/`, retrieved on 19-5-2016
[12] The making of glass fiber, `http://www.compositesworld.com/articles/the-making-of-glass-fiber`, retrieved on 19-5-2016
[13] Epichlorohydrin, `https://www3.epa.gov/airtoxics/hlthef/epichlor.html`, retrieved on 19-5-2016
[14] Bisphenol A general toxicity, `http://www.bisphenol-a.org/human/herGeneralToxicity.html`, retrieved on 19-5-2016

# 5

# Design Prerequisites

In this chapter the prerequisites for the design process are outlined. These procedures facilitate the concurrent design of the subsystems and integrate contingencies and margins into the design process. First the system interface definition in the form of an $N^2$ chart is shown. Next the functional flow diagram (FFD) is shown. This diagram shows the steps during the mission in a chronological order. And finally, the functional breakdown structure (FBS) is included, which gives a clear overview of what each step in the mission consist of.

## 5.1. System Interface Definition

A system interface definition is an essential prerequisite to an adequate design process. An often applied tool to visualise the system interface definition is the $N^2$ chart, which gives a clear overview of the interdependence of the individual subsystem design processes. Now, based on the design, all the functions are shown in square blocks. Meanwhile all the output-input blocks are shown as rounded rectangles. Each of these blocks are an output of the horizontally aligned function block and an input of the vertically aligned function block. In this way, all interfaces of the design can be identified at a glance. The $N^2$ chart is given in Figure 5.1

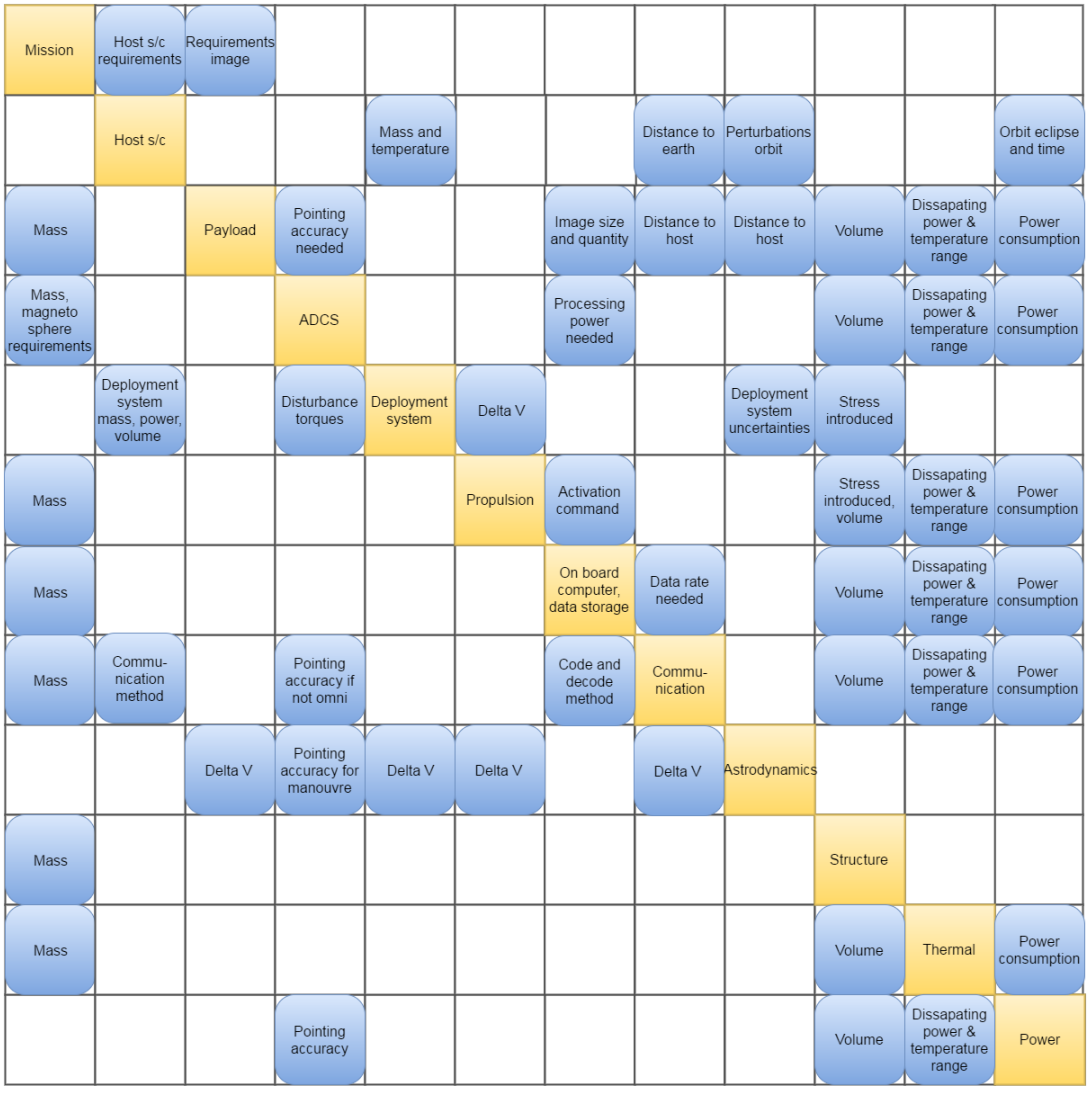


Figure 5.1: $N^2$ chart for the detailed design phase

## 5.2. Functional Flow Diagram

The FFD gives a good overview of the mission operations in a chronological order. Here each step during the mission operations is shown. The functional flow diagram is shown in Figure 5.2. First a top-level overview of the mission is shown, this is the most upper diagram. Next, where needed, the sub-levels of the steps are shown, these diagrams are beneath the first diagram. The sub-levels give a more detailed overview of the mission steps. The starting time of each activity is given in the block. The time zero is chosen in such a way that the mission of the femto-satellite starts at time is zero. Initialisation of the board computer, the start of spinning up the momentum wheels and the initialisation of the camera can all be done within the first second. So therefore the start time is given as approximately zero. The functions are performed in the sequence of the diagram.

Function 7.3, *Send telemetry* will continue until the battery runs out of power or the femto-satellite will get out of range from the host spacecraft. Also there is no clear ending for function 7.4, *Host send data to ground*. This is due to the fact that this heavily depends on the host spacecraft's communication to the ground. One needs to know how much of the femto-satellite's data can be sent per contact period with the ground without compromising its own mission.

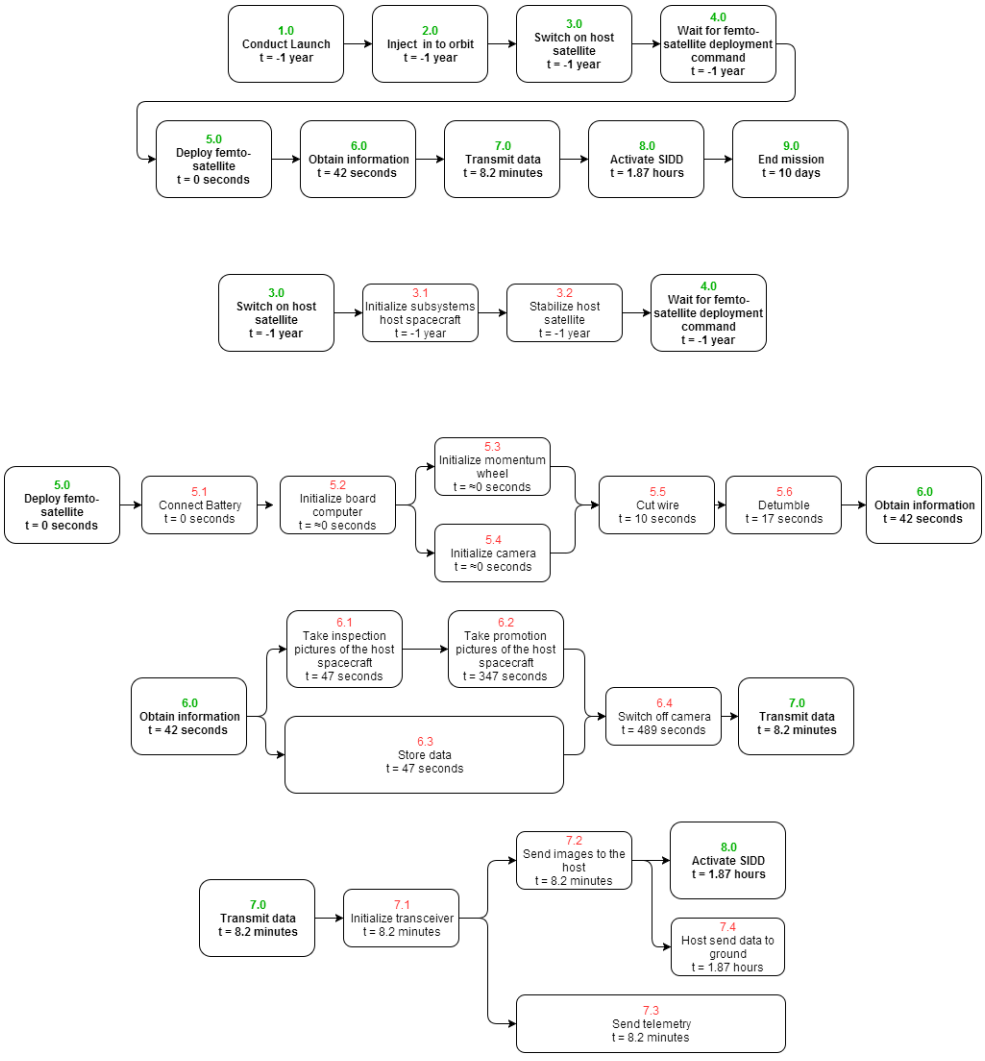


Figure 5.2: Functional flow block diagram

## 5.3. Functional Breakdown Structure

The FBS, given in Figure 5.3 gives an overview of the main actions on the top level. The sub-level indicates detailed actions which together form the top level action. Note that the FBS and FFD visualise the same process only from a different perspective since the FFD shows the chronological order of the femto-satellite's operations while the FBS

shows their hierarchal order.

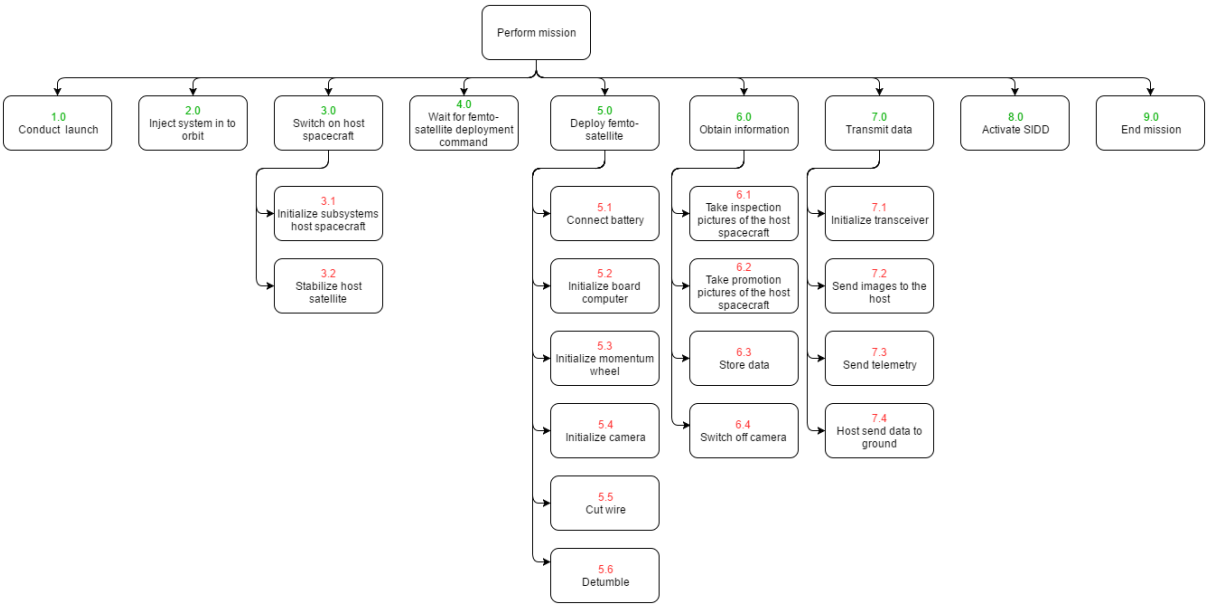


Figure 5.3: Functional breakdown structure

## 5.4. Contingencies and Margins

In this section the contingencies and margins for the design process will be elaborated upon and how they are used in the design process is explained. A contingency is defined as the difference between the current best estimate and the maximum expected value [22].

The expected contingencies, measured as a percentage of the current best estimate are obtained from NASA's Green Book [23]. Since there is no statistical design method for the design of a femto-satellite the design begins with searching for components to get idea what each subsystem weighs. This approach gives a relatively good approximation of the mass from the start compared to a conventional design process which is based merely on statistical data in the beginning stages. Thus the lower bound of the contingencies from the Green Book is used. However, the volume budget is hard to define. The size of the satellite should be smaller than 125 $cm^3$ but the satellite can never be packed in a way that the full satellite is filled without redundant space. Therefore during the start of the design a cube of $5 \times 5 \times 5$ $cm$ is assumed so the parts should not exceed 5 $cm$ in any direction. Further on in the design an investigation is performed for the optimal shape. The mass budget is much better to quantify. The spacecraft mass should not exceed a 100 $g$. The contingency for the baseline review is 25%, for the Conceptual Design stage (*Midterm Report* [5]) 20% and for the Preliminary Design stage (*Final Report*) 15%. The contingencies and margins for the power and velocity increment are not taken into account since the target values cannot be fixed during the design.

The margins during a conventional spacecraft design process are 25% [2][p.316]. Thus these will be taken into account while designing the femto-satellite so that when it is being built the final mass does not exceed the requirements. It should be noted that due to the novel nature of the femto-satellite concept these contingencies and margins are not considered leading. If the design deviates from the target value slightly during a step in the design this will be noted as a deviation but will not be fully mitigated since deviations are expected. However, if large deviations occur (causing the mass to exceed 100 $g$) they will be mitigated.

With contingencies and margins it is possible to calculate the target mass in the current design step using Equation (5.1). In this equation $m_{fr}$ is the target mass at the final review, $m_T$ is the target mass of 100 grams, $n_{CM}$ represents the contingency margin and $n_{DM}$ represents the design margin. The mass target for the final review is 69.6 grams.

$$m_{fr} = \frac{m_T}{(1+n_{CM})(1+n_{DM})} \tag{5.1}$$

# 6

# Requirements

Defining the requirements is one of the most important steps that needs to be done before and during the design process. Requirements will give an insight to the expectations set by the customer and constraints for the design team. Well-defined requirements will make the design process go more smoothly and can be easily validated afterwards. Requirements can evolve and change over time and can have significant effect on the iterations. When a requirement has been changed or removed, the reason behind the changes will be documented. First the mission and stakeholder requirements are stated in Section 6.1. Section 6.2 will elaborate on the system requirements leading from the mission and stakeholder requirements. Section 6.3 will elaborate on the subsystem requirements leading from the system requirements and payload design. Section 6.4 will elaborate on the changes and removal of requirements due to design iterations. When a requirement has been changed or removed the new requirement will end in **-A** for the first iteration, **-B** for the second iteration, etc. Section 6.5 will give an overview of the top-level, driving, key and killer requirements of the final design. Verification and validation of the requirements defined in this chapter will be be performed in Chapter 20.

## 6.1. Mission and Stakeholder Requirements

Before in the group's *Midterm Report* [5] the mission requirements and stakeholder requirements were defined. The mission requirements are defined by complying with the constraints set by the stakeholder requirements. However, following the evaluation of the *Midterm Report* some requirements were adjusted according to the updated mission outline. An overview will be given of these requirements as present in the final design.

**Orbit requirements**
**TS-MIS-ORB-03** The femto-satellite shall be released from the host-spacecraft in the downrange direction.

**Inspection requirements**
**TS-MIS-IMG-INS-01-B** The femto-satellite shall provide data aimed at modelling space debris and micro-meteoroid impact.

**Promotion requirements**
**TS-MIS-IMG-PRO-01-B** The femto-satellite shall promote the mission of its host spacecraft.

**Sustainability requirement**
**TS-STH-SUS-01-A** The femto-satellite shall comply with the existing regulation to mitigate space debris, which requires the femto-satellite to de-orbit within 25 years.

**Safety and reliability requirements**
**TS-STH-SAR-01** Safety requirements for piggyback launches shall be adhered to.
**TS-STH-SAR-02** The femto-satellite shall withstand the launch loads.
**TS-STH-SAR-03** The femto-satellite shall be integrated into the host-spacecraft for launch.

**Performance requirements**
**TS-STH-PER-02** Telemetry shall be available with a maximum latency of one day.
**TS-STH-PER-03-A** The design shall employ commercial off-the-shelf components where possible.
**TS-STH-PER-05** The femto-satellite shall accommodate a payload with a mass greater than or equal to 15% of its mass.

**Engineering budget requirements**
**TS-STH-ENB-01** The spacecraft launch mass shall not exceed 100 $g$.
**TS-STH-ENB-02** The spacecraft volume shall not exceed 125 $cm^3$.

**Cost requirements**
**TS-STH-CST-01** The cost of each individual spacecraft shall not exceed €10,000.
**TS-STH-CST-02** The cost of the total mission (excluding launch) shall not exceed €500,000.

## 6.2. System Requirements

Based on the mission and stakeholder requirements, the following system requirements can be formulated. Table 6.1 gives a clear picture from which mission or stakeholder requirement the system requirements are derived from.

Table 6.1: Flow down of system requirements from the mission and stakeholder requirements

| Requirement | Orbit req. | Inspection req. | Promotion req. | Sustainability req. | Safety req. |
|---|---|---|---|---|---|
| TS-SYS-POD-01-B | × | | | | |
| TS-SYS-POD-04 | | × | × | | |
| TS-SYS-POD-05 | | × | × | | |
| TS-SYS-POD-07 | | | | × | |
| TS-SYS-POD-09 | | | | | × |
| TS-SYS-POD-11 | | | | | × |
| TS-SYS-POD-12 | | × | × | | |
| TS-SYS-POD-13 | | × | | | |
| TS-SYS-POD-14 | | | × | | |

**TS-SYS-POD-01-B** The femto-satellite shall provide a velocity increment of 1.3 $cm/s$ for release from the host spacecraft in the downrange direction.
**TS-SYS-POD-04** The femto-satellite shall be able to store images on board.
**TS-SYS-POD-05** The femto-satellite shall be able to transfer stored data to the host spacecraft.
**TS-SYS-POD-07** The femto-satellite shall be able to increase its orbital decay rate.
**TS-SYS-POD-09** The femto-satellite shall have a natural frequency higher than 35 $Hz$.
**TS-SYS-POD-11** The femto-satellite shall withstand accelerations up to 10.8 $g$.
**TS-SYS-POD-12** The femto-satellite shall take pictures of the host spacecraft when the host spacecraft is placed in direct sunlight.
**TS-SYS-POD-13** The femto-satellite shall be able to identify space debris and micro-meteoroid impact damage on the solar arrays and bus of the host spacecraft.
**TS-SYS-POD-14** The femto-satellite shall provide images of the host spacecraft that can be used for promotion of its mission.

## 6.3. Subsystem Requirements

Based on the system requirements formulated in Section 6.2 the following subsystem requirements were formulated. All requirements are summarised from the individual subsystem chapters and can be referred to for more specific elaboration. Furthermore the relation between subsystem requirements can be seen in Table 6.2 and 6.3. The subsystem requirements are present on the horizontal and the subsystem they depend on on the vertical axis.

**Payload**
**TS-SYS-POD-PL-06** The femto-satellite shall be able to capture visual images with a smallest feature size of 0.1 $mm$.
**TS-SYS-POD-PL-07** The femto-satellite shall be able to take colour pictures.
**TS-SYS-POD-PL-08** The femto-satellite shall capture images on which the diagonal of one side of the host spacecraft occupies at least 10 % of the horizontal dimension of the picture.

**Communication System**
**TS-SYS-POD-COM-01** The communication system shall provide a closing link budget during the mission.
**TS-SYS-POD-COM-02** The communication system shall provide a data rate of at least 1 $Mb/s$.
**TS-SYS-POD-COM-03** The communication system shall be able to send data to Earth.
**TS-SYS-POD-COM-04** The communication system shall have an omnidirectional radiation pattern.

**Attitude Determination and Control System**
**TS-SYS-POD-ADC-01** The ADC subsystem shall be able to keep the host spacecraft within the field of view of the payload subsystem, which is 63 ° horizontal and 45 ° vertical.
**TS-SYS-POD-ADC-02** The ADC subsystem shall be able to de-tumble the femto-satellite within 25 seconds from release.
**TS-SYS-POD-ADC-03** The ADC subsystem shall be able to counter the disturbance torques that act on it during the ADCS lifetime.
**TS-SYS-POD-ADC-04** The ADC subsystem shall be able to have sufficient momentum storage about a single axis to store worst-case disturbance torque for the entire ADCS lifetime acting about this orbit.
**TS-SYS-POD-ADC-05** The ADC subsystem shall be able to point the payload towards the host spacecraft for the duration of the imaging process.

**De-orbit Device**
**TS-SYS-POD-DOD-01-A** The femto-satellite shall be able to de-orbit within 25 years up to an orbital altitude of 1000 $km$.
**TS-SYS-POD-DOD-02** The femto-satellite shall be made detectable from the Earth after its operational lifetime.

**Command & Data Handling System**
**TS-SYS-POD-CDH-01** The C&DH subsystem shall process the ADCS sensor input data and send commands to the ADCS actuators.
**TS-SYS-POD-CDH-02** The C&DH subsystem shall process incoming commands from the host from the communications system.
**TS-SYS-POD-CDH-03** The C&DH subsystem shall send commands to the payload and store the data that the payload gathers.
**TS-SYS-POD-CDH-04** The C&DH subsystem shall send the payload data to the communications subsystem to be transmitted to the host spacecraft.
**TS-SYS-POD-CDH-05** The C&DH subsystem shall monitor the power subsystem and switch operation modes if problems occur.
**TS-SYS-POD-CDH-06** The C&DH subsystem shall communicate with the de-orbit device and tell it when to de-orbit.
**TS-SYS-POD-CDH-07** The C&DH subsystem shall be able to interface with the ADCS sensors, which use the $I^2C$ communication protocol.
**TS-SYS-POD-CDH-08** The C&DH subsystem shall be able to interface with the ADCS actuators which require a $PWM$ signal.
**TS-SYS-POD-CDH-09** The C&DH subsystem shall be able to interface with the payload, which uses $I^2C$ as the input protocol and $CSI-2$ as the output protocol.
**TS-SYS-POD-CDH-10** The C&DH subsystem shall be able to interface with the communications subsystem which uses $SPI$ and $I^2C$ as a protocol.
**TS-SYS-POD-CDH-11** The C&DH subsystem shall be able to interface with the de-orbit device which requires a GPIO-high signal.
**TS-SYS-POD-CDH-12** The C&DH subsystem shall be able to receive data from the payload with a data rate of 111.02 $MB/s$.
**TS-SYS-POD-CDH-13** The C&DH subsystem shall have a storage capacity of at least 42 $GB$.
**TS-SYS-POD-CDH-14** The C&DH subsystem shall transmit the data to the communication system with a data rate of 6.75 $MB/s$.
**TS-SYS-POD-CDH-15** The C&DH subsystem shall be able to interface with the power monitor, which uses $I^2C$.

**Power System**
**TS-SYS-POD-POW-01-A** The power subsystem shall deliver a total energy of 3.69 $Wh$ to the femto-satellite.
**TS-SYS-POD-POW-04-A** The power subsystem shall be able to power the femto-satellite for 6749 $s$.
**TS-SYS-POD-POW-05** The power storage shall have a safety margin of 15 %.
**TS-SYS-POD-POW-06** The power subsystem shall be able to provide up to 2.79 $W$.
**TS-SYS-POD-POW-07** The power subsystem shall be able to power the de-orbiting device.
**TS-SYS-POD-POW-08** The power subsystem shall provide the specific voltage to each component.
**TS-SYS-POD-POW-09** The power subsystem shall have no power leakage before deployment.

**Thermal Control System**
**TS-SYS-POD-TC-01** The femto-satellite shall not get colder than -10 $^\circ C$ during its operational lifetime while the camera is offline.
**TS-SYS-POD-TC-02** The femto-satellite shall not get colder than 5 $^\circ C$ during the time it takes pictures.
**TS-SYS-POD-TC-03** The femto-satellite shall not get warmer than 50 $^\circ C$ during its operational lifetime while the camera is offline.
**TS-SYS-POD-TC-04** The femto-satellite shall not get warmer than 40 $^\circ C$ during the time it takes pictures.

**Deployment System**
**TS-SYS-POD-SM-01** The deployment system shall be electrically conductive to minimise chance of electrostatic discharge.
**TS-SYS-POD-SM-02** The components of deployment system shall not resonate with the launch load vibrations.
**TS-SYS-POD-SM-03** The spring deployment mechanism shall not allow the femto-satellite to move in any direction before the deployment.
**TS-SYS-POD-SM-04** The spring deployment mechanism shall contain an actuator that can touch the pin switch on the femto-satellite.
**TS-SYS-POD-SM-05** The deployment system shall be able to contain the femto-satellite from the launch until the deployment.
**TS-SYS-POD-SM-06** The spring index of the spring of the deployment mechanism shall have a value within a range of 4 and 25.

**TS-SYS-POD-SM-07** The spring force shall not exceed the yield force of the spring.
**TS-SYS-POD-SM-08** The spring shall not be subject to buckling.
**TS-SYS-POD-SM-09** The diameter of the spring wire shall have a value greater than the minimum manufacturable wire diameter.

Table 6.2: The dependency between subsystem requirements

| Subsystem | Payload | | | ADCS | | | | | Communication | | | | Deployment | | | | | | | | | Thermal control | | | |
|---|---|---|---|---|---|---|---|---|---|---|---|---|---|---|---|---|---|---|---|---|---|---|---|---|---|
| Requirement | PL | | | ADC | | | | | COM | | | | SM | | | | | | | | | TC | | | |
| | 06 | 07 | 08 | 01 | 02 | 03 | 04 | 05 | 01 | 02 | 03 | 04 | 01 | 02 | 03 | 04 | 05 | 06 | 07 | 08 | 09 | 01 | 02 | 03 | 04 |
| System requirements | × | × | × | × | | × | × | × | × | × | × | | × | × | × | × | × | × | × | × | × | | | | |
| Payload | | | | × | × | | | × | | | | | | | | | | | | | | × | × | × | × |
| ADCS | | | | | | | | | | | | | | | | | | | | | | | × | | × |
| Communication | | | | | | | | × | | | | | | | | | | | | | | × | | × | |
| C&DH | | | | | | | | | | | | | | | | | | | | | | × | × | × | × |
| De-orbit | | | | | | | | | | | | | | | | | | | | | | × | | × | |
| Power | | | | | | | | | | | | × | | | | | × | | | | | × | × | × | × |

Table 6.3: The dependency between subsystem requirements

| Subsystem | C&DH | | | | | | | | | | | | | | | De-orbit | | Power | | | | | | |
|---|---|---|---|---|---|---|---|---|---|---|---|---|---|---|---|---|---|---|---|---|---|---|---|---|
| Requirement | CDH | | | | | | | | | | | | | | | DOD | | POW | | | | | | |
| | 01 | 02 | 03 | 04 | 05 | 06 | 07 | 08 | 09 | 10 | 11 | 12 | 13 | 14 | 15 | 01-A | 02 | 01-A | 04-A | 05 | 06 | 07 | 08 | 09 |
| System requirements | | | | × | | | | | | | | × | × | × | | × | × | × | × | × | | | | × |
| Payload | | | × | × | | | | | × | | | × | × | | | | | × | × | × | × | | × | × |
| ADCS | × | | | | | | × | × | | | | | | | | | | × | × | × | × | | × | × |
| Communication | | × | | × | | | | | | × | | | | × | | | | × | × | × | × | | × | × |
| C&DH | | | | | | | | | | | | | | | | | | × | × | × | × | | × | × |
| De-orbit | | | | | | × | | | | | × | | | | | | | × | | | | × | × | × |
| Power | | | | | × | × | | | | | | | | | × | | | | | | | | | |

## 6.4. Requirement Iterations

Due to iterations during the design process changes were made. This will influence the requirements set previously. This section is dedicated to the elaboration of requirements that were changed or removed. At the end of each subsection an overview is given of the removed requirements, the requirement number is crossed out.

### 6.4.1. Previous Mission and Stakeholder Requirement Changes

Following the evaluation of the *Midterm Report* and the presentation during the *Midterm Review* some requirements were adjusted according to the updated mission outline. Firstly, requirements **TS-MIS-ORB-01** and **TS-MIS-ORB-02** were added to define the characteristics of the inspection orbit in iteration 0 (see Section 18.1). However, during iteration 1 it was concluded that this orbit design is not feasible due to orbit perturbations which put too stringent requirements on the $\Delta V$ budget, please see Section 18.2. Hence, **TS-MIS-ORB-01** and **TS-MIS-ORB-02** were deleted and **TS-MIS-ORB-03** was added to replace them. Requirements **TS-MIS-IMG-INS-01** was changed into **TS-MIS-IMG-INS-01-A** in iteration 0 to become more specific about the features of the spacecraft to be inspected. However, it was moved to system requirements as **TS-SYS-POD-13** in order to comply with the requirement hierarchy. As a result, **TS-MIS-IMG-INS-01-B** needed to be defined. The statement of requirement **TS-MIS-IMG-PRO-01** was slightly changed by changing "promotion" into "promotion of its space mission" to emphasize the fact that the promotion concerns the host spacecraft rather than the femto-satellite, therefore resulting in requirement **TS-MIS-IMG-PRO-01-A**. Analogous to **TS-MIS-IMG-INS-01-A** it was moved to system requirements as **TS-SYS-POD-14** and **TS-MIS-IMG-INS-01-B** was defined. Requirement **TS-STH-PER-01** was changed into **TS-STH-PER-01-A** since it was decided in consultation with the supervisor that the one-year lifetime requirements concerns the mission as a whole instead of an individual femto-satellite considering the fact that the mission could consist of multiple femto-satellites instead of only one. Furthermore, requirement **TS-STH-PER-03** was changed into **TS-STH-PER-03-A** because it was concluded that commercial off-the-shelf (COTS) products cannot always be used. Sometimes components will have to be designed by the project group itself, while sometimes one has to anticipate future developments. Lastly, requirement **TS-STH-SUS-01** was changed into **TS-STH-SUS-01-A** to become more specific.
~~**TS-MIS-ORB-01**~~ The femto-satellite shall be injected into an oscillating orbit with <TBD> ° inclination relative to the

host spacecraft.
~~**TS-MIS-ORB-02**~~ At its maximum distance to the host spacecraft within the oscillating orbit, the femto-satellite shall be injected into a football orbit with an eccentricity of <TBD>, resulting in a combined oscillating and football orbit relative to the host spacecraft.
~~**TS-MIS-IMG-INS-01**~~ The femto-satellite shall be able to identify outside damage on the host spacecraft.
~~**TS-MIS-IMG-INS-01-A**~~ The femto-satellite shall be able to identify space debris impact on the solar arrays of the host spacecraft.
~~**TS-MIS-IMG-INS-02**~~ The femto-satellite shall be able to identify the current state of the host spacecraft.
~~**TS-MIS-IMG-PRO-01**~~ The femto-satellite shall provide images of the host spacecraft that can be used for promotion.
~~**TS-MIS-IMG-PRO-01-A**~~ The femto-satellite shall provide images of the host spacecraft that can be used for promotion of its space mission.
~~**TS-STH-PER-01**~~ The femto-satellite's lifetime shall be greater than one year.
~~**TS-STH-PER-03**~~ The design shall employ commercial off-the-shelf components.
~~**TS-STH-PER-04**~~ The femto-satellite design shall be compatible with existing launch systems. of its mass.
~~**TS-STH-SUS-01**~~ The spacecraft shall comply with existing regulations to mitigate space debris.

### 6.4.2. Previous System Requirement Changes

Requirement **TS-SYS-POD-01** was deleted since it did not comply with the so-called "requirements on requirements" [22], which states that every requirement should be solution-free. Since the spring deployment mechanism as previously described in **TS-SYS-POD-01** is in fact a solution for the injection of the femto-satellite into an oscillating orbit this requirement was deleted and requirement **TS-SYS-POD-02** was changed in iteration 0 (see Section 18.1). In relation to that, it was concluded that the orbit characteristics should be stated in the mission requirements rather than the system requirements. To this purpose, requirements **TS-MIS-ORB-01** and **TS-MIS-ORB-02** were set up in Section 6.1. Then from these new mission requirements a velocity increment follows as described by requirements **TS-SYS-POD-01-A** and **TS-SYS-POD-02-A**. However, in iteration 1 **TS-MIS-ORB-01** and **TS-MIS-ORB-02** were deleted and replaced by **TS-MIS-ORB-03**, from which **TS-MIS-ORB-01-B** can be derived. Furthermore, requirement **TS-SYS-POD-03** was changed into **TS-SYS-POD-03-A** to comply with the re-evaluated value of the smallest feature size. Lastly, requirement **TS-SYS-POD-10** was deleted since it was considered redundant when looking at **TS-SYS-POD-09**.
~~**TS-SYS-POD-01**~~ The femto-satellite shall be able to be released with a spring mechanism from the host spacecraft.
~~**TS-SYS-POD-02**~~ The femto-satellite shall be able to perform the football orbit.
~~**TS-SYS-POD-01-A**~~ The femto-satellite shall provide a velocity increment of <TBD> $m/s$ for injection into an oscillating orbit.
~~**TS-SYS-POD-02-A**~~ The femto-satellite shall provide a velocity increment of <TBD> $m/s$ for injection into a football orbit.
~~**TS-SYS-POD-03**~~ The femto-satellite shall be able to capture optical images with a smallest feature size of 5 $mm$.
~~**TS-SYS-POD-10**~~ The femto-satellite shall be able to remain operable after vibrations experienced during launch.

### 6.4.3. Previous Subsystem Requirement Changes

Since some of the system requirements changed during iteration 1, some of the already established subsystem requirements were also changed accordingly. Firstly, since the mission outline was altered and the inspection satellite will no longer periodically flyby the host spacecraft anymore, requirement **TS-SYS-POD-03A-PL-01** was re-evaluated, as a result of which **TS-SYS-POD-03A-PL-01-A** was defined. Requirement **TS-SYS-POD-PL-05** was deleted and moved to the system requirements as **TS-SYS-POD-12** in order to comply with the requirement hierarchy. Also, since the propulsion system was removed from the design in iteration 1, requirements **TS-SYS-POD-02B-PROP-01** to **TS-SYS-POD-02B-PROP-04** were deleted. Moreover, due to the fact that the femto-satellite is also not equipped with solar arrays anymore, requirements **TS-SYS-POD-POW-02** and **TS-SYS-POD-POW-03** were scrapped. In addition **TS-SYS-POD-POW-01** was changed into **TS-SYS-POD-POW-01-A** since the power budget changed. Besides, **TS-SYS-POD-POW-04** was changed into **TS-SYS-POD-POW-04-A** to comply with the fact that it should be solution-free. **TS-SYS-POD-DOD-01** was dismissed because it did not have a good basis on how the requirement was created.
~~**TS-SYS-POD-03A-PL-01**~~ The payload shall capture 35 frames within the 4 seconds during which the femto-satellite is closest to the host satellite.
~~**TS-SYS-POD-PL-05**~~ The payload shall take pictures of the host spacecraft when the host spacecraft is placed in direct sunlight.
~~**TS-SYS-POD-02B-PROP-01**~~ The propulsion system shall carry <TBD> $m^3$ of krypton cold gas propellant.
~~**TS-SYS-POD-02B-PROP-02**~~ The propellant tank shall withstand a stress of <TBD> $Pa$.
~~**TS-SYS-POD-02B-PROP-03**~~ The propulsion system shall have a maximum propellant leakage of <TBD> $kg/s$.

~~**TS-SYS-POD-02B-PROP-04**~~ The thrust generated by the propulsion system shall produce a maximum torque of <TBD> $N$.
~~**TS-SYS-POD-POW-01**~~ The power system shall deliver a total power of <TBD> $W$ to the femto-satellite.
~~**TS-SYS-POD-POW-02**~~ The solar arrays shall have a total area of <TBD> $m^2$.
~~**TS-SYS-POD-POW-03**~~ The solar arrays shall have an efficiency of <TBD> %.
~~**TS-SYS-POD-POW-04**~~ The battery shall have a storage capacity of <TBD> $J$.
~~**TS-SYS-POD-DOD-01**~~ The femto-satellite shall de-orbit 10 times faster than its passive decay rate.

## 6.5. Requirements Categorisation

As is known from systems engineering theory [22] requirements can be divided among different categories. Some requirements are the most important ones to adhere to during the design process, these are know as top level requirements. Other requirements drive the design more than average. These are known as driving requirements. Certain requirements are of primary importance to the customer: the key requirements. Some requirements may drive the design to an unacceptable extent: the killer requirements [22]. For every category, the corresponding requirements are listed below, including an explanation why they belong to this category.

### 6.5.1. Top-level requirements

**TS-STH-SUS-01-A** According to the group's supervisor P.P. Sundaramoorthy[1], the biggest concern of the space community (including the UN and the International Telecommunications Union) with femto-satellites is that their low price will make it possible for many corporate and private to launch their own satellite, which is unfavourable in light of the increasing threat of space debris. Moreover, due to their small size, femto-satellites may not be detected at all by existing space debris detectors, posing an even larger danger. Hence, it is of utmost importance to fulfil the de-orbiting requirement in order to convince the space community of the capability of femto-satellites.

### 6.5.2. Driving requirement

**TS-SYS-POD-PL-06** Identifying space debris impact means the images taken by the femto-satellite should have a certain smallest feature size of 0.1 $mm$. This aspect is heavily dependent on the camera characteristics and the distance from the femto-satellite to the host spacecraft. Therefore, the type of camera should be carefully selected. Also the inspection orbit is extremely stringent and therefore the velocity increments should be accurately determined and applied with minimum misalignments. Hence, this requirement drives the design of the mission, the payload, the propulsion system and the ADCS.
**TS-SYS-POD-DOD-01-A** and **TS-SYS-POD-DOD-02** Limiting space debris is paramount and it is possible to show the potential of femto-satellites without contributing to more space debris. Making sure that the femto-satellite will de-orbit faster will contribute to the sustainability of the future of femto-satellites and thus is a driving requirement.
**TS-STH-ENB-01** and **TS-STH-ENB-02** The low mass and volume of the femto-satellite are its main aspects. Hence, miniaturisation of the femto-satellite's components is a main driver in the design.

### 6.5.3. Key requirements

**TS-SYS-POD-13** Identifying space debris impact on the solar arrays of the host spacecraft is the core of the femto-satellite's mission and forms the customer's main interest. Failure to meet this requirement means a failure to demonstrate the femto-satellite's potential to the customer and the spaceflight community.
**TS-STH-CST-01** One of the major advantages of the femto-satellite is its low cost. A cost that exceeds the requirement could result in the customer losing his interest in the product.

### 6.5.4. Killer requirements

**TS-STH-PER-01** This requirement was already identified as a killer requirement in iteration 1 because the components selected during the Conceptual Design do not survive for one year. For example, the rechargeable battery's capacity reduces to 70 % within 30 days. This could be extended to 150 days, though at the expense of the battery mass which increases by a factor 2. Furthermore, the momentum wheels of the ADCS are limited to a lifetime of 8 months. The customer suggested during the Conceptual Design to fulfil the one year lifetime by multiple femto-satellites, stating that the mission lifetime should be one year instead of an individual femto-satellite. However, the group believes that this means creating a mission with multiple femto-satellites merely for the sake of fulfilling the requirement and therefore thinks it is a killer requirement.
During iteration 1 the group came to the conclusion that the mission outline from iteration 0 was not feasible anymore since orbit maintenance would put too stringent requirements on the design (see Section 18.2). Hence, a simpler orbit design was made from which it became clear that the femto-satellite's lifetime was limited to 2 orbits. Therefore, the requirement was definitely scrapped in iteration 1.

[1] Professor TU delft, interviewed on 07-06-2016

# II
# Design

# 7

# Astrodynamics

In this chapter the astrodynamics of the mission will be elaborated upon. First a closer look will be taken into relative motion. Then the effect of perturbations on the host spacecraft and femto-satellite will be evaluated. This information is used to determine an orbit for the femto-satellite. Lastly information is given concerning eclipses and de-orbiting.

## 7.1. Relative Motion

The Clohesy-Wiltshire (CW) equations used to describe the relative motion of two satellites are given by Equation (7.1) through (7.6). They are derived in [24] and [1]. These equations describe the motion of a femto-satellite relative to the host spacecraft. The $x$, $y$, $z$ components form a reference frame with the origin in the centre of mass of the host spacecraft. The $z$-axis points in the radial direction and is also called the altitude component, the $y$-axis is perpendicular to the orbital plane in the direction of motion and is also called the cross-track component and the $x$-axis complements the right handed reference frame and is also called the down-range component. The $x$-axis usually points in the direction of the velocity vector. These equations are simplified and do not account for orbit perturbations, J2 effect etc. and are only valid if the distance between the two satellites is small compared to the semi-major axis. Here $n$ is the mean motion given by Equation (7.7). The $\Delta V$ in each direction can be calculated by solving for the $\dot{x}_0$, $\dot{y}_0$ and $\dot{z}_0$ component.

$$x(t) = \left(6z_0 + \frac{4\dot{x}_0}{n}\right)\sin(nt) + \frac{2\dot{z}_0}{n}\cos(nt) - (6nz_0 + 3\dot{x}_0)\,t + \left(x_0 - \frac{2\dot{z}_0}{n}\right) \tag{7.1}$$

$$y(t) = y_0\cos(nt) + \frac{\dot{y}_0}{n}\sin(nt) \tag{7.2}$$

$$z(t) = \frac{\dot{z}_0}{n}\sin(nt) - \left(3z_0 + \frac{2\dot{x}_0}{n}\right)\cos(nt) + \left(4z_0 + \frac{2\dot{x}_0}{n}\right) \tag{7.3}$$

$$\dot{x}(t) = (6nz_0 + 4\dot{x}_0)\cos(nt) - 2\dot{z}_0\sin(nt) - (6nz_0 + 3\dot{x}_0) \tag{7.4}$$

$$\dot{y}(t) = -y_0 n\sin(nt) + \dot{y}_0\cos(nt) \tag{7.5}$$

$$\dot{z}(t) = \dot{z}_0\cos(nt) + (3nz_0 + 2\dot{x}_0)\sin(nt) \tag{7.6}$$

$$n = \sqrt{\frac{\mu}{a^3}} \tag{7.7}$$

$$\epsilon = \frac{v^2}{2} - \frac{\mu}{r} = -\frac{\mu}{2a} \tag{7.8}$$

In order to have the femto-satellite perform a periodic motion near the host spacecraft the orbital energy $\epsilon$ of the two satellites should be equal, given by Equation (7.8). An equal orbital energy guarantees periodic motion. Thus it is important to apply a $\Delta V$ which only changes the direction of the velocity vector, not the magnitude. With this knowledge two different manoeuvres can be defined.

### 7.1.1. Football Orbit

To start this manoeuvre a $\Delta V$ should be applied in the radial direction. If this $\Delta V$ does not change the magnitude of the velocity its orbit changes as shown in Figure 7.1 and 7.2. A $\Delta V$ will result in a slightly elliptical orbit of the femto-satellite. Assuming $z_0 = 0$ and $\dot{x}_0 = 0$, Equation (7.1) and (7.2) simplifies to (7.9) and (7.10).

$$x(t) = \frac{2\dot{z}_0}{\omega}\left[\cos(\omega t) - 1\right] + x_0 \tag{7.9}$$

$$z(t) = \frac{\dot{z}_0}{\omega}\sin(\omega t) \tag{7.10}$$

It is important to note that the football manoeuvre should be started with a non-zero $x_0$ to avoid a collision between the femto-satellite and the host spacecraft after one orbit.

### 7.1.2. Oscillating Orbit

If a $\Delta V$ in the cross-track direction is applied it will result in an oscillating motion around the cross-track axis. This is visualised in Figure 7.3 and 7.4. If one assumes $y_0 = 0$, Equation (7.2) simplifies to (7.11). Note that is important to start this manoeuvre downrange of the host spacecraft to avoid a collision.

$$y(t) = \frac{\dot{y}_0}{\omega}\sin(\omega t) \tag{7.11}$$

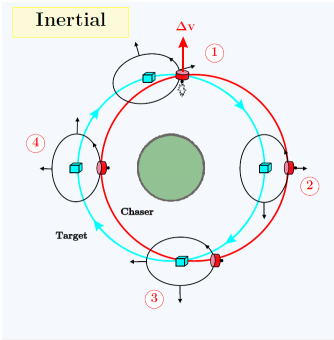


Figure 7.1: Football orbit inertial view [1]

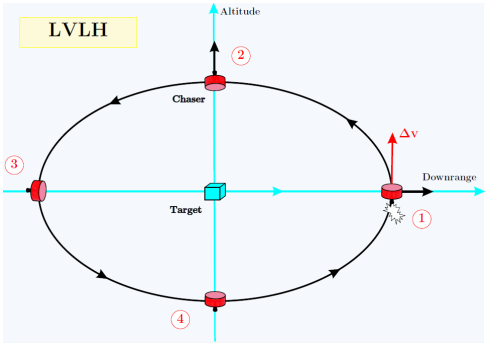


Figure 7.2: Football orbit LVLH view [1]

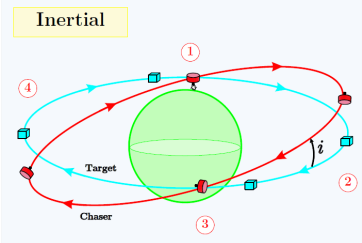


Figure 7.3: Oscillating orbit inertial view [1]

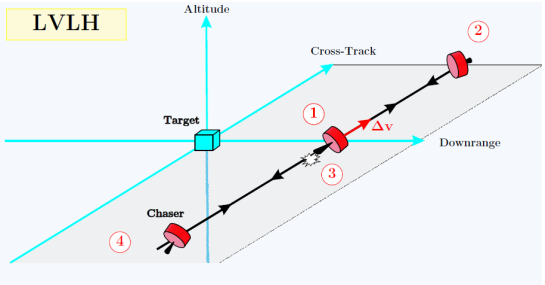


Figure 7.4: Oscillating orbit LVLH view [1]

## 7.2. Orbit Perturbations

In this stage of the design it is important to consider orbit perturbations and their effect on both the host and inspection satellite. Especially the drift caused by different accelerations between the two satellites is important. Two different perturbations are considered, atmospheric drag and solar radiation pressure (SRP). Perturbations caused by the asymmetric mass distribution of the Earth are not considered since they do not cause a drift between the two satellites, although it does cause an entire orbit to drift. Perturbations caused by third bodies like the Sun or the Moon are not considered either. Orbital analysis is done using the General Mission Analysis Tool (GMAT) made by NASA and collaborators from the private industry. This tool was verified and validated, see [25]. The satellite characteristics and orbit parameters used as initial values are given in Table 7.1 and Table 7.2.

Table 7.1: Satellite characteristics

| | **Mass** $[kg]$ | $C_D$ $[-]$ | **Coefficient of Reflectivity** | **Drag Area** $[m^2]$ | **SRP Area** $[m^2]$ | $A/m$ |
|---|---|---|---|---|---|---|
| **Host spacecraft** | 100 | 2.2 | 0.3 | 0.81 | 0.81 | 0.0081 |
| **Femto-satellite** | 0.1 | 2.2 | 0.8 | 0.0035 | 0.0035 | 0.035 |

Table 7.2: Orbit parameters

| **SMA** $[km]$ | **Eccentricity** | **Inclination** $[\circ]$ | **Atmospheric model** |
|---|---|---|---|
| 6828 | 0 | 97 | MSISE90 |

The MSISE90 model was developed at the NASA Goddard Space Flight Center and is based on satellite mass spectrometer data and ground based radar observations [24].

### 7.2.1. Perturbations from Atmospheric Drag

As a result of atmospheric particles surrounding the Earth the femto-satellite experiences atmospheric drag. This force acts in the opposite direction of its velocity vector and thus decreases the satellite's kinetic energy. As a result, the orbit altitude decreases, again leading to an increased atmospheric drag since the satellite moves closer to the Earth where the atmospheric density is higher [2]. The acceleration due to atmospheric drag is described by Equation

(7.12).

$$\mathbf{a_D} = -\frac{1}{2}\rho C_D \frac{A}{m} |\mathbf{v_{S/A}}| \mathbf{v_{S/A}} \tag{7.12}$$

Here $\mathbf{v_{S/A}}$ is the satellite's velocity vector relative to the atmosphere. $C_D$ is the drag coefficient, which is set to 2.2. $A$ is the surface area and $m$ the mass. $\rho$ comes from the atmospheric model. The value of $\rho$ can not be determined exactly, the value provided by the astrodynamic model is only an approximation. In practise the density of the air is dependant on the diurnal variation, the rotation of the Sun around its own axis, the semi-annual variation and the 11 year solar activity cycle [24]. The influence of the solar activity is the highest on $\rho$ and can cause variations up to a factor 10 at an altitude of $450km$ [24]. Exact consequences of the variations on $\rho$ are not considered in this report and left to later design stages and the recommendations.

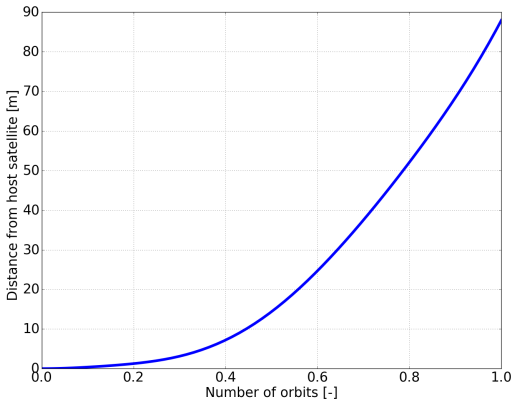


Figure 7.5: Distance between the host spacecraft and femto-satellite at an altitude of $450km$

The only difference between the host spacecraft and femto-satellite is the ratio of $A$ over $m$, all other components are (nearly) identical. Consider the (hypothetical) case where the femto-satellite is released into the same orbit as the host spacecraft. Only taking atmospheric drag into account the distance between the host spacecraft and femto-satellite as function of the number of orbits is given by Figure 7.5. The femto-satellite drifts away very fast, after one orbit the distance has already increased to $87m$. This drift is caused by the big difference in $A/m$, the area over mass ratio of the femto-satellite is more than four times larger.

### 7.2.2. Perturbations from Solar Radiation Pressure

Due to solar radiation pressure, periodic variations arise in all of the Keplerian orbital elements. This phenomenon most strongly affects light-weight bodies with large sunlit areas [2]. The acceleration resulting from solar radiation pressure is described by Equation (7.13) [26].

$$\mathbf{a_R} = -\frac{\Phi}{c}(1+\alpha)\frac{A_S}{m}\mathbf{e_S} \tag{7.13}$$

Here, $c$ is the speed of light, $A_S$ is the total sunlit surface area of the satellite, $m$ is the mass of the satellite and $\mathbf{e_S}$ the unit vector from the satellite to the Sun. $\Phi$ is the solar flux, which is described by Equation (7.14) [26]. $\alpha$ is the reflection coefficient of the satellite ($\alpha = 0$ for absorption, $\alpha = 1$ for specular reflection at normal incidence [2]). $\alpha$ is estimated to be 0.3 for solar panels[1] while $\alpha$ for kapton foil (the outside of PICS) is estimated to be around 0.8.

$$\Phi = \frac{P}{4\pi r^2} \tag{7.14}$$

Here, $P$ represents the mean radiative power of the Sun ($P = 3.805 \cdot 10^{26}$ $W$ [26]) and $r$ is the distance of the satellite to the Sun. At an altitude of $450km$ the drift of the femto-satellite with respect to the host spacecraft caused by SRP is between 300 to 100 times less than the drift caused by atmospheric drag. It is much harder to show the effect of SRP in a plot because it is not just simply a function of altitude, it depends on various orbital parameters and the time of the year. It shows a periodic motion with a period of one orbit. Also the direction of the acceleration shows large variations, while the atmospheric drag always acts in the negative velocity vector, $\mathbf{e_S}$ deviates much more.

Although atmospheric drag has a much larger influence on the relative motion of the two satellites it can not be discarded. Its effect will be taken into account when considering relative motion.

## 7.3. Orbit Determination

When plotting the distance of the femto-satellite to the host spacecraft it quickly becomes clear that the femto-satellites drifts away. This is mainly attributed to the difference in atmospheric drag. The SRP slows the drift down under certain circumstances, but this does not help much because it is so small. The question now arises how much $\Delta V$ the femto-satellite needs to keep it in an acceptable range from the host spacecraft. In the next two subsections a

[1] Solar Panels, `http://www.treehugger.com/renewable-energy/ask-pablo-do-solar-panels-contribute-to-the-heat-island-effect.html`, retrieved on 15-6-2016

higher and a lower bound for the required $\Delta V$ is calculated.

### 7.3.1. Velocity Increment Estimate Using GMAT

To calculate the required velocity increment ($\Delta V$) the following mission profile was determined and programmed into GMAT.

1. Apply a $\Delta V$ that would, in ideal circumstances, initiate a football manoeuvre.
2. Determine the distance between the host spacecraft and femto-satellite.
3. Allow the femto-satellite to drift. If the distance is greater than 100m and the femto-satellite is moving away from the host spacecraft, a $\Delta V$ is applied to compensate for this drift. The magnitude and the direction of the $\Delta V$ are calculated by GMAT's own *Target* and *Achieve* functions by varying the $x$, $y$ and $z$ components of the $\Delta V$.
4. Propagate the orbits and return to step 2.

This results in a required $\Delta V$ of around 6 $km/s$ after 9 orbits. This is as high as the $\Delta V$ required to transfer from LEO to the moon[2], so this estimate is likely too high. The reason for this is that the burns are not applied in an efficient manner, see also Figure 18.1.

### 7.3.2. Theoretical Minimum Velocity Increment

The minimum required $\Delta V$ can be calculated by computing the acceleration due to differential drag according to Equation (7.15) [27].

$$\Delta a_D = \frac{1}{2}\left(C_{D1}\frac{A_1}{m_1}\rho_1 - C_{D2}\frac{A_2}{m_2}\rho_2\right)v_a^2 \tag{7.15}$$

$C_D$ is set to 2.2 [28] and $v_a$ is 7626 $m/s$ for both satellites. According to Table 7.1 the $A/m$ ratios are 0.0081 and 0.035 for the host and femto-satellite, respectively. The density $\rho$ is $9.2\times10^{-14}$ $kg/m^3$ and $2.1\times10^{-11}$ $kg/m^3$ for low and extremely high solar activity, respectively.[3] By mulitplying the resulting acceleration with the orbital period of 5648 $s$, one gets a required $\Delta V$ of 0.907 $mm/s$ per orbit for the case with low solar activity and 207 $mm/s$ per orbit for extremely high solar activity.

### 7.3.3. Final Trajectory

It becomes clear that a larger amount of $\Delta V$ is needed than the propulsion subsystem can deliver. This large amount of $\Delta V$ arises from the large difference in $A/m$ (more than 4 times larger). The excessive drift of the femto-satellite could be solved in two ways. Unfortunately both are unfeasible.

1. Lower the $A/m$ ratio of the femto-satellite by assuming a cube of $4\times4\times4$ instead of $5\times5\times5$. This would reduce the $A/m$ with 36% and would cause the femto-satellite to only drift 87$m$ each orbit. However, the required $\Delta V$ to stay in close proximity of the host spacecraft is still too much for the propulsion system to deliver, without even considering the reduced size of the propulsion system.
2. Choose a different host with a more suitable $A/m$. However, when scaling down a satellite, the $A$ scales quadratically while $m$ scales with the power 3. Also, the SkySat is one the few satellites with a constant $A/m$. This value can vary if satellites keep their solar panels pointed towards the Sun. This makes host selection a very tricky process.

The options presented above are all not realistic, and so it was decided that the requirement of a lifetime of one year was dropped but another trajectory had to be chosen. As discussed in Subsection 18.2 the femto-satellite would no longer have propulsion. By utilising the difference in drag in a clever way a trajectory could be computed which maximises the lifetime of the mission. The maximum distance from the host spacecraft should not exceed 242$m$ as long as possible and be within 4.01$m$ of the host satellite as long as possible. Furthermore the femto-satellite should stay within 5.61$m$ of the host satellite as long as possible too. 242$m$ is the maximum distance the communications subsystem can send data over while a distance closer than 4.01$m$ is needed for inspection. 5.6$m$ is the maximum distance used for promotion pictures.

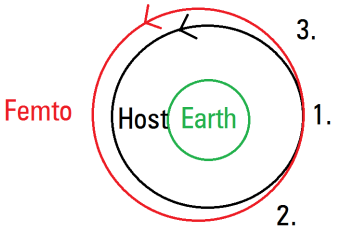


Figure 7.6: Stages during the orbit of the host spacecraft and femto-satellite

Consider the hypothetical case where the femto-satellite is injected downrange of the host spacecraft. Due to its higher velocity the femto-satellite initially drifts away. Its eccentricity also increases slightly due to the higher velocity. This also increases the time it takes to complete one orbital period. The distance

[2] Wikimedia Commons, `https://commons.wikimedia.org/wiki/File:Delta-Vs_for_inner_Solar_System.svg`, retrieved on 27-06-2016
[3] MSISE-90 model, `http://www.braeunig.us/space/atmos.htm`, retrieved on 27-06-2016

profile from the host satellite would approximately have the shape of Figure 7.7. The different stages of the orbit are shown in Figure 7.6 and explained below.

1. A $\Delta V$ is applied in the direction of the velocity to initiate the manoeuvre. This causes an increase in eccentricity and orbital period and a drift away from the host spacecraft, corresponding to the initial increase in distance in Figure 7.7.
2. The femto-satellite reaches its furthest point from the host spacecraft. As seen from the host spacecraft the femto-satellite is behind the host spacecraft. From this point the femto-satellite catches up on the host spacecraft due to a higher velocity. Meanwhile the drag causes the femto-satellite to decay faster than the host spacecraft, bringing the two closer together.
3. The femto-satellite decelerates further, leaving the host spacecraft behind.

Note that the shape of Figure 7.7 varies with the amount of applied $\Delta V$. The time it takes to drift further than $242m$ also varies with applied $\Delta V$, but lies in the range of 7500 to 17000 seconds. After evaluating various options for $\Delta V$ and their corresponding difference profiles the range for $\Delta V$ was set to 1.0 to $1.7cm/s$. For a full derivation, see Appendix A.

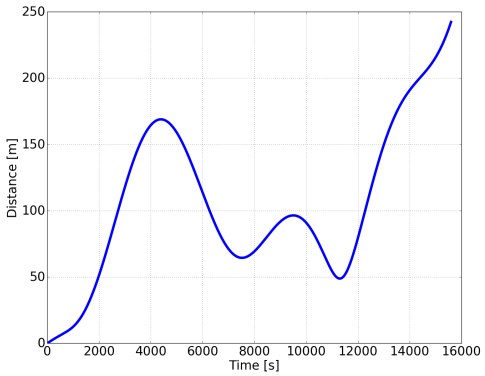


Figure 7.7: Distance from the host spacecraft. $\Delta V = 1.3cm/s$, TA = 45°

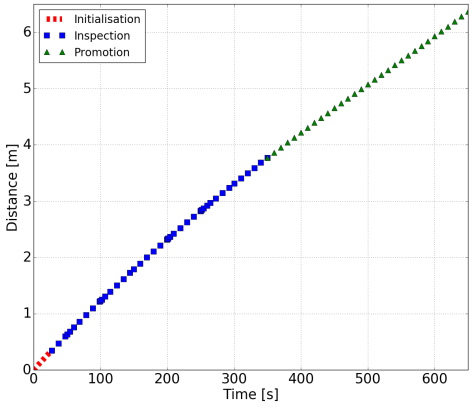


Figure 7.8: Activities during the first stage of the mission

## 7.4. Probability of Collision

Because a $\Delta V$ is applied in the direction of the velocity vector, the relative motion of the host spacecraft and the femto-satellite is no longer periodic according to Equation (7.8). This means that the two spacecrafts will never return to the same location at the same time. However, this theory does not take orbit perturbations into account. From Figure 7.7 and Appendix A it can be seen that the distance to the host spacecraft decreases to a minimum of $12.5m$ but due to the uncertainty in atmospheric drag it is difficult to predict the absolute distance. Because the femto-satellite takes longer to complete one orbit, it will always lag relative to the host spacecraft. Combined with a higher drag this reduces the probability of collision significantly. Considering the situation plotted in Figure 7.7 the velocity difference between the two spacecrafts does not exceed $4cm/s$. Although this is no indicator of the consequences of the collision, it does show that the relative velocities are small.

## 7.5. Eclipses and De-orbiting

Because the orbit of the SkySat is highly inclined, sun-synchronous orbits are possible, especially if one only considers the short lifetime of the femto-satellite. For a very small range of the RAAN ($\Omega$) of $-2° to + 2°$ the orbit is sun-synchronous. According to [24] the $\Omega$ of this specific orbits drift with approximately $0.04deg/hr$ due to the J2 effect. Thus a sun-synchronous orbit is certainly possible, although it will have to be carefully timed. A more detailed discussion of the possibility of a sun-synchronous orbit is given in the chapter about thermal control, Chapter 14.

As discussed in Chapter 4 the de-orbiting requirement is very important to adhere to. Because of the high $A/m$ the femto-satellite will de-orbit itself quite fast. A more detailed explanation of the de-orbiting system is given in Chapter 11.

# 8

# Payload

The payload of the femto-satellite is a miniaturised camera that is able to take pictures of the host spacecraft from a distance. In this chapter the camera module is explained. First a research in shown in to the characteristics of a camera, this is shown in Section . Next the camera selection is presented. Ending with and finally the size of the payload data is determined.

## 8.1. Requirements

The payload is driven by the following system requirements for the femto-satellite:

**TS-SYS-POD-03** The femto-satellite shall be able to capture visual images with a smallest feature size of 0.1 $mm$.
**TS-SYS-POD-06** The femto-satellite shall be able to take colour pictures.
**TS-SYS-POD-08-A** The femto-satellite shall capture images on which the diagonal of one side of the host spacecraft occupies 10 % or more of the horizontal dimension of the picture.

## 8.2. Imaging Geometry

In order to assess the camera's capabilities in terms of picture resolution and quality the geometry of the imaging operation is investigated in this section. The field of view (FOV) is the observation angle of the camera module which can be measured vertically, horizontally and diagonally as shown in Figure 8.1.

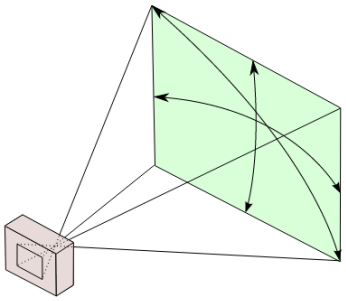

Figure 8.1: Horizontal, vertical and diagonal FOV

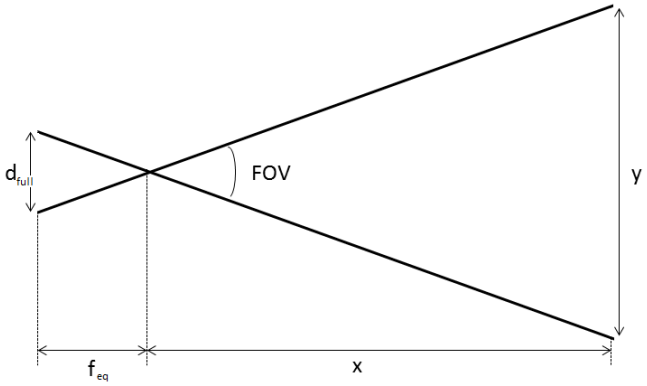


Figure 8.2: Imaging geometry

The field of view $FOV$ can be calculated by Equation 8.1:

$$FOV = 2\arctan\left(\frac{d_{full}}{2f_{eq}}\right) \tag{8.1}$$

$$IFOV = 2\arctan\left(\frac{p}{2f_{real}}\right) \tag{8.2}$$

where $d_{full}$ is the full frame sensor size and $f_{real}$ is the equivalent focal length of the lens.[1] The dimensions of the full frame sensor size are the dimensions of the image sensor multiplied by the crop factor.[2] The equivalent focal length is the focal length which results in the same field of view on a full frame (35 $mm$) camera. The instantenous field of view ($IFOV$) is the field of view provided by one pixel which can be calculated by Equation (8.2) where $p$ is the pixel size and $f_{real}$ is the physical focal length. The distance $x$ between the host spacecraft and the femto-satellite can be calculated by Equation (8.3):

$$x = \frac{r}{2\tan\left(\frac{IFOV}{2}\right)} \tag{8.3}$$

[1] Oregon Small Satellite Project, `http://oresat.org/field-of-view/`, retrieved on retrieved on 01-06-2016
[2] Apple Iphone SE specifications, `http://www.devicespecifications.com/en/model/7a423ad7`, retrieved on 01-06-2016

where $r$ is the coverage of one pixel, or the size of the smallest feature in the picture.[3]

## 8.3. Image Quality

The performance of a digital camera mainly depends on the performance of the most important camera module elements: the lens module (including diaphragm and shutter) and the image sensor which processes the incoming light by liberating electrons on its silicon semiconductor [29]. The shutter can close more rapidly in order to avoid blurry pictures when the object is moving relative to the camera. The diaphragm can be adjusted to regulate the amount of light falling on the sensor in order to avoid under- and overexposure. Figure 8.1 is a sketch of a simple digital camera. In commercial context it is common to describe the performance of a camera by its amount of mega pixels (or picture elements), although the final sharpness of a picture taken by the camera depends on an extensive amount of factors. Figure 8.3 summarises the literature study performed on picture sharpness [4] [5] [6] [29], [30], [31].

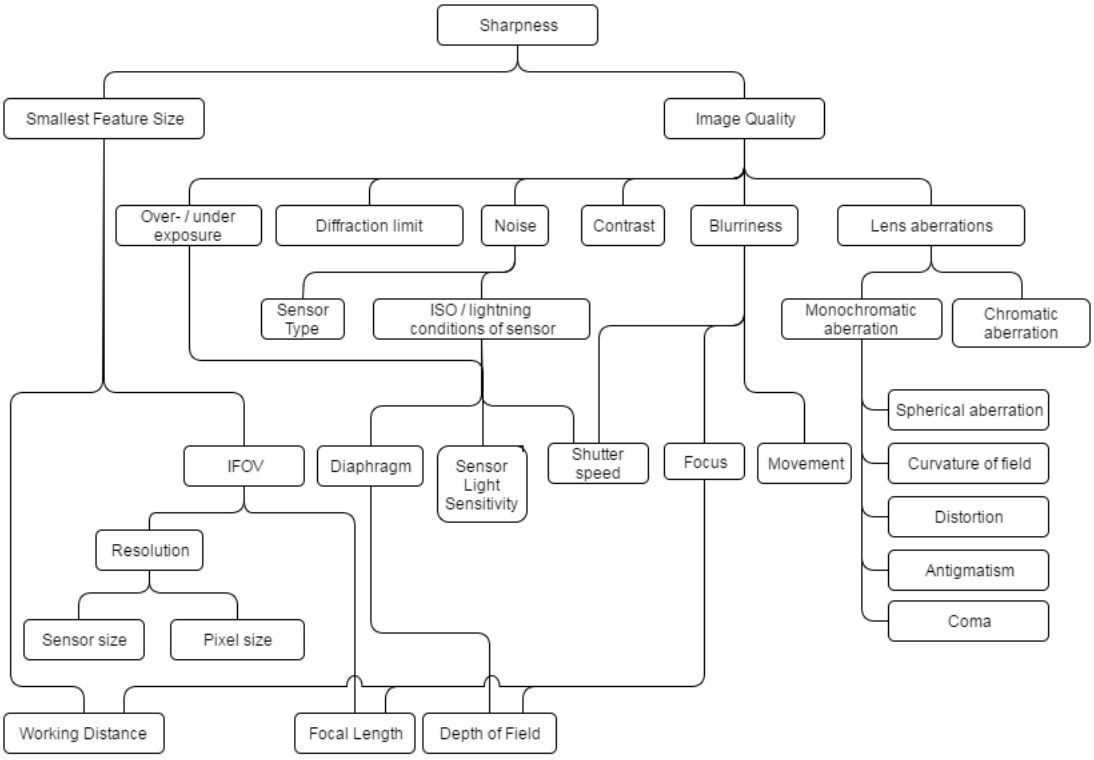


Figure 8.3: Image sharpness breakdown structure

The 'sharpness' of a picture is hard to quantify since it is the combination of smallest feature size and image quality. The smallest feature size decreases with increasing resolution, increasing focal length and decreasing working distance (as was explained in Section 8.2). The image quality depends on the amount of over-/under exposure, diffraction limit, noise, contrast, blurriness and the presence of lens aberrations. Lens aberrations are a result of the assumption of an idealised thin lens that all rays are converging to one point which is called the image point. Lens aberrations are negligibly small for small lens apertures which increases the sharpness, although this aperture decrease is limited by the so called diffraction limit.[29] The diffraction limit is neglected in this report since it is in the range of micrometers for small camera modules.[7]

In order to minimise the blurriness of a picture of an object that moves relative to the femto-satellite the picture should be taken with an high shutter speed. The depth of field (DOF) should not be only one single point but at least in the range of 0.5 till 1 meter (according to the dimensions of the *SkySat C series*, Section 2). For that reason

[3] Oregon Small Satellite Program
[4] Oregon Small Satellite Project, `http://oresat.org/field-of-view/`, retrieved on 06-06-2016
[5] Sharpness: what is it and how is it measured? `http://www.imatest.com/docs/sharpness/`, retrieved on 06-06-2016
[6] DSLR Camera Basiscs, `http://imaging.nikon.com/lineup/dslr/basics/04/02.htm`, retrieved on 06-06-2016
[7] Lens diffraction and photography, `http://www.cambridgeincolour.com/tutorials/diffraction-photography.htm`, retrieved on 06-06-2016

the diaphragm can not be opened signficantly (to avoid DOF reduction) but the light sensitivity of the image sensor, expressed as the so called ISO-value, should increase. The noise and therefore image quality decrease with increasing ISO-value [30]. However, noise is only problematic when the detail of the picture is important. That is, if digital zoom is not applied after a picture for promotional purposes is taken, a difference between a low and high quality picture is hardly noticeable. Therefore, noise needs to be reduced by post-processing techniques only for the pictures for inspection of impact craters which will be explained in Section 8.5.

Another argument for the expectation of low resulting image quality for the inspection pictures originates from the image sensor type. As can be seen from Figure 8.3 the amount of noise depends on the type of sensor as well. In mobile phone devices CMOS (complementary metal oxide semiconductor) sensors are used instead of CCD (charge-coupled device) sensors because of the large amount of power reduction [8]. The main disadvantage of the CMOS sensor is the high read-out noise. This characteristic of CMOS sensors puts limits on the image quality for taking detailed pictures with mobile phone cameras. [9]

## 8.4. Camera Selection

In this section several camera modules are compared. The specifications of the Iphone 6S, Samsung S6, Sony FCB MA 130, Sony FCB MA 132 and Sony FCB MA 133 camera modules are listed in Table 8.1. [10] [11] [12] The latter cameras are commonly used in document scanning, UAVs and other security and industrial applications.

Table 8.1: Camera specifications

| | **Iphone 6S** | **Samsung S6** | **Sony FCB MA 130** | **Sony FCB MA 132** | **Sony FCB MA 133** |
|---|---|---|---|---|---|
| **Specifications** | | | | | |
| Mass [g] | 1-1.5 | 1.9 | 2.2 | 9.7 | 8.7 |
| Width [mm] | 8.6 | 27.2 | 16.5 | 28.0 | 28.0 |
| Height [mm] | 8.31 | 12.4 | 10.3 | 26.0 | 25.6 |
| Depth [mm] | 5.6 | 4.6 | 18.0 | 18.9 | 18.9 |
| Volume [mm^3] | 400.2 | 1551.5 | 3059.1 | 13759.2 | 13547.5 |
| Power [mW] | 600-800 | 600-800 | 710-730 | 710 | 710 |
| Sensor Model | Sony IMX315 | Sony IMX240 | Sony IMX169CQK | Sony IMX169CQK | Sony IMX169CQK |
| Physical Sensor Size X [mm] | 4.8 | 5.95 | 5.9 | 5.9 | 5.9 |
| Physical Sensor Size Y [mm] | 3.6 | 3.35 | 4.38 | 4.38 | 4.38 |
| Equivalent Sensor Size X [mm] | 36 | 36 | 36 | 36 | 36 |
| Equivalent Sensor Size Y [mm] | 24 | 24 | 24 | 24 | 24 |
| Physical Focal Length [mm] | 4.02 | 4.35 | 5.3 | 3.8 | 2.8 |
| Equivalent Focal Length [mm] | 29.0 | 27.6 | 31.2 | 22.4 | 16.5 |
| Resolution [Mpix] | 12.19 | 15.87 | 13.19 | 13.19 | 13.19 |
| Pixel Size [mm] | 0.00119 | 0.00112 | 0.0014 | 0.0014 | 0.0014 |
| **field of view** | | | | | |
| FOV X [deg] | 64 | 66 | 60 | 78 | 95 |
| FOV Y [deg] | 45 | 47 | 42 | 56 | 72 |
| IFOV [deg] | 0.017 | 0.015 | 0.015 | 0.021 | 0.029 |
| **Inputs** | | | | | |
| Feature Size [mm] | 0.1 | 0.1 | 0.1 | 0.1 | 0.1 |
| **Outputs** | | | | | |
| Working Distance [m] | 0.34 | 0.39 | 0.38 | 0.27 | 0.20 |
| Coverage X [m] | 0.42 | 0.51 | 0.44 | 0.44 | 0.44 |
| Coverage Y [m] | 0.28 | 0.34 | 0.29 | 0.29 | 0.29 |
| **Inputs** | | | | | |
| Coverage X [m] | 11.2 | 11.2 | 11.2 | 11.2 | 11.2 |
| **Outputs** | | | | | |
| Working Distance [m] | 9.02 | 8.57 | 9.72 | 6.97 | 5.13 |
| Coverage Y [m] | 7.47 | 7.47 | 7.47 | 7.47 | 7.47 |
| Feature Size [mm] | 2.67 | 2.21 | 2.57 | 2.57 | 2.57 |

[8] CCD vs CMOS: what is the difference? http://www.steves-digicams.com/knowledge-center/how-tos/digital-camera-operation/ccd-vs-cmos-whats-the-difference.html#b, retrieved on 06-06-2016

[9] CCD and CMOS Image Sensor Technologies, https://courses.cs.washington.edu/courses/cse467/08au/pdfs/lectures/07-cmos-ccd-imagers.pdf, retrieved 07-06-2016

[10] DeviceSpecifications, http://www.devicespecifications.com/, retrieved on 02-06-2016

[11] FCB Microseries, https://pro.sony.com/bbsc/assetDownloadController/FCB-Micro-print-ready-brochure.pdf?path=Asset%20Hierarchy%24Professional%24SEL-yf-generic-153703%24SEL-yf-generic-153736SEL-asset-478893.pdf&id=StepID%24SEL-asset-478893%24original&dimension=original, retrieved on 08-06-2016

[12] IMX168CQK, IMX169CQK, http://www.sony.net/Products/SC-HP/new_pro/september_2013/imx168_169cqk_e.html, retrieved on 08-06-2016

The field of view and instantaneous field of view presented in Table 8.1 are calculated according to Equations (8.1) till (8.3). Note that a distinction is made for the horizontal (X) and vertical (Y) components.

As was described in Chapter 2 the impact craters of space debris and micrometeoroids on the EuReCa satellite are of the size of 100 microns till 6.4 millimeters. According to Requirement **TS-SYS-POD-ADC-02**, a $\Delta V$ 0.013 $m/s$ is required and a picture can be taken from a distance larger than 9 $cm$. The average working distance, or distance from the object to the femto-satellite, equals 32 $cm$ for a smallest feature size of 0.1 $mm$ where the size range of interest for impact craters starts. Due to the limited FOV of the cameras, the mean coverage is 45 $cm$ by 30 $cm$ at this distance. Table 8.1 shows that the mobile phone camera module for the Samsung S6 can provide the largest working distance and largest coverage for a smallest feature size of 0.1 $mm$.

The performance of the camera module for the promotion pictures is assessed by checking the smallest feature size and working distance for a required horizontal coverage. For promotion pictures it is assumed that the bigger sides of the SkySat are sides of interest since they are covered with solar panels. From requirement **TS-SYS-POD-08** the femto-satellite shall capture images on which the diagonal of one side of the host spacecraft occupies 10 % or more of the horizontal dimension of the picture. The diagonal of the biggest side of the host spacecraft (60 $cm$ by 95$cm$) equals 1.12 $m$. The average working distance for a horizontal coverage of 11.2 $m$ (= $10 \cdot 1.12$) equals 7.88 $m$. The average smallest feature size at this distance is 2.5 $mm$. All working distances for the promotion pictures are reachable in the first revolution of the relative orbit as can be seen in Figure 7.7. The smallest feature size is of less importance for the promotion pictures.

From Table 8.1 and the discussion in the last paragraphs it can be concluded that the Samsung S6 camera has the best performance in terms of smallest feature size and working distance. In terms of mass and volume only the Iphone 6S camera has a better performance. However, because the FOV is bigger for the Samsung S6 camera and also because at a larger working distance inspection pictures can be taken, it is decided to use the Samsung S6 camera. The price of the Samsung S6 camera is relatively low (33.60 Euro[13]) like the prices of the other camera modules and was therefore not taken into account in the trade-off. The precise mass and dimensions of the Samsung S6 camera module were measured at the Aerospace Laboratory of the Faculty of Aerospace Engineering TU Delft. The Samsung S6 camera module was provided for research during the DSE-phase by GSM Berkel [14]. The final imaging specifications using the Samsung S6 camera are summarised in Table 8.2.

Table 8.2: Final imaging specifications using the Samsung S6 camera

| | **Minimum Working Distance** | **Maximum Working Distance** |
|---|---|---|
| Distance [$m$] | 0.39 | 8.57 |
| Coverage[$m$] | 0.51×0.34 | 11.2×7.47 |
| Smallest Feature Size [$mm$] | 0.1 | 2.21 |

## 8.5. Post-Processing Techniques

As discussed in Section 8.3 the image quality is expected to be relatively low. Under this circumstance, the image needs to be reconstructed with post-processing techniques.
As both host satellites and femto-satellites are moving and rotating, it will result in a blurry image. With regard to this circumstance, a set of pictures can be taken to calculate the relative motion. Based on analysing the change of different pixel points in a certain area, the relative motion can be predicted. After the relative motion is established, the image can be reconstructed to erase the blur of the picture. By checking multiple frames which are taken in a short period, the noise level of the final picture can be reduced. After predicting the possible movement, the noise of the camera can be distinguished. Meanwhile the blur can be limited to a low level. Then based on the motion, the picture can be reconstructed with a clear and accurate view. This technology is called mutiframe super resolution[15]. Basically the higher the frame rate used, the better the picture that can be recovered. However achieving a big amount of pictures in a short time period is not possible as the shutter speed will be high at the same time which will result in a low brightness of the picture. Besides this, the Samsung camera can only take 7 pictures per second, which limits

[13] Samsung galaxy S6 camera module-compatibel, `https://www.mytrendyphone.nl/shop/samsung-galaxy-s6-171810p.html?gclid=CjOKEQjw1v66BRCV-6rh6s-Biu8BEiQAelpui5D9tEI1bb2TOXGPixkEHPoR-JmLOW-Kv-ev9413zgAaAm2I8P8HAQ&tagcl=1&trackid=google.nl_google.nl&refHost=https%3A%2F%2Fwww.google.nl%2F`, retrieved on 16-06-2016

[14] GSM Berkel, http://gsmberkel.nl/, retrieved on 04-06-2016

[15] Fast and Robust Multiframe Super Resolution,`http://people.duke.edu/~sf59/srfinal.pdf`

the maximum frames that can be captured and used[16]. Under this circumstance, at maximum, 7 frames per second can be used for multiframe super resolution in this case.

## 8.6. Data Size Determination

The amount of data gathered needs to be known for the link budget, since the data rate depends on the contact time with the ground and the amount of data that needs to be sent. Every pixel in a picture is an information package where a pixel can be in colour or black and white. The amount of different tints depends on how many bits the system is. For a 2 bits system one can have $2^2 = 4$ different combinations, or in this case, colour tints. So for a 8 bits system there are $2^8 = 256$ different colour tints. For a black and white image one sample per pixel is enough. This sample presents a scale from white to black. Three samples are needed for a colour image. Because with red, green and blue one can make every colour. So one sample presents all the different tints of red, the other presents all different tints of green and the last sample presents all different tints of blue. So Equation (8.4) is used to determine the amount of bits in a picture. [2] This data can be sent as raw data to the ground station. Another option is compression, but for compression one needs a more powerful board computer.

$$D = n_b \cdot s \cdot p_p \tag{8.4}$$

Here $D$ stands for the amount of data in bits for one picture, $n_b$ is the number of bits per sample, $s$ is the number of samples per pixel, $p_p$ is the amount of pixels. So for a 3 colours picture of 16 mega-pixels with 256 tints, so an 8 bits system, the amount of raw data is 384 megabit, or 48 megabyte for one single picture.

## 8.7. Number of Pictures

The total number of pictures depends on several different aspects. As presented before, multi-frame technology will be applied which will lead to a tremendous number of pictures. These pictures will be captured in several different positions to generate different views of the host spacecraft. However, the number of pictures is constrained by the light condition, the data rate into storage, the camera property, data transfer rate and the photographing plan. The light condition implies that the imaging can only be performed under some position which will not result in a too dark or too bright scene. Based on the astrodynamic model the total time can be used for shooting is limited as it has to stay within the range of $3.8m$ for inspection and $8.57m$ for promotion. As the data handling rate can only achieve $128MB/s$, the total size of the image captured is limited.

Another thing that needs to be considered is the data transfer rate. As WiFi is used, the transfer rate is limited to 6.75 $MB/s$. Meanwhile the camera used in the femto-satellite can take 7 pictures per second at maximum with a relatively lower resolution. Together with these is the photographing plan, as the communication with host and taking imaging cannot be performed at the same time. The total time of imaging is limited which will also limit the total number of pictures. Based on all this information, the maximum number of pictures can be obtained by Equations (8.5) to (8.7).

$$T_{transfer} + T_{imaging} = T_{tot} \tag{8.5}$$

$$N_{persecond} \cdot T_{imaging} \cdot S_{picture} = T_{transfer} \cdot R_{datatranser} \tag{8.6}$$

$$N_{tot} = N_{persencod} \cdot T_{imaging} \tag{8.7}$$

With the requirements on minimum imaging distance and data transfer, the data transfer time and imaging time can be obtained from the astrodynamic model, which is shown in Chapter 7. Meanwhile based on the selected camera, the number of pictures that can be taken per second and the size of each picture are also known. With so many restrictions, the final shooting rate is chosen as 2.33 fps. Meanwhile, due to power issues, the transferring time is limited to 6250 seconds, which is shown in Section 9.4. However the communication time is also limited by the power system, which does not allow the camera to take pictures for more than 442 seconds.
After 30 seconds the femto-satellite is at 0.39 $m$ distance from the host and it starts imaging. For the first 300 seconds, 700 inspection pictures can be taken, and after the inspection the femto-satellite will be 4.04 $m$ away from the host spacecraft. Then 178 promotional pictures can be taken in the next 142 seconds. The latest picture will be taken at 5.61 $m$ and is therefore still in the range of $0-8.57m$. These numbers are the maximum number of pictures the femto-satellites can achieve. For customers, they can choose their own imaging plan if it is in this range.

[16] Burst mode of samsung s6,`http://gadgetguideonline.com/galaxys6/galaxy-s6-camera-guide/how-to-use-galaxy-s6-camera-burst-mode/`,retrived on 8/6/2017

# 9

# Communication System

For this mission, the femto-satellite needs to be able to communicate to the ground. To be able to do this, a communication architecture needs to be designed. This is presented in this chapter. First, the subsystem requirements are listed. Secondly, the general communication flow design is shown. Thirdly, the trade-off between different communication methods is presented. Fourthly, the design choice is presented and finally the effects of radiation for the communication is described.

## 9.1. Subsystem Requirements

The communication sub-system design needs requirements for the design. The communication needs to be able to send the data during the mission. Otherwise there is no point in collecting data. This results in requirement **TS-SYS-POD-05-COM-01**. Also a high data rate is needed to be able to send the pictures, which are large data packages. So assuming the mission wants to make at least 25 pictures, with each picture a size of 48 MB, during a three hours mission gives a data rate of 0.9 Mb/s. Rounding this number gives requirement **TS-SYS-POD-05-COM-02**. The images need to be send to Earth. Otherwise collecting data is pointless. This results in requirement **TS-SYS-POD-05-COM-03**. And finally the antenna needs to have an omnidirectional radiation pattern. This way it is possible to send data without needing the ADCS to be operational. This way the system uses less power and therefore the design can be lighter.

The requirements for the communication sub-system are as follows. These requirements will be verified in Chapter 20 about verification and validation.

**TS-SYS-POD-05-COM-01** The communication system shall provide a closed link budget during the mission.
**TS-SYS-POD-05-COM-02** The communication system shall provide a data rate of at least 1 $Mb/s$.
**TS-SYS-POD-05-COM-03** The communication system shall be able to send data to Earth.
**TS-SYS-POD-05-COM-04** The communication system shall have an omnidirectional radiation pattern.

## 9.2. Communication Flow Design

In this section the communication flow design is going to be discussed. The information from the femto-satellite needs to be transmitted to the ground. Four configurations are proposed which will be investigated. The proposals are given below. The distance from the femto-satellite to the host spacecraft increases over the duration of the mission. After 2 orbits the distance is between 50 and 200 meters.

- Communication from the femto-satellite direct to the ground
- Communication from the femto-satellite via a relay femto satellite to the ground
- Communication from the femto-satellite via a relay satellite grid to the ground
- Communication from the femto-satellite via the host to the ground

### 9.2.1. Communication Directly to the Ground

For this design an antenna and a transceiver are part of the femto-satellite. This system should than be able to communicate to the ground. For this system the communication flow design is independent of the distance between the host spacecraft and the femto-satellite. Communication to the ground by small satellites is mostly done by S-band- or UHF/VHF transceivers.[1] The advantage of UHF/VHF transceivers are that they have a relatively low power consumption and a relatively low mass. Also the free space losses are low due to their low frequency. The disadvantage is that it can only handle low data rates. They also need a long antenna, since the antenna needs to be at least a quarter wavelength. The advantage of the S-band transmitter is that it can handle higher data rates, high enough to send high data packages like pictures. Also the antenna can be smaller. The disadvantage is that it has a higher mass and uses more power than the UHF/VHF transceiver. An example of a cubesat S-band transmitter is the *ISIS TXS S-Band Transmitter*. It weighs 62 grams without antenna and uses a maximum power consumption of 3.5 watts.[2] The mass of only the transceiver is already more than 60 % of the maximum mass of the femto-satellite. This leaves an unacceptably low amount of mass budget for the rest of the subsystems and the power needed is

[1] Delfispace, `http://www.delfispace.nl/`, retrieved on 03-06-2016
[2] S-band transmitter, `http://www.cubesatshop.com/index.php?page=shop.product_details&flypage=flypage.tpl&product_id=9&category_id=5&option=com_virtuemart&Itemid=67`, retrieved on 03-06-2016

high for a system like the femto-satellite. An example of the UHF/VHF transceiver is the *NanoCom AX100*. The transceiver weight without antenna is 24.5 grams and the power consumption is 2.64 watts.[3] This is less than 25 % of the mass and leaves room for the other subsystems. However, the power consumption is again high. Stefano Speretta[4] explained that there are no smaller transceivers since there is no market now for these transceivers. So with these values it is concluded that direct communication to the ground on the inspection femto-satellite is not possible with the technology of today.

### 9.2.2. Communication via a Relay Femto-Satellite

This communication flow design consists of an inspection satellite which sends its data with a short range transceiver to a communication relay femto-satellite which in turn sends the data to Earth. The relay femto-satellite will be deployed with the inspection satellite. The advantage of this design is that the communication is independent of the host spacecraft. So when the ground loses contact with the host, both femto-satellites can be deployed via a fail safe protocol. Then the inspection femto-satellite can inspect the host spacecraft and the relay femto-satellite can send the data to Earth. This will help determining the reason for losing contact. Also the relay femto-satellite could relay commands from the ground to the host spacecraft.

As discussed in Section 9.2.1, the transceivers needed to communicate to the ground are not yet small enough for femto-satellites. But a relay satellite can consist of only a transceiver, solar panels and/or power storage device. A simple ADCS is required so that the tumbling rates do not become to large. This is done on the Delfi-C$^3$.[5] So this design could work with the UHF/VHF transponder discussed earlier.[3] But due to the almost 17 centimetre long antenna and the 6.5 by 4 centimetre transponder, the relay femto-satellite can not be designed in a $5 \times 5 \times 5$ centimetre cube. The relay femto-satellite needs to be in range of the inspection satellite to be able to communicate via a short range transceiver. The relay femto-satellite can not be designed in the same shape as the inspection satellite. Therefore the ballistic coefficient will differ and they will drift away from each other. Over time the inspection- and relay satellite will be out of communication range from each other. So because of the high mass of the transceiver, non cubic shape and therefore loss of contact over time, it is decided that this communication flow design will not be used for PICS.

### 9.2.3. Communication via a Grid of Relay Satellites

This communication flow design consists of a femto-satellite which sends its data to a satellite in a grid of relay satellites that are used for satellite telephones etc. and which in turn send the data to the ground. There are relay satellites in GEO and LEO. For missions in LEO the distance to Earth is smaller than the distance to the relay satellites in GEO. So the GEO relay satellites are not useful for this scenario. The relay satellites in LEO are closer by for LEO missions than the Earth, therefore research is done in the LEO relay satellites. These relay satellites are owned by companies, for example *orbcomm*. Due to the low data rate [6] and high power consumption [7] it is concluded that this is not applicable to femto-satellites.

### 9.2.4. Communication via the Host Spacecraft

This communication flow design consists of a femto-satellite which sends its data to the host spacecraft which sends the data to the ground. During the mission the femto-satellite takes pictures of the host spacecraft. So the distance between the host and femto-satellite is relatively small compared to the distance to the Earth. For this reason not the same transceivers are used for communication to the host with respect to direct communication to the ground. So research is done into WiFi and Bluetooth modules. The advantage of WiFi is the larger data rate and the advantage of Bluetooth is the low power consumption.[8] Because of the relatively low masses compared to UHF/VHF or S-band transceivers these communication modules are preferred. Also, both methods meet the requirements for the communication subsystem. So this communication flow design is chosen over the other methods. In the next section, Section 9.3, the trade-off between WiFi and Bluetooth is presented.

### 9.2.5. Selecting Communication Flow Design

The communication flow design from the femto-satellite via the host to the ground is selected. The disadvantage of this design is that it heavily depends on the host's capability to relay the data to Earth. Yet the technology is not mature enough for other possibilities. This design can really be improved when there are transceivers small enough for femto-satellites that can reach the ground. Figure 9.1 shows the communication flow diagram. Each arrow has

[3] UHF/VHF transceiver `http://www.gomspace.com/index.php?p=products-ax100`,retrieved on 03-06-2016

[4] Research engineer, chair space system engineering at the TU Delft, Former RF Systems Engineer at ISIS, interviewed on 30-06-2016

[5] Delfi attitude control,`http://www.delfispace.nl/delfi-c3/attitude-determination-control`,retrieved on 06-06-2016

[6] orbcom data rate,`http://www.orbcomm.com/en/networks/satellite/isatdata-pro`,retrieved on 06-06-2016

[7] Datasheet orbcomm,`http://www.orbcomm.com/PDF/datasheet/OG2-OG-ISAT-Satellite-Modems.pdf`,retrieved on 06-06-2016

[8] Bluetooth versus WiFi,`http://www.engineersgarage.com/contribution/difference-between-bluetooth-and-wifi`,retrieved on 05-06-2016

text above it, this text explains the data flow. For this mission the pictures taken are the data that needs to be sent. The commands from the ground determine when the femto-satellite will be released. Also since the femto-satellite does not have propulsion on board, it has no control over its orbit. So if one wants to have active inspection, where one wants to inspect a specific place, the host spacecraft needs to aid the inspection by turning the specific location to the camera of the femto satellite. Therefore the diagram shows that the femto-satellite can give commands to the host spacecraft. Furthermore, the femto-satellite will perform the mission completely autonomously after deployment. This is due to the short mission duration.

The data rate of the SkySat is 480 Mb/s on X-band. So this communication link can send the amount of data of the femto-satellite to the ground.

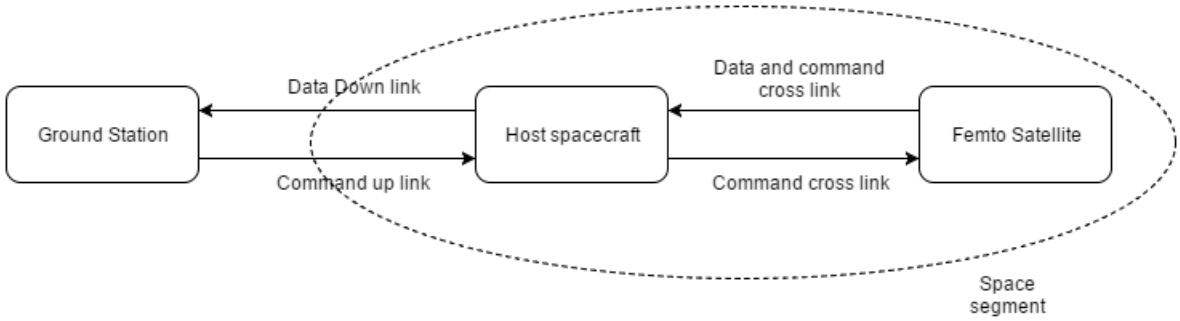


Figure 9.1: Communication flow diagram

## 9.3. Communication Methods

From the communication flow design it is determined that a short range communication device is needed to communicate to the host. Also, a large amount of data needs to be sent since the inspection satellite takes a high amount of pictures in a short time. From these requirements research was done in WiFi and Bluetooth chips. As discussed earlier, the advantage of WiFi is the large data rates and the advantage of Bluetooth is the low power consumption. For this application the research on Bluetooth is focused on class 1 Bluetooth chips. These chips have a range of at least 100 meters. Table 9.1 shows examples of WiFi and Bluetooth chips. These are used to determine whether WiFi or Bluetooth is the better choice.

Table 9.1: Wifi versus Bluetooth trade-off

| **Component** | **Data rate** $[Mb/s]$ | **Range** $[m]$ | **Power usage** $[mW]$ | **Data rate** × **distance** $[Mb/s \times m]$ | **Data per joule** $[Mb/J]$ |
|---|---|---|---|---|---|
| **WIFI** | | | | | |
| LM820 [9] | 120 | 180 | 625 | 21600 | 192 |
| ESP8266[10] | 54 | 200 | 462 | 10800 | 117 |
| **Bluetooth** | | | | | |
| WT11i [11][12] [13] | 2.1 | 350 | 500 | 735 | 4 |
| LM930 [14] | 1 | 500 | 82.5 | 500 | 12 |

The first column shows different example parts for the Bluetooth and WiFi systems. The second, third and fourth column show the data rate, range and power usage, respectively. The fifth column shows the data rates multiplied with the distance. This number is an indication for which system can send the most data. The relatively speed of the femto-satellite with respect to the host satellite is independent of which communication protocol is going to be used. So the range of the communication is an one to one relation with the communication time. And therefore

[9] LM820 http://lm-technologies.com/product/wifi-smt-module-150mbps-with-onboard-antenna-lm820/, retrieved on 09-06-2016
[10] ESP8266, https://cdn-shop.adafruit.com/product-files/2471/0A-ESP8266__Datasheet__EN_v4.3.pdf, retrieved on 09-06-2016
[11] WTIIi, https://www.bluegiga.com/en-US/products/wt11i-bluetooth-class-1-module/, retrieved on 09-06-2016
[12] WT11i http://pdf1.alldatasheet.com/datasheet-pdf/view/608558/ETC2/WT11I.html, retrieved on 09-06-2016
[13] WT11i https://www.bluetooth.org/tpg/RefNotes/WT11i_Datasheet.pdf, retrieved on 09-06-2016
[14] LM930, http://lm-technologies.com/product/bluetooth-smart-module-4-1-class-1-lm930/, retrieved on 09-06-2016

these numbers give an indication which part can send the most data. The sixth column gives the amount of data sent per joule. The weight for these modules are all relatively low so these are not driving in the trade-off.

The last two columns of Table 9.1 show a significant difference between WiFi and Bluetooth. Wifi can send more data than the Bluetooth chips. The femto-satellite is going to take pictures, which will generate a large amount of data. So a high amount of data needs to be sent and therefore a high data rate times distance is preferred. Also the data per joule is significantly higher for WiFi compared with Bluetooth. With this it is concluded that WiFi is going to be used for communication to the host.

## 9.4. Subsystem Design Trade-off

After selecting WiFi for the communication, a WiFi module needs to be selected. Table 9.2 shows a selection of WiFi chips. The advantage of the *LM820* is that is has a high speed output. Yet the operational temperature range is very limiting. The advantage of the *WF121* is that it has a larger operational temperature range than the *LM820*, yet it uses relatively high power. The *ESP8266* has a favourable operational temperature range and a relatively low power input. The drawback with respect to the *LM820* is the lower data rate. With this data rate and assuming 3 hours send time the total amount of data that can be sent is 72.9 gigabytes. With a picture size of 48 megabytes, this gives a total amount of 1518 pictures that can be sent. This is already a large amount of pictures, so the higher data rate is not needed.

Table 9.2: WiFi modules trade-off

| **Component** | **Power** $[W]$ | **Temperature range** $[^{\circ}C]$ | **Size** $[mm]$ | **Speed** $[Mb/s]$ |
|---|---|---|---|---|
| LM820 [15] | 0.625 | -10 / +60 | $25\times12\times2$ | 120 |
| WF121 [16] | 0.8 | -40 / 85 | $15.4\times26.2\times2$ | 54 |
| ESP8266 [17] | 0.46 | -40 / 125 | $25\times38\times5$ | 54 |

So with this reasoning the *ESP8266* is selected with a built-in PCB trace antenna. The radiation pattern of a PCB antenna is omnidirectional.[18] The WiFi module will be mounted on the host spacecraft and on the femto-satellite. The specifications of the communication are as follows. An IEEE 802.11g with orthogonal frequency-division multiplexing (OFDM) modulation and a data rate of 54 $Mb/s$ is going to be used. For a 54 $Mb/s$ data rate and this modulation, the input power is 0.46 watts and the output power is 15 $dBm$. The minimum signal to noise ratio is 21 $dB$ when there are interfering channels. Assuming a 60 degrees Celsius temperature, no antenna gains, and 2 $dB$ losses gives a range of 242 meters. Since there are almost no interfering channels in space the 21 $dB$ is not a hard requirement. So with this, one can safely conclude that the femto-satellite can communicate with the host during the whole mission duration. The mass of the WiFi chip is 5 grams, the dimensions are $25\times38\times5$ millimetres.

The communication range can be increased significantly by using a better transceiver at the host spacecraft to receiver the signal. Also other antennas can be used to improve the distance. However, the *ESP8266* with PCB trace antenna can send all the data within mission duration. If the customer wants to take more pictures to be sent, he also has to accept extra mass on the host satellite.

The minimum clearance distance should be ideally half a wave length for the best results. Yet this distance can be decreased at the expense of performance.[19] The clearance should be 62.5 mm and the cube is $50\times50\times50$ mm. Therefore no clearance can be made inside the satellite. So the WiFi is placed on the top corner of the PCB, to maximise the clearance. 12.5% of the free space is filled with the femto-satellite so when this is in line with the host, the performance is less. Also the effect of the kapton foil needs to be analysed since no literature about the effect of kapton foil on signal strength is available.

The battery can provide an extra 204 seconds of power with only the communication active. This is a 3.3% increase of time and will not cover the whole loss. Also the orientation is hard to determine, so it is hard to determine how much of the time the femto-satellite is in the way of the communication. The effect of the femto-satellite in line of communication needs to be tested experimentally. With these results better estimates can be made to determine if all the pictures can be sent.[19] In the worst case scenario, not all promotion pictures are sent to the host. This is an

[15] LM820,http://lm-technologies.com/product/wifi-smt-module-150mbps-with-onboard-antenna-lm820/,retrieved on 06-06-2016

[16] WF121,https://media.digikey.com/pdf/Data%20Sheets/BlueGiga%20PDFs/WF121_Datasheet.pdf,retrieved on 06-06-2016

[17] ESP8266,https://cdn-shop.adafruit.com/product-files/2471/0A-ESP8266__Datasheet__EN_v4.3.pdf,retrieved on 06-06-2016

[18] Radiation pattern,http://www.cypress.com/file/136236/download,retrieved on 09-06-2016

[19] Antenna clearance,https://www.lsr.com/white-papers/antenna-design-gain-and-range,retrieved on 24-06-2016

acceptable risk.

## 9.5. Data Transmitting

The amount of data transmitted is dependent on several factors: Amount of data gathered, data rate, communication time and power usage. The total amount of data gathered should be equal to the data sent and it should fit in the power budget. The solution is 442 seconds of taking pictures, which will gather a maximum of 878 pictures, with a total data size of 42.1 $GB$. With the power constrains it is determined that the optimal transmitting time is 6250 seconds. A transmitting rate of 53.9 $Mb/s$ will be used. The telemetry of the femto-satellite will be sent with the pictures during these transmissions. After finishing transmitting the pictures the femto-satellite is at 85 meters from the host spacecraft, which is till within transmitting range. This is due to the fact that the power budget was the most limiting factor. Since the battery uses a 15% margin there is a possibility that there is still power available after ending transmission. This power will be used to send telemetry to the host spacecraft as long as it is possible. This telemetry will be used to analyse the behaviour of the femto-satellite.

# 10

## Attitude Determination & Control System

In this chapter the Attitude Determination and Control System will be designed. The design will be separated into four steps, which are as follows:[2]

- Define control modes
- Derive subsystem requirements from control modes & system requirements
- Select the type of attitude determination & control to be used
- Select and size the ADCS hardware

These four steps are worked out in sections 10.1 through 10.4 and are concluded with a subsystem summary in Section 10.5.

## 10.1. Control Modes

The control modes of the attitude determination and control system will need to make sure that the satellite is able to maintain/restore attitude at all times. During the lifetime of the femto-satellite there will be two distinct operation modes:

- Nominal operation
- De-tumbling/deployment operation

The nominal operation mode will be used while the femto-satellite is orbiting on its own and its main task is to point the payload towards the host spacecraft to sense it. In this mode the gyroscopes are used to sense the current attitude and the payload camera will be used periodically to (re-)determine the location of the host spacecraft.

The de-tumbling and deployment operation mode will be used during the launch of the femto-satellite in which the primary task of the ADCS is to get the satellite to stop tumbling and gain control over its orientation. When this goal has been achieved the femto-satellite will turn to the nominal operation mode.

## 10.2. Subsystem Requirements

The subsystem requirements of the attitude determination and control system are specified below:

**TS-SYS-POD-ADC-01** The ADC subsystem shall be able to keep the host spacecraft within the field of view of the payload subsystem, which is 63 ° horizontal and 45 ° vertical.
**TS-SYS-POD-ADC-02** The ADC subsystem shall be able to de-tumble the femto-satellite within 25 seconds from release.
**TS-SYS-POD-ADC-03** The ADC subsystem shall be able to counter the disturbance torques that act on it during the ADCS lifetime.
**TS-SYS-POD-ADC-04** The ADC subsystem shall be able to have sufficient momentum storage about a single axis to store worst-case disturbance torque for the entire ADCS lifetime acting about this orbit.
**TS-SYS-POD-ADC-05** The ADC subsystem shall be able to point the payload towards the host spacecraft for the duration of the payload.

## 10.3. Type of Attitude Determination & Control

In the design of the attitude determination and control system various parts are used, separated into sensors and actuators. In this section the sensors and actuators used will be documented and the reasoning behind why they are being used is explained.

### 10.3.1. Sensors

Ordinary satellites require two types of sensors to accurately monitor the femto-satellite orientation, *relative* and *absolute* sensors. The combination of these two sensors will allow the femto-satellite to point the payload towards the host spacecraft.

The relative sensors will provide fast readings of the satellite's attitude relative to previous known attitudes. These relative readings can be integrated to provide the current femto-satellite attitude, however these sensors are known to have a bias, which causes drift because the bias is being amplified through the integration. This is why periodic correction using absolute sensors is required. Due to the short lifespan of the femto-satellite it was decided that

instead of utilising separate absolute ADCS sensors a periodic image will be taken with the payload camera to determine the attitude relative to the host.

**Relative Sensors**
In this section a series of sensors are presented that can be used as relative sensors. Relative sensors often come in the shape of full Inertial Measurement Units (IMU) and/or Attitude Heading Reference Systems (AHRS).

There are however some problems with the use of IMUs in space. The gyroscopes will function normally as expected, however the accelerometers will not register the location of the Earth relative to the satellite, which is due to the fact that the satellite is in permanent free-fall. Other than accelerations due to thrusters and disturbances no accelerations will be registered by it.

The magnetometers will work, however the readings are only useful if a model of the Earth magnetic field is present. Given that the femto-satellite has the highest priority in targeting the host the orientation relative to Earth is not of importance. This means that the gyroscope is the only component that is going to be used during the mission. In Table 10.1 a selection of possible gyroscope candidates for the satellite can be seen. The temperature sensitivity is given over the entire temperature range of the component.

Table 10.1: Gyroscope specifications

| **Product** | **Mass** $[g]$ | **Dimensions** $[mm]$ | **Voltage** $[V]$ | **Current** $[mA]$ | **Power** $[mW]$ | **Gyroscope Accuracy** $[°/s]$ | **Temp. Sensitivity** |
|---|---|---|---|---|---|---|---|
| InvenSense ITG-3701[1] | 0.015 | 3.0×3.0×0.75 | 1.71-3.6 | 3.3 | 11.88 | 0.015 | ±4% |
| STM L3GD20H[2] | 0.02 | 3.0×3.0×1.0 | -0.3 - 4.8 | 5 | 24.0 | 0.00875 | ±2% |
| Kionix KXG03[3] | 0.02 | 3.0×3.0×1.0 | 1.8 - 3.3 | 1.85 | 6.1 | 0.0078 | ±2.5% |

When choosing which gyroscope is going to be used special attention is paid to the temperature sensitivity, accuracy and power consumption. Out of these three categories the Kionix KXG03 performs the best, with the highest accuracy, lowest power consumption and average temperature sensitivity.

As mentioned before these sensors tend to have a bias. The exact bias from the sensor chosen is not given by the manufacturer, however it is known from a variety of IMU datasets that were used as literature study in the midterm report[5] the average bias is 10 °/hr.[4, 5, 6] This is plotted vs time and the total gyroscope bias at the end of the ADCS lifetime can be seen in Figure 10.1. If this error is integrated during this time in a single direction, which will determine the worst-case deviation, it is seen in Figure 10.2 that the drift at the end of the ADCS lifetime is very large. This means that just using the gyroscopes is not an option for the mission. This is why the absolute sensors are necessary. This sensing will be done by using periodic host detection, which is elaborated upon in the next section.

**Periodic Host Detection**
Detection of the host spacecraft will be done by using edge detection algorithms on images taken by the payload camera. In order to not stress the on-board processor too much with these algorithms, minimum size images will be used. These images are at the VGA resolution (640x480). In Figure 10.3 an example is given of what a simple edge detection algorithm can produce. When the edges have been found the enclosed area of the edges can be used to find the host spacecraft geometric centre. Since this is exactly what the camera should be pointed at this type of algorithm can be used to detect the host spacecraft and correct for the gyroscope drift.

[1] ITG-3270 Datasheet, `https://www.invensense.com/wp-content/uploads/2015/02/ITG-3701-Datasheet.pdf`, retrieved on 13-06-2016
[2] STM L3GD20H Datasheet, `http://www.st.com/content/ccc/resource/technical/document/datasheet/35/b1/e0/39/71/57/43/01/DM00060659.pdf/files/DM00060659.pdf/jcr:content/translations/en.DM00060659.pdf`, retrieved on 13-06-2016
[3] Kionix KXG03 Datasheet, `http://kionixfs.kionix.com/en/datasheet/KXG03%20Preliminary%20Specifications%20Rev%200.19.pdf`, retrieved on 13-06-2016
[4] vectornav,`http://www.vectornav.com/products/vn100-smd/specifications`, retrieved on 09-05-2016
[5] xsens,`https://www.xsens.com/download/pdf/documentation/mti-1/mti-1-series_datasheet.pdf`, retrieved on 09-05-2016
[6] yostlabs,`https://www.yostlabs.com/sites/default/files/3-Space_Sensor_Users_Manual_Embedded_1.1_r20_18Oct2012_0.pdf`, retrieved on 10-05-2016

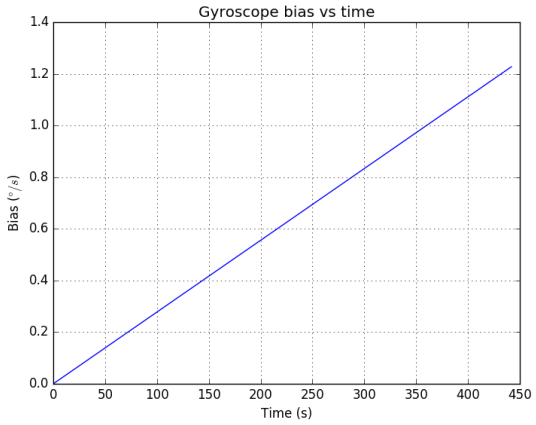


Figure 10.1: Gyroscope Bias vs Time

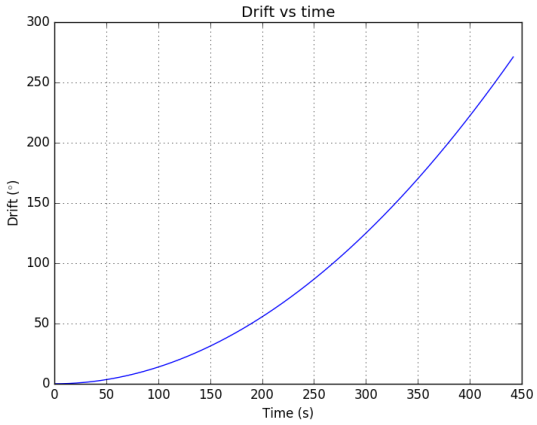


Figure 10.2: Gyroscope Drift vs Time

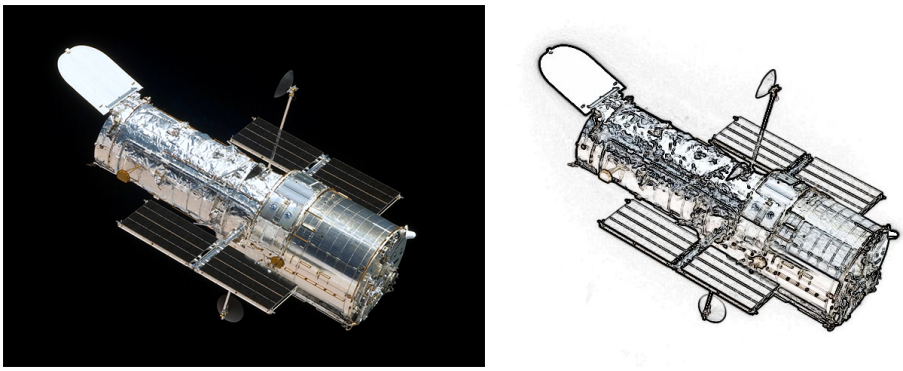

Figure 10.3: Edge detection algorithm example with an image of the Hubble telescope

The dimensions of the host spacecraft can be seen in Table 2.3 and taking the smallest surface the face with 60×60 centimetre becomes the leading factor for accuracy. Due to limitations set by the payload a maximum distance of 8.57 $m$ where imaging is taking place is assumed (further elaboration can be found in Section 8.7) this becomes the distance where the accuracy of the camera system will still matter.

At a distance of 8.57 $m$ the horizontal and vertical distance that is within the field of view of the femto-satellite is equal to 10.9 and 7.3 $m$ respectively. Knowing this distance the size of each pixel can be calculated which is equal to 1.7 and 1.5 $cm$ respectively. Since the host spacecraft will be 60×60 cm at the minimum this is enough to detect the host with sufficient accuracy since every side will be more than 30 pixels long at the maximum distance.

In order to determine how fast these periodic measurements must be taken, two factors are of importance: the drift of the gyroscopes and the uncertainties in the relative orbit. The field of view of the camera as specified by requirement **TS-SYS-POD-ADC-01** is equal to 63° horizontal and 45° vertical. The femto-satellite must remain pointed within this field of view to sense the host.

The minimum field of view of 45°is taken, meaning that a total deviation of 22.5°from the centre is possible. According to Figure 10.2 this occurs after 127.3 seconds. A conservative estimate will be taken which means that the imaging must be done every 100 seconds if only the gyro drift is considered.

If the orbit deviates much from what was determined before launch a situation may arise where the femto-satellite believes that it is pointing itself to the host, but in fact the host is in another location due to variations in the $\Delta V$ provided during separation and uncertainties about the atmosphere.

The relative orbit in the XZ, XY and YZ planes from separation until the end of the imaging period has been evaluated. This time is the time in which the ADCS must be on-line to point the payload. From this evaluation it has become clear that there is very little deviation in the path-angle between the femto-satellite and the host. This means that deviations in the orbit model will be negligible. The orbit will always form a near-straight line.

### 10.3.2. Actuators

Momentum wheels are preferred to be used for the attitude control part of the ADCS. The reason for this is that this allows the usage of brushless DC motors, which have a very bad response for low rotation rates, but excellent characteristics when spinning at nominal velocity.

## 10.4. Hardware Sizing

The sizing of the ADCS hardware will be done by using a combination of the requirements set by the mission and the disturbance torques. This will allow to determine the size of the momentum wheels.

### 10.4.1. Disturbance Torques

The environment where the satellite will be orbiting is home to several different disturbances. The ADCS will need to be able to counteract these torques throughout the femto-satellite lifetime. In order to size the ADCS these disturbances will need to be determined. This will be done in this section.

In LEO there are three relevant disturbance torques that act on the femto-satellite [28].

1. Aerodynamic
2. Solar radiation
3. Residual dipole

For the determination of the torques it is assumed that the high symmetry of the femto-satellite causes the gravity gradient torque to be negligible. In a standard 1U CubeSat the centre of gravity must lie within 2 $cm$ of the geometric centre [28]. For a 5×5×5 $cm$ femto-satellite this reduces to a distance of 1 $cm$. In the equations in this section this distance will be assumed. The shape and dimensions of the design will have a profound influence on the magnitude of the disturbances [32] [28].

**Aerodynamic Torque**

The aerodynamic torque can be calculated using Equation (10.2) where $C_D$ for a cubic shaped satellite is assumed to be 2.2, $\rho$ is the air density, $V$ is the orbital velocity and $(C_{CP}-C_{CG})$ is the distance between the centre of pressure and the center of gravity [28]. Finally $A_p$ is the projected area, which can be calculated using Equation (10.1) where $a$ is the length of a single dimension of the cube [28].

$$A_p = \frac{a^2}{2}\left(a+\sqrt{6}\right) \tag{10.1}$$

$$T_a = C_d \frac{1}{2}\rho V^2 A_p \cdot (C_{CP}-C_{CG}) \tag{10.2}$$

**Solar Radiation Torque**

The torque due to solar radiation can be calculated using Equation (10.3), where $S_0$ is the solar energy flux, $\rho_{body}$ is the body reflectance of the femto-satellite and $i$ is the incidence angle. The worst-case $S_0$ near Earth is 1428 $\frac{W}{m^2}$, which is when the Earth is the closest to the sun. The worst-case incidence angle $i$ is 0°.

$$T_{sp} = \frac{S_0}{c} A_p (1+\rho_{body}) cos(i)(C_{CP}-C_{CG}) \tag{10.3}$$

**Residual Dipole Torque**

The residual dipole torque can be calculated using Equation (10.4). In this equation $D$ is the dipole of the femto-satellite, which can be assumed to be 0.005 $Am^2$ and $B$ is the strength of the Earth magnetic field [28].

$$T_m = D \cdot B \tag{10.4}$$

Equation (10.6) is the relationship for the magnetic field strength $B$ as a function of the Earth radius $R_E$, radial distance from the Earth centre of mass $r$ and the angle with the axis from the centroid through the north pole $\theta$. This equation gives a result in *Tesla* [33].

$$H_E = \frac{\mu_0}{4\pi}\left(\frac{1}{R_E^3}\right)M \tag{10.5}$$

$$B = H_E\left(\frac{R_E}{r}\right)^3 \cdot \sqrt{1+3cos^2(\theta)} \tag{10.6}$$

By going for the worst case scenario on the proposed orbit of 450km altitude and assuming all torques to act in the same direction, the total disturbance torque is rated at $2.55 \cdot 10^{-7} Nm$.

### 10.4.2. Momentum Wheel Capacity

Sizing of the momentum wheels will depend on the disturbance torques acting over the duration of the orbit or the slew torque needed for manoeuvres and pointing. The design will take the maximum of these two requirements and size the wheels accordingly.

**Disturbance Torque**
In this section the momentum wheels will be sized for the maximum disturbance torque that was previously determined. Given that the ADCS lifetime is 442 seconds a worst-case scenario assumption will be taken where this torque is applied about a single axis for the entire mission duration. The total momentum storage required is equal to the previously established value of disturbance torque of $2.55 \cdot 10^{-7} Nm$ over a duration of 442 seconds. The total momentum that is added to the femto-satellite will be equal to $1.13 \cdot 10^{-4} Nms$.

**Slew Rate for Turning**
Because the femto-satellite will be launched in such a way that the payload is already pointed towards the host when separation occurs and the fact that the relative orbit is very straight, the slew rate will not form a requirement for the ADCS. This is why the momentum wheels will not be sized according to a minimum slew rate.

**De-tumbling after Separation**
Depending on the preciseness of the initial separation of the femto-satellite from the host spacecraft, the femto-satellite might experience the spring force on a slight offset from its centre of gravity. This will introduce a torque on the femto-satellite and cause it to spin. The spinning should be countered fast enough because in the initial phase after deployment the distance between the two satellites are small and thus crucial for taking detailed pictures.

The time required for de-tumbling should be kept low to meet this requirement. The camera used on the payload will start taking images when a distance of 0.39 $m$ has been reached, which means that when this distance is reached the camera should be ready to take images. According to the orbit model from Chapter 7 this distance is reached after roughly 30 seconds. A conservative estimate of 25 seconds will be used which will ensure that not only the femto-satellite is de-tumbled when the minimum distance is reached but also the fact that the femto-satellite will be in position to start the imaging sequence.

In order to size the tumbling caused by the separation system a similar approach is taken to the disturbance torques where it is assumed that the force can be applied to the femto-satellite in such a way that a maximum deviation from the centre of gravity of 1 $cm$ will occur.

The spring system will apply the force to the geometric centre of the femto-satellite and if the c.g. is 1 $cm$ off from this centre there will be a residual moment. This residual moment will cause a build-up in angular momentum over the deployment time. The magnitude of this angular momentum will be used to size the momentum wheels. This angular momentum can be calculated using Eq. (10.7). In this equation $F_{sp}$ is the average spring force, $\Delta cg$ the deviation of the centre of gravity and $\Delta t$ the time for which this force is applied.

$$h_{detumble} = F_{sp} \cdot \Delta cg \cdot \Delta t \tag{10.7}$$

The total angular momentum that is added to the femto-satellite during the de-tumbling phase will be equal to $3.9 \cdot 10^{-6} Nms$.

### 10.4.3. Momentum Wheel Sizing
The mass moment of inertia of the flywheel depends on the required momentum storage and the torque that needs to be applied. The wheels will be sized so that they can provide enough torque to counteract the disturbance torques, change the femto-satellite attitude and store momentum for long-term disturbances.

**Wheel Moment of Inertia**
In sections 10.4.2 and 10.4.2 the total momentum that needs to be stored by the momentum wheel is calculated. The total momentum stored in a momemtum wheel is given by Eq. (10.8) where $h$ is the total stored momentum, $I$ is the moment of inertia and $\omega$ is the angular velocity.

$$h = I \cdot \omega \tag{10.8}$$

Using the total momentum storage required in the wheel $h_{total}$, the nominal rotational velocity of the motor $n_N$ and the maximum deviation from this nominal velocity in fractions of the total $\beta$, it is possible to calculate the required moment of inertia of a single momemtum wheel. The resulting equation is Eq. (10.9). In normal spacecraft designs $\beta$ is normally restricted to around 10 % to prolong the longevity of the electromotors, however due to the novel design of the femto-satellite and limited lifespan the value for $\beta$ can be set much higher than normal.

For the design a $\beta$ of 1 is selected which means that in the worst-case scenario the femto-satellite will be fully saturated at the end of lifetime, which is not a problem.

$$I_{wheel} = \frac{h_{total}}{n_N \cdot \beta} \tag{10.9}$$

**Electromotor & Speed Controller**

The electromotor that will be used to drive the momentum wheels is the Faulhaber 0308-B [7]. This electromotor is chosen for its very compact design, good performance and low energy usage.

This electromotor is of a 2-pole design and requires a signal that is generated by an electronic speed controller (ESC). When ESCs are considered there are two options, ESCs with sensor input and ESCs without sensor input. Given that the motor chosen is sensorless a speed controller of the latter category is chosen. The controller that will be used is the SuperMicro Systems MX-3A speedcontroller [8] which is based on the SIL F330 MCU [9]. This ESC is chosen due to its low mass and small volume.

The motor is capable of an angular velocity between 100 and 30 000 $rpm$ with a speed controller, so a velocity of 15000 $rpm$ is chosen to be the nominal speed of the momentum wheel. PWM, short for pulse width modulation, is required for regulating the speed and thus the attitude of the femto-satellite and this will be covered by the command & data handling discussed in Chapter 12.

**Wheel Material**

Three different materials are considered for the construction of the momentum wheel. The 310 stainless steel is resistant to oxidation due to higher chromium content and is easily manufactured and obtained[10]. Aluminium 7000 series is commonly used in the spacecraft industry, has good properties against corrosion, is easily manufactured and is lighter than steel [34] [11]. An even lighter solution would be achieved by utilising beryllium. Beryllium has a higher elasticity than steel, has excellent thermal conductivity and is resistant to oxidation. It is also often used in femto-satellite construction and is generally a very desired material due to its very low density and relatively high Youngs Modulus. The downside of this material is that it is toxic and should be handled with care.[12]

Table 10.2: Flywheel material properties

| **Material** | **Density** $[kg/m^3]$ | **Yield Strength** $[MPa]$ |
|---|---|---|
| 310 stainless steel | 7750 | 205 |
| Aluminium EN AW-7010 | 2830 | 440 [13] |
| Beryllium | 1850 | 240 [14] |

**Final Wheel Sizing**

With Eq. (10.9) it is possible to calculate the required moment of inertia of a momentum wheel. In order to comply with the minimum required momentum storage a wheel moment of inertia of $7.4{\cdot}10^{-8} kgm^2$ is required. Disk shaped momentum wheels have a mass moment of inertia around their turning axis defined by Equation (10.10) [35]. Since the mass of the flywheel depends on the material density and the dimension of the flywheel it is also possible to express it in terms of material density and volume as seen in Equation (10.11). The volume of the flywheel can be depicted as a cylinder and is shown in Equation (10.12) [35].

$$I = \frac{m \cdot r^2}{2} \qquad (10.10) \qquad m = \rho_m V \qquad (10.11) \qquad V = \pi r_f^2 h \qquad (10.12)$$

Combining Equation (10.10), (10.11) and (10.12) the expression for mass moment of inertia is seen in Equation (10.13). With the inertia the radius and thickness can be varied for the flywheel and corresponding mass can be determined. As can be seen by Eq. (10.10) it is beneficial to maximise the radius of the momentum wheel since this will provide a higher moment of inertia a lower wheel mass.

$$I = \frac{\rho_m \pi r_f^4 h}{2} \qquad (10.13)$$

In Table 10.3 the sizes of momentum wheels with different material, radius, mass and thickness is given. A lower limit of 0.8 $mm$ for the thickness is set for manufacturability. From this table it is clear that the beryllium wheels are the lightest of all options. The wheel size of 13 $mm$ radius and 0.88 $g$ is chosen as a suitable option.

[7] Electro motor datasheet, `https://fmcc.faulhaber.com/resources/img/EN_0308_B_DFF.PDF`, retrieved on 9-06-2016

[8] SuperMicro MX-3A Datasheet, `http://www.hobbyking.com/hobbyking/store/__44315__SuperMicro_Systems_Brushless_ESC_3_0A.html`, retrieved on 14-06-2016

[9] SIL F330 Datasheet, `https://www.silabs.com/Support%20Documents/TechnicalDocs/C8051F33x.pdf`, retrieved on 14-06-2016

[10] 310 Stainless steel specifications `http://www.azom.com/article.aspx?ArticleID=966`, retrieved on 11-05-2016

[11] Aluminium 7010, `http://www.aubertduval.com/uploads/tx_obladygestionproduit/7010_GB.pdf`, retrieved on 11-05-2016

[12] Beryllium properties, `http://periodic.lanl.gov/4.shtml`, retrieved on 11-05-2016

[13] Aluminium 710 strength, `http://aviationmetals.net/products/item/316`, retrieved on 11-05-2016

[14] Beryllium strength, `http://www.azom.com/article.aspx?ArticleID=7646`, retrieved on 11-05-2016

Beryllium can be manufactured in sheets of 0.04" according to ESPI Metals [15]. The thickness of 0.89 mm is equal to 0.035". In order to reduce manufacturing costs a standard size of 0.04" will be taken. This will result in final wheels that are 13 $mm$ in radius, have a thickness of 1.016 $mm$ and a mass of 1 $g$.

These wheels were sized by making use of the required momentum which was created with the assumption that the centre of gravity deviates by $1cm$ from the geometric center. In reality this deviation is only $0.46cm$ meaning that the wheels are oversized. However up to this point no safety margins have been taken into account, thus it will be assumed that because a worst-case scenario is assumed everywhere and that the actual distance to the centre of gravity is less than what was assumed no further safety margins are required.

Table 10.3: Wheel parameters of different materials

| **Material** | **Wheel radius** $[mm]$ | **Mass** $[g]$ | **Wheel thickness** $[mm]$ |
|---|---|---|---|
| Steel | 8 | 2.31 | 1.48 |
| | 8.5 | 2.05 | 1.17 |
| | 9 | 1.83 | 0.92 |
| Aluminium | 11 | 1.22 | 1.13 |
| | 11.5 | 1.12 | 0.95 |
| | 12 | 1.03 | 0.80 |
| Beryllium | 12 | 1.03 | 1.23 |
| | 12.5 | 0.94 | 1.05 |
| | 13 | 0.88 | 0.89 |

The last thing that needs to be checked is whether the momemtum wheels are capable of detumbling the satellite within 25 seconds. The deployment will give the satellite a maximum worst-case angular velocity of:

$$\omega_{SC} = \frac{h_{SC}}{I_{SC}} = \frac{3.9 \cdot 10^{-6}}{0.03} = 0.00013 \frac{rad}{s}$$

The control torque that can be provided by the momemtum wheels is limited by the motors and is equal to 0.000013 Nm. The maximum angular acceleration then becomes:

$$T = I\alpha \Rightarrow \alpha = \frac{T}{I} = \frac{0.000013}{0.03} = 0.0004 \frac{rad}{s}$$

Countering the angular velocity of 0.00013 $\frac{rad}{s}$ will then take 0.3 seconds. This however does not re-point the femto-satellite back to its original orientation. How long this re-pointing will take can not be determined since it depends on the PID settings on the flight controller. It can however be safely assumed that this countering and re-pointing can be countered within 25 seconds.

## 10.5. Subsystem Overview

The attitude determination and control subsystem consists of sensors that are able to determine the position of the femto-satellite relative to the host spacecraft, the Kionix KXG03 IMU is chosen for this task. Three momentum wheels are used for maintaining three-axis control for imaging positioning. The ADCS will only stay active for the duration of the de-tumbling and imaging phase. The total mass of the system is 5.15 $g$ and the power consumption is equal to 0.201 $W$.

[15] ESPI Metals, `http://www.espimetals.com/index.php/online-catalog/349-Beryllium`, retrieved on 16-06-2016

# 11

## De-orbit Device

This chapter will elaborate on the active de-orbit device of the femto-satellite. This device will ensure that the femto-satellite will not end-up as space debris and extend the applicable range for similar future missions. First the requirements are explained, then the research in de-orbit devices is shown and finally the final de-orbit device is shown.

## 11.1. Subsystem Requirements

Space debris is a real issue for now and the future. So the femto-satellite will be designed such that it will de-orbit itself much quicker than the in regulations required 25 years as seen in requirement **TS-STH-SUS-01-A**. To extend the applicable range of the femto-satellite and make femto-satellites more attractive in general the two requirements have been set up. In this section an investigation in different de-orbiting systems is done and one is selected to be put on the femto-satellite.

**TS-SYS-POD-DOD-01-A** The femto-satellite shall be able to de-orbit within 25 years up to an orbital altitude of 1000 $km$.
**TS-SYS-POD-DOD-02** The femto-satellite shall be made detectable from the Earth after its operational lifetime.

Requirement **TS-SYS-POD-DOD-02** is satisfied by the fact that the FGAN and Teide Observatory can detect space objects at an altitude of $800km$ with a diameter of $2cm$ and $2-6cm$ respectively. Since the femto-satellite is $5cm$ wide the femto-satellite is detectable[13]. It is of importance since the femto-satellite can not communicate its status to Earth after it is leaving the host-spacecraft, so it needs to be tracked from the ground.

## 11.2. Investigation Into De-orbit Devices

First the Terminator Tape™ made by Tethers Unlimited, Inc. is investigated. Terminator Tape™ uses a conducting electrodynamic tether called Hoytether™, with a mass equal to 1% of the host spacecraft mass, which makes use of the Earth magnetic field to decelerate the spacecraft [36]. The current smallest size of this device is made for Cubesats[1], its properties are listed in Table 11.1.

Secondly the use of a propulsion is investigated. For de-orbiting from an altitude of $450km$ a $\Delta V$ of $116.2m/s$ is needed [18]. However, this means that the femto-satellite de-orbits directly after the burn, it could be sufficient to lower the altitude such that it de-orbits by natural causes quicker. For example with the $10.0g$ system with $10m/s$ it would reduce the orbit decay time by maximum 40%, resulting in a range of 875 to 83 days de-orbit time. Summarised data is given in Table 11.1.

The third option would be the gravity gradient tape [37], however no real developments or available products of this system could be found.

The fourth proposed system is the Gossamer Orbit Lowering Device (GOLD) developed by Global Aerospace Corporation, it involves a Kapton balloon that can be inflated to decrease the mass-over-area parameter $\beta$ and thus increasing the orbit decay rate [38]. The system mass is on average between 2.8% and 7.8% of the satellite's mass and for now theoretically as small as $60g$ on the $1kg$ CubeSat called PolySat-6. The advantage of this concept is that it does not use power after the device is deployed, so the battery only needs to provide power at the time of deployment. After contacting Global Aerospace Corporation it seemed theoretically doable, but further research needs to be done in combination with femto-satellites to determine the exact parameters. General parameters on the GOLD device can be seen in Table 11.1, where the mass is 7.8% of $100g$ based on the worst case average system mass.

As last the AEOLDOS (Aerodynamic End Of Life De-orbit System) is considered, but due to the weight and the petal-hub deploy system it will not be available in smaller sizes soon [39].

Based on this data a GOLD like de-orbiting and propulsion system are favourable due to their small size. However the GOLD system is far less complex than an integrated propulsion system and since it does not require any operational power and does not require the ADCS to work such a system is favourable. Since Global Aerospace Corporation could not give any information for now on the rescaling of the device for femto-satellite usage, a small investigation will be

[1] CubeSat Terminator Tape™, `http://www.tethers.com/SpecSheets/Brochure_CubeSatTermTape.pdf`, retrieved 3-6-2016

Table 11.1: Different de-orbit systems. For small satellites with an mass-over-area $\beta$ less than $100 kg/m^2$ at an altitude of $450 km$. Normal de-orbit time is $0.4 yr - 2.7 yr$ (based on solar radiation levels) [2].

| **De-orbit system** | **Mass** $[g]$ | **Volume** $[cc]$ | **Depl. power** $[W]$ | **Op. power** $[W]$ | **De-orbit time** $[yrs]$ |
|---|---|---|---|---|---|
| CubeSat Terminator tape | 83 | 53.95 | 0.9 | <0.9 | <0.5 |
| Propulsion | 10.0 | 4.3 | 0 | 0.0003 | 1.73 |
| GOLD | 7.8 | N/A | N/A | 0 | 0.03 |
| AEOLDOS | 372 | 400 | N/A | 0 | 0.01 - 1.6 |

done on similar technology (spherical inflatable de-orbit device), mainly based on a technical report from the Delft University of Technology and literature on the GOLD device [37, 38, 40].

## 11.3. Spherical Inflatable De-orbit Device

For now a Spherical Inflatable De-orbit Device (SIDD) is considered and investigated as an option to de-orbit the femto-satellite, since no thorough information was obtained on the GOLD system.

### 11.3.1. Balloon Sizing

First it is assumed that the femto-satellite is $100g$ and the smallest, worst case, frontal area facing forward with the velocity vector or to the sun is one side only and thus $0.05 \times 0.05 = 0.0025 m^2$. This leads to a $\beta$ of $40 kg/m^2$, this value needs to be as small as possible to de-orbit faster. For comparison, a satellite with a $\beta$ of $200 kg/m^2$ at an altitude of $450 km$ under maximum solar radiation de-orbits in 502 days, whilst a satellite with a $\beta$ of $50 kg/m^2$ under the same conditions only needs 157 days to de-orbit. [18] A way to increase $\beta$ is to decrease the area as explained before. This will be done with an inflatable balloon attached directly to the femto-satellite. Other options would be a cocoon or a towed configuration but those options are either too complex or bring higher risks than the directly attached balloon. [40] The material used will be Kapton of $6.35 \mu m$ thick with a density of $9 g/m^2$ like in the GOLD. The diameter of the balloon normally depends on within what time the system is required to be de-orbited, however for this design the mass of the de-orbit device is leading. Though the impact on the de-orbit time has to be sufficient. Therefore two different options are proposed. The first system has a balloon of just under $10g$, namely $9.5g$, which means the balloon has a radius of $0.29m$. The second system has a radius of $0.1m$ which will lead to a mass for the balloon of $1.13g$. These values are both found via calculating the area of the sphere and using the density of the used Kapton thickness. With the found values, predictions can be done to see what the impact is of the SIDD on the de-orbit time. The results can be found in Table 11.2. The simulation has been done with GMAT, using the atmospheric model MSISE90 and SMAD [18]. The de-orbit decay-time-over-mass for the balloon itself at 450 km for the $R = 0.1m$ is equal to 9.29 and for the $R = 0.29m$ is equal to 0.13. This means that the bigger the system is the more efficient it is per mass. From Table 11.2 can be seen that in any case with the de-orbit device the femto-satellite will de-orbit within 25 years (9125 days) at an altitude of 950 $km$, satisfying requirement **TS-STH-SUS-01-A** but not yet **TS-SYS-POD-DOD-01-A**.

Table 11.2: Amount of days till de-orbit ($130 km$) and the mass-over-area $\beta$ for each SIDD configuration. † indicates simulated with GMAT, ‡ indicates taken from SMAD.

| | **Time to de-orbit** $[days]$ | | | | **Satellite parameters** | | |
|---|---|---|---|---|---|---|---|
| SIDD | 450 km alt | 700 km alt | 900 km alt | 950 km alt | A $[m^2]$ | m$[kg]$ | $\beta$ $[kg/m^2]$ |
| Without | 120 † | 9884 ‡ | $>1.3 \times 10^5$ ‡ | $2.11 \times 10^5$ ‡ | 0.0025 | 0.1 | 40 |
| $R = 0.1m$ | 10.5 † | 470 † | 4002 † | 9100 † | 0.031 | 0.1 | 3.23 |
| $R = 0.29m$ | 1.2 † | 46.6 † | 490 † | 2131 † | 0.264 | 0.1 | 0.38 |

From the values found in Table 11.2, a SIDD of with a radius of $0.1m$ decreases the orbit decay time by a factor 11, thus satisfying the system requirement **TS-SYS-POD-07**. This factor is enough for the demonstration of technology and the decay rate shall be validated so it is indeed applicable up to the orbital altitude of $950 km$. Considering the fact that the device should be as light as possible, the SIDD with a radius of $0.1m$ is chosen. This means that the inflatable structure weights $1.13g$, a contingency margin is taken of 25%, leading to a mass of a round-off mass of $1.5g$. The volume of the not-inflated balloon is calculated with a packing factor of 5 like in the IDOD design. The surface area is again calculated with $R = 0.1m$, then multiplied with the thickness of $6.35 \mu m$, leading to a volume of $0.8cc$. Using the packing factor of 5 this leads to a volume of $4cc$. [40]

### 11.3.2. Balloon Storage

The storage system design will be lead by the required $4cc$ for the balloon and made of AL 2090-T83. Assuming the CGG will take up $1cc$ inside the storage, the needed volume inside the storage will become roughly $5cc$. The cool gas generator will be put on the backside of the storage, $8.8mm$ inside the storage, so it can feed the balloon with gas. Due to constraints for the layout the storage will have an internal dimension of $1.6 \times 1.6 \times 1.95$ centimetres to store

the balloon. The system will have a lid and opening system just as the IDOD system. Assuming a thickness for the AL 2090-T83 of $1mm$ will lead to an estimation mass just for the use of aluminium alloy of $5.08g$. From the IDOD system the hold down and release mechanism will weight about $3.75g$ assuming a smaller circuit board of just $1g$. It comprises two small resistors and a wire that can be melted with a simple command so the lid can be opened. For the SIDD system it will be scaled down to about $0.5cc$. This means that the SIDD will take up a total of $9.85cc$. The IDOD also has a deploy sensor, but this is left out for the SIDD. Observations from Earth should be able to verify the deployment. The SIDD will have a spring for opening the lid, like the IDOD. However the lid should open sufficiently, to allow the balloon to deploy, this means the SIDD has to stick out of the side by the hinge thickness so the lid can be rotate 180 degrees. [40]

### 11.3.3. Inflation System

For inflation of the device a gas is needed which will be generated by a Cold Gas Generator (CGG) developed by TNO with a volume of $3.4cc$ of which $1cc$ inside the storage. The inflation for the GOLD required about $135g$ gas total for a $37m$ diameter balloon, which means the femto-satellite system will require much less. About $2.14\times10^{-5}g$ for $R = 0.1m$. No specific gas is mentioned for the GOLD design, Nitrogen or Oxygen however seem reasonable options since they can be stored in micro cool gas generators[2]. The temperature range of the CGG is $-10$ to 40 degree Celsius and is the only leading temperature range in the system[3]. [38] The CGG from TNO is about $2g$[4], it produces $174.75mg$ Nitrogen or $200mg$ Oxygen, which is too much for the mission. However there might be options to reduce the mass and the gas released by the CCG, but for now this one is taken. It uses about 2.2 Ampere and 4.3 Volts for 4 to 10 seconds[5]. This amount of power required is too high for main battery of the system. So two small batteries of each $5W-5.7W$ with a length of $3.6cm$, a volume of $1.3cc$ and a mass of $3g$ will be added[6]. The connection of the CGG is assumed to be placed behind the middle of the storage and connected onto the PCB. No cabling is needed, unlike the IDOD. It is also assumed no special commands needs to be send to the CGG, just applying the current and voltage should be enough. It can be shown in similar matter as has been done for the IDOD that for Nitrogen the pressure inside the envelope will be $0.04bar$ after fully igniting the CGG [40], this leads to a hoop stress of $29MPa$ which is below the yield stress of $69Mpa$ at 23°$C$ up to $46MPa$ which is above the yield stress of $41MPa$ at 200°$C$[7], but this latter temperature is not expected to be reached. Maximum temperature is 150°$C$. This leaves this parts mass at a total of $2g$.

### 11.3.4. Subsystem Overview

The total mass, power and costs can be found in Section 17.4. It should be noted that this system is the result of an investigation in the GOLD and IDOD together to get an estimation of what the GOLD would weight. Since the GOLD is fully developed it should be used over the SIDD, since the SIDD is not an actual completely designed de-orbit device. No extra contingency margins have been applied since the values found for the IDOD already had contingencies. The SIDD for a orbital altitude of $1000km$ has to be done in another iteration, but the de-orbit up to an altitude of $950km$ is covered with the current design. Costs are based on found values in stores and scaled down to the amount of material needed, so no bulk buying is considered unless specified. Batteries belong to the power part for costs and mass and are included in brackets. The storage is made of AL 2090-T83 which for this amount of material costs less than 1 Euro, manufacturing can be deep drawn and is estimated to cost about 100 Euro. The Kapton film needs to be custom ordered but a two times as thick Kapton film as needed can be bought in 2 pieces of $300\times300cm$ for 305 Euro[8]. Only $0.125cm^2$ is needed for the envelop, but it is expected that some Kapton is wasted in the process. The cool gas generator is estimated by ISIS to cost about 4000 Euro per unit [9], getting cheaper if bought in bulk. When the de-orbit device is activated, beforehand the trajectory should be simulated and crosschecked with the known objects to see if any collision might occur. This is needed to reduce the risk of damage to operating satellites or generating additional space debris. This system can also be used to accelerate the decay rate beyond the 25 years regulation when in lower orbits.

---

[2] The Cool Gas Generator, `http://cgg-technologies.com/cool-gas-generator/`, retrieved 9-6-2016

[3] The CGG, `http://www.isispace.nl/brochures/ACQ-CGS-PRM-001%200.15%20nL%20Micro%20CGG%20flyer.pdf`, retrieved 14-6-2016

[4] 0.15 nL N2 Micro-Cool Gas Generator, `http://www.cubesatshop.com/index.php?page=shop.product_details&flypage=flypage.tpl&product_id=120&category_id=21&option=com_virtuemart&Itemid=99`, retrieved 20-5-2016

[5] Interface Control Document 0.15 nL N2 Micro Cool Gas Generator, `http://www.isispace.nl/brochures/ACQ-CGS-RP-001%20Interface%20Control%20Document%200.15%20nL%20N2%20Micro%20Cool%20Gas%20Generator.pdf`, Retrieved on 01-06-2016

[6] Turnigy nano-tech Cell, `http://www.hobbyking.com/hobbyking/store/__23310__Turnigy_nano_tech_90mah_1S_15C_Round_Cell.html`, Retrieved 10-6-2016

[7] DuPont Kapton film, `http://www.dupont.com/content/dam/dupont/products-and-services/membranes-and-films/polyimde-films/documents/DEC-Kapton-summary-of-properties.pdf`, retrieved 24-6-2016

[8] DuPont Kapton 13$\mu m$, `http://www.goodfellow.com/catalogue/GFCat4J.php?ewd_token=W6WjRlZxNFjCusgamzHMikZEKbsYBe&n=FZrCleUcrhb80tXI31ww3TjDjfD6dY`, Retrieved 15-6-2016

[9] Sales Engineer at ISIS, contacted on 14-06-2016

# 12

## Command & Data Handling System

In this chapter the design of the command and data handling subsystem is presented. First the requirements put on the system are defined in sections 12.1. Second, the system architecture is determined in section 12.2. The central processing unit is selected in section 12.3 and finally the mass storage interface is given in section 12.5. The chapter is concluded with a summary of the system in section 12.6.

## 12.1. Subsystem Requirements

The command and data handling subsystem will be performing the following tasks for all the other subsystems:
**TS-SYS-POD-CDH-01** The C&DH subsystem shall process the ADCS sensor input data and send commands to the ADCS actuators.
**TS-SYS-POD-CDH-02** The C&DH subsystem shall process incoming commands from the host from the communications system.
**TS-SYS-POD-CDH-03** The C&DH subsystem shall send commands to the payload and store the data that the payload gathers.
**TS-SYS-POD-CDH-04** The C&DH subsystem shall send the payload data to the communications subsystem to be transmitted to the host spacecraft.
**TS-SYS-POD-CDH-05** The C&DH subsystem shall monitor the power subsystem and switch operation modes if problems occur.
**TS-SYS-POD-CDH-06** The C&DH subsystem shall communicate with the de-orbiting device and tell it when to de-orbit.

The command and data handling subsystem will consist of a processor and data storage unit that will need to interface with all the subsystems on board of the femto-satellite. This is why a set of requirements will be created for the interface with the subsystems.

**TS-SYS-POD-CDH-07** The C&DH subsystem shall be able to interface with the ADCS sensors, which use the $I^2C$ communication protocol.
**TS-SYS-POD-CDH-08** The C&DH subsystem shall be able to interface with the ADCS actuators which require a $PWM$ signal.
**TS-SYS-POD-CDH-09** The C&DH subsystem shall be able to interface with the payload, which uses $I^2C$ as the input protocol and $CSI-2$ as the output protocol.
**TS-SYS-POD-CDH-10** The C&DH subsystem shall be able to interface with the communications subsystem which uses $SPI$ and $I^2C$ as a protocol.
**TS-SYS-POD-CDH-11** The C&DH subsystem shall be able to interface with the de-orbiting device which requires a GPIO-high signal.
**TS-SYS-POD-CDH-12** The C&DH subsystem shall be able to receive data from the payload with a data rate of 111.02 $MB/s$.
**TS-SYS-POD-CDH-13** The C&DH subsystem shall have a storage capacity of at least 42 $GB$.
**TS-SYS-POD-CDH-14** The C&DH subsystem shall transmit the data to the communication system with a data rate of 6.75 $MB/s$.
**TS-SYS-POD-CDH-15** The C&DH subsystem shall be able to interface with the power monitor, which uses $I^2C$.

In summary this means that the device will require the following interfaces:

- 2x Interface with the Inter-Integrated Circuit ($I^2C$) protocol
- 1x Interface with the Camera Serial Interface 2 ($CSI-2$) protocol
- 1x SPI
- 3x PWM output
- 1x GPIO port

## 12.2. System Architecture

When it comes to the architecture of the C&DH system there are three main options, which can be seen in Figure 12.1.[2] For the design of the femto-satellite a combination between the *Ring* and *Bus* structure is going to be used.

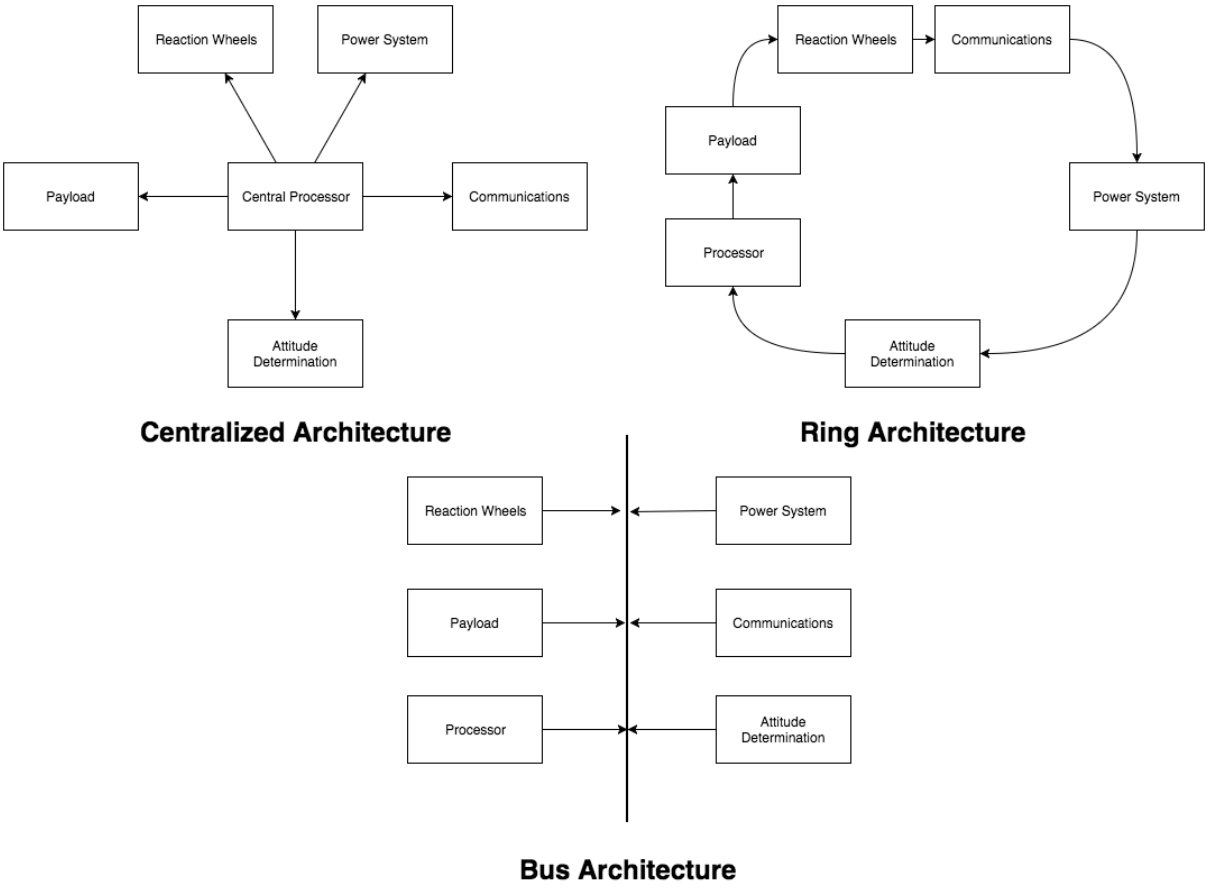


Figure 12.1: Three command and data handling architectures [2]

Due to the usage of the $I^2C$ protocol on many of the connected components a bus-structure is automatically created since $I^2C$ makes use of two communication lines (SDA & SDL), meaning that all components are connected to a shared bus. However within subcomponents, like for example the payload there are interconnections using other protocols. The camera is connected using $I^2C$ but the output of the camera will need to loop through other components to translate it to a useful signal before it gets delivered to the storage device. These components are not all directly connected to the central bus.

With the architecture chosen the list of components will need to be determined, this is done by looking at each of the subsystems and see what they require. The C&DH system is separated into three categories: processing, payload data gathering and mass storage.

## 12.3. Data Processing

In order to perform the processing on the femto-satellite a micro controller will need to be chosen. This selection is presented in this section. The processing unit is only tasked with processing the femto-satellite attitude and sending commands to the camera. This is due to the fact that the payload data storage and transmission is handled by a separate USB controller and a flash storage manager which has a smaller micro controller built-in. (see section 12.5).

Sending commands to the camera is a very trivial task and requires very little processing power, it just needs to be timed. The ADCS system requires the processing of the IMU data and the processing of the camera-input when required. As a reference the ADCS of the *Delfi N3XT* femto-satellite is taken since it has a similar set-up for the ADCS with the addition of magnetorquers.[1]

The Delfi N3XT uses a micro controller based on the ARM9 architecture that is clocked at 400 $MHz$. For the femto-satellite a similar clock frequency is taken. The decision had to be made between an 8-bit micro controller and a 32-bit micro controller. If an 8-bit controller is used it is only possible to calculate the angular orientation with an

[1] Delfi N3XT ADCS, `http://www.delfispace.nl/delfi-n3xt/attitude-determination-and-control-subsystem`, retrieved on 08-06-2016

accuracy of 1.4° which when combined with gyroscope bias and possible inaccuracies in the pointing algorithm using the camera makes the system very inaccurate. This is why 32-bits of accuracy is used.

After all considerations are taken into account the following demands are put on the central processing unit:

1. Power consumption as low as possible
2. A clock frequency of approx. 400 $MHz$
3. Sufficient interface capabilities.

In Table 12.1 two possible candidates are listed from the Atmel corporation which is also known for the microprocessor used in the Arduino platform. Both of these meet the demands set above but the **SAMA5D31** uses less power, which means that this is the best choice for the platform. This processor is larger and a little bit heavier but given that this difference is marginal the preference is given to the lower power consumption vs the lower size. It should be noted that the **SAMA5D31** can also run at higher frequencies up to 600 $MHz$ which means that the core clock can be temporarily increased during high-intensity manoeuvres like the deployment or camera-edge detection cycles.

Table 12.1: Microprocessor candidates
*Mass estimated using density of silicon

| | **Mass** [$g$] | **Size** [$mm \times mm \times mm$] | **Core speed** [$MHz$] | **Voltage** [$V$] | **Current** [$mA$] | **Power** [$mW$] |
|---|---|---|---|---|---|---|
| **Atmel AT91SAM9G15**[2] | 0.4* | 12×12×1.2 | 400 | Core: 1.2<br>IO: 3.3 | 109 | ≈248 |
| **Atmel SAMA5D31**[3] | 0.47 | 16×16×0.8 | 396 | Core: 1.2<br>IO: 3.3 | 90 | ≈205 |

## 12.4. Payload Data Acquisition

According to requirement **TS-SYS-POD-CDH-03** and **TS-SYS-POD-CDH-04** the C&DH subsystem must be able to interact with the payload by sending commands and receiving data. This data must then be relayed to the communications system.

In section 8.4 the payload camera has been selected. This camera is based on a Sony CMOS sensor, which uses the D-PHY CSI-2 protocol.[4] This protocol allows for the fast transfer of imaging data which is required for high-resolution cameras like the one selected. This protocol supports very high speeds but does not interface with storage or communication directly and thus has to be translated.

The processing of this signal will be done by utilising the *CYUSB306X* module which is able to convert the CSI-2 signal to a USB rev3.0 or USB rev2.0 compliant signal so that it can be sent to the mass-storage device and the communications array. The specifications for this device are in Table 12.2. The USB rev2.0 interface can not be used since it is too slow (480 $Mb/s$) and thus the USB3.0 interface is used which can run at 5 Gbps maximum.

## 12.5. Mass Storage

In order to provide mass storage to the system a set of components are required. In order to make sure that the main processor is relieved as much as possible from this task all storage from the payload will not go through the processor, freeing up processing time for other systems.

In order to achieve this separation of systems the architecture as depicted in Figure 12.2 is used.

[2] AT91SAM9G15 Datasheet, `http://www.atmel.com/Images/Atmel-11052-32-bit-ARM926EJ-S-Microcontroller-SAM9G15_Datasheet.pdf`, retrieved on 09-06-2016

[3] SAMA5D31 Datasheet, `http://www.atmel.com/images/Atmel-11121-32-bit-Cortex-A5-Microcontroller-SAMA5D3_Datasheet.pdf`, retrieved on 09-06-2016

[4] Sony Sensor Sheet, `https://pro.sony.com/bbsc/assetDownloadController/FCB-Micro-print-ready-brochure.pdf?path=Asset%20Hierarchy%24Professional%24SEL-yf-generic-153703%24SEL-yf-generic-153736SEL-asset-478893.pdf&id=StepID%24SEL-asset-478893%24original&dimension=original`,retrieved on 09-06-2016

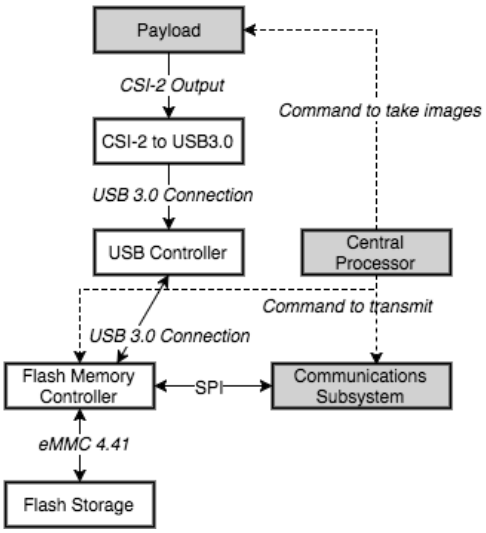


Figure 12.2: The mass storage architecture

The camera is capable of generating 2.33 pictures per second at 48 MB/picture, as seen in section 8.7. This means that the required storage speed of the entire system is $2.33 \cdot 48 = 112 MB/s$. The $CSI-2$ output supports a speed of up to 125 $MB/s$ which is sufficient. The required speed from the camera to the storage device must always be above this value.

The components that are selected for the mass-storage device are listed in Table 12.2. These components all have transfer/storage speeds that are greater than the required 112 $MB/s$. The *CSI-2 to USB3.0* interface was already discussed in section 12.4. The masses for these components are not publicly available so the assumption is made that they are a solid block of silicon.

Table 12.2: Mass storage component summary
*Mass estimated using density of silicon

| | **Mass** $[g]$ | **Size** $[mm \times mm \times mm]$ | **Voltage** $[V]$ | **Current** $[mA]$ | **Power** $[mW]$ | **Task** |
|---|---|---|---|---|---|---|
| **CYUSB306X**[5] | 0.186* | 10 × 10 × 0.8 | **Core**: 1.2<br>**IO**: 3.3<br>**USB**: 5 | **Core**: 0.5583<br>**IO**: 0.0045<br>**USB**: 4.672 | 24.0 | CSI-2 to USB3.0 |
| **TUSB8041**[6] | 0.188* | 9 × 9 × 1 | 3.3 | 0.015 | 0.0495 | USB Controller |
| **CYUSB302X**[7] | 0.186* | 10 × 10 × 0.8 | **Core**: 1.2<br>**USB**: 5 | **Core**: 200<br>**USB**: 60 | 540 | Flash Memory Controller |
| **iNAND 7030**[8] | 0.418* | 11.5 × 13 × 1.2 | 1.8 | 1.8 | 630 | 64 GB Flash Storage |

The SPI connection that is between the flash memory controller and the communications subsystem is limited by the frequency at which the memory controller works. SPI data transfer requires two pulses between bytes. [9] The selected controller has a frequency of 33 $MHz$, which means that the effective number of bytes that can be transmitted per second is $33/2 = 16.5 MB/s$ which is more than the communications subsystem can transmit and thus forms no bottleneck.

## 12.6. Subsystem Overview

The command and data handling subsystem has now been fully designed. In Figure 12.3 the command and data handling diagrams is presented. This will give an overview of the command and data handling subsystem on board of the subsystem. The final mass of the command and data handling subsystem is 1.454 g, the volume is 0.6252 $cm^3$ and the power consumption is 1.4 $W$.

[5] CYUSB306X Datasheet, `http://www.cypress.com/file/133591/download`, retrieved on 07-06-2016
[6] TUSB8041 Datasheet, `http://www.ti.com/lit/ds/symlink/tusb8041.pdf`, retrieved on 07-06-2016
[7] CYUSB302X Datasheet, `http://www.cypress.com/file/123816/download`, retrieved on 08-06-2016
[8] Sandisk iNAND 7030 Datasheet, `http://www.mouser.com/ds/2/669/iNAND_06012016_SDIN9DW4-948140.pdf`, retrieved on 08-06-2016
[9] SPI with Arduino, `http://arduino.stackexchange.com/questions/16348/how-do-you-use-spi-on-an-arduino`, retrieved on 09-06-2016

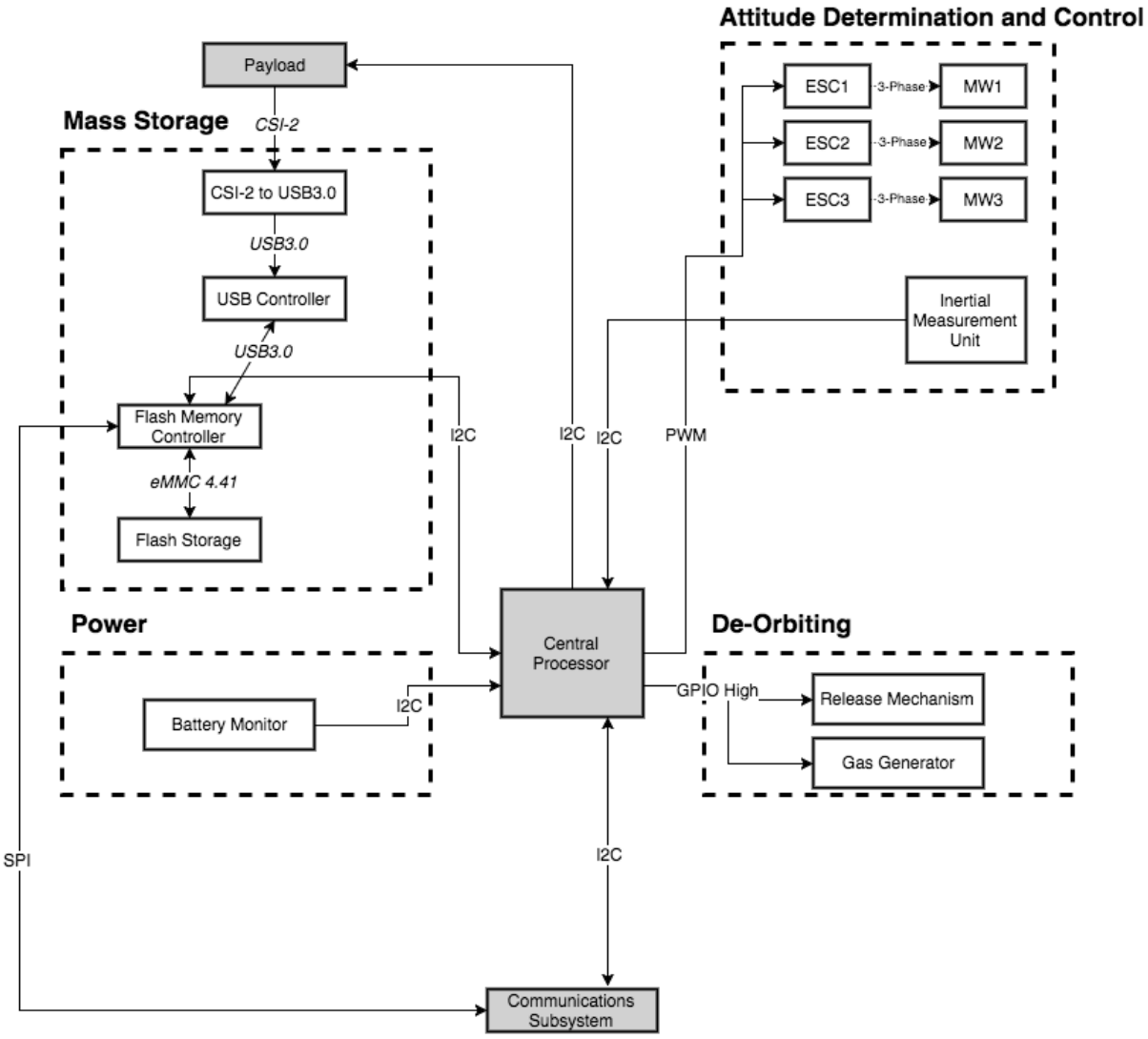


Figure 12.3: Command and Data Handling diagram

# 13

## Power System

This chapter discusses the power subsystem. The requirements for the subsystem are set in Section 13.1. After the requirements are known, first in Section 13.2 the power budget is set up for the whole femto-satellite. Then Subsection 13.3 will elaborate more on the possibility of storing the power using a non-rechargeable power system. Afterwards Section 13.4 will show the architecture of the subsystem. Finally Section 13.5 an overview of the subsystem is given. For a complete overview and steps leading to the final iteration design Chapter D in the appendices can be viewed.

## 13.1. Subsystem Requirements

The power subsystem shall be able to meet the following set of requirements. The numbers have been filled in during the design of the power subsystem.

**TS-SYS-POD-POW-01-A** The power subsystem shall deliver a total energy of 3.69 $Wh$ to the femto-satellite.
**TS-SYS-POD-POW-04-A** The power subsystem shall be able to power the femto-satellite for 6749 $s$.
**TS-SYS-POD-POW-05** The power storage shall have a safety margin of 15 %.
**TS-SYS-POD-POW-06** The power subsystem shall be able to provide up to 2.79 $W$.
**TS-SYS-POD-POW-07** The power subsystem shall be able to power the de-orbiting device.
**TS-SYS-POD-POW-08** The power subsystem shall provide the specific voltage to each component.
**TS-SYS-POD-POW-09** The power subsystem shall have no power leakage before deployment.

## 13.2. Power Budget

In order to size the budget an initial estimation of the power consumption per subsystem will be made. This gives an insight to the required power the whole system should provide. The operational lifespan of the femto-satellite consists of six operation phases: Initialisation, deployment, de-tumbling, imaging, transmitting and de-orbiting phase. It is divided in phases due to the significant changes in distance to the host-spacecraft. Only during the first part of its orbit after release is the femto-satellite in range for the payload. In Table 13.1 the power consumption of different subsystems and their total for the durations is stated for the six phases. The duration of different phases are also shown in the same table and from this data the total power can be derived. A separate battery is needed for the de-orbiting device due to the high power requirement. However this is separated from the main battery and other subsystems and is only activated at the end of its operations.

Table 13.1: The amount of power consumption of each operational phase (*is only for the secondary battery)

| **Subsystem** | **Initialisation** [$mW$] | **Deployment** [$mW$] | **De-tumbling** [$mW$] | **Imaging** [$mW$] | **Transmitting** [$mW$] | **End of life** [$mW$] |
|---|---|---|---|---|---|---|
| ADCS | 201 | 201 | 201 | 201 | 0 | 0 |
| C&D | 1400 | 1400 | 1400 | 1400 | 1400 | 1400 |
| Communications | 460 | 0 | 0 | 0 | 460 | 0 |
| Payload | 600 | 0 | 0 | 600 | 0 | 0 |
| De-orbit | 0 | 0 | 0 | 0 | 0 | 10500* |
| **Total** | **2661** | **1601** | **1601** | **2201** | **1860** | **1400** |

## 13.3. Non-Rechargeable Power Solution

Since the spacecraft lifetime is very short a non-rechargeable battery is used since these have a much higher energy density compared with rechargeable batteries. By calculating the amount of power used by all the subsystems and knowing the lifespan of the femto-satellite, it is possible to select a single or set of batteries for the power system. Because it is possible to provide this amount of power with a primary battery, separate power generation would be obsolete. A battery monitor, the DS2745, will be used to continuously know the capacity of the battery system and to be able to tell the board computer the state of the battery [1].

[1] Smart battery monitor, `https://datasheets.maximintegrated.com/en/ds/DS2745.pdf`, retrieved on 2-06-2016

### 13.3.1. Main battery

There are a few different options for the type of batteries that can be used where the largest selection criteria are the energy capacity and the continuous current it can provide.

Because of the limitations set on the mass and the relatively high continuous current requirement, lithium manganese dioxide batteries are preferred for the non-rechargeable power source[2]. A list has been made to provide possible non-rechargeable batteries which can be seen in Table 13.2.

Table 13.2: Non-rechargeable battery selection

| **Type** | **Model** | **Nominal Voltage** $[V]$ | **Nominal Capacity** $[mAh]$ | **Continuous current** $[mA]$ | **Mass** $[g]$ | **Dimensions** $[mm]$ | **Power density** $[mW/g]$ | **Temperature range** $[^{\circ}C]$ |
|---|---|---|---|---|---|---|---|---|
| Li/MnO2 | CR17335 [3] | 3 | 1400 | 1500 | 20 | 17∅ x 34.5 | 210.0 | -40 – +60 |
| Li/MnO2 | CR123A [4] | 3 | 1500 | 1000 | 16 | 17.1∅ x 34.5 | 281.3 | -30 – +60 |
| Li/MnO2 | CR17450 [5] | 3 | 2400 | 1000 | 23 | 16.5∅ x 44.5 | 313 | -40 – +60 |

When the voltages of different components of other subsystems are not equal to the nominal voltage of the battery, buck-boost converters [6] are used to regulate the voltage. A step-down converter [7] is required to reduce the voltage to 1.2V for components of the C&DH. Because of these conversions a 5% increase of power is added to the total usage because many components require a converter. A 15% safety margin is added to the battery capacities due to temperature fluctuations and self-discharge if the hibernation time is long. Now the total power consumption per operating phase can be updated and is seen in Table 13.3. The battery CR123A meets the requirements and has been chosen to be the main battery. The total times for the imaging and transmitting phase are dependent on each other due to the data rate of the communication, payload and command and data handling subsystems. The larger the amount of pictures taken, the longer it takes to send them all to the host-spacecraft and thus will lead to a higher power consumption. The current ratio between the imaging and transmitting phase duration is optimal to keep the 15% safety margin. The time specified in Table 13.3 is the upper boundary for the imaging to stay within the capacity of the main battery.

Table 13.3: Operational phases with their corresponding time and power usage

| **Operational Phase** | **Power consumption** $[mW]$ | **Time** $[s]$ | **Total energy** $[mWh]$ |
|---|---|---|---|
| Initialisation | 2794 | 10.2 | 7.9 |
| Deployment | 1681 | 7 | 3.3 |
| De-tumbling | 1681 | 30 | 14 |
| Imaging | 2311 | 442 | 283.7 |
| Transmitting | 1953 | 6250 | 3390.6 |
| De-orbiting | 1470 | 10 | 4.1 |

### 13.3.2. Secondary Battery

For the de-orbiting device a separate power source is needed because the main battery is unable to provide enough power. Two high C-rate batteries that can provide up to 11 $W$ are chosen for their low mass and high discharge rate [8]. They will be on a separate circuit and are only activated at the end of the femto-satellite's operational lifespan. An additional battery monitor will be added to the secondary battery to know the state of the battery during release from the host. More information can be found in Chapter 11 about de-orbiting.

### 13.3.3. Activation from Host

A small switch is placed between the main battery and the rest of the system. This will be activated before release from host by a rod actuator built into the deployment system. This is done using a simple switch with a pin plunger,

[2] Li/MnO2 advantages, `http://www.powerstream.com/LiPMnO2.htm`, retrieved on 6-06-2016

[3] CR17335 Battery datasheet, `http://www.voltec-sunmoon.com/cgi/search-en.cgi?f=product_en+product_en1_1_&id=19038&t=product_en_1_`, 6-06-2016

[4] CR123A Battery datasheet, `http://www.vitzrocell.com/sub04/product_list.php?ca_id=40&id=10`, retrieved on 6-06-2016

[5] CR17450 Battery datasheet, `http://www.vitzrocell.com/sub04/product_list.php?ca_id=40&id=12`, retrieved on 6-06-2016

[6] Buck-boost converter datasheet, `http://cds.linear.com/docs/en/datasheet/3533fb.pdf`, retrieved on 8-06-2016

[7] Step-down converter datasheet, `http://cds.linear.com/docs/en/datasheet/340612fa.pdf`, retrieved on 8-06-2016

[8] Battery datasheet, `http://www.hobbyking.com/hobbyking/store/__23310__Turnigy_nano_tech_90mah_1S_15C_Round_Cell.html`, retrieved on 10-06-2016

the D2F ultra sub-miniature basic switch which will add 0.5 $g$ to the total mass,[9] and will be activated before release using an electric cylinder rod actuator, the ERD06.[10] The actuator will be powered by the host-spacecraft. It will be positioned and programmed to extend the rod and press the switch 10.2 seconds before release. This will give the system adequate time to start up and be ready for operations and is limited by the spin up time of the momentum wheels. During this time everything is on to perform a test on each component before deploment.

### 13.3.4. Degradation

If the femto-satellite does not deploy for several years, the internal leakage of power might drain the battery such that the operational lifespan will not be reached. For maximum retention of the battery if the femto-satellite has a long hibernation duration before deployment, a physical disconnection mechanism will be present between the battery and the whole femto-satellite bus. This mechanism should keep the current from flowing into the different systems of the femto-satellite. This needs to be done because even if it is inactive there will be a very small consumption of power by the electrical components. (leakage current) The self-discharge rate of the battery itself is less than 2% per year so this is not a large factor if the hibernation time is long [11].

## 13.4. Power Architecture

In this section the architecture is detailed for the chosen design. An electrical block diagram, which can be seen in Figure 13.1, gives the interaction of different parts of subsystems with the power source. The de-orbiting module is separated from the main architecture.

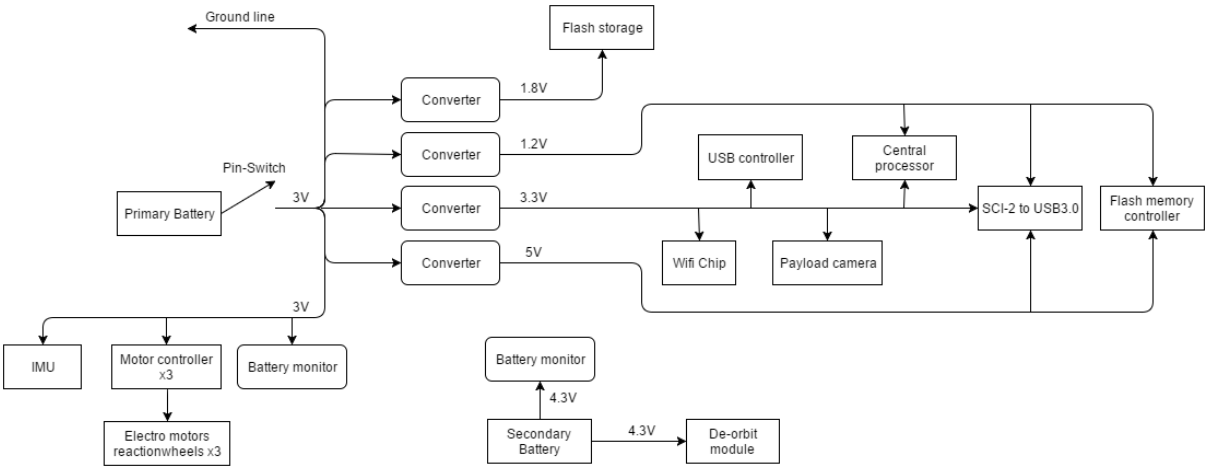


Figure 13.1: The electrical block diagram specifying the voltages of different parts

## 13.5. Subsystem Overview

Due to the short operational lifespan of the mission a non-rechargeable power solution is chosen for simplicity and cost efficiency. It will consist of a main battery and 4 converters to change the voltage to the required one for each subsystem. A switch is placed between the main battery and the rest of the circuit that connects shortly before release so the whole system can start up. A separate battery set is used for activating the de-orbiting device due to high power demand. Battery monitors are used to check the state of the batteries during operation. Connections are needed to provide power from the power source to the components of each subsystem. The total mass of the subsystem is 24 grams. See Section 17.4 for the mass and cost breakdown of all the individual parts.

[9] Switch datasheet, `https://www.omron.com/ecb/products/pdf/en-d2f.pdf`, retrieved on 10-06-2016

[10] Actuator datasheet, `http://www.tolomatic.com/products/product-details/erd-low-cost-electric-cylinders-for-pneumatic-cylinder-replacement#/features-options`, retrieved on 13-06-2016

[11] Battery specification, `http://www.vitzrocell.com/sub04/product_list.php?ca_id=40&id=10`, retrieved on 03-06-2016

# 14

## Thermal Control System

For successful operation of the femto-satellite, design of the thermal control subsystem is crucial. Many components, especially the batteries and the camera, have to be kept within a narrow temperature range. This can be achieved by applying appropriate coatings or foil. In Section 14.1 the thermodynamic model that was developed to model the satellite's temperature evolution is described. Later this model is verified by comparing it to the reference values for a sphere in Section 20.3.1 and validated with FUNcube telemetry in Section 20.3.1. The requirements of the thermal system are established and the mission profile is explained. Based on these the thermal design is given in the final section.

## 14.1. Thermodynamic Model

The temperature of the satellite is determined by the incoming and outgoing radiation as well as the internal power dissipation. As the satellite has a heat capacity, it takes time for the temperature to change.

For the thermodynamic analysis the femto-satellite is taken as a uniform, perfectly conducting mass. Also the orbit is assumed circular. For simplicity it is assumed to be a sphere with the same surface area as the actual satellite. It is not divided into nodes with different temperatures due to the small size of the satellite. This is the first thermal analysis of the system so further on in the design a more detailed thermal model can be developed. For now adequate margins on the temperature limits are taken into account.

The incoming radiation is composed of solar radiation, radiation from the sun reflected off Earth and infrared radiation coming from Earth. They are given by Equations (14.1) to (14.3)[2][p.454].

$$Q_{solar} = \alpha I_{solar} A \tag{14.1}$$

$$Q_{albedo} = \alpha I_{solar} \rho_{albedo} F_{albedo} A \tag{14.2}$$

$$Q_{EarthIR} = \epsilon I_{EarthIR} F_{EarthIR} A \tag{14.3}$$

Here the $Q$ are the incoming heats in $W$, the $I$ are the incoming radiations, $\alpha$ is the satellite's absorptivity, $\epsilon$ is its emissivity, $\rho_{albedo}$ is the Earth's albedo and $A$ is the projected area, i.e. a circle or one fourth of the total surface area. The values that apply for Earth orbit are given in Table 14.1. Furthermore $F$ are the view factors which are given by Equation (14.4) [41].

Table 14.1: Heat radiation environment around Earth [2][p.455]

| Parameter | Value | Unit |
|---|---|---|
| $I_{solar}$ | 1420 | $[W/m^2]$ |
| $\rho_{albedo}$ | 0.265 | [-] |
| $I_{EarthIR}$ | 231 | $[W/m^2]$ |

$$F_{albedo} = F_{EarthIR} = \left(\frac{R_E}{a}\right)^2 \tag{14.4}$$

Here $R_E$ is the radius of the Earth and $a$ is the satellite orbit's semi-major axis.

For internal power dissipation, the total power consumption of the satellite is used. This is a simplification as some power leaves the femto-satellite by radiation. This lost power is small however; it is only about 0.03 $W$ for the femto-satellite communication.[1] All other power is eventually converted to heat inside the femto-satellite.

The power radiated away from the satellite depends on its temperature:

$$Q_{out} = \epsilon \sigma A_S T^4 \tag{14.5}$$

where $\sigma$ is the Stefan-Boltzmann constant ($5.670\,51 \times 10^{-8}\ W/m^2K^4$), $A_S$ is the satellite's surface area and $T$ is its temperature.

[1] ESP8266EX datasheet, `https://cdn-shop.adafruit.com/product-files/2471/0A-ESP8266__Datasheet__EN_v4.3.pdf`, retrieved on 08-06-2016

Adding up these heat flows gives the total heat flow towards the satellite:

$$Q = Q_{solar} + Q_{albedo} + Q_{EarthIR} + Q_{diss} - Q_{out} \tag{14.6}$$

Finally, the temperature change $\Delta T$ over a short time period $\Delta t$ is given by:

$$\Delta T = \frac{Q\Delta t}{mC} \tag{14.7}$$

where $m$ is the satellite's mass and $C$ is its specific heat in $J/(kgK)$.

These equations where implemented into a Python code with time step $\Delta t = 10s$. This code also takes into account eclipse times. During eclipse $Q_{solar}$ and $Q_{albedo}$ are zero.

## 14.2. Subsystem Requirements

To establish the thermal requirements, the other subsystem designers have to be consulted. The temperature ranges of various components are given in Table 14.2.

By using Table 14.2, the requirements on temperature floor and ceiling can be established. The table shows the different temperature ranges for each of the parts. Here it is seen that the camera during operation has the most limiting temperature range, which is from minus 5 until 50 $^\circ C$. The camera will only be operational for 9.2 minutes. So this minimum temperature is not leading for the whole mission duration. During the communication phase of the mission the camera is offline. So the leading temperature range for this phase is from -20 to 60 $^\circ C$. The cold gas generator of the de-orbit device has a range of -10 to 40 $^\circ C$. When the de-orbit device is activated is dependent on the temperature of femto-satellite. So the internal temperate should be in the temperature range of the de-orbit device to be able to deploy it.

In addition a margin of 10 $^\circ C$ is taken to account for uncertainties in the model and an uneven temperature distribution across the satellite. The magnitude of 10 $^\circ C$ is standard in the thermal control discipline. Furthermore the FUNcube telemetry in Figure 20.3 shows that the temperature differences across the satellite can be up to $\pm 12^\circ C$, however since the femto-satellite is smaller than that, the temperature differences are also expected to be smaller. Taking the ranges from the table and applying the margin leads to the following requirements:
**TS-SYS-POD-TC-01** The femto-satellite shall not get colder than -10 $^\circ C$ during its operational lifetime while the camera is offline.
**TS-SYS-POD-TC-02** The femto-satellite shall not get colder than 5 $^\circ C$ during the time it takes pictures.
**TS-SYS-POD-TC-03** The femto-satellite shall not get warmer than 50 $^\circ C$ during its operational lifetime while the camera is offline.
**TS-SYS-POD-TC-04** The femto-satellite shall not get warmer than 40 $^\circ C$ during the time it takes pictures.

Table 14.2: Temperature ranges of various components

| Component | $T_{min}[^\circ C]$ | $T_{max}[^\circ C]$ |
|---|---|---|
| **Payload** | | |
| Samsung S6 Camera Operational [2] | -5 | 50 |
| Samsung S6 Camera Storage [3] | -20 | 60 |
| **Communication** | | |
| ESP8266 wifi module [4] | -40 | 125 |
| **ADCS** | | |
| IMU Xsens MTi Sensor[5] | -40 | 85 |
| Momentum wheel motor [6] | -30 | 60 |
| Speed controller [7] | -40 | 85 |
| **Active de-orbit device** | | |
| Spherical inflatable de-orbiting device [8] | -10 | 40 |
| **Command and data handling** | | |
| SAMA5D31 [9] | -40 | 105 |
| CYUSB306X [10] | -40 | 85 |
| TUSB8041 [11] | -40 | 85 |
| CYUSB302X [12] | -40 | 85 |
| iNAND 7030 [13] | -25 | 85 |
| **Power** | | |
| Battery (discharging)[14] | -30 | 60 |
| **Structure** | | |
| FR-4 PCB[15] | – | 140 |

## 14.3. Mission Profile

In the start of the mission one wants to start directly with taking pictures. This temperature needs to be at least 5 $^{\circ}C$ to be able to operate the camera. So the internal temperature of the host spacecraft needs to be known.

SkySat uses solar panels and bateries for power regulation.[16] Batteries are, in general, the most limiting factor for the thermal range of a spacecraft.[18][p.428] The general temperature ranges of batteries are between 0 and 15 $^{\circ}C$.[18][p.428] Assuming that this is the operational temperature range of the host one can say that the internal temperature of host spacecraft has to be between 0 and 15 $^{\circ}C$. Where the coldest temperature will be at the end of eclipse and the hottest temperature will be at the beginning of the eclipse. At 450 kilometres the orbital period is 93.6 minutes and the maximum eclipse time is 35.92 min.[18] So the time that the satellite is in the view of the sun for a minimum 57.68 minutes Assuming a linear temperature increase with the time that the femto-satellite is in the sun, the femto satellite can only deploy after 19.2 minutes from the end of the eclipse since the internal temperature needs to be at least 5 $^{\circ}C$. Also the femto-satellite should be released 9.2 minutes before it enters the eclipse because it takes 9.2 minutes to take all the pictures and one needs light to take the pictures. This leaves a rough 29 minutes deployment window to deploy the femto-satellite. At the beginning of the deployment window the internal temperature of the host is 5 $^{\circ}C$. At the end of the deployment window the temperature will be 12.5 $^{\circ}C$.

For the deployment window of the de-orbit device there are no limitations with these assumptions. Since the coldest internal temperature is zero degrees, which is the lower bound of the temperature range. And the hottest temperature is 15 degrees which is well within the temperature range of the de-orbit device.

This analysis is a rough estimate with the two big assumptions, a linear temperature increase and the operational range of the battery. To improve the estimate one needs to know the thermal model of the host spacecraft. So in the next design phase the thermal model of the host satellite will be used to update the deployment window. Also the IMU has a temperature sensor, which will be placed as close to the camera as possible. With this data the internal temperature can be checked before activating the camera.

## 14.4. Thermal Design

A passive thermal design is used for the femto-satellite. That is, an appropriate surface finish for the outsides of the satellite is chosen from Table 11-46 in [2][p.436]. Furthermore, to minimise thermal gradients across different parts of the satellite, dark-coloured parts are used inside the satellite and metals like the pins and the beryllium flywheels are painted black. To determine which surface finish is appropriate for the outside, the temperature development is simulated with the thermodynamic model. According to Table 13.3, the power consumption – which is approximately equal to the internal power dissipation – is 2.7 $W$ during the first 472 $s$ after deployment while pictures are taken and 1.95 $W$ for the remaining time until satellite shutdown. Like SkySat, the femto-satellite's orbit has a semi-major axis of 6854.5 $km$ which gives an orbital period of 5647.7 $s$. With the orbital model in GMAT it was established that the eclipse times range from 1546 to 2155 $s$ but sometimes there is a sun-synchronous orbit and therefore no eclipse. The satellite should be kept within the thermal requirements for all these conditions.

$A_s$ is the satellite's surface area which is $6\times(5cm)^2 = 150cm^2 = 0.015m^2$ and the projected area $A$ is a fourth of this,

[2] FCB Mircro serries,https://pro.sony.com/bbsc/assetDownloadController/FCB-Micro-print-ready-brochure.pdf?path=Asset%20Hierarchy%24Professional%24SEL-yf-generic-153703%24SEL-yf-generic-153736SEL-asset-478893.pdf&id=StepID%24SEL-asset-478893%24original&dimension=original, retrieved on 10-06-2016

[3] FCB Mircro series,https://pro.sony.com/bbsc/assetDownloadController/FCB-Micro-print-ready-brochure.pdf?path=Asset%20Hierarchy%24Professional%24SEL-yf-generic-153703%24SEL-yf-generic-153736SEL-asset-478893.pdf&id=StepID%24SEL-asset-478893%24original&dimension=original, retrieved on 10-06-2016

[4] ESP8266 Temperature range,https://cdn-shop.adafruit.com/product-files/2471/0A-ESP8266__Datasheet__EN_v4.3.pdf,retrieved on 10-06-2016

[5] IMU Xsens MTi,https://www.xsens.com/download/pdf/documentation/mti-1/mti-1-series_datasheet.pdf,retrieved on 10-06-2016

[6] Momentum wheel moter, https://fmcc.faulhaber.com/resources/img/EN_0308_B_DFF.PDF,retrieved on 10-06-2016

[7] Speed controller,https://www.silabs.com/Support%20Documents/TechnicalDocs/C8051F33x.pdf, retrieved on 14-06-2016

[8] The Mirco Cool Gas Generator, http://www.isispace.nl/brochures/ACQ-CGS-PRM-001%200.15%20nL%20Micro%20CGG%20flyer.pdf, retrieved 14-6-2016

[9] SAMA5D31,http://www.atmel.com/images/Atmel-11121-32-bit-Cortex-A5-Microcontroller-SAMA5D3_Datasheet.pdf, retrieved on 10-06-2016

[10] CYUSB306X,http://www.cypress.com/file/133591/download, retrieved on 10-06-2016

[11] TUSB8041,http://www.ti.com/lit/ds/symlink/tusb8041.pdf, retrieved on 10-06-2016

[12] CYUSB302X,http://www.cypress.com/file/123816/download, retrieved on 10-06-2016

[13] iNAND 7030,http://www.mouser.com/ds/2/669/iNAND_06012016_SDIN9DW4-948140.pdf, retrieved on 10-06-2016

[14] CR123A Battery datasheet, http://www.vitzrocell.com/sub04/product_list.php?ca_id=40&id=10, retrieved on 06-06-2016

[15] FR-4 epoxy insulation board data sheet, http://www.newlytrend.com/172-fr-4-epoxy-insulation-board.html

[16] SkySat, http://space.skyrocket.de/doc_sdat/skysat-3.htm, retrieved on 10-06-2016

i. e. 0.00375 $m^2$.

The specific heat of the satellite is calculated by a weighted average of its main components. This calculation is given in Table 14.3.

Table 14.3: Main components of the femto-satellite

| **Component** | **Material** | **Mass** $[g]$ | **Specific heat** $[J/(kgK)]$ | **Source** |
|---|---|---|---|---|
| Structure | Aluminium | 22.16 | 940 | [42][p.112] |
| Flywheels | Beryllium | 4 | 1925 | [43] |
| Battery | $Li/MnO_2$ | 16 | 1062 | [44] |
| Electronics | Copper, FR-4, Silicon | 29.83 | 600 | [17] |
| Total | Various | 71.99 | 886 | – |

Manual optimisation of the model yields 1 $mil$ (25.4 $\mu m$) of aluminised kapton as ideal surface material. It has an absorptivity of 0.38 and an emissivity of 0.67. That is the entire surface (except the camera and SIDD openings) has to be enclosed with kapton foil.

The resulting temperature development is modelled for a hot case and a cold case. The result for the hot case with an initial temperature of 15 $^\circ C$ and with no eclipses given in Figure 14.1. The temperature evolution for the cold case with an initial temperature of 5 $^\circ C$, starting time 9.2 $min$ before eclipse and maximum eclipse time of 2155 $s$ is shown in Figure 14.2. Although the temperature at the end of the deployment window is actually 12.5 $^\circ C$, it is taken as 5 $^\circ C$ to account for the worst possible case. The red lines indicate the temperature floor and ceiling given by the requirements. As one can see, the temperature floor and ceiling are not crossed and hence the requirements **TS-SYS-POD-TC-01** through **-04** are verified by analysis.

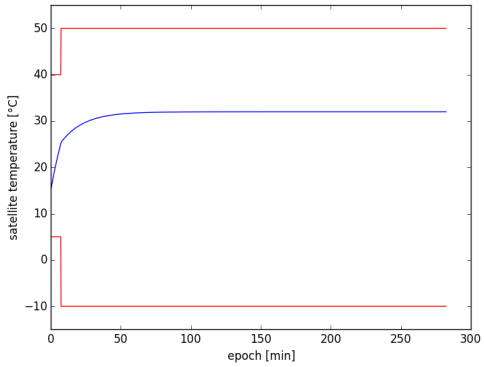


Figure 14.1: Temperature development over mission lifetime plotted against the requirements, hot case.

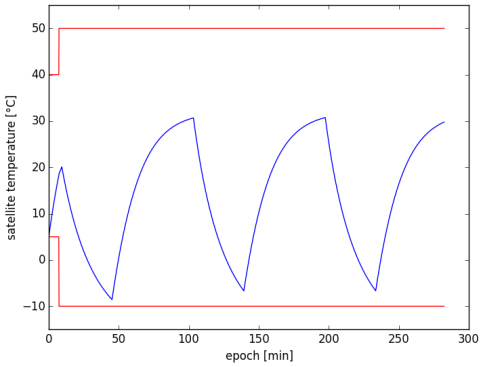


Figure 14.2: Temperature development over mission lifetime plotted against the requirements, cold case.

In addition a sensitivity analysis was performed. That is the impact of changing $\alpha$ and $\epsilon$ by 0.1 on the temperature development was investigated. The resulting maximum and minimum temperatures are given in Table 14.4.

Table 14.4: Sensitivity analysis: maximum (hot case) and minimum (cold case) temperatures for varying absorptivity and emissivity

| $\boldsymbol{\alpha}$ [-] | $\boldsymbol{\epsilon}$ [-] | $\boldsymbol{T_{min}}$ $[^\circ C]$ | $\boldsymbol{T_{max}}$ $[^\circ C]$ |
|---|---|---|---|
| 0.38 | 0.67 | -8.6 | 32.0 |
| 0.28 | 0.67 | -9.5 | 21.6 |
| 0.48 | 0.67 | -7.7 | 41.6 |
| 0.38 | 0.57 | -0.3 | 43.4 |
| 0.38 | 0.77 | -15.6 | 22.7 |

As the thermal control system is passive, it does not require any power. The only part of the thermal subsystem is the aluminised kapton foil. Multiplying its density of 1420 $kg/m^3$ with the surface area of 0.015 $m^2$ and thickness of 25.4 $\mu m$ yields a weight of 0.54 $g$. The foil can be ordered from GoodFellow as a $150 \times 150 mm$ sheet for 202 euros.[18]

[18] GoodFellow online catalogue, `http://www.goodfellow.com/catalogue/GFCat4J.php?ewd_token=upWKTZR3slKqpuIVIdrEaDOAP1PmzZ&n=Spqtl3YUvDe7c7AWZ5IUCBJkzLl78r`, retrieved on 13-06-2016

# 15

## Deployment System

In this chapter the deployment system used to separate the femto-satellite from the host spacecraft is designed. Its purpose is to deliver a velocity increment to the femto-satellite to ensure a safe separation from the host spacecraft. This velocity increment should not be too large since this will cause excessive drift from the host spacecraft, which is not beneficial since the time close to the host is the most valuable period with the highest image clarity and detail. Hence, finding an optimum between these two constraints is the main driver in the deployment system design. This chapter is divided into five sections. First in Section 15.1 the subsystem requirements for the deployment subsystem are restated. Based on these requirements, different design options are explored in Section 15.2. Through this study it is decided that a nichrome wire cutter release mechanism will be used as a deployment mechanism. In Section 15.3 the aspects related to the design of the springs, the most essential element of the nichrome wire cutter, will be discussed. Then in Section 15.4 the design aspects of the exterior structure of the deployment system, the components supporting the springs and the nichrome wire are outlined. Finally, in Section 15.5 the design strategy of the integral deployment system is worked out in detail and the design is finalised.

## 15.1. Subsystem Requirements

The subsystem requirements of the deployment system are stated below.

**TS-SYS-POD-SM-01** The deployment system shall be electrically conductive to minimise chance of electrostatic discharge.
**TS-SYS-POD-SM-02** The deployment system components shall not resonate with the launch load vibrations.
**TS-SYS-POD-SM-03** The deployment system shall not allow the femto-satellite to move any direction before the deployment.
**TS-SYS-POD-SM-04** The deployment system shall contain an actuator that can touch the pin switch on the femto-satellite.
**TS-SYS-POD-SM-05** The deployment system shall be able to contain the femto-satellite from the launch until the deployment.

## 15.2. Design Justification

Various design options exist for the deployment of the femto-satellite. The most common options (pyrotechnics, memory metal actuators, high energy paraffin actuators and nickel chromium wire cutters [45] [46]) are discussed below.

- **Pyrotechnics**, which operate a simple mechanical device by combustion pressure have always been the most widely used means of deployment in space applications. Hence, they are well-engineered and thus very reliable. They are also characterised by high energy efficiency and rapid operation (less than 10 $ms$). Disadvantages include the occurrence of stray currents and electrostatic discharge which pose a threat to safety and hence require complex protection system aimed at absorbing electrostatic discharge [45]. This would significantly increase the mass of the femto-satellite, adding to the mass already added due to the fact that the release mechanism would be installed on the femto-satellite rather than on the host spacecraft. Even more importantly, use of pyrotechnics is currently prohibited on some spacecraft like the Hubble Space Telescope [45] and by CubeSat regulations due to the occurrence of mechanical shocks. [1] It is expected that these regulations will apply to femto-satellites as well.
- **Memory metal actuators** are based on the principle of shape memory alloys (SMAs) which, when heated above a certain critical temperature, can return to their original shape after having been deformed at a temperature below this critical temperature. By applying this procedure the strain energy added to the metal by deformation is released and exploited to exert work required for the deployment [45] [47]. A design example which employs this technique is the Frangibolt manufactured by the company TiNi Aerospace. It consists of an actuator (an SMA) and a notched fastener which is pre-stressed. By powering the actuator, the SMA inside it expands, causing the fastener to fracture [47]. [2] One disadvantage of this concept is that part of the mechanism needs to

[1] CubeSat Design Specification, `http://org.ntnu.no/studsat/docs/proposal_1/A8%20-%20Cubesat%20Design%20Specification.pdf`, retrieved on 06-06-2016
[2] Frangibolt, `http://www.tiniaerospace.com/fbconcept.html`, retrieved on 06-06-2016

be installed on the femto-satellite. Another possible disadvantage is that the release force generated by the frangibolt is too large. [2]

- **High Energy Paraffin actuators** basically rely on the same principle as memory metal actuators. Instead of the expansion of a metal, it employs the expansion of paraffin when it changes from the solid to the liquid phase [47].
- **Nichrome wire cutters** as a device used for release of deployables in space is a concept addressed by various researchers, such as J. Gardiner (Utah State University) [46] and A. Thurn (Naval Research Laboratory, Washington D.C.) [48]. It employs the compression of two springs, which upon relaxation generate a force used to release the deployable. The springs, which are each wound around a cylinder moving freely through shafts connected to the host spacecraft, are compressed by connecting the two ends of the cylinder to a tensioned Vectran (or Kevlar) cable by a V-shaped nichrome (nickel-chromium) wire. A design invented by A. Thurn is shown in Figure 15.1 [48]. In Figure 15.1 the cylinders are stowed, with the springs compressed by the nichrome wire, which is wrapped around the Vectran cable shown on the right. To release the deployable the wire is heated, causing it to cut through the Vectran cable upon which the springs are relaxed and push the deployable outwards with a force equal to the compression force [47]. [3] The deployment process is visualised by Figure 15.2 [48]. Several advantages lie in this concept. Firstly, the entire mechanism is installed on the host spacecraft, consequently adding no mass to the femto-satellite. Also, the concept of springs is widely applied in aerospace and mechanical engineering and is deemed simple and reliable. Moreover, although the concept is yet only applied for the deployment of CubeSats, it is expected that it can be downscaled for femto-satellite use since spring parameters can be varied to comply with the small force needed for the deployment.

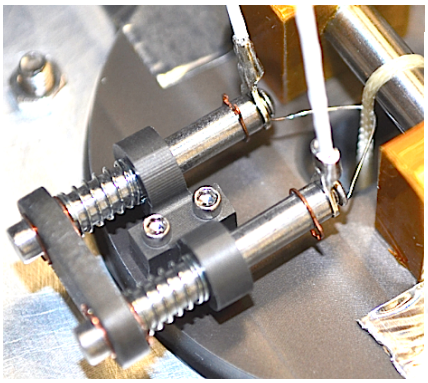

Figure 15.1: The nichrome wire cutter deployment mechanism designed by A. Thurn, Naval Research Laboratory

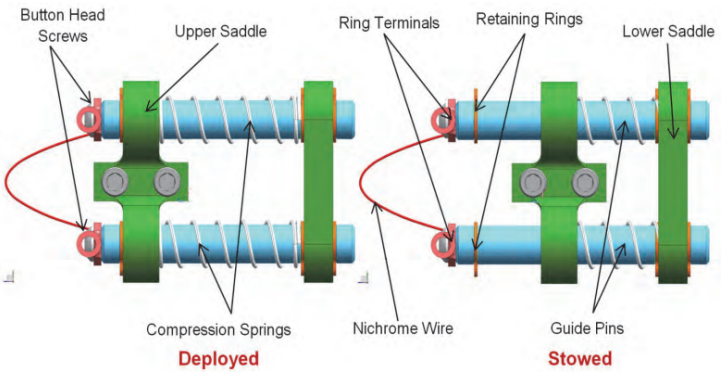


Figure 15.2: The process of deployment in the nichrome wire cutter release concept

For the justification of the design choice, no trade-off is performed since insufficient quantitative data is available and time constraints play a role. Instead, a qualitative analysis of the four options is provided here. Taking into account the features of the four design concepts described above, it can be immediately concluded that the pyrotechnics concept can be discarded since the occurrence of mechanical shocks pose an unacceptable risk to the design. Memory metal actuators and High Energy Paraffin actuators seem to be more viable options. However, these mechanisms are regarded as being more complex than the nichrome wire cutters and hence require much additional research into their mechanical properties which is deemed unfavourable due to the time constraints related to the project. Also, these mechanisms require installation of parts on the femto-satellite and hence add mass. Therefore, it is concluded that the nichrome wire cutter concept is the most viable option due to its relative simplicity and reliability and because it does not add mass to the femto-satellite but can be installed entirely on the host spacecraft.

The springs used in the nichrome wire cutters add the following requirements to the already stated subsystem requirements of the deployment system in Section 15.1:

**TS-SYS-POD-SM-06** The spring index of the spring of the deployment system shall have a value within a range of 4 and 25.
**TS-SYS-POD-SM-07** The spring force shall not exceed the yield force of the spring.
**TS-SYS-POD-SM-08** The spring shall not be subject to buckling.

[3] NRL Invents CubeSat Release Mechanism: To Deploy Solar Panels, Tethers, `http://www.nrl.navy.mil/media/news-releases/2014/nrl-invents-cubesat-release-mechanism-to-deploy-solar-panels-tethers`, retrieved on 03-06-2016

**TS-SYS-POD-SM-09** The diameter of the spring wire shall have a value greater than the minimum manufacturable wire diameter.

## 15.3. Spring Design

In this section, the spring for the nichrome wire cutter deployment mechanism will be designed. The driver for the design is the velocity increment required to launch the femto-satellite into orbit, which is provided by the springs. Hence, in Subsection 15.3.1 the velocity increment is transferred to spring properties. Subsequently, relations are set up for stress, deflection and buckling stabaility and length of the spring in Subsections 15.3.2 to 15.3.4.

### 15.3.1. Implications of the Velocity Increment for the Spring Design

The spring for the deployment of the femto-satellite from the host spacecraft is an elastic structure which stores energy when a compressive load is applied. The performance of the spring is mainly determined by the energy storage capacity $C_{spring}$, which is described by Equation (15.1).

$$C_{spring} = \frac{1}{2} k s_{\max}^2 \tag{15.1}$$

where $s_{max}$ is the spring's maximum deflection and $k$ is the spring stiffness, which will be further discussed in Subsection 15.3.3.

Using equation (15.1) the energy storage capacity of the spring can be expressed in terms of the velocity increment $\Delta V$. To this purpose, the equations of conservation of energy of the system containing the femto-satellite and the host spacecraft are analyzed before and after the deployment of the femto-satellite. The system before deployment is sketched in Figure 15.3. The femto-satellite $m_f$ is attached to the host spacecraft $m_h$ by means of a spring represented by a stiffness $k$. It should be noted that the spring is compressed before release.

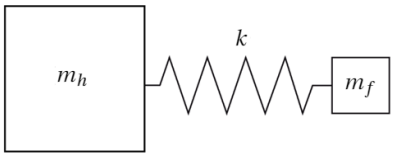


Figure 15.3: Schematic representation of the deployment mechanism before release

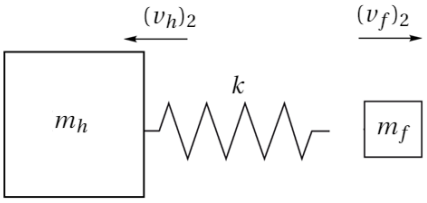


Figure 15.4: Schematic representation of the deployment mechanism after release

After the release the host spacecraft and femto-satellite move away from each other as shown in Figure 15.4. The velocities of the femto-satellite and the host spacecraft after release can be determined using the conservation of energy principle [49], which states that the sum of the kinetic and potential energy of the total system stays constant before and after release. The energy equation is a summation of the potential and kinetic energy at two points in time and is expressed by Equation (15.2).

$$\frac{1}{2} k s_1^2 + \frac{1}{2}(m_h + m_f) v_1^2 = \frac{1}{2} k s_2^2 + \frac{1}{2} m_h (v_h)_2^2 + \frac{1}{2} m_f (v_f)_2^2 \tag{15.2}$$

where $k$ is the stiffness of the spring, $s$ is the springs' deflection, $m_h$ is the mass of the host spacecraft including the spring, $m_f$ is the mass of the femto-satellite, $v_1$ is the velocity of the host spacecraft and femto-satellite together before release, $(v_f)_2$ is the velocity of the femto-satellite after release and $(v_h)_2$ is the velocity of the host spacecraft after release, which acts in the direction opposite to $(v_f)_2$.

Before release, the spring has a maximum compression $s_{max}$. It is assumed that at the initial velocity of the total system equals zero using the initial position of the host spacecraft as a reference position. For that reason, $v_1 = 0$. It is also assumed that no residual stresses act on the spring after release so $s_2 = 0$. Hence, Equation (15.2) can be rewritten to Equation (15.3) since the velocity of the femto-satellite after deployment is equal to the velocity increment ($(v_f)_2 = \Delta V$).

$$C_{spring} = \frac{1}{2} m_h (v_h)_2^2 + \frac{1}{2} m_f (\Delta V)^2 \tag{15.3}$$

Then application of conservation of momentum equation yields Equation (15.4)

$$(m_h + m_f) v_1 = m_h (v_h)_2 + m_f (v_f)_2 \tag{15.4}$$

Substituting Equation (15.4) for $(v_h)_2$ in Equation (15.3), noting that $v_1 = 0$, finally yields Equation (15.5), which

expresses the spring energy storage capacity as a function of $\Delta V$.

$$C_{spring} = \frac{1}{2} m_h \left( \frac{m_f \Delta V}{m_h} \right)^2 + \frac{1}{2} m_f (\Delta V)^2 = \frac{1}{2} \left[ \frac{m_f^2}{m_h} + m_f \right] (\Delta V)^2 \tag{15.5}$$

Since the spring energy storage capacity $C_{spring}$ is a function of important spring sizing parameters Equation (15.5) is the starting point for the design process of the spring given the $\Delta V$ that the spring needs to provide.

### 15.3.2. Stresses in Springs

It is assumed that the spring is subjected to an axial load only as shown in Figure 15.5 [50], based on which the Free Body Diagram (Figure 15.6 [50]) can be derived. Here $F$ is the axial force, $d$ is the wire diameter and $D$ is the diameter of the spring. Given that the maximum shear stress on the cross section of the wire is given by Equation (15.6) it can be rewritten to (15.7) using the information from Figure 15.6 [50].

$$\tau_{max} = \frac{Tr}{J} + \frac{F}{A} \tag{15.6}$$

$$\tau = \frac{8FD}{\pi d^3} + \frac{4F}{\pi d^2} \tag{15.7}$$

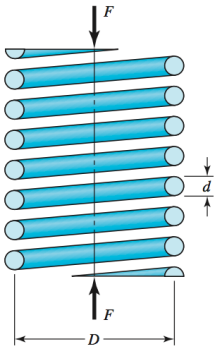


Figure 15.5: Axial load applied on the spring

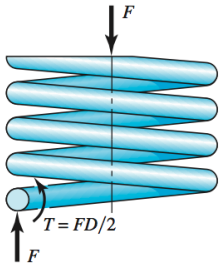


Figure 15.6: Free Body Diagram of the spring

Defining the spring index $C$ (Equation (15.8)) Equation (15.7) can now be rewritten to Equation (15.9). Here, $K_B$ (expressed by Equation (15.10)) is the Bergsträsser factor, which accounts for the localized stress increase on the inner surface of the coil due to the curvature of the wire [50].

$$C = \frac{D}{d} \tag{15.8}$$

$$\tau = K_B \frac{8FD}{\pi d^3} \tag{15.9}$$

$$K_B = \frac{4C+2}{4C-3} \tag{15.10}$$

### 15.3.3. Deflection and Buckling Stability of Springs

By using Castigliano's theorem [51] it follows that the strain that the spring deflection is expressed by Equation (15.11) where $G$ is the shear modulus of the spring material [50].

$$y \approx \frac{8FD^3N}{d^4G} \tag{15.11}$$

Using the well-known spring equation (15.12) it is found that the spring stiffness $k$ is expressed by Equation (15.13) [50].

$$F = ky \tag{15.12}$$

$$k = \frac{d^4G}{8D^3N} \tag{15.13}$$

Springs may buckle when the deflection $y$ becomes too large. The critical deflection is expressed by Equation (15.14), where $y_{cr}$ is the deflection such that the spring becomes unstable in terms of buckling [50].

$$y_{cr} = L_0 C_1' \left[ 1 - \left( 1 - \frac{C_2'}{\lambda_{eff}^2} \right)^2 \right] \tag{15.14}$$

In Equation (15.14) $\lambda_{eff}$ is the effective slenderness ratio of the spring given by Equation (15.15), where $\alpha$ is the end condition constant of the spring. Assuming the spring is fixed between two parallel flat plates, the end condition is given to be $\alpha = 0.5$ [50].

$$\lambda_{eff} = \frac{\alpha L_0}{D} \tag{15.15}$$

Furthermore, $C_1'$ and $C_2'$ are elastic constants expressed by Equations (15.16) and (15.17) [50].

$$C_1' = \frac{E}{2(E-G)} \tag{15.16}$$

$$C_2' = \frac{2\pi^2 (E-G)}{2G+E} \tag{15.17}$$

Analyzing Equation (15.14), it can be observed that the spring displays absolute buckling stability if $C_2'/\lambda_{eff}^2 > 1$.

Hence, combining Equations (15.15), (15.16) and (15.17) it appears that the free length $L_0$ should adhere to the inequality expressed by Equation (15.18) in order for the spring to fulfil absolute stability [50].

$$L_0 < \frac{\pi D}{\alpha}\left[\frac{2\,(E-G)}{2G+E}\right]^{\frac{1}{2}} \tag{15.18}$$

### 15.3.4. Spring Length

Compression springs exhibit different types of ends, each having different expressions for the spring length and number of coils. These ends will not be discussed in detail here. It is assumed that the spring of the deployment will have squared and ground ends since it needs to be connected to two flat surfaces as will be described in Section 15.4. Therefore, the spring will have $N_e = 2$ end coils. Hence, the total number of coils is expressed by Equation (15.19), in which $N_a$ is the number of active coils [50].

$$N_t = N_a + N_e = N_a + 2 \tag{15.19}$$

The solid length $L_s$, the length at which the spring is fully compressed, is then given by Equation (15.20). On the other hand, the free length $L_0$, at which the spring is uncompressed, is given by Equation (15.21). Here, $p$ is the spring pitch [50].

$$L_s = dN_t \tag{15.20}$$

$$L_0 = L_s + y_{max} = pN_a + 2d \tag{15.21}$$

### 15.3.5. Spring Materials

There exists a wide variety of materials applicable for springs. Material properties that play a role in the design of springs are tensile strength, Young's modulus and shear modulus, minimum manufacturable wire diameter, relative mass and cost, degradation resistance, fatigue resistance and resistance to shock and impact loading [50] [52]. Due to the vacuum conditions and the aggressive space environment additional material properties related to these aspects need to be taken into account for the spring design. The considerations for the material properties taken into account in the spring design are listed below.

- **Tensile strength** For springs, the ultimate tensile strength (UTS) is heavily dependent on the wire diameter. It has been demonstrated that the relationship between the UTS and the wire diameter graphically is a straight line when plotted on a log-log scale. Calling the slope of this line $m$ and the intercept with the $d = 0$ axis $A$, the UTS is expressed by Equation (15.22) [50].

  $$S_{ut} = \frac{A}{d^m} \tag{15.22}$$

  Obviously, it is unfavourable for the springs to be deformed plastically. Hence, the springs should only be deformed up to their elastic limit. For most materials this elastic limit is expressed as a percentage of their UTS.
- **Young's modulus and shear modulus** From Equation (15.13) it appears that the spring constant $k$ is proportional to the shear modulus $G$. As will become apparent in Section 15.3 this implies that the spring length is directly related to $G$. Hence, the value of $G$ greatly influences the dimensions of the spring and should therefore be minimised. The Young's modulus $E$ appears in Equations (15.16) and (15.17) related to the spring design. However, the spring dimensions appear to be less sensitive to $E$ than to $G$ since no direct proportionality exists. These considerations are outlined in Section 15.5.
- **Minimum manufacturable wire diameter** This parameter greatly varies among spring materials [52] [50]. Since the wire diameter directly affects important spring characteristics (as becomes apparent from Subsections 15.3.2 and 15.3.3) it plays an important role in the selection of the material for the spring.
- **Relative mass and cost** As will become apparent in Subsection 15.5 the mass of the spring will be negligible with respect to the host spacecraft's mass. Hence, since the spring will be installed on the host spacecraft and not on the femto-satellite, the mass of the spring is no point of concern. The cost, however, differs greatly among different spring materials. Also, since little research has been done into manufacturability of springs except for minimum manufacturable wire diameter, manufacturing of the spring designed in Section 15.5 may require adjustment of existing tools or production of new dedicated tools. Since these aspects are considered to be outside the scope of this report, the additional costs associated to them remain to be determined.
- **Electrical conductivity** Interactions of the spacecraft with the plasma and high-energy particle environments in space can cause differential charging of spacecraft materials and electronics, which results into electrostatic discharge (ESD). Therefore, ESD design guidelines state that all exterior surfaces of the spacecraft should be preferably at least partially conductive [53]. The deployment mechanism could arguably be considered part of the femto-satellite's exterior surface since it is directly connected to the femto-satellite prior to deployment. Hence, electrical conductivity should be aimed for when selecting the spring material.
- **Degradation resistance** Degradation of materials in space arises from several factors, including UV radiation,

ionising radiation, micrometeoroids and atomic oxygen (ATOX). Especially ATOX is considered one of the most serious hazards to materials used in space for altitudes between 200 and 700 $km$ [54]. Although the spring will be located internally during most of its operational time (for the layout and operation of the deployment interface see Section 15.4) and therefore protected against ATOX [55] it will be directly subjected to the space environment during deployment. Hence, resistance against corrosion is taken into account in selecting the spring material. In this report only a qualitative analysis on this matter is presented.

- **Fatigue resistance** For dynamically loaded springs investigating the fatigue resistance is of great importance. However, it is assumed that in the deployment mechanism the spring is under a mere constant load due to it being protected by the deployment interface. Therefore, fatigue resistance is not considered here.
- **Resistance to shock and impact loading** Similar to fatigue resistance, it is assumed that the deployment interface protects the spring against shocks and impact loading. Hence, these aspects are left out of consideration.
- **Effects of temperature** Many materials in space display impact resistance (toughness) problems due to the low temperatures they are exposed to during the mission. Springs are an exception to this rule since they are designed to be deflected under impact. Also, most common spring materials maintain satisfactory toughness even at cryogenic temperatures. For that reason, the minimum service temperature is less critical than the maximum service temperature [52]. However, according to Budynas and Nisbett [50] certain materials cannot be applied below subzero temperatures, see Table 15.1 As appeared from the equations presented in Subsection 15.3.3 the Young's modulus $E$ and the shear modulus $G$ play an important role in the spring design. In general, most common spring materials show approximately a 2% change in their moduli for each 55 $^{o}C$ change in temperature [52]. Since the operative temperature range of the femto-satellite is $-14.4\ ^{\circ}C$ to $55.2\ ^{\circ}C$ (see Chapter 14) it is concluded, assuming linear behaviour, that one should design for either a 1.3 increase or decrease in $E$ and $G$, depending on which case is critical.

Various spring materials and their properties as stated above are presented in Table 15.1. This table was produced by combining data both from literature [50] [52] and manufacturers [56].[4,5] In case of conflicting values, manufacturer data was used. Note that the A digits in the first column represent the ASTM designation of the corresponding materials.[6] The exponent $m$ and the intercept value $A$ in the second and third columns correspond to the quantities appearing in Equation (15.22). The minimum diameter in the seventh column represents the minimum manufacturable wire diameter as discussed above. For the corrosion resistance and application at subzero temperatures (last two columns) no quantitative data was found. Hence, qualitative data obtained from literature [50] [52] was used. The signs -, +, ++ represent poor, good, excellent performance in terms of corrosion resistance, while +++ designates immunity to corrosion [52]. The designations NA and A stand for 'not applicable' and 'applicable' [50]. In case no data was found for a particular quantity, the corresponding cell is left blank.

[4] MatWeb Material Property Data, `http://www.matweb.com/`, retrieved on 13-06-2016
[5] Titanium wire, `http://www.sigmaaldrich.com/catalog/product/aldrich/266019?lang=en&region=DK`,retrieved on 16-06-2016
[6] ASTM International, `http://www.astm.org/DIGITAL_LIBRARY/JOURNALS/MPC/index.html`, retrieved on 16-06-2016

Table 15.1: Properties of common spring materials

| **Material** | **Exp. *m*** [-] | **Interc. A** [$MPa \cdot mm^m$] | **Min. elastic limit** [%**UTS**] | **Young's Modulus** [$GPa$] | **Shear Modulus** [$GPa$] | **Min. diam.** [$mm$] | **Density** [$kg/m^3$] | **Elect. resist.** [$\mu\Omega \cdot cm$] | **Corr. resist.** | **App. at subzero temp.** |
|---|---|---|---|---|---|---|---|---|---|---|
| Music wire (A228) | 0.145 | 2211 | 45 | 207.0 | 79.3 | 0.3 | 7720 | | - | NA |
| OQ&T wire (A229) | 0.187 | 1855 | 45 | 207.0 | 79.3 | 0.5 | 7720 | | | NA |
| Hard-drawn wire (A227) | 0.19 | 1783 | 45 | 198.6<br>197.9<br>197.2<br>196.5 | 80.7<br>80.0<br>79.3<br>78.6 | 0.71<br>0.84<br>1.63<br>3.18 | 7861 | | | NA |
| Cr-Va (A6150) | 0.168 | 2005 | 65 | 203.4 | 77.2 | 1.09 | 7860 | 19 | - | A |
| Cr-Si (A9254) | 0.108 | 1974 | 65 | 203.4 | 77.2 | 0.61 | 7860 | 19 | - | A |
| Steel (A313) | 0.146<br>0.263<br>0.478 | 1867<br>2065<br>2911 | 45 | 193.0 | 69.0 | 0.33<br>2.5<br>5.1 | 7900 | 73 | ++ | A |
| Steel (17-7PH) | 0<br>0.146 | 2300 | 55 | 203.0 | 75.8 | 0.2<br>0.5 | 7670 | 84 | ++ | A |
| Phosphor-bronze wire (CA510) | 0<br>0.028<br>0.064 | 1000<br>913<br>932 | 45 | 103.4 | 41.4 | 0.3<br>0.56<br>1.9 | 8860 | 10.5 | ++ | A |
| Titanium (Ti-13V-11Cr-3Al) | 0 | 1140 | 40 | 110.0 | 41.0 | 0.508 | 4840 | 178 | +++ | A |
| Titanium (Beta-C) | 0 | 1310 | 45 | 106.0 | 41.0 | 0.127 | 4840 | 42 | + | A |

## 15.4. Deployment Interface Design

The spring is integrated into the deployment system by a deployment interface which will be installed on the host spacecraft. In this section the design of this deployment interface is presented. The femto-satellite will be deployed from the host spacecraft with a springs as discussed in Section 15.3. Before deployment the femto-satellite is attached to the host spacecraft. Hence, the springs should be compressed before deployment, ensuring that the femto-satellite will be attached to the host spacecraft until deployment. Examples of deployment systems for small satellites that currently perform this task are the Poly-Picosatellite Orbital Deployer (P-POD) and the NanoRacks CubeSat Deployer (NRCSD).[7] In the NRCSD the CubeSats are ejected using a combination of a spring and a plunger at the rear of the NRCSD.[8] Like in the P-POD, the CubeSat pushes open the door of the deployment mechanism by the spring force transferred through the CubeSat structure. The design of the deployment interface for the femto-satellite is based on the P-POD and the NRCSD. However, the following adjustment are made to their design:

- Since the means of the release of the springs are not specified in the design of the P-POD [7] and the NRCSD [8] the nichrome wire cutter deployment mechanism is integrated in their design concept. Also, an electric rod-style actuator (ERSA) needs to be included in the deployment system due to the fact that the femto-satellite needs to be activated before deployment (see Subsection 13.3.3). Hence, space needs to be reserved in the centre of the deployment interface. Therefore, two nichrome wire cutter mechanisms are positioned around the ERSA in order to provide a pure linear force in the deployment direction.
- The deployment door is opened before the springs are released. In this way the door does not have to be opened by the femto-sallite. The first reason for this design choice is the uncertainty added to the system due to the door opening by the spring force. Since a precise velocity increment of 1.3 $cm/s$ has to be delivered for the injection into the relative orbit around the host spacecraft any uncertainty is undesired. The second reason is the small spring force applied. If the femto-satellite does not have to push the door open the risk of the deployment system decreases. Implications for the design of the door will be discussed in the Recommendations (Chapter 29).
- After the deployment door has been opened, the deployment is initialised by a nichrome wire that releases the

[7] CubeSat Concept and the Provision of Deployer Services, `https://directory.eoportal.org/web/eoportal/satellite-missions/c-missions/cubesat-concept`, retrieved on 16-06-2016

[8] NanoRacks CubeSat Deployer, `http://www.nasa.gov/mission_pages/station/research/experiments/1350.html`, retrieved on 16-06-2016

springs.

### 15.4.1. Deployment Interface Layout

A sketch of the 3D configuration of the deployment interface is shown in Figure 15.7. The technical drawings are presented in Figure 15.8 and Figure 15.9.

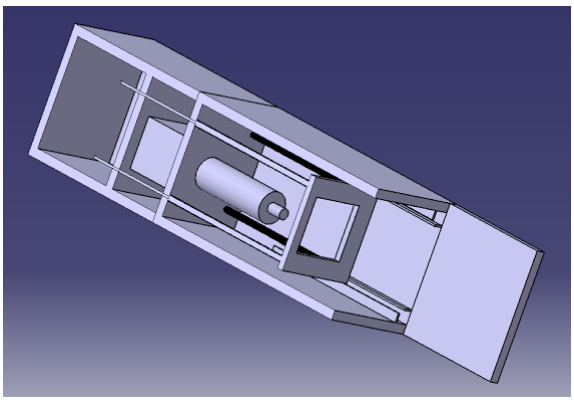

Figure 15.7: 3D Catia drawing of the Deployment Interface

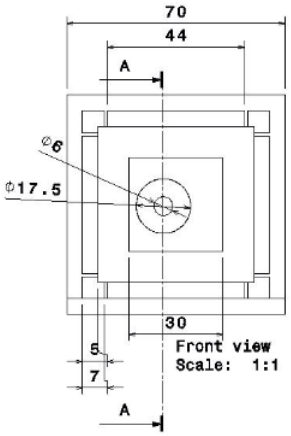


Figure 15.8: Technical Drawing Deployment Interfact: Topview

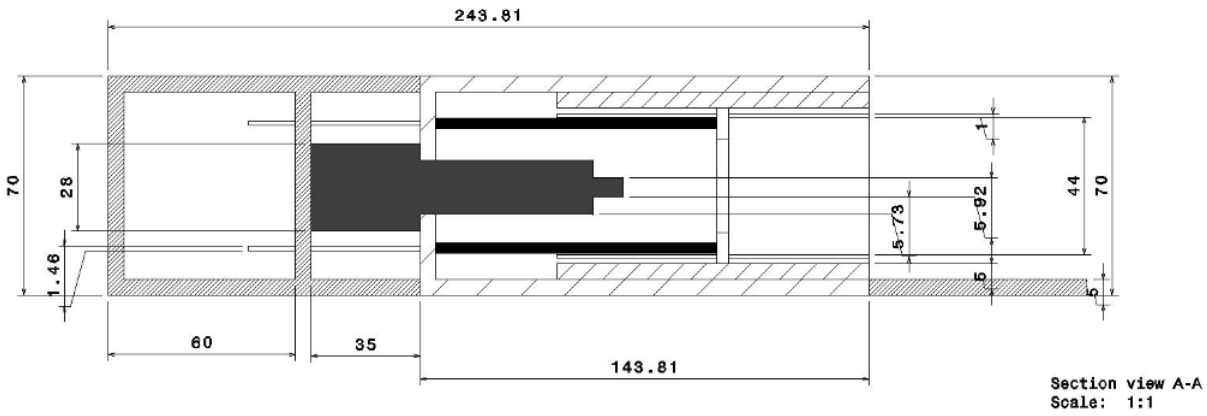


Figure 15.9: Technical Drawing Deployment Inerface: Sideview

The key features of deployment interface are the following:

- A femtosatellite of dimensions 5 $cm$ x 5 $cm$ x 5 $cm$ can be placed between the supporting plate and deployment door.
- An ERSA activates the femto-satellite by a movable extension that pushes the switch located on the femto-satellite's surface.
- A nichrome wire attached to the left wall of the deployment interfaces burns the loop connecting the Vectran cables attached to the spring-supporting steel pins when heated by a current.
- Four springs in stowed position provide the initial separation of the femto-satellite during deployment.

The ERSA [9] type ERD06 [10] will turn on the femto-satellite before release. The actuator and nichrome wire will be powered by the host-spacecraft. In analogy with the P-POD design [57] [11], the rails is hard anodised with Teflon impregnation to reduce friction.

[9] ERD ELECTRIC ROD-STYLE ACTUATOR, `file:///C:/Users/TUDelft/Downloads/2190-4000_0504_erd-cat.pdf`, retrieved on 16-06-2016

[10] Actuator datasheet, `http://www.tolomatic.com/products/product-details/erd-low-cost-electric-cylinders-for-pneumatic-cylinder-replacement#/features-options`, retrieved on 13-06-2016

[11] PTFE Impregnation, `http://www.globalmetalfinishing.com/ptfe-impregnation`, retrieved on 27-06-2016

### 15.4.2. Supporting components

In the stowed condition the femto-satellite is fixed in the deployment interface structure. Before release the femto-satellite is refrained from movement by the deployment door. At the other side the femto-satellite is held by a steel supporting plate connected to four springs. The springs are supported by pins which can not freely move to the left due to their extensions with smaller diameters through the right aluminium (7075T-3) plate. The satellite-supporting plate and the spring pins are made of carbon (C1020) steel since a certain mass is needed for the manufacturability of the springs as will be explained in Section 15.5.3.

The thin part of the pins are extended to the left in Figure 15.9. Due to the smaller diameter of $1mm$ of these parts and their corresponding holes in the aluminium vertical plate they prevent the pins, supporting plate and therefore the femto-satellite from moving to the left. The thin part of the pins have a length of 60 $mm$ such that they are extended 20 $mm$ to the left from the second vertical aluminium plate. In this way they avoid the freedom of movement of the pins during deployment, given a maximum spring deflection of $10mm$ .

The ERSA [12] type ERD06 has an extension rod diameter of $6mm$ and the pin switch to turn on the femto-satellite is located $15.6mm$ from the top aluminum sliding in Figure 15.9. For that reason, the steel supporting plate has cross-sectional dimensions of $50mm$ x $50mm$ with a square hole of $30mm$ x $30mm$ as shown in Figure 15.8.

### 15.4.3. Nichrome wire

Since in the design of the deployment mechanism four springs are used instead of two, also two nichrome wires would be applied and hence two separate Vectran cables are cut if one wants to design according to A. Thurn's nichrome wire cutter deployment mechanism [48]. However, due to the addition of the ERSA to the deployment system design, the distance between each pair of spring-supporting pins is 39.27 $mm$. That would mean the length of the nichrome wires would become larger than 39.27 $mm$ while A. Thurn mentions that at "free length greater than $32mm$ the apex of the nichrome wire when heated becomes very hot and the resulting loss in tensile strength can cause necking of the wire which would impact further use of the nichrome wire" [48]. Hence, it is chosen that instead of connecting the ends of the spring-supporting pins by nichrome wires they will be connected by two diagonally crossing Vectran cables, in turn connected by a Vectran loop which will be cut by a nichrome wire attached to the leftmost wall of the deployment interface.
Now, the minimum length 10 $mm$ of the nichrome wire [48] is chosen as the design length. Modelling the nichrome wire as a parabola $y = \frac{1}{2}x^2$, the separation of its two ends along the wall can be estimated by Equation (15.23) [13] where $b-a$ equals the distance between the two ends of the nichrome.

$$L_{wire} = \int_a^b \sqrt{1+\left(\frac{dy}{dx}\right)^2}\,dx = \int_a^b \sqrt{1+x^2}\,dx = \frac{1}{2}\left[x\sqrt{1+x^2}+\sinh^{-1}(x)\right]_a^b \tag{15.23}$$

With $L_{wire} = 10$ $mm$ it can be computed that $b-a = 5.58$ $mm$. Hence, the distance from the apex of the nichrome wire to the wall is 7.78 $mm$. Given the distance from the ends of the spring-supporting pins to the wall is 40 $mm$, the Vectran cables should span 32.22 $mm$ in the horizontal direction as in Figure 15.8. Hence, with a vertical distance of 39.27 $mm$, using Pythagoras theorem the diagonal distance the Vectran cables span equals 50.80 $mm$. Also modelling the Vectran cables as parabolas Equation (15.23) can be used again to find that the length of each Vectran cable should be 650 $mm$. To estimate the time to burn the wire and hence deploy the femto-satellite, test data produced by A. Thurn [48] are used. These show the failure currents, electrical resistances and failure times for the nichrome wire under only the tension of its own weights for different lengths. It can be assumed that the wire is loaded under only the tension of its own weight since the spring force is very small (see Subsection 15.5.3). For the sake of simplicity the first value of $L_{wire} = 12.7$ $mm$ is used, which yields a failure current of 2.15 $A$, an electrical resistance of 0.8Ω and a failure time of 7 $s$. Using the electrical power expression for a circuit $P = I^2R$ where $I$ is the electrical current and $R$ is the electrical resistance, it is found that the power required for operating the nichrome wire cutter deployment mechanism is $P = 3.60$ $W$.

## 15.5. Integral Design Strategy

Using the equations presented in Section 15.3, the material properties outlined in Table 15.1 and the configuration of the deployment interface (Section 15.4) the spring design can be numerically implemented. First in Subsections 15.5.1 and 15.5.2 the sequence of design steps is outlined for respectively the spring and the deployment interface, including relevant assumptions and constraints for each design step. Then in Subsection 15.5.3 the results of the design process are presented and the dimensions and material of the spring and the deployment interface are

[12] ERD ELECTRIC ROD-STYLE ACTUATOR, `file:///C:/Users/TUDelft/Downloads/2190-4000_0504_erd-cat.pdf`, retrieved on 16-06-2016

[13] Arc Length, `https://cims.nyu.edu/~kiryl/Calculus/Section_7.4--Arc_Length/Arc_Length.pdf`, retrieved on 17-06-2016

selected.

### 15.5.1. Spring Design Steps

The sequence of the spring design process is as follows.

1. The first design step is to calculate the required energy storage capacity of the spring $C_{spring}$, expressed by Equation (15.5). However, the term $m_f$ representing the mass of the femto-satellite will be altered since, if one recalls the schematic representation of the deployment displayed by Figure 15.3 and Figure 15.4 has to include the mass of the pins around which the springs are wound and the supporting plate pushing away the femto-satellite during deployment. Also, the energy storage capacity is divided over four springs so to obtain the energy storage capacity per spring the total energy storage capacity is divided by four. Hence Equation (15.5) is rewritten to Equation (15.24).

$$C_{spring} = \frac{1}{8}\left[\frac{m_{f+con}^2}{m_h} + m_{f+con}\right](\Delta V)^2 \tag{15.24}$$

   In Equation (15.24), $m_{f+con}$ is equal to $m_{f+con} = m_f + m_{con} = m_f + m_{pins} + m_{plate}$ where $m_{con}$ represents the components that connect the femto-satellite to the spring; the pins around which the springs are wound ($m_{pins}$) and the mass of the satellite-supporting plate ($m_{plate}$).
2. Based on the minimum manufacturable wire diameter of the spring material in question (see Table 15.1) a wire diameter $d$ is chosen. Then a spring index is also chosen, which is constrained to $4 \leqslant C \leqslant 25$. [14] Subsequently, using Equation (15.8) the spring diameter $D$ can be determined.
3. The maximum spring deflection is arbitrarily determined to be $y_{max} = 0.01\ m$. It is checked whether it fulfils the buckling stability requirement imposed by the critical deflection $y_{cr}$, which is expressed by Equation (15.14).
4. Combining Equation (15.1) and Equation (15.12) the maximum spring force can be determined by Equation (15.25).

$$F = \frac{2C_{spring}}{y} \tag{15.25}$$

   Then, the spring constant $k$ can be determined by using Equation (15.25).
5. After having calculated $F$ the magnitude of the force needs to be examined by calculating the yield force of the spring. First, using Equation (15.22) the yield stress in the spring is calculated by Equation (15.26) where $K_E$ is the elastic limit corresponding to the selected material and wire diameter as a fraction of the UTS as specified in Table 15.1. Also the values of $A$ and $m$ follow from Table 15.1.

$$S_{yield} = \frac{K_E}{100}\frac{A}{d^m} \tag{15.26}$$

   Having obtained $S_{yield}$ the Bergsträsser factor is computed by applying Equation (15.10). Then the yield force is calculated by substituting $S_{yield}$ for the shear stress $\tau$ in Equation (15.9) to obtain Equation (15.27).

$$F_{yield} = \frac{\pi d^3 S_{yield}}{8K_B D} \tag{15.27}$$

6. Rewriting Equation (15.13) to Equation (15.28) the number of active coils can be calculated.

$$N_a = \frac{d^4 G}{8kD^3} \tag{15.28}$$

   Then the number of total coils can be calculated by Equation (15.19).
7. In the final step the dimensions of the spring are calculated. First the solid length $L_s$ (the length of the spring at compression) is calculated using Equation (15.20). Then the free length $L_0$ (the length of the spring after release) can be calculated by Equation (15.21). Finally the spring pitch $p$ is determined by rewriting Equation (15.21) to Equation (15.29)

$$p = \frac{L_0 - 2d}{N_a} \tag{15.29}$$

### 15.5.2. Deployment Interface Design Steps

1. The dimensions of the thick parts of the steel pins are driven by the spring design. Their length is expressed by Equation (15.30) (where $L_s$ is the solid length of the spring) and their diameter by Equation (15.31). In the latter equation an arbitrary clearance of 1% of the wire diameter has been applied to ensure the springs are not directly connected to the pins.

[14] Compression Spring Design, `http://www.mrspring.com/docs/Compression%20%20Spring%20Design%20Info.pdf`, retrieved on 15-06-2016

$$L_{pin,thick} = L_s \quad (15.30) \qquad D_{pin,thick} = D - 2d - 0.01d \quad (15.31)$$

2. The length of the thin pin part is chosen to make sure that it will not move out of the deployment interface during deployment by putting a safety factor of 2 on the expected pin movement $\Delta x$.

$$L_{pin,thin} = 2\Delta x + t_{al,plate} + t_{elec,actuator} \quad (15.32)$$

The diameter of the thin pin part is half the diameter of the thick pin part to prevent movement of the pins during launch.

$$D_{pin,thin} = 0.5 \cdot D_{pin,thick} \quad (15.33)$$

3. The mass of the thin pin part and wide pin part are calculated with Equations (15.34) and (15.35) respectively.

$$m_{pin,thick} = \rho_{C1020,steel}\left(\frac{D_{pin,thick}^2}{4} L_{pin,thick}\right) \quad (15.34)$$

$$m_{pin,thin} = \rho_{C1020,steel}\left(\frac{D_{pin,thin}^2}{4} L_{pin,thin}\right) \quad (15.35)$$

4. The mass of the structure to be pushed away by the spring minus the femto-satellite, denoted as $m_{con}$, is determined by the spring as explained in the Section 15.5.1. The mass of the steel plate can be derived from that by Equation (15.36).

$$m_{plate} = \rho_{C1020,steel}\left(m_{con} - 4m_{pin,thick} - 4m_{pin,thin}\right) \quad (15.36)$$

5. Subsequently the thickness of the plate is calculated by Equation (15.37) where $w_0 = 50mm$ is the outer dimension of the square steel supporting plate and $w_i = 30mm$ is the dimension of the square hole in the steel supporting plate.

$$t_{plate} = \frac{m_{plate}}{\rho_{C1020,steel}(w_0^2 - w_i^2)} \quad (15.37)$$

### 15.5.3. Selection of Dimensions and Material

The design steps discussed in Subsections 15.5.1 were applied to different combinations of materials and wire diameters as outlined in Table 15.1. It appeared that the wire diameter has a profound impact on the length of the spring, which upon analysis can also be concluded from Equation (15.28) which shows that $N_a$ scales with $d^4$. Decreasing the spring index $C$ also has a dramatic effect since it $N_a$ is inversely proportional to $C^3$ through the spring diameter $D$. The shear modulus $G$ also directly affects $N_a$, though only by a power one. Since the velocity increment required is very small the required energy storage capacity also has a very low value, which implies that the spring force $F$ and spring constant $k$ become very small. As a result, $N_a$, $L_s$ and $L_0$ acquire very large values. Hence, it was decided that $L_s$ and $L_0$ should have a length not larger than around twice the dimensions of the femto-satellite to have a reasonable design guideline.

In the previous design approach $N_a$ was set according to information acquired from Conley [50], which states that values of $3 \leqslant N_a \leqslant 15$ are recommended and spring manufacturers such as Murphy and Read Spring Manufacturing Co. which state $N_a = 200$ as an upper limit for the coil number. [15] However, this would imply $y_{max}$ to be in the order of $10^{-1}$ $mm$ and $L_s$ and $L_0$ in the order of $mm$ which was deemed undesirable because of temperature and manufacturing tolerances. Hence the maximum deflection was set to $y_{max} = 0.01$ $m$, from which $N_a$ was derived. However, this resulted in a high number of coils which, in combination with the small values for $p$ (in the order of $10^{-1} mm$), raises the question of manufacturability, an issue which will be discussed in Section 29.8.

In an effort to resolve the concerns about manufacturability, the following design guidelines were applied.

- Minimise the wire diameter $d$
- Maximise the spring index $C$
- Minimise the shear modulus $G$
- Increase the energy storage capacity $C_{spring}$ by increasing $m_{f+con}$ (see Equation (15.24)). This can be achieved by increasing the mass of the supporting plate $m_{plate}$ up to acceptable values. By using carbon steel as the plate material the dimensions of the supporting plate can still be kept to a minimum.

Applying the design steps outlined in Subsection 15.5.1 and the design considerations explained above, different spring designs can be achieved. A couple of design options are outlined in Table 15.2 which is meant to show how the spring design characteristics vary with varying the material, the mass of the spring-satellite connections (the pins and the supporting plate), the wire diameter and the spring index. Note that for options 1,3 and 5 no critical deflection exists.

[15] Custom Compression Springs, `http://www.mrspring.com/compression-springs.html`, retrieved on 10-06-2016

Table 15.2: A selection of spring designs options

| | *Input* | | | | *Output* | | | | |
|---|---|---|---|---|---|---|---|---|---|
| | **Material** | $m_{con}$ [$g$] | $d$ [$mm$] | $C$ [-] | $F_{yield}$ [$N$] | $F$ [$10^{-4}N$] | $N_a$ [-] | $L_0$ [$cm$] | $y_{cr}$ [$cm$] |
| **Option 1** | Ti (Beta-C) | 50 | 0.508 | 25 | 2.27 | 5.16 | 3294 | 168 | - |
| **Option 2** | Steel (17-7PH) | 50 | 0.5 | 25 | 14.3 | 5.16 | 5994 | 301 | 4.29 |
| **Option 3** | Ti (Beta-C) | 10 | 0.127 | 25 | 0.14 | 3.47 | 1226 | 16.6 | - |
| **Option 4** | Ti (Beta-C) | 50 | 0.127 | 4 | 0.67 | 5.16 | 201053 | 2554 | 0.217 |
| **Option 5** | Ti (Beta-C) | 50 | 0.127 | 25 | 0.14 | 5.16 | 824 | 11.5 | - |

Conclusively, beta-C titanium was selected as the material for the spring since it has the lowest manufacturable wire diameter in combination with a minimum shear modulus value. From Table 15.1 it can be concluded that Titanium beta-C is electrically conductive due to its relatively low electrical resistance of 42 $\mu\Omega$. A wire diameter of $d = 0.127\ mm$ was selected, combined with a spring index of $C = 25$ and a mass of the spring-satellite connections of $m_{con} = 50\ g$. These result in a spring with $N_a = 824$ active windings and a free length of $L_0 = 11.5\ cm$.

Once the spring design parameters are calculated the design of the deployment interface is determined following the Design Steps of Section 15.5.2. The dimensions of the pins are: $L_{pin,thick} = 104.8mm$, $D_{pin,thick} = 2.9mm$, $m_{pin,thick} = 0.0055kg$, $L_{pin,thin} = 60mm$, $D_{pin,thin} = 1.5mm$, $m_{pin,thin} = 0.00108kg$. Using Equation (15.36) the plate mass equals $0.026kg$ with a plate thickness of $1.9mm$. Fore these calculations an Al 7075 t-3 material density of 2800 $kg/m^3$ and a Steel C1020 material density of 7850 $kg/m^3$ is used. The price of Al 7075 t-3 is 1.61 €/$kg$ [16] and the price of Steel C1020 is 0.50 €/$kg$ [17] (June 2016). The final mass, volume, power and cost budgets for the deployment system are specified in Table 17.4 in Section 17.4.

[16] InvestmentMine: Aluminum Prices and Aluminum Price Charts, `http://www.infomine.com/investment/metal-prices/aluminum/`, retrieved on 17-06-2016

[17] MIT Open Sourceware, `http://ocw.mit.edu/courses/materials-science-and-engineering/3-11-mechanics-of-materials-fall-1999/modules/props.pdf`, retrieved on 17-06-2016

# 16

# Structural and Vibrational Analysis

## 16.1. Requirements

In this chapter the structural and vibrational analysis is performed, it is needed to check whether the whole satellite and key subsystems can withstand the launch loads and operational loads if present. With this it is investigated if requirement **TS-STH-SAR-02** is fullfilled.

**TS-STH-SAR-02** The spacecraft shall withstand the launch loads.

The structural analysis comprises the evaluation of the launch loads onto the structure, because during launch and stage separation huge forces and accelerations act upon the satellite and subsystems, which can reach up to several $g$'s.

The vibrational analysis is to check whether the design can withstand certain vibrations and does not vibrate in the natural frequency of the system. This is important because if the system starts to resonate in its natural frequency with the driving frequency large deflections may occur which exceed the elastic limits and thus let the structure fail. [58] The latter means that the satellite and equipment on the satellite need to have a natural frequency higher than the vibrations occurring during the launch on the launcher. [45] After that the random and harmonic vibrations need to be analysed for the satellite. This means to look for the deflection of the satellite due to the launcher and the stresses that rise from those deflections as advised by Stefano Speretta[1]. The shock analysis and specific non-structure part analysis are left for actual testing as said in literature due to its complexity. [18]

For most launchers the vibrational and acceleration envelopes are known. For example the Delta III and Ariane 4 have minimal vibration requirements of $100 Hz$, due to this for equipment. This means that if the satellite has a natural frequency below this value it will resonate and probably will collapse under the bigger growing deflections. [45] Since the chosen mission is launched along a SkySat satellite by TerraBella, the launchers of these satellites is investigated as well for vibrational analysis, namely the Dnepr rocket and the Soyuz-2-1b Fregat-M [2]. The launch accelerations and minimal fundamental frequencies for both launch systems, and the Ariane 5 for comparison, are given in Table 16.1. [59–61] The DNEPR also has requirement for the use of safety factors, for flight this one is set to 1.3.

This leads to two new system requirements:

**TS-SYS-POD-09** The femto-satellite shall have a natural frequency higher than 35 $Hz$.
**TS-SYS-POD-11** The femto-satellite shall be able to remain operable after launch accelerations up to 10.8 $g$.

Table 16.1: Launch system accelerations and vibrations. (+ = tension; – = compression)

| **Launch system** | **Longitudinal Acceleration (x)** $[g]$ | **Lateral Acceleration (y, z)** $[g]$ | **Lateral Fund. Frequency** $[Hz]$ | **Longitudinal Fund. Frequency** $[Hz]$ |
|---|---|---|---|---|
| DNEPR | -8.3 to +1 | -1 to +0.8 | 10 | 20 |
| Soyuz-2-1b | –5.0 to +1.8 | -1.8 to +1.8 | 15 | 35 |
| Ariane 5 | -6.0 to +2.5 | -2 to +2 | 10 | 31 |

The structural analysis will conduct analysis on stresses occurring in the structure during launch and deployment. This will be done both by FEM analysis in CATIA and hand calculations to verify the CATIA model. The structural and vibrational analysis includes but is not limited to the analysis of the momentum wheels, aluminium pins and the PCBs.

## 16.2. Vibrational Analysis

In this section the vibrational analysis is performed for system requirement **TS-SYS-POD-09**. First the fundamental frequency of the femto-satellite is computed after which the momentum wheels, aluminium pins and PCBs are analysed for both the natural frequency and the harmonic and random vibrations.

[1] Staff TU delft, Former RF system engineer at ISIS, contacted on 13-06-2016

[2] SkySat-1 , `http://www.satimagingcorp.com/satellite-sensors/skysat-1/`, retrieved 6-6-2016

### 16.2.1. Fundamental Frequency

First off to calculate the natural frequency, the system can be modelled as an undamped mass spring system. The stiffness of the system can be calculated following beam theory. The results are shown in Equation (16.1) till (16.4).

$$\delta_a = \frac{FL}{AE} \tag{16.1}$$

$$k_a = \frac{F}{\delta} = \frac{EA}{L} \tag{16.2}$$

$$\delta_l = \frac{FL^3}{3EI} \tag{16.3}$$

$$k_l = \frac{F}{\delta} = \frac{3EI}{L^3} \tag{16.4}$$

From the stiffness the angular natural frequency $\omega_n$ can be calculated via Equations (16.5) and (16.6), which can be converted to the natural frequency $f_n$ by dividing by $2\pi$.

$$\omega_{n-a} = \sqrt{\frac{k_a}{m}} = \sqrt{\frac{EA}{mL}} \tag{16.5}$$

$$\omega_{n-l} = \sqrt{\frac{k_l}{m}} = \sqrt{\frac{3EI}{mL^3}} \tag{16.6}$$

Now for all the parts their natural frequency can be calculated with their known dimensions and material properties. Also for every part except the motorshafts the equivalent spring constants are determined with Equations (16.2) and (16.4). This way later a simplified model of the femto-satellite can be made to determine its natural frequency.

**Motorshaft**

In this section a small analysis will be done on the momentum wheels and the motors, to see what their natural frequency is and whether it is high enough to withstand launch loads. The momentum wheels will be modelled as a mass on a clamped beam under loading. Now with Equations (16.5) and (16.6), the natural frequency of the motors can be calculated, given a shaft length of $2mm$ and shaft diameter of $0.6mm$ which is needed for the area moment of inertia $I$ and the cross-sectional area $A$ of the shaft. This leads to two fundamental frequencies, one axial and one lateral. The findings are given in Table 16.2. Aluminium material is considered since no materials for the shaft were specified by the manufacturer[3].

**Aluminium Rods**

The rods made of AL 2090 T83 have a diameter of $2.5mm$ with a thickness of $0.2mm$ and are $5cm$ long. With this their cross-sectional area and moment of inertia can be calculated. The mass for the calculations is the mass of the aluminium rod itself. The calculated natural frequencies can be seen in Table 16.2.

**Printed Circuit Boards**

The PCBs are roughly $5 \times 5$ centimetres and were initially $0.2mm$ thick. However this led to a lateral natural frequency of $12Hz$ which is far below the specified minimum natural frequency by the launchers. Therefore the PCB effective FR4 thickness was increased to $0.5mm$ ($0.71mm$ with copper layer) which led to a lateral natural frequency of $37.6Hz$ which is sufficient. The mass was calculated with an online tool[4] and the eventual calculated values can be found in Table 16.2.

**L-beams**

The L-beams are $2mm$ wide in both axis with a thickness of $0.5mm$ and are roughly $5cm$ long. The calculated area and moment of inertia and the thus following natural frequencies can be found in Table 16.2. Again the mass is the mass of the L-beam itself.

**Flanges**

The Flanges are simplified for the model, their cross-sectional area stays about the same over the flange despite the changing cutout shapes. Therefore their moment of inertia is simplified as well as a plate of $12mm$ wide, $2.5cm$ long and $0.2mm$ thick. The shortened length follows from the fact that they are pinned at top and bottom and are much less rigid than the pieces they are attached to. The simplification leads to a lower moment of inertia than the actual one, but this is a more worse case, so if the found fundamental frequency is still within the requirements it is justified. Fundamental frequencies in both lateral directions are shown with their respective moment of inertia in Table 16.2.

**Whole Structure**

Now all the parts have been checked the whole satellite can be modelled and checked on its natural frequency. This is done by cutting the femto-satellite in the middle in both axial and lateral direction. Since parallel spring constants can be merged together by simply adding them up, the natural frequency can be simply calculated by using the Equations (16.5) and (16.6), taking the the total mass of the femto-satellite of $72g$. Since in both section cuts an axial and lateral vibration can occur these are shown separately. For this analysis the flanges have an effective length of $5cm$. See Table 16.2. As shown the natural frequency, in any direction, of the whole structure is more than 5 times the required natural frequency of the launchers, satisfying requirement **TS-SYS-POD-09**. All separate parts also satisfy this requirement as can be seen from 16.2.

[3] Electro motor datasheet, `https://fmcc.faulhaber.com/resources/img/EN_0308_B_DFF.PDF`, retrieved on 13-06-2016

[4] Leiton circuit boards, `http://www.leiton.de/leiton-tools-weight-calculation.html`, retrieved 16-6-2016

Table 16.2: Fundamental frequencies for critical parts and total structure. * indicates matching lateral direction.

| | **Rods** | **Motorshaft** | **PCB** | **L-beams** | **Flanges** | **Flanges** | **Axial Struc.** | **Lat. Struc.** |
|---|---|---|---|---|---|---|---|---|
| I $[m^4]$ | $9.6\times10^{-13}$ | $6.4\times10^{-15}$ | $5.2\times10^{-13}$ | $5.9\times10^{-13}$ | $5.8\times10^{-15}$ | $5.8\times10^{-15}$ | - | - |
| I $[m^4]$ | - | - | - | - | $2.9\times10^{-11}*$ | $2.9\times10^{-11}$ | - | - |
| A $[m^2]$ | $1.4\times10^{-6}$ | $2.8\times10^{-7}$ | 0.0025 | $1.75\times10^{-6}$ | $2.4\times10^{-6}$ | $2.4\times10^{-6}$ | - | - |
| E $[GPa]$ | 76 | 69 | 210 | 76 | 76 | 76 | - | - |
| L $[mm]$ | 50 | 2 | 50 | 50 | 25 | 50 | - | - |
| m $[g]$ | 0.19 | 0.99 | 4.7 | 0.18 | 1.295 | 1.295 | 72 | 72 |
| $k_a$ $[N/m]$ | $2.2\times10^{6}$ | - | $1.1\times10^{9}$ | $3.4\times10^{6}$ | $7.3\times10^{6}$ | $3.6\times10^{6}$ | $1.6\times10^{7}$ | $3.3\times10^{9}$ |
| $k_l[N/m]$ | 1756 | - | 263 | 2339 | 85 | 11 | $1.13\times10^{5}$ | $1.16\times10^{5}$ |
| $k_l[N/m]$ | - | - | - | - | $4.3\times10^{5}$ | $5.3\times10^{4}$ | - | - |
| Axial $f_n$ $[Hz]$ | 17243 | 15719 | 7523 | 22335 | 37787 | - | 2373 | 34073 |
| Lateral $f_n$ $[Hz]$ | 488 | 2042 | 37.6 | 582 | 40.5 / 2900* | - | 199 | 202 |

### 16.2.2. Harmonic and Random Vibration

After natural frequency the harmonic and random vibrations will be checked, in the Soyuz and DNEPR manuals [59, 60] these are given in forms of frequency versus amplitude in $g's$ and as frequency versus Power Spectral Density (PSD). Since acceleration $g$ is an acceleration it can replace $\ddot{x}(t)$ in Equation (16.9), which is derived from a standard sine wave like in Equations (16.7) and (16.8). With the known frequency $f$, the value of $g$ equal to 9.81 and the fact that a standard sinusoid can never be bigger than 1, and taking this value as worst case, the actual amplitude $A$ can be calculated, as can be seen in Table 16.3. The Soyuz is taken as main launcher to analyse the vibrations since it has the biggest deflections. Also in this analysis it is assumed that the femto-satellite is in its deployment interface and is only deflected on its principal axes and if so, has contact on the whole of one of its surfaces. Analysis is performed on the whole femto-satellite rather than specific subsystems.

$$x(t) = Asin(2\pi f t) \tag{16.7}$$

$$\dot{x}(t) = A2\pi f cos(2\pi f t) \tag{16.8}$$

$$\ddot{x}(t) = -A(2\pi f)^2 sin(2\pi f t) \tag{16.9}$$

$$\frac{X}{Y} = \left(\frac{1+(2\zeta r)^2}{(1-r^2)^2+(2\zeta r)^2}\right)^{1/2} \tag{16.10}$$

However this does not yet say anything about what the femto-satellite is experiencing during the launch, so with the use of Equation (16.10) [58] this can be investigated. Assuming no damping, $X$ the femto-satellite amplitude, $Y$ the launcher amplitude and $r = \omega_b/\omega_n = f_b/f_n$, where $\omega_b$ and $f_b$ are the frequency of the base excitation exerted by the launcher. This equation states that the femto-satellite moves with the launcher for small values of $r$, since then both deflections are close to each other. The biggest difference occurs when the natural frequency of the femto-satellite is reached, which is about $199Hz-202Hz$, then $r$ is close to 1, and resonance occurs. After that $r$ gets even smaller than 1, but $\frac{X}{Y}$ decreases again, meaning the femto-satellite and the launcher start to move alike again. The amplitudes calculated before show that the biggest deflections occur at the lower frequencies and gradually get less with the higher frequencies. This means that at the lower frequencies $\frac{X}{Y}$ should be as close as possible to 1 to make sure the femto-satellite moves together with those deflections. The amplification factor $\frac{X}{Y}$ is calculated with a arbitrary natural frequency of $207Hz$ and the input of the frequency from the launcher, as can be seen in Table 16.3. After that a value of 1 is subtracted from the calculated value to find the difference of amplitude, after which this is multiplied by the deflection present at that frequency. This way the relative deflection compared to the launcher is calculated. For the simulation the natural frequency of the femto-satellite is set to $207Hz$ and at this frequency the maximum deflection is about $0.0139mm$ due to random vibrations, as can be seen the harmonic vibrations do not dominate the spectrum. To reach $0.195mm$ of total deflection due to difference in amplitude $\frac{X}{Y}$ needs to be a factor 14. The assumption for now that no damping occurs brings the fact that the amplification can go way beyond that value to infinity, in realistic scenarios there is always some kind of damping, and with a damping ratio as small as 0.05 the amplification gets maximum to about factor 10. This means that in that case the found value of $0.0139mm$ will amplify to a maximum of $0.125mm$ and not $0.195mm$. This also means that with the 0.05 damping ratio the $0.125mm$ will result in the L-beams to a maximum stress of $190MPa$, if all the deflection is resulting in equal compression, using Equation (16.1). This damping ratio is derived from a value for Q=10 from the launch manuals. The stress value found is also far below the yield stress of $520MPa$ of AL 2090T83. Since all axis contain the L-beams, they are all well protected

against these vibrations and compression. With this analysis can be concluded that the structure can withstand the harmonic and random vibrations and thus fulfilling requirement **TS-SYS-POD-09**, however actual testing should be performed as well in a later design phase. Also in realistic scenarios the high enough natural frequency will make sure that only small amplitudes get amplified and the compression of the femto-satellite because of that will lead to within acceptable stress levels.

Table 16.3: Vibration analysis of Soyuz harmonic and random vibrations. Based on the femto-satellite's natural frequency of 207$Hz$.

| **Harmonic Vibrations Soyuz** | | | | | | **Random Vibrations Soyuz** | | | | | |
|---|---|---|---|---|---|---|---|---|---|---|---|
| f [$Hz$] | g | A [$mm$] | X/Y [-] | X/Y-1 [-] | $\delta$[$mm$] | f [$Hz$] | PSD [$g^2/Hz$] | A [$mm$] | X/Y [-] | X/Y-1 [-] | $\delta$[$mm$] |
| 1 | 0.4 | 99.396 | 1 | 2E-05 | 0.00232 | 20 | 0.005 | 0.1964 | 1.0094 | 0.0094 | 0.0019 |
| 5 | 0.6 | 5.9638 | 1.0006 | 0.0006 | -1E-06 | 50 | 0.010 | 0.0703 | 1.062 | 0.062 | 0.0044 |
| 10 | 0.8 | 1.9879 | 1.0023 | 0.0023 | 0.00035 | 100 | 0.025 | 0.0393 | 1.3044 | 0.3044 | 0.012 |
| 20 | 0.8 | 0.497 | 1.0094 | 0.0094 | -0.0022 | 200 | 0.025 | 0.0139 | 15.04 | 14.04 | 0.195 |
| 30 | 0.5 | 0.1381 | 1.0215 | 0.0215 | -4E-05 | 500 | 0.025 | 0.0035 | 0.2068 | -0.793 | -0.003 |
| 40 | 0.5 | 0.0777 | 1.0388 | 0.0388 | 0.00011 | 1000 | 0.110 | 0.0026 | 0.0448 | -0.955 | -0.002 |
| 60 | 0.5 | 0.0345 | 1.0917 | 0.0917 | 0.00027 | | | | | | |
| 100 | 0.3 | 0.0075 | 1.3044 | 0.3044 | 0.00106 | | | | | | |

## 16.3. Structural Analysis

In this section the structural analysis and FEM analysis is performed to check the system requirement **TS-SYS-POD-11**. All non-FEM findings are based on beam theory. First the motorshafts are analysed on bending, buckling, tension and compression, taking the wheel mass as the load inducer. After that the L-beams and aluminium rods are analysed on compression, tension and buckling, with one fourth of the femto-satellite mass as load inducer, because 4 beams and rods are always present. For the aluminium rods the PCBs are considered to be pinned points. As last the FEM analysis on the PCBs is done.

The highest load present is 8.3$g$, taken from Table 16.1. This in combination with the safety factor of 1.3 gives a maximum load of 10.8$g$. For compression and tension stresses the load is divided over the area of the part. For bending stresses Equation (16.11) is used and for buckling Equation (16.12). In which $M$ is the moment in $Nm$, $y$ the distance to the centre of gravity in $m$, $I$ the moment of inertia in $m^4$, $n$ the number of harmonic waves, $E$ the Young's modulus in $Pa$ and L the length of the beam in $m$. All properties of the parts can be found in Table 16.2. The findings of the analysis can be found in Table 16.4. From the analysis can be concluded that system requirement **TS-SYS-POD-11** is satisfied.

$$\sigma = \frac{My}{I} \tag{16.11}$$

$$F_{crit} = \frac{n^2\pi^2 EI}{L^2} \tag{16.12}$$

Table 16.4: Data on structural analysis.

| | Motorshaft ($\sigma_y = 370MPa$) | | | L-beam ($\sigma_y = 520MPa$) | | Aluminium rod ($\sigma_y = 520MPa$) | |
|---|---|---|---|---|---|---|---|
| | **Compression** | **Buckling** | **Bending** | **Compression** | **Buckling** | **Compression** | **Buckling** |
| $\sigma$ [MPa] | 0.37 | - | 9.89 | 1.09 | - | 0.066 | - |
| $F/F_{crit}$ [N] | - | $9.68\times10^{-5}$ | - | - | $6.42\times10^{-3}$ | - | $6.6\times10^{-3}$ |

### 16.3.1. Printed Circuit Boards

The PCBs are analysed with the finite element method (FEM) module of CATIA V5 R21. This allows the analysis of quasi two-dimensional objects like the PCBs as opposed to narrow beams which could be analysed by hand using beam theory. The FEM algorithm in CATIA relies on the following three hypotheses:[5]

- small displacement in translation and rotation
- small strain
- linear elasticity

CATIA divides the component into a mesh consisting of tetrahedrons. The mesh size is set to 0.5 $mm$, the minimum that CATIA can handle without shutting down. FR-4, the material of the PCBs has a tensile strength of 310 $MPa$, a

[5]CATIA documentation, `http://catia.tudelft.nl/b20doc/English/online/CATIAfr_C2/estugCATIAfrs.htm`, retrieved on 15-06-2016

Young's modulus of 21 $GPa$ and a Poisson's ratio of 0.127 [6]. The boundary conditions are assumed to be the following: the PCBs are clamped at the pinholes and forces are applied corresponding to the masses of the components on the PCBs. I. e. the masses are multiplied with an acceleration of 8.3 $g$, the maximum acceleration given in Table 16.1 and with 1.3, the safety factor required for the DNEPR rocket and given in the beginning of this chapter.

The resulting stresses for PCB1, the PCB with the highest loading, are shown in 16.1. The displayed displacement is exaggerated. For all PCBs the highest stresses occur right next to the clamping positions and the highest displacements occur in the middle of the plate. Table 16.5 summarises the results of the FEM analysis.

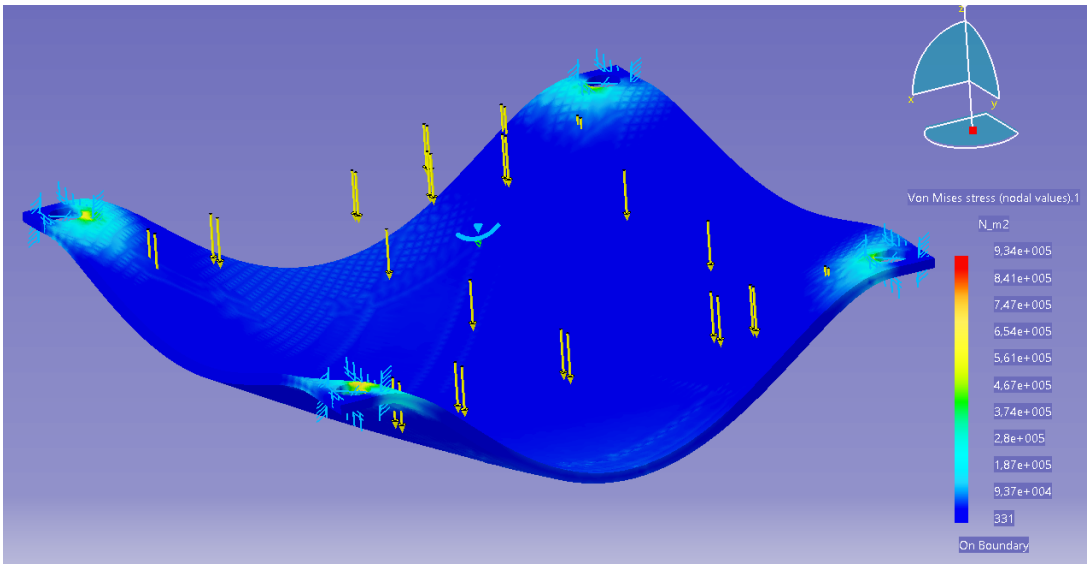


Figure 16.1: FEM-analysis of PCB1

Table 16.5: Maximum stress and displacement of PCBs under 8.3 $g$ launch load

| | **Max. stress** $[MPa]$ | **Max. displacement** $[\mu m]$ |
|---|---|---|
| PCB1 | 0.934 | 1.89 |
| PCB2 | 0.240 | 0.46 |
| PCB3 | 0.608 | 1.59 |

Obviously the PCBs are extremely over-designed with regard to static loading as the maximum stress is 3 orders of magnitude below the tensile strength. However the result of the vibrational analysis requires them to be that thick.

The verification and the validation plan of the FEM model are explained in Subsection 20.3.2.

[6] FR-4 epoxy insulation board data sheet, `http://www.newlytrend.com/172-fr-4-epoxy-insulation-board.html`, retrieved on 17-06-2016

# 17

# Configuration and Structure

This chapter starts with a trade-off for the optimal shape of the satellite. After that the components of the structure are selected. Then the final architecture of femto-satellite will be discussed. The placement of different subsystems, the shape of the satellite and a primary view of the whole system. Also the hardware and software diagram are also introduced as it will also influence the configuration.

## 17.1. Shape of the Femto-Satellite

The shape of the femto-satellite is determined by several different parts. The first one is integration difficulty, as the whole system needs to be integrated within the shape, it need to provide enough spaces for these subsystems. Second one is the manufacturing difficulty: as the femto-satellite is small, the difficulty of manufacturing should be limited to a relatively low range. The third is mountability of the shape, as the femto satellite need to be installed on the host spacecraft. The last one is the structural efficiency. From the research of different satellites, four different shapes are normally used as octagonal prism, sphere, cube and hexagonal prism. Besides these shapes, the single plate structure is also considered. The advantages and disadvantages are given in Table 17.1.

- **Cube** *Advantages*: Easy to manufacture, larger surface area for the same volume, easy integration, smaller number of joints.
  *Disadvantages:* Problems in arranging items in the sharp corner, surface for solar panel maybe not sufficient for the power usage.
- **Octagonal prism** *Advantage:* Slightly larger volume than cube, less sharp corners.
  *Disadvantage:* More number of joints which brings extra weight and risk. Difficult to assemble.
- **Sphere** *Advantage:* Larger volume for less material
  *Disadvantage:* Hard to manufacture, difficult to integrate with the launch, cannot utilise full space available due to the curved surface
- **Hexagonal prism** *Advantage:* Larger volume than cube with the same amount of material used, sharp corners are less.
  *Disadvantage:* Difficult to build a perfect structure due to the angular constraints, too many joints which need many bolts and nuts that increases the weight
- **Single plate structure** *Advantage:* Easy manufacturing, easy integration with host satellite, larger surface area.
  *Disadvantage:* Hard to integrated with subsystems like momentum wheel, weak in structure.

Table 17.1: Comparison of different shapes

| | Manufacturing difficulty | Ease of integration | Structural efficiency | Mountability | Volume efficiency |
|---|---|---|---|---|---|
| Cube | Good | Good | Good | Good | Moderate |
| Sphere | Bad | Bad | Good | Bad | Good |
| Octagonal prism | Bad | Moderate | Moderate | Good | Good |
| Hexagonal prism | Bad | Moderate | Moderate | Good | Good |
| Single plate stucture | Good | Bad | Bad | Good | Good |

In conclusion, based on the analysis of these advantages and disadvantages the cube is selected as the final shape of femto-satellite. Starting from the volume of different subsystems, the structure should be able to provide enough space to contain these subsystems. Based on the total volume, the size of the cube is chosen as $5cm \times 5cm \times 5cm$.

## 17.2. Components of the Structures Subsystem

The structural subsystem of the femto-satellite has to provide strength and stiffness during operation and especially in face of the launch loads. Since all equipment is installed within the structure, the structure has to connect and support this equipment. When these masses are accelerated during launch, the structure has to transfer the forces to the host satellite. First the structure is sized based on engineering experience, the structural analysis is conducted in Chapter 16 to check if it fulfils requirements **TS-SYS-POD-09** and **TS-SYS-POD-11**. A few iterations were required to come up at the final structure represented here. The steps in between are not documented.

All equipment is mounted to three PCBs. These are fixed to 4 hollow aluminium pins of 2.5 $mm$ diameter and 0.2 $mm$ thickness which are held together by two holders. The holders are quadratic structures made up of L-profiles with a

height of 2 $mm$ and a thickness of 0.5 $mm$. 6 grid plates are mounted to the outside of the holders. Their function is to provide support for the kapton foil required by the thermal subsystem. The pins and holders are made from an aluminium-titanium because of that alloy's superior strength and the grid plates are made from aluminium-lithium 8090 because it is comparatively light. The PCBs have a size of $47.5 \times 47.5 mm$, slightly smaller than the satellite. They have a carrier thickness of 0.5 $mm$. This is similar to PCB thicknesses used by TU Delft's Micro Aerial Vehicle Lab. A copper thickness of 35 $\mu m$ and copper density of 50% were assumed. The layer count is assumed to be 6[1] but it remains to be seen during PCB design whether this is the right choice. Using Leiton's online tool[2] the mass was calculated as 4.7 $g$ per board and the total thickness was calculated to be 0.71 $mm$. Table 17.2 summarises the mass of each component of the structures subsystem. Except for the PCBs, the masses were obtained from the CATIA model. The structure can be manufactured at Metaalwinkel BV for €821.99, including material cost.

Table 17.2: Component masses of the structures subsystem

| **Component** | **Number** | **Component mass** [$g$] |
|---|---|---|
| PCB | 3 | 4.7 |
| Side panel | 4 | 0.52 |
| Camera side panel | 1 | 0.63 |
| SIDD side panel | 1 | 0.61 |
| Pins | 4 | 0.16 |
| Holders | 2 | 2.00 |
| **Total mass** | | **21.66** |

## 17.3. Configuration of Femto-Satellite

The internal configuration of the femto-satellite consists of different subsystems. As one of the challenges brought by the limited volume and weight, the femto-satellite will be highly compact in order to accommodate all the subsystems. As all the subsystems will be connected together by PCBs, based on a surface area calculation, at least 3 PCB are needed. However, the femto-satellite also imposes a limit in height, the more PCBs used the smaller each layer's height is. Also sub-systems like the spherical inflatable de-orbiting device and battery are relative large parts which will be the limiting factor for the distance between the PCBs. Due to these limits, 3 PCBs are chosen. The top PCB panel includes the communication system and all the chips for data handling. On the other side of the PCB all the batteries are installed. On the second PCB, two of the momentum wheels and their speed controllers are included. In the bottom panel, the other momentum wheel and its speed controller is installed together with the de-orbiting system. Integrating different systems is not just about putting them there, all the placements need to be carefully considered. In this case, three momentum wheels are placed in 3 mutually perpendicular planes in order to provide 3-axis control. The communication module is installed near the surface to ensure communication quality. Similarly, the de-orbiting system, the camera and the power switch are also placed on one surface in order to deploy the balloon easily. The satellite configuration is given in Figure 17.1.

[1] welldone blog, `http://www.fedevel.com/welldoneblog/2013/09/3-steps-how-to-determine-calculate-number-of-pcb-layers/`, retrieved on 14-06-2016

[2] Leiton PCB weight calculator, `http://www.leiton.de/leiton-tools-weight-calculation.html`, retrieved on 15-06-2016

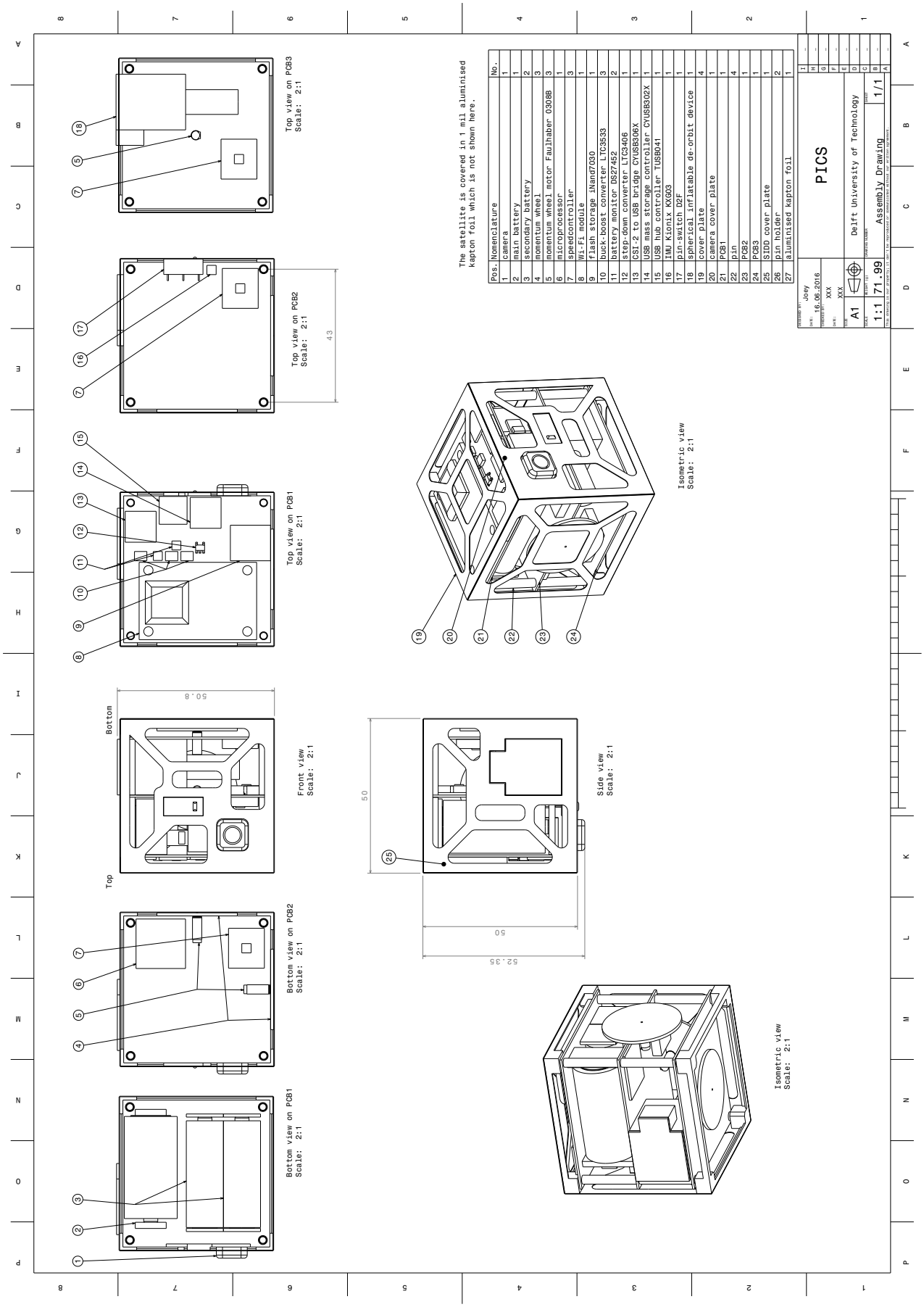


Figure 17.1: Configuration drawing of the PICS femto-satellite

## 17.4. Resource Allocation

After showing the layout of the design a concise overview of all the parts is presented. The resource allocation of the femto-satellite is shown in Table 17.3 and the resource allocation of the deployment system is shown in Table 17.4. These tables shows the mass, dimensions, power usage and cost for all of the individual parts of the system

Table 17.3: Resource allocation

| **Components (amount)** | **Mass** [$g$] | **Dimensions** [$mm$] | **Power use**[$mW$] | **Cost** [€] |
|---|---|---|---|---|
| | | **Payload** | | |
| Samsung S6 camera | 1.9 | 27.2×12.4×4.6 | 600-800 | €33.60 |
| Sub total | 1.9 | 1551 [$mm^3$] | 600-800 | €33.60 |
| | | **Communication** | | |
| ESP8266 Wifi module [3] | 5 | 25×38×5 | 460 | €8.84 |
| Sub total | 5 | 4750 [$mm^3$] | 460 | €8.84 |
| | | **ADCS** | | |
| Kionix KGX03 [4] | 0.02 | 3×3×1 | 6.1 | €3.79 |
| Faulhaber 0308 B (x3) | 0.35 (×3) | ∅0.6 ×10.4 (×3) | 195 | €300 (×3) |
| MX-3A ESC (x3) [5] | 0.36 (×3) | 12.9×11.6×3.4 (×3) | - | €8.5 (×3) |
| Momentum wheel(x3) | 1 (×3) | ∅26 ×1.016 (×3) | - | €16.67 (×3) |
| Sub total | 5.15 | 15 092 [$mm^3$] | 201.10 | €979.29 |
| | | **Active de-orbit device** | | |
| Envelope | 1.5 | - | - | €305 |
| Storage | 5.08 | 18×18×21.5 | - | €100 |
| Inflation system | 2 | ∅12 ×21.2 | 9500 | €4000 |
| Hold and release mechanism | 3.75 | 5×10×10 | <1000 | €10 |
| Sub total | 12.33 | 9864 [$mm^3$] | <10 500 | €4415 |
| | | **Command and data handling** | | |
| SAMA5D31[6] | 0.47 | 16×16×0.8 | 205 | €7.41 |
| CYUSB306X [7] | 0.186 | 10×10×0.8 | 24 | €17.20 |
| TUSB8041 [8] | 0.188 | 9×9×1 | 0.0495 | €6.78 |
| CYUSB30×2 [9] | 0.186 | 10×10×0.8 | 540 | €17.47 |
| iNAND 7030 [10] | 0.418 | 11.5×13×1.2 | 630 | €57.58 |
| Sub total | 1.45 | 657 [$mm^3$] | 1399.05 | €106.44 |
| | | **Power** | | |
| Main battery [11] | 16 | ∅17.1 ×34.5 | - | €10.11 |
| Secondary battery (x2)[12] | 3 (×2) | ∅6 × 36 (×2) | - | €1.07 (×2) |
| Battery monitor (x2)[13] | 0.02 (×2) | 2.9 × 2.9 × 1.1 (×2) | - | €1.61 (×2) |
| Converter 1.2V [14] | 0.01 | 2.9 × 1.5 × 1 | - | €2.93 |
| Converter 1.8,3.3,5V (x3)[15] | 0.02 (×3) | 4 × 3 × 0.75 (×3) | - | €5.69 (×3) |
| Micro switch [16] | 0.5 | 12.7 × 5.8 × 5.5 | - | €0.06 |
| Wiring | 1.39 | - | - | - |
| Sub total | 24.00 | 10 414 [$mm^3$] | - | €35.55 |
| | | **Thermal & structures** | | |
| Kapton foil [17] | 0.5 | 0.0254×15 000 $mm^2$ | - | €202.00 |
| PCB(x3) [18] | 4.7 (×3) | 0.71×47.5×47.5 (×3) | - | €75.33 (×3) |
| Side panel(x6) | 0.55 (×6) | 0.2×49.6×49.6 (×6) | - | €106.39 (×6) |
| Pins(x4) | 0.06 (×4) | ∅2.5×44 (×4) | - | €3.70 (×4) |
| Holders(x2) | 2 (×2) | 5×49.6×49.6 (×2) | - | €76.00 (×2) |
| Aluminium parts: delivery | - | - | - | €16.85 |
| Sub total | 22.16 | 33 605 [$mm^3$] | - | €1226.84 |
| **Total** | **71.99** | **75,933** [$mm^3$] | - | **€6805.56** |

Table 17.4: Resource allocation (ctd.)

| Components (amount) | Mass [$g$] | Dimensions [$mm$] | Power use[$mW$] | Cost [€] |
|---|---|---|---|---|
| **Deployment System** | | | | |
| Springs (×4) [19] | 0.505 (×4) | ∅ 3.18 x 105 (×4) | - | €479 (×4) |
| Spring guiding pins (wide) (×2) [20] | 11.02 (×2) | ∅ 2.92 x 105 (×2) | - | €3.515 (×2) |
| Spring guiding pins (narrow) (×2) [21] | 2.16 (×2) | ∅ 1.46 x 60 (×2) | - | €3.515 (×2) |
| Exterior structure [22] | 547 | 244 x 70 x 5 (×2)<br>70 x 70 x 5 (×1) | - | |
| Satellite-supporting plate [23] | 23.6 | 50 x 50 x 1.88 (outer)<br>30 x 30 x 1.88 (inner) | - | |
| Deployment door [24] | 68.6 | 70 x 70 x 5 | - | €11.50 |
| Electric rod-style actuator | 119 | 28 x 35 x 30<br>∅ 17.5 x 50.5<br>∅ 6 x 9.5 | 6000 | €300 |
| Nichrome wire (×2) [25] | 0.166 (×2) | ∅0.254 x 10 (×2) | 3400 | €1.31 (×2) |
| Vectran cables (×2) [26] | $0.6 \cdot 10^{-6}$ (×2) | ∅ 0.90 x 650 (×2) | - | €10.64 (×2) |
| Sliding rails (×8) [27] | 1.4 (×8) | 100 x 5 x 1 (×8) | - | €0.38 (×8) |
| **Total** | **798** | **271,892 $mm^3$** | **9400** | **€2268** |

The parts of the femto-satellite are given in the first column. Behind some parts a multiplication with a number is given, which means how many of this part are in the femto-satellite. The same goes for the mass, dimensions and costs. The provided power is not given in this table since not all the systems are active at the same time. Therefore showing the power input and output will be confusing. Also the total power uses is not given since not all the systems will be active at the same time. Chapter 13 shows more information about the power architecture. In the bottom the total mass, part volume and bus cost of the femto-satellite are given. A cube of 125000 [$mm^3$] is used, so 60.7% of the space is occupied and the total bus cost is €6805.56.

During the design the mass was tracked. Table 17.5 shows the evolution of the design mass and target value up till the midterm review. The mass budget from the midterm review on is tracked on day to day basis. This evolution can be

[4] ESP8266 Pricing, https://www.adafruit.com/product/2471, retreived on 16-06-2016
[5] Kionix KGX03 Pricing http://www.digikey.com/product-detail/en/kionix-inc/KXG03-1034-FR/1191-1043-1-ND/5972707, retrieved on 15-06-2016
[6] MX-3A Pricing, http://www.hobbyking.com/hobbyking/store/__44315__SuperMicro_Systems_Brushless_ESC_3_0A.html, retrieved on 14-06-2016
[7] SAMA5D31 Pricing,http://www.atmel.com/devices/ATSAMA5D31.aspx, retrieved on 14-06-2016
[8] CYUSB306X Pricing,http://www.digikey.com/product-detail/en/cypress-semiconductor-corp/CYUSB3065-BZXI/CYUSB3065-BZXI-ND/4917723, retrieved on 14-06-2016
[9] TUSB8041 Pricing,http://nl.mouser.com/Texas-Instruments/Semiconductors/Interface-ICs/USB-Interface-IC/TUSB8041-Series/_/N-451w3?P=1yv9xliZ1z0zls6, retrieved on 14-06-2016
[10] CYUSB30×2 Pricing,http://www.cypress.com/part/cyusb3025-bzxi, retrieved on 14-06-2016
[11] iNAND 7030 Pricing,http://nl.mouser.com/Search/Refine.aspx?Keyword=inand+7030, retrieved on 14-06-2016
[12] Tekcell CR123 Pricing, http://www.aliexpress.com/store/product/100-original-battery-for-TEKCELL-CR123A-3V-non-rechargeable-lithium-battery/1898672_32577080525.html, retrieved on 14-06-2016
[13] Turnigy nano tech battery Pricing, http://www.hobbyking.com/hobbyking/store/__23310__Turnigy_nano_tech_90mah_1S_15C_Round_Cell.html, retrieved on 14-06-2016
[14] DS2745 Pricing, http://www.distrelec.nl/nl/batterij-lader-ic-umax-maxim-ds2745u/p/17386192?wt_mc=x.fed.chips.x.-&utm_source=chipsX&utm_medium=feed, retrieved on 14-06-2016
[15] LTC3406-1.2 Pricing, http://www.linear.com/purchase/LTC3406-1.2, retrieved on 14-06-2016
[16] LTC3533 Pricing, http://www.linear.com/purchase/LTC3533, retrieved on 14-06-2016
[17] D2F Pricing, http://www.ebay.com/bhp/omron-micro-switch, retrieved on 14-06-2016
[18] PCB Pricing, http://www.pcbway.com/orderonline.aspx, retrieved on 16-06-2016
[20] Stainless Steel Rod, http://www.ebay.com/bhp/stainless-steel-rod-3-16, retrieved on 17-06-2016
[21] Stainless Steel Rod, http://www.ebay.com/bhp/stainless-steel-rod-3-16, retrieved on 17-06-2016
[22] Metals Depot, http://www.metalsdepot.com/catalog_cart_view.php?msg=, retrieved on 17-06-2016
[23] Metals Depot, http://www.metalsdepot.com/catalog_cart_view.php?msg=, retrieved on 17-06-2016
[24] Metals Depot, http://www.metalsdepot.com/catalog_cart_view.php?msg=, retrieved on 17-06-2016
[25] Nichrome Resistance Wire, http://www.ebay.com/bhp/nichrome-resistance-wire, retrieved on 17-06-2016
[26] Braided Vectran 200 - Spools, http://estore.twinline-usa.com/products/braided-vectran-200-spools-black, retrieved on 19-06-2016
[27] Metals Depot, http://www.metalsdepot.com/catalog_cart_view.php?msg=, retrieved on 17-06-2016

seen in Figure 17.2. The black horizontal line at 69.6 grams is the target value for this design phase. At the second of June it was concluded that an appropriate propulsion system for this mission can not be designed. So the nature of the mission changed and propulsion was no longer needed. More information can be found in Chapter 18. At the eight of June the active de-orbit device was added to reduce the de-orbit time since preventing space debris is an important factor in this design. The final design is still 2.39 grams above the target value for this design phase. As explained in the Contingencies and margins Section 5.4, small deviation will not be fully investigated. The final design is expected to stay below 100 grams with this deviation.

Table 17.5: Mass and Volume budget for the orbiting spacecraft

| **Mass** [*g*] | **Payload** | **ADCS** | **Propulsion** | **Comm.** | **Power** | **Structure** | **Total** | **Target** |
|---|---|---|---|---|---|---|---|---|
| Baseline | 8.9 | 6 | 15 | 1.8 | 18 | 10 | 59.7 | 59.4 |
| Midterm | 1.5-9 | 9.5-21 | 7.5-8.5 | 1-4 | 14.9 | 15 | 49.4 - 60.9 - 72.4 | 61.5 |
| Final | 1.9 | 5.15 | 0 | 5 | 24 | 22.16 | 71.99 | 69.6 |

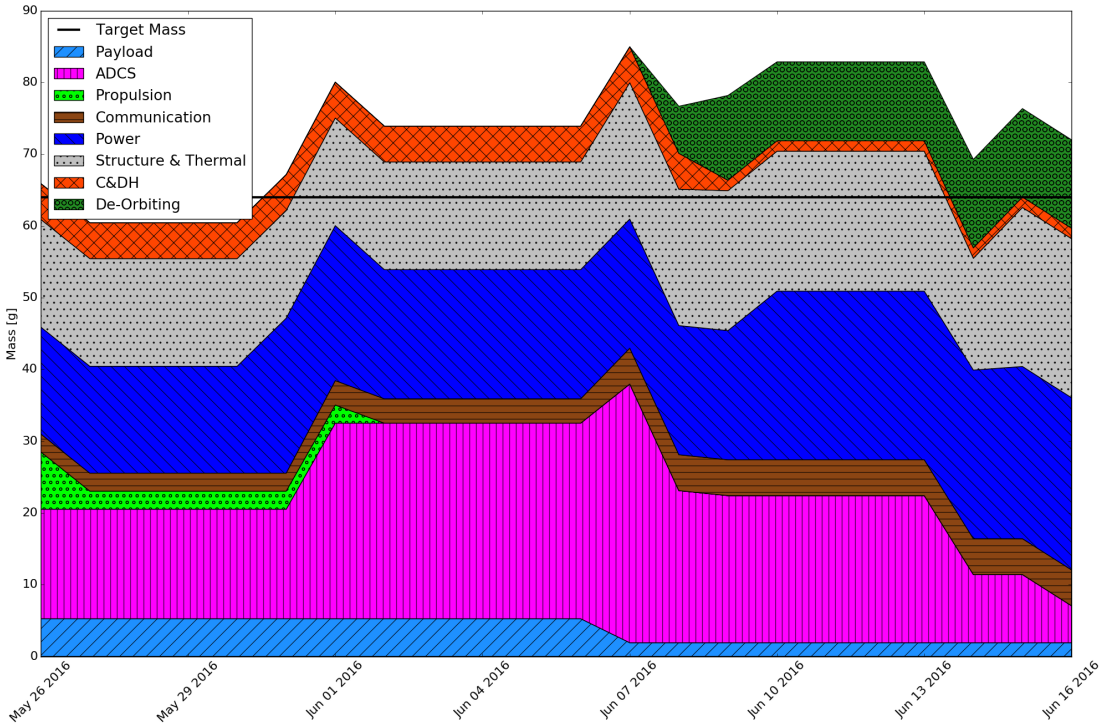


Figure 17.2: The evolution of the mass budget the detailed design duration.

## 17.5. Hardware and Software Diagrams

The hardware diagram is shown in Figure 17.3. This diagram shows how the components are connected to the other components. This will give a clear and concise overview of all the hardware on board of the femto-satellite. The software block diagram can be seen in Figure 17.4. This diagram shows which software is active in what phase of the mission. Also it shows the interaction and dependence of each of the software elements. This diagram shows that each of the systems will be tested before the release and when all systems are checked, the femto-satellite will be launched.

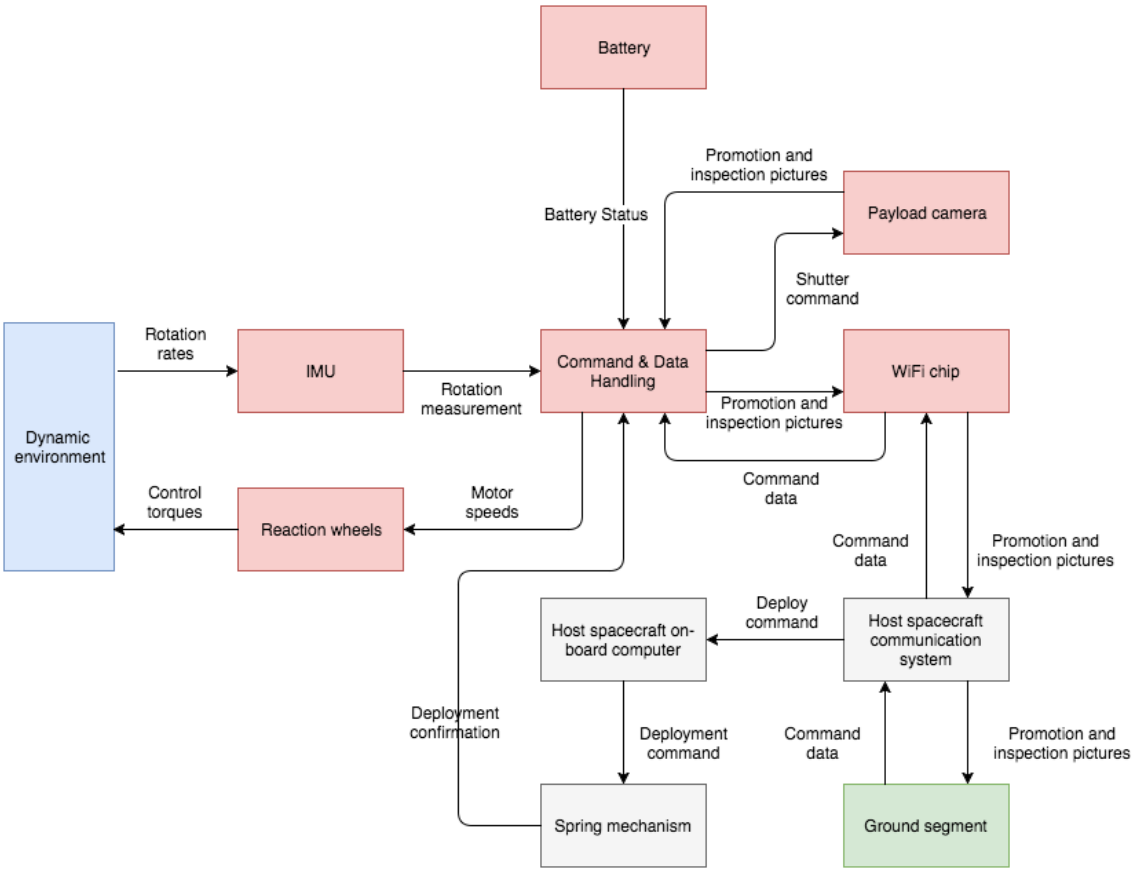


Figure 17.3: Hardware diagram of the femto-satellite

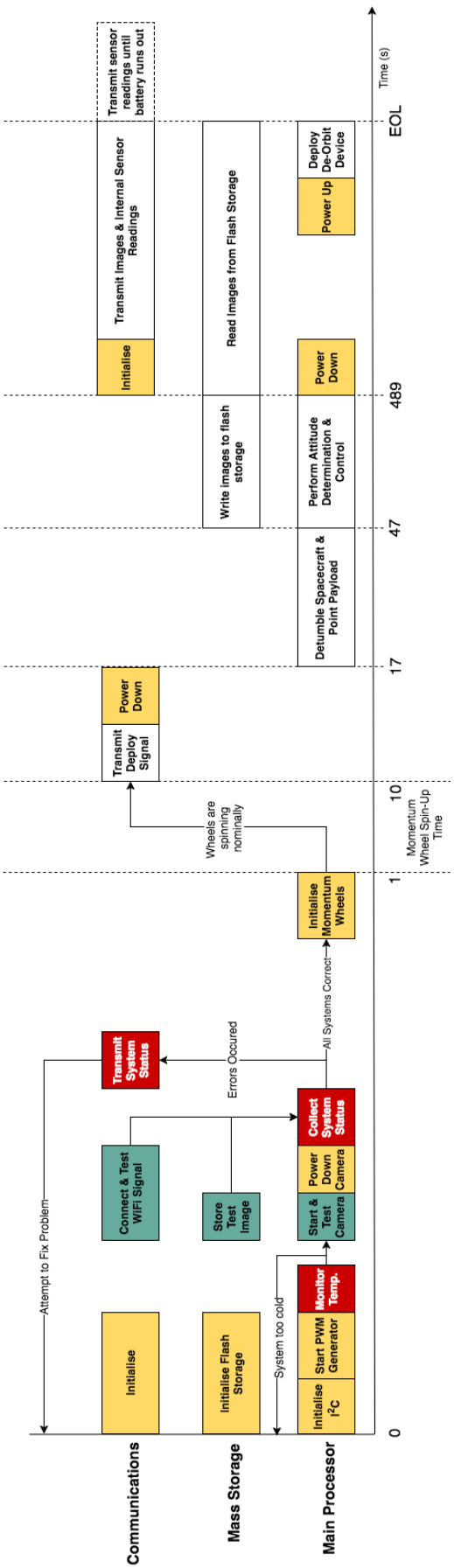


Figure 17.4: Software diagram for the femto-satellite throughout the mission

# 18

# Design Iterations

During the technical design process of the femto-satellite a series of iterations were made, this chapter documents these iterations. Design iterations were made every day but only a few major iterations are identified and presented in this chapter. In Section 17.4 a day-to-day change of the mass budget can be seen. In this section the major design iterations that were made are documented.

## 18.1. Iteration 0 on 26-05-2016

This iteration is the iteration from the midterm report [5]. This iteration will be used as a baseline and the iterations in the future sections will only explain the differences with this and previous iterations.

In the midterm the mission statement was as follows:
*"DSE group S13 at the Faculty of Aerospace Engineering at TU Delft will design a femto-satellite to demonstrate its inspection and promotion potential."[5]*

This mission was to be executed by a free-orbiting femto-satellite that is using a combination of a football and oscillating orbit around the host spacecraft to inspect and take promotion pictures. This femto-satellite is launched from the host using a spring system and will perform its orbit injection using an on-board propulsion system. The femto-satellite will communicate with the host satellite via Bluetooth because of its low power usage. The data rate is low but the contact time with the host satellite is long. So this will not be a problem. The host satellite will relay the information between the ground station and the femto-satellite. At the midterm the average mass is 60.9 grams, which is 0.6 grams below target, the power budget is 2.8 watts under operation of all components simultaneously and the $\Delta V$ is 0.0567 meters per second.

## 18.2. Iteration 1 on 02-06-2016

By using the astrodynamic model GMAT R2015a, it was found that the $\Delta V$ required for orbit maintenance is far too high. Furthermore, the ADCS turned out to be heavier than anticipated. Therefore a major re-design effort was required.

**Orbit**

The motion of the host spacecraft and femto-satellites were modelled in GMAT and their relative distance was measured. Without orbit corrections, the satellite drifts away by 110 $m$ over the course of the first orbit. This drift is mainly due to the difference in drag which in turn stems from the difference in area over mass ratio between the two satellites. The area over mass ratio of the femto-satellite is much higher because the area only scales with the square while the mass scales with the cube of a satellite's dimensions.

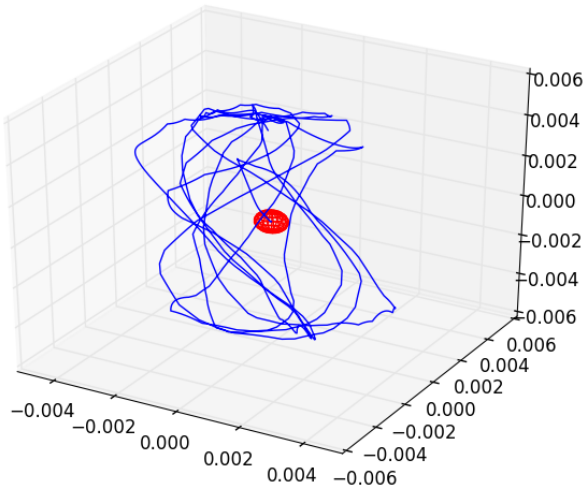


Figure 18.1: Motion of the femto-satellite in a non-rotating reference frame centred at the host spacecraft in 24 hours. Delta-Vs are applied to keep the distance between the two satellites within 3.38 $m$. The red ball in the centre symbolises a host spacecraft with a diameter of 1 $m$. The axis scale is kilometres.

A script was programmed to apply impulse burns that keep the femto-satellite within 3.38 metres of the host spacecraft which is the minimum working distance of the i-Phone 6S camera (See Table 8.1). This camera was selected as payload in design iteration 0. The script also kept track of the cumulative delta-V. It has to be noted that the script for calculating the required burns is not very efficient although some optimisation steps have been conducted. It results in a delta-V of about 10 $m/s$ per orbit. Even though the script for computing the burns is not totally optimised, this is way too high. The propulsion system proposed can only deliver $5 m/s$ total, which would be all used in less than half an orbit. It appears unlikely that the algorithm's efficiency can be increased sufficiently to make up for this. The trajectory of the femto-satellite

with respect to the host spacecraft is shown in Figure 18.1. The reference frame is non-rotating and centred at the host spacecraft.

**Attitude Determination and Control**
During the technical design of the momentum wheel system it was discovered that a major oversight was made during the conceptual design stages, which is that electronic speed controllers were forgotten to be included to the mass per momentum-wheel setup. These speed controllers weigh around 4 $g$ and would add another 12 $g$ to the system if 3 momentum-wheels are used, which would make it far too heavy to be used on the femto-satellite.

**Iteration Change**
In the new iteration the femto-satellite will no longer be inserted into a football and oscillating orbit but will instead be inserted into a simpler orbit with the spring system. After insertion the femto-satellite will slowly drift away from the host spacecraft. This change has the following consequences:

- No propulsion system is required due to the fact that the insertion can be done directly.
- The power subsystem is greatly simplified since the mission duration is shortened. This means there is no longer a need for a rechargeable battery or solar panels.
- The ADCS can be simplified since with the short on-orbit lifetime it is no longer necessary to de-saturate the momentum wheels. This means that the increased weight with the speed controllers can be compensated by having no mass for propulsion and no mass for magnetorquers.
- The ADCS can be simplified further by removing the cameras and GPS for attitude determination since the drift of the IMU is small enough that the femto-satellite will not lose sight of the host-spacecraft.

Also a de-orbiting system will be added to the spacecraft to make sure that the spacecraft will be able to de-orbit quickly. This addition can be made since a lot of mass was saved on the other subsystems. All of the research that was performed into the propulsion system up to this point is still available in Appendix C.

## 18.3. Iteration 2 on 08-06-2016
On this day there was a major revision to the attitude determination and control subsystem. After the previous iteration the mass went down, however the mass kept increasing after this again which meant that something had to be done to make sure that the system does not go over the design mass. The maximum femto-satellite mass on this day reached 86 $g$, while the target mass was still 64 $g$.

Combined with the changes from iteration 1 it was decided that the ADCS can be greatly simplified since there is no need for the complicated camera system. This helps greatly with reducing power consumption and mass. Due to the short mission lifetime there will only be reliance on the IMU and periodic images from the payload camera. All of the research that was performed into the absolute sensors up to this point is still available in Appendix B.

## 18.4. Iteration 3 on 16-06-2016
This iteration flows very naturally from the modifications made after the last one and no major redesigns were required. Due to the ever-decreasing femto-satellite mass and the fact that the force exerted by the spring during deployment the requirements on ADCS were greatly reduced, causing it to have a very low mass. The final iteration budgets can be found in Section 17.4.

## 18.5. Iteration 4 on 27-06-2016
Previously it was anticipated that the $\Delta V$ required for orbit maintenance was in the order of magnitude of a few kilometres per second for 9 orbits. With new, updated information the minimum and maximum $\Delta V$ required is 0.907 and 207 $mm/s$ per orbit, respectively. This can be found in Section 7.3. The propulsion system that was considered up till *iteration 1* could deliver a $\Delta V$ of 5 $m/s$, which will result in a mission duration between 358.3 and 1.6 days.

Adding this propulsion system adds 8.84 grams to the design. Also when the mission duration increases the momentum wheels will need de-saturation. For this magnetorquers are required, which will add mass, power and volume. Next, the non-rechargeable batteries need to be replaced by rechargeable batteries and solar panels, this will add extra mass and volume. Also the ADCS needs to be active so that the propulsion system applies the $\Delta V$ in the correct direction. This will result in larger batteries. The communication can use a lighter Bluetooth chip since there is a longer transmitting time, yet this decrease of mass and power is negligible with respect to the other additions that are needed. Also the design is already 2.9% over the target weight. So concluding, implementing these changes will make the design heavier than the required 100 grams and therefore the design after *iteration 3* will be continued.

# 19

# Risk Management

During the scope of the design process there are many events that could contribute to delays and potential failure of the project. It is paramount to ensure these risks are reduced where possible. These events should thus be identified and categorised into probabilities of occurrence and their respective impact to be fully aware of the risks.

## 19.1. General Process Risks

To avoid or mitigate the risks in occurrence and severity some steps should be taken. The general process risks are to be mitigated at the very start of the design process to ensure maximum efficiency. Elaboration and mitigation techniques are given for each potential risk. When shown in the initial risk map these are already mitigated since it is important for the design process.

Table 19.1: The potential risks faced during the design process with their respective ID

| ID | Potential risk |
|---|---|
| P1 | Laptop failure |
| P2 | Data loss |
| P3 | Software failure |
| P4 | Absence of group member |
| P5 | Miscommunication |
| P6 | Tutors not available |
| P7 | Design too complex |
| P8 | Planning not adequate |

**P1** *Laptop failure.* Laptops are primarily used for most of the tasks during the project. If one of them fails it will reduce the productivity of the overall group. As a backup other computers can be used that are available at the same table or same building if necessary.
**P2** *Data loss.* Data loss is not a large issue because the data is not stored locally. In event of data loss efficiency is lost during the recovery or reproduction of the same content. Backups of documentation is made daily to increase redundancy and reduce the risk. Data is stored individually and on-line to make sure the impact from eventual data loss is lowered.
**P3** *Software failure.* Software failure can become a larger issue if it is a critical component, such as 'ShareLateX', in reporting. Alternatives can be used to continue the work process without sacrificing much efficiency. Since backups are made frequently a different software can be used without causing big issues but it does require some time to get use to.
**P4** *Absence of group member.* When a group member is absent for a short period it will reduce the overall productivity of the group. Less work can be done in the same time. However this risk can be $MHz$d by informing the other group members before they are absent and the willingness of working in his own time.
**P5** *Miscommunication.* Miscommunication can lead to efficiency loss during the design process, but this can be mitigated by having daily meetings to make sure every group member is on the same page and has complete understanding of the current status of the project.
**P6** *Tutors not available.* If the tutors are not available it might cause some small delays due to questions remaining unanswered. However it is unlikely that all the tutors are unavailable at the same time and a big part of the communication is done via email, so the risk is negligible.
**P7** *Design too complex.* If the design becomes too complex at a point several subsystems might cause conflicts with each other. The design philosophy to adhere to is KISS (keep it simple stupid) and utilising COTS products wherever possible. Maintaining this philosophy will reduce the chance that the design becomes too complex.
**P8** *Planning not adequate.* If the workload has been underestimated delays will occur in the design process. These should be mitigated by constantly communicating with each other, documenting every decision and remaining flexible with the allocated work. People should be able to spend time outside of office hours if significant delays are present.

## 19.2. Development and Operation Risks

Next to the general process risks the technical risks during the design process and operational risks when in orbit are also present. These risks have to be evaluated accordingly and mitigated whenever the risk becomes high enough that it causes major issues for completing the designated mission. During the design process the concept has endured several changes due to iterations. Therefore some risks became obsolete and others were created. The obsolete risks have been crossed out and omitted from the risk map. These will first be elaborated upon in Section 19.3.

Table 19.2: The potential risks faced during mission development (D) and operation (O) with their respective ID

| ID | Potential risk |
|---|---|
| ~~D1~~ | ~~An adequate propulsion system cannot be developed.~~ |
| D2 | An adequate camera cannot be found. |
| D3 | The power budget does not close. |
| D4 | The mass budget does not close. |
| ~~D5~~ | ~~A docking mechanism cannot be developed.~~ |
| D6 | The link budget does not close. |
| D7 | Adequate radiation shielding cannot be developed within the mass constraints. |
| D8 | The mission goes over budget. |
| D9 | An adequate ADCS cannot be developed within the mass and volume constraints. |
| ~~D10~~ | ~~An accurate astrodynamical model cannot be developed.~~ |
| D11 | The centre of gravity has a large offset to the geometric centre. |
| D12 | The volume budget does not close. |
| D13 | Adequate testing facilities not available. |
| O1 | The femto-satellite crashes into the host spacecraft. |
| ~~O2~~ | ~~The femto-satellite runs out of fuel.~~ |
| O3 | The lens-mechanism gets stuck. |
| O4 | The processor crashes. |
| O5 | A momentum wheel fails. |
| O6 | Two momentum wheels fail. |
| ~~O7~~ | ~~A thruster fails.~~ |
| ~~O8~~ | ~~Multiple thrusters fail.~~ |
| O9 | A launch vehicle failure occurs. |
| O10 | Space debris impacts the femto-satellite. |
| O11 | A structural failure occurs. |
| O12 | Commands sent to the femto-satellite are misinterpreted. |
| O13 | Communication with the femto-satellite is lost. |
| ~~O14~~ | ~~The battery runs out before a charging cycle is engaged.~~ |
| ~~O15~~ | ~~The solar panel deployment mechanism fails.~~ |
| O16 | Separation from the host spacecraft fails. |
| O17 | Storage of data fails. |
| O18 | Failure due to thermal damage. |
| ~~O19~~ | ~~Loss of propellant due to leakage.~~ |
| O20 | Attitude determination of the femto-satellite fails. |
| ~~O21~~ | ~~Propellant tank rupture.~~ |
| O22 | The femto-satellite does not survive launch vibrations. |
| O23 | Communication with host spacecraft is lost. |
| O24 | Battery runs out before end of operational lifetime. |

## 19.3. Risk Iteration

This section will elaborate on which risks are no longer applicable to the final design iteration. These risks have lost relevancy due to removing different aspect of the mission or subsystems. In the following list the risk can be seen and the reason for removal.

**D1** *An adequate propulsion system cannot be developed.* Because a previous concept iteration involves a permanently orbiting solution where the femto-satellite stays close to its host-spacecraft the propulsion system had to provide an unrealistic amount of $\Delta V$ for the duration of its lifespan. In fact this risk would lead to unacceptable budgets for the

whole system. This has promptly led to an iteration with a concept that does not rely on a propulsion system that provides orbital corrections. In the end the risks involving the propulsion subsystem are no longer present in the final design.
**D5** *A docking mechanism cannot be developed.* One of the potential concepts of the mission involves a docking system on the host-spacecraft so the femto-satellite is able to re-dock after a certain amount of time. For this concept a new docking mechanism had to be designed and this would bring additional risks to the overall mission. Due to an iteration where the chosen concept did not contain docking as a part the risks involving the docking mechanism are no longer present in the final design.
**D10** *An accurate astrodynamical model cannot be developed.* Because a more accurate astrodynamical model (GMAT) that has been verified and validated has been found during the design process the need to completely develop an astrodynamical model was redundant. Further calculations on astrodynamics were made using the GMAT model, and thus effectivly mitigating the risk.
**O2** *The femto-satellite runs out of fuel.* This risk is part of the propulsion subsystem and has been removed. See D1 for more information.
**O7** *A thruster fails.* This risk is part of the propulsion subsystem and has been removed. See D1 for more information.
**O8** *Multiple thrusters fail.* This risk is part of the propulsion subsystem and has been removed. See D1 for more information.
**O14** *The battery runs out before a charging cycle is engaged.* Because a previous concept iteration involves a permanently orbiting solution where the femto-satellite should have an independent power generation and management, the power subsystem also had to consider generating power. This was important to maintain a long operational lifetime. The recharging would be done by utilising solar panels on one side of the femto-satellite and working in charging cycles. The femto-satellite would have to point itself for charging before the battery drained. Because the operational lifetime of the mission is significantly less the need for power generation has become obsolete. In the final design risks involving power generation and recharging are no longer present.
**O15** *The solar panel deployment mechanism fails.* This risk is part of the power generation part and is no longer present in the final design. See O14 for more information.
**O19** *Loss of propellant due to leakage.* This risk is part of the propulsion subsystem and has been removed. See D1 for more information.
**O21** *Propellant tank rupture.* This risk is part of the propulsion subsystem and has been removed. See D1 for a complete overview.

## 19.4. Risk Analysis

For the final design the risks are ranked in the initial risk map, presented in Table 19.3, in the probability that the potential risk happens and the impact of the potential risk. The cells of the tables are categorised to indicate the seriousness of the risk, where the upper right corner poses a critical risk and the lower left a low risk. This means that a risk that is likely to happen and simultaneously has a significant impact will pose a problem for the design of the femto-satellite. The probability scale varies from *rare* to *almost certain*. The impact scale of the risk has been defined as follows:

- **Negligible:** The event does not prevent any mission objectives from being achieved.
- **Low:** A few secondary mission objectives cannot be accomplished and technical performance might be slightly lower than expected.
- **Moderate:** Several major mission objectives cannot be realised but the mission remains operational for its minimum lifetime.
- **Major:** The event cuts the mission short after some mission objectives have been accomplished and technical performance will become questionable.
- **Catastrophic:** The event prevents the spacecraft from achieving any of its objectives and will be classified as total mission failure.

## 19.5. Risk Mitigation

Since the risks are categorised by their impact on the mission success the more profound ones should be evaluated and. For all risks that fall into the upper right region of the risk map, risk mitigation measures have to be developed. For risks currently in the middle region measures have to be proposed too but are not strictly necessary when none are available. For risks in the lower left region no measures are needed since the severity of the risk is low. The following subsections will explore the mitigation techniques for each risk stated earlier. Extra attention will be drawn to risk **O1** due to its potentially high probability and impact. Afterwards a posterior risk map is made to show how the implementation of the risk mitigation measures will influence the risks. This will be shown in Table 19.4.

Table 19.3: Risk map

| | | Probability | | | | |
|---|---|---|---|---|---|---|
| | | Rare | Unlikely | Possible | Likely | Almost certain |
| **Impact** | Catastrophic | D2, O10, O16 | D9, O9, O11, O22 | D11, D12 | O1 | |
| | Major | O3, O6, O13, O17, O23 | D6, D13, O4, O18 | D3, D4, D7, | | |
| | Moderate | O20 | P5, D8, O12 | P7, D6, O5, | | |
| | Low | | P2, P3, P6, O24 | P1, P4, P8, | | |
| | Negligible | | | | | |

### 19.5.1. Development risks

**D2** *An adequate camera cannot be found.* The payload is leading in the design process, if a certain requirement is unable to be met different approaches should be investigated to make sure there is an adequate camera to fulfil the mission.
**D3** *The power budget does not close.* By careful designing the power subsystem to conform to the power demands of the other subsystems and establishing rules for different operating phases, the risk of the power budget not closing can be mitigated.
**D4** *The mass budget does not close.* By keeping the design simple the total mass of the system can be kept relatively low. During the design process parts should be chosen with low mass as an important criteria. The mass budget of the femto-satellite will be closely monitored and the risk of exceeding will be mitigated by applying the steps mentioned above.
**D6** *The link budget does not close.* By relying on the host-spacecraft for communications the distance for transmitting data can be kept low. This will be beneficial to closing the link budget. By also assigning extra personnel resources from start of the design phase the risk shall be mitigated.
**D7** *Adequate radiation shielding cannot be developed within the mass constraints.* This risk shall be mitigated by analysing the effect of radiation on the sensitive parts of the satellite and if possible preferably use space qualified products. By reducing the operational lifetime and limiting the hibernation time of the satellite the severity of radiation can be mitigated.
**D8** *The mission goes over budget.* This risk shall be mitigated by choosing COTS products where possible.
**D9** *An adequate ADCS cannot be developed within the mass and volume constraints.* This risk shall be mitigated by allocating extra personnel resources from the start and where possible keeping the design simple. By reducing the operational lifetime of the satellite the size of the ADCS can be made smaller.
**D11** *The centre of pressure has a large offset to the centre of gravity.* This risk shall be mitigated by careful analysing the different components and finding the optimal configuration before construction of the satellite.
**D12** *The volume budget does not close.* This risk shall be mitigated by carefully analysing the different components and finding the optimal configuration before construction of the satellite.
**D13** *Adequate testing facilities not available.* This risk shall be mitigated by appropriate planning of testing phases in later parts of the design process to ensure testing is done properly and thoroughly.

### 19.5.2. Operational risks

**O1** *The femto-satellite crashes into the host spacecraft.* This is the primary risk of the mission and needs to be looked into carefully. This risk shall be mitigated by modelling the behaviour of the satellite and ensuring the femto-satellite will not come within a certain distance to its host spacecraft. Preliminary research has been done in the Chapter about astrodynamics and can be seen in Section 7.4. The minimum distance has been determined to be sufficiently large but with high uncertainty. The chance of impact was deemed low after modelling several different delta V's. An important note is that the relative velocity is very small and thus will further reduce the impact of the risk. Extensive testing with astrodynamical models should be performed in further design stages to model every possible outcomes of the trajectory with varying atmospheric densities to confirm it will not come close to its host-spacecraft. The host-spacecraft should also able to apply manoeuvres to evade the femto-satellite in case a collision is imminent, which will further mitigate the risk.
**O3** *The lens-mechanism gets stuck.* The risk cannot be effectively mitigated since it depends on the manufacturer. It is only possible to design the satellite in a way to reduce the amount of vibrations the components experience.
**O4** *The processor crashes.* This risk shall be mitigated by testing the components under similar conditions and having multiple redundant processors if budgets allow.
**O5** *A momentum wheel fails.* This risk shall be mitigated by careful integration procedures, thorough testing and selecting electircal motors with excellent reliability. Analysis shall be done to ensure the components will survive the

loads experienced during its lifetime.
**O6** *two momentum wheels fail.* This risk shall be mitigated by careful integration procedures, thorough testing and selecting electro motors with excellent reliability. Analysis shall be done to ensure the components will survive the loads experienced during its lifetime.
**O9** *A launch vehicle failure occurs.* This risk shall be mitigated by selecting launchers with a favourable track record, although this is up to the costumer since the femto-satellite is designed to be launched together with the host spacecraft.
**O10** *Space debris impacts the femto-satellite.* This risk is outside of the development team's control and therefore no risk mitigation measures are proposed.
**O11** *A structural failure occurs.* This risk shall be mitigated by careful design, testing and construction of the structural elements.
**O12** *Commands sent to the femto-satellite are misinterpreted.* Software shall be developed in a way this risk is highly unlikely by ensuring that improper commands are filtered out.
**O13** *Communication with the femto-satellite is lost.* This risk shall be mitigated by developing a safe-mode which allows the femto-satellite to operate autonomously until contact is established again at a later stage.
**O16** *Separation from host spacecraft fails.* This risk shall be mitigated by careful design, extensive testing of the mechanism and keeping the mechanism simple and less prone to failure.
**O17** *Storage of data fails.* This risk shall be mitigated by testing the components under similar conditions and having redundancy of storage system if the budgets allows.
**O18** *Failure due to thermal damage.* This risk shall be mitigated by carefully designing the thermal control of the femto-satellite. A thermal analysis shall be conducted to assess the performance of the shielding to ensure adequate protection. By choosing parts with a high operating temperature range and setting constraints on release window the risk can be further mitigated.
**O20** *Attitude determination of the femto-satellite fails.* This risk shall be mitigated by careful design and having redundancy in case of partial failure.
**O22** *The femto-satellite does not survive launch vibrations.* This risk shall be mitigated by thoroughly testing and optimising the design to ensure the satellite shall survive the initial phase of the mission. Vibrational analysis shall be performed on the components and the satellite as a whole to create a clear picture of forces present.
**O23** *Communication with host spacecraft is lost.* This risk shall be mitigated by exploring the possibility of an extra femto-satellite specifically designed for relaying communications to the ground. Additional information can be found in Section 9.2.1. By having a safe-mode which allows the femto-satellite to operate autonomously until contact is established again at a later stage.
**O24** *Battery runs out before end of operating lifetime.* This risk shall be mitigated by setting a sufficient margin to the capacity of the main battery. With a battery monitor the current state of the battery can be checked and if deemed necessary the power plan can be adjusted to remain operational until de-orbiting.

Table 19.4: Posterior risk map

| | | **Probability** | | | | |
|---|---|---|---|---|---|---|
| | | Rare | Unlikely | Possible | Likely | Almost certain |
| **Impact** | Catastrophic | D2, O9, O10, O11, O16, O22 | D12 | | | |
| | Major | D6, D9, D13, O3, O6, O13, O17, O23 | D3, D4, O1, O4 | | | |
| | Moderate | D8, O12, O18, O20 | P5, D7, O5 | P7, | | |
| | Low | O24 | P2, P3, P6, D11 | P1, P4, P8 | | |
| | Negligible | | | | | |

## 19.6. Conclusion on Risk Management

By identifying possible risks that can occur during the design process and mission and developing risk mitigation techniques for events with a high probability and high impact the posterior risk map, seen in Table 19.4, has been drawn. It is visible that no risks are present in the upper right corner. Risks that are in the other sections should be monitored during the next design phase. Operational risk 1 has been preliminarily mitigated by modelling the trajectory but will require more extensive testing in further design stages to verify all possible deviations from nominal deployment. This will mitigate the risk of collision.

# 20

## Verification and Validation

Verification and validation are procedures used to determine if a (sub)system meets the predefined set of requirements or specifications. Verification and validation can be done at every level of the (sub)system. The verification and validation procedure according to the V-diagram can be seen in Figure 20.1. This chapter contains all the verification

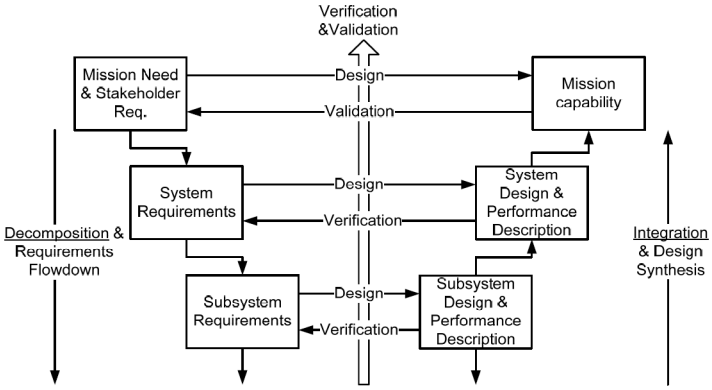


Figure 20.1: Designing according to the V-diagram

and validation procedures for the PICS. It starts with the lower levels of Figure 20.1, and continues to the higher levels. After that verification and validation procedures for the different models are discussed. In the end a compliance matrix that checks all the requirements is presented together with a sensitivity analysis. Every requirement are drafted according to the VALID criteria[22]:

**V Verifiable (i.e. objective, preferably quantitative)**
**A Achievable (i.e. sufficient resources available)**
**L Logical (i.e. traceability, flow-down)**
**I Integral (i.e. complete, all-encompassing)**
**D Definitive (i.e. unambiguous)**

## 20.1. Requirements Verification

**Payload**

**TS-SYS-POD-PL-06** *The femto-satellite shall be able to capture visual images with a smallest feature size of* $0.1mm$. The camera will be tested on the ground and the final output image will be checked for the smallest feature size.
**TS-SYS-POD-PL-07** *The femto-satellite shall be able to take colour pictures.* Comparable to **TS-SYS-POD-03-A** it can be verified with a test.
**TS-SYS-POD-PL-08** *The femto-satellite shall capture images on which the diagonal of one side of the host spacecraft occupies 10% or more of the horizontal dimension of the picture.* This requirement can be verified by testing it on Earth, by taking a replica of the host spacecraft and simulating the distances between the host spacecraft and femto-satellite while taking pictures. After analysing the pictures it can be decided if the requirement is met.

**Communication System**

**TS-SYS-POD-05-COM-01** *The communication system shall provide a closed link budget during the mission.* The range of the wifi chip is 242 meters and according to the calculations all the pictures are sent 1.9 hours after release from the host spacecraft. At this point the distance to the host spacecraft is 85 meters. This verifies the requirement
**TS-SYS-POD-05-COM-02** *The communication system shall provide a data rate of at least 1* $Mb/s$. The data rate is 54 $Mb/s$ which is higher than 1 $Mb/s$ so the requirement is verified.
**TS-SYS-POD-05-COM-03** *The communication system shall be able to send data to earth.* The femto-satellite itself can not send images to the ground. Yet the communication flow is designed in such a way that it uses the ability of the

host spacecraft to send data to the ground. Also it is established that the host spacecraft is able to send images to the ground. So the communication system as a whole is able to send images to the ground and therefore the requirement in verified.
**TS-SYS-POD-05-COM-04** *The communication system shall have an omnidirectional radiation pattern.* The PCB trace antenna built into the wifi module has a omnidirectional radiation pattern. So with this information the requirement is verified.

**Attitude Determination and Control System**
**TS-SYS-POD-ADC-01** *The ADC subsystem shall be able to keep the host spacecraft within the field of view of the payload subsystem, which is 63° horizontal and 45° vertical.* The combination of the periodically checking camera system and gyroscopes are able to keep the spacecraft within the field of view of the camera. Hence this requirement is verified.
**TS-SYS-POD-ADC-02** *The ADC subsystem shall be able to de-tumble the spacecraft within 25 seconds from release.* The momentum wheels have been sized in such a way that they are capable of storing the momentum generated during deployment and can counter the rotation within 0.3 seconds. Hence this requirement is verified.
**TS-SYS-POD-ADC-03** *The ADC subsystem shall be able to counter the disturbance torques that act on it during the ADCS lifetime.* The wheels have been sized in such a way that they are large enough to store all the momentum generated during the deployment and all the disturbance torques about a single axis. Thus each wheel is large enough to counteract the disturbances. Hence this requirement is verified.
**TS-SYS-POD-ADC-04** *The ADC subsystem shall be able to have sufficient momentum storage about a single axis to store worst-case disturbance torque for the entire ADCS lifetime acting about this orbit.* According to the same reasoning as used in requirement **TS-SYS-POD-ADC-04** this requirement is verified.
**TS-SYS-POD-ADC-05** *The ADC subsystem shall be able to point the payload towards the host spacecraft for the duration of the payload.* There is only a small disturbances in the spacecraft orbit during the sensing period and the actuators are powerful enough to counter these. The sensors are able to provide the spacecraft with accurate input and thus this requirement is verified.

**De-orbit Device**
**TS-SYS-POD-DOD-01-A** *The femto-satellite shall be able to de-orbit within 25 years up to an orbital altitude of 1000 $km$.* This requirement is verified by analysis and can be demonstrated after launch to see the actual decay rate increase. **TS-SYS-POD-DOD-02** *The femto-satellite shall be made detectable from the Earth after its operational lifetime.* This requirement is verified by analysis, that is, objects larger than 2 $cm$ can be detected [13].

**Command & Data Handling System**
**TS-SYS-POD-CDH-01** *The C&DH subsystem shall process the ADCS sensor input data and send commands to the ADCS actuators.* The ADCS actuators communicate over PWM, which the central processor can generate. The ADCS sensors use $I^2C$ and camera input, which the central processor can also handle. The central processor has 3-bit addressing on $I^2C$ meaning that it has enough channels to support all the $I^2C$ devices.
**TS-SYS-POD-CDH-02** *The C&DH subsystem shall process incoming commands from the host from the communications system.* The central processor can communicate over $I^2C$ with the communications subsystem. The flash memory controller can communicate over the higher speed $SPI$ protocol with the communications subsystem.
**TS-SYS-POD-CDH-03** *The C&DH subsystem shall send commands to the payload and store the data that the payload gathers.* The central processor can send commands to the payload over $I^2C$ and the mass storage section of the C&DH is capable of transferring the data to flash memory.
**TS-SYS-POD-CDH-04** *The C&DH subsystem shall send the payload data to the communications subsystem to be transmitted to the host spacecraft.* The flash storage interface can communicate over $SPI$ with the communications subsystem.
**TS-SYS-POD-CDH-05** *The C&DH subsystem shall monitor the power subsystem and switch operation modes if problems occur.* The power subsystem contains a $I^2C$ battery monitor which can be read by the central processor.
**TS-SYS-POD-CDH-06** *The C&DH subsystem shall communicate with the de-orbiting device and tell it when to de-orbit.* The de-orbiting device will require a $GPIOhigh$ signal from the central processor to start the deployment, this signal can ben sent by the processor.
**TS-SYS-POD-CDH-07** *The C&DH subsystem shall be able to interface with the ADCS sensors, which use the $I^2C$ communication protocol.* This requirement is verified for the same reasons that **TS-SYS-POD-CDH-01** is verified.
**TS-SYS-POD-CDH-08** *The C&DH subsystem shall be able to interface with the ADCS actuators which require a $PWM$ signal.* This requirement is verified for the same reasons that **TS-SYS-POD-CDH-01** is verified.
**TS-SYS-POD-CDH-09** *The C&DH subsystem shall be able to interface with the payload, which uses $I^2C$ as the input protocol and $CSI-2$ as the output protocol.* This requirement is verified for the same reasons that **TS-SYS-POD-CDH-03** is verified.

**TS-SYS-POD-CDH-10** *The C&DH subsystem shall be able to interface with the communications subsystem which uses SPI and $I^2C$ as a protocol.* This requirement is verified for the same reasons that **TS-SYS-POD-CDH-04** and **TS-SYS-POD-CDH-02** are verified.
**TS-SYS-POD-CDH-11** *The C&DH subsystem shall be able to interface with the de-orbiting device which requires a GPIO-high signal.* This requirement is verified because the selected processor has a GPIO port that can be used for this purpose.
**TS-SYS-POD-CDH-12** *The C&DH subsystem shall be able to receive data from the payload with a data rate of 111.02 $MB/s$.* The subsystem is capable for eaching 125 $MB/2$ and is thus fast enough.
**TS-SYS-POD-CDH-13** *The C&DH subsystem shall have a storage capacity of at least 42 $GB$.* The subsystem has a storage of 64 GB and is thus large enough.
**TS-SYS-POD-CDH-14** *The C&DH subsystem shall transmit the data to the communication system with a data rate of 6.75 $MB/s$.* The $SPI$ connection is fast enough to handle this.
**TS-SYS-POD-CDH-15** *The C&DH subsystem shall be able to interface with the power monitor, which uses $I^2C$.* The subsystem can communicate over $I^2C$ and thus this requirement is verified.

**Power System**
**TS-SYS-POD-POW-01-A** *The power subsystem shall deliver a total energy of 3.69 $Wh$ to the femto-satellite.* The main battery chosen for the power subsystem is able to deliver up to 4.5 $Wh$. For that reason, this requirement is verified.
**TS-SYS-POD-POW-04-A** *The power subsystem shall be able to power the femto-satellite for 6749 $s$.* The main battery chosen for the power subsystem is able to deliver its maximum continuous current for up to 8640 $s$. For that reason, this requirement is verified.
**TS-SYS-POD-POW-05** *The power storage shall have a safety margin of 15 %.* The main battery is still able to provide enough power after applying a safety margin of 15%. For that reason, this requirement is verified.
**TS-SYS-POD-POW-06** *The power subsystem shall be able to provide up to 2.79 $W$.* The main battery is able to deliver a maximum continuous current of 1 $A$ on a voltage of 3 $V$, which is equal to 3 $W$. For that reason, this requirement is verified.
**TS-SYS-POD-POW-07** *The power subsystem shall be able to power the de-orbiting device.* The secondary battery is able to deliver the high constant power for the de-orbiting device to active. For that reason, this requirement is verified.
**TS-SYS-POD-POW-08** *The power subsystem shall provide the specific voltage to each component.* 4 voltage converters are used to manage the voltages supplied to the different components if they do not operate on the same voltage as the main battery. For that reason, this requirement is verified.
**TS-SYS-POD-POW-09** *The power subsystem shall have no power leakage before deployment.* The main battery is physically disconnected by means of a switch, this means that no leakage is present before the switch is actuated. For that reason, this requirement is verified.

**Thermal Control System**
**TS-SYS-POD-TC-01** *The femto-satellite shall not get colder than -10 °C during its operational lifetime while the camera is offline.*
**TS-SYS-POD-TC-02** *The femto-satellite shall not get colder than 5 °C during the time it takes pictures.*
**TS-SYS-POD-TC-03** *The femto-satellite shall not get warmer than 50 °C during its operational lifetime while the camera is offline.*
**TS-SYS-POD-TC-04** *The femto-satellite shall not get warmer than 40 °C during the time it takes pictures.* These requirements are verified by the thermodynamic analysis shown in Figures 14.1 and 14.2. According to this analysis the temperature remains within the floor and ceiling established by the requirements.

**Deployment System**
**TS-SYS-POD-SM-01** *The deployment system shall be electrically conductive to minimise chance of electrostatic discharge.* The spring material used is titanium beta-C. From Table 15.1 it can be concluded that Titanium beta-C is electrically conductive due to its relatively low electrical resistivity of 42 $\mu\Omega \cdot cm$.
**TS-SYS-POD-SM-02** *The deployment system components shall not resonate with the launch load vibrations.* The spring pins, supporting plate and femto-satellite are not able to move in any direction before the deployment due to the closed deployment door and pin diameter difference as explained in Section 15.4.2. For that reason, the spring is stowed and is not able to cause resonating vibrations with the launch loads. For that reason, this requirement is verified.
**TS-SYS-POD-SM-03** *The deployment system shall not allow the femto-satellite to move any direction before the deployment.* The spring pins, supporting plate and femto-satellite are not able to move in any direction before the deployment due to the closed deployment door and pin diameter difference as explained in Section 15.4.2. For that reason, this requirement is verified.

**TS-SYS-POD-SM-04** *The deployment system shall contain an actuator that can touch the pin switch on the femto-satellite.* The deployment system contains an ERSA that will touch the pin switch before deployment. For that reason, this requirement is verified.
**TS-SYS-POD-SM-05** *The deployment system shall be able to contain the femto-satellite from the launch until the deployment.* As sketched in Figure 15.9 the femto-satellite can be integrated in the $5 \times 5 \times 5cm$ free space in the deployment interface. For that reason, this requirement is verified.
**TS-SYS-POD-SM-06** *The spring index of the spring of the deployment system shall have a value within a range of 4 and 25.* A spring index of 25 is used. For that reason, this requirement is verified.
**TS-SYS-POD-SM-07** *The spring force shall not exceed the yield force of the spring.* The spring force equals $F = 5.1610^{-4} N$ and the yield force equals $F_{yield} = 0.142N$ for the chosen spring design, which verifies this requirement.
**TS-SYS-POD-SM-08** *The spring shall not be subject to buckling.* The maximum spring deflection is arbitrarily determined to be $y_{max} = 0.01\ m$. It is checked whether it fulfils the buckling stability requirement imposed by the critical deflection $y_{cr}$, which is expressed by Equation (15.14). Since no critical deflections exists this requirement is verified.
**TS-SYS-POD-SM-09** *The diameter of the spring wire shall have a value greater than the minimum manufacturable wire diameter.* The diameter of the spring wire is $0.127m$ which is the minimum manufacturable wire diameter for titanium beta-C according to Table 15.1. For that reason, this requirement is verified.

### 20.1.1. System Requirements

**TS-SYS-POD-01-B** *The femto-satellite shall provide a velocity increment of 1.3 $cm/s$ for release from the host spacecraft in the downrange direction.* This is the hardest system requirement to verify. Simulating the micro gravity environment in which the femto-satellite will deploy on Earth is very hard, but not impossible. A complex test structure can verify this requirement.
**TS-SYS-POD-04** *The femto-satellite shall be able to store images on board.* Fulfilment of this requirement will be demonstrated by storing data in the on board memory and reading it out during a ground demonstration.
**TS-SYS-POD-05** *The femto-satellite shall be able to transfer stored data to the host spacecraft.* A test setup can be made to simulate the connection between the host spacecraft and femto-satellite. Based on the test, the requirement can be verified.
**TS-SYS-POD-07** *The femto-satellite shall be able to increase its orbital decay rate.* The system used to increase the orbital decay rate should be analysed. Based on the analysis, the requirement can be verified. A demonstration can verify this requirements as well.
**TS-SYS-POD-09** *The femto-satellite shall have a natural frequency higher than 35 $Hz$.* This requirement is verified by modelling and analysing the natural frequency of the components and the total spacecraft. It can be further verified by testing.
**TS-SYS-POD-11** *The femto-satellite shall be able to remain operable after launch accelerations up to 10.8 $g$.* This requirement is verified by creating a structural stress model. With this model it is proven that the femto-satellite can withstand the launch accelerations. A full scale test simulating the launch accelerations can also be conducted.
**TS-SYS-POD-12** *The payload shall take pictures of the host spacecraft when the host spacecraft is placed in direct sunlight.* The femto-satellite is released when it comes in the sunlight. The imaging part takes 442 seconds ands starts 30 seconds after the wire is cut. This total time interval is small enough to perform in the sunlight period of the orbit after analysis. For that reason, this requirement is verified. **TS-SYS-POD-13** *The femto-satellite shall be able to identify space debris and micro-meteoroid impact damage on the solar arrays and bus of the host spacecraft.* To test this requirement images of a satellite on Earth will be taken. Then these images will be analysed to see which features on the satellite can be distinguished.
**TS-SYS-POD-14** *The femto-satellite shall provide images of the host spacecraft that can be used for promotion of its mission.* Like the previous requirement, this requirement will be verified by test.

### 20.1.2. Stakeholder Requirements

**TS-STH-SAR-01** *Safety requirements for piggyback launches shall be adhered to.* A failure model shall be made and used to find out the probability that the femto-satellite inflicts damage on the host spacecraft.
**TS-STH-SAR-02** *The spacecraft shall withstand the launch loads.* This requirement shall be verified by creating a structural stress model. With this model it can be proven whether the femto-satellite can withstand the launch loads. A full scale test simulating the launch loads can also be conducted.
**TS-STH-SAR-03** *The femto-satellite shall be integrated into the host spacecraft for launch.* This can be verified by making a design which demonstrates that the femto-satellite is integrated in the host spacecraft.
**TS-STH-SUS-01-A** *The spacecraft shall comply with the existing regulation to mitigate space debris, which requires the femto-satellite to de-orbit within 25 years.* This requirement shall be verified by analysis of the de-orbit system. In case of failure of the orbital decay system various tools exist that can analyse the de-orbit time.

**TS-STH-PER-02** *Telemetry shall be available with a maximum latency of one day.* This requirement shall be verified by analysing the orbit and the link budget.
**TS-STH-PER-03-A** *The design shall employ commercial off-the-shelf components where possible.* The design includes a COTS camera, C&DH system, communication system and battery.
**TS-STH-PER-05** *The femto-satellite shall accommodate a payload with a mass greater than or equal to 15% of its mass.* This requirement can be verified by analysing the payloads mass percentage. However, the definition of payload is not fixed. It is unclear if the de-orbiting systems counts as payload. This should be negotiated with the customer.
**TS-STH-ENB-01** *The spacecraft launch mass shall not exceed* $100g$. According to Section 17.4, the mass is 72 $g$. The mass has to be monitored against the target values throughout the project and during production it has to be verified.
**TS-STH-ENB-02** *The spacecraft volume shall not exceed* $125cm^3$. With dimensions of $5\times5\times5cm$ the femto-satellite has a volume of exactly 125 $cm^3$.
**TS-STH-CST-01** *The cost of each individual spacecraft shall not exceed €10,000.* This requirement shall be verified by drawing up a budget. This is done in Section 17.4.
**TS-STH-CST-02** *The cost of the total mission (excluding launch) shall not exceed €500,000.* Like the previous requirement, this one can be verified with a budget.

### 20.1.3. Mission Requirements
**TS-MIS-ORB-03** *The femto-satellite shall be released from the host-spacecraft in the downrange direction.* This requirement can only be verified after deployment since the host spacecraft is responsible for proper alignment of the release system. To properly release the PICS in the correct direction the host spacecraft needs a sufficiently accurate ADCS system. Assuming the host spacecraft has an ADCS system capable of properly aligning the release direction this requirement can be verified by demonstration and by analysing the orbit of the PICS.
**TS-MIS-IMG-INS-01-B** *The femto-satellite shall provide data aimed at modelling space debris and micro-meteoroid impact.*
**TS-MIS-IMG-PRO-01-B** *The femto-satellite shall promote the mission of its host spacecraft.*

## 20.2. System Validation
After assembly of the PICS it should be validated that it actually works as specified. Although actual validation can only happen once it is deployed, certain aspects can be simulated on Earth. The first thing to validate is if the PICS is designed for the right purpose. When taking a look at the mission statement, stated in Chapter 2, it becomes clear that the PICS is designed for the right purpose. It is very suited for demonstrating the inspection and promotional potential of a femto-satellite.

For the product validation the focus lies on practise rather than on requirements. It is essential to validate that the different subsystems of the PICS work together. The first test that needs to be performed is the end-to-end information test [62]. Its purpose is to identify system discrepancies and to ensure that information is passed to the correct subsystems[1]. In a simulated environment the PICS should prepare itself to take a picture, take the picture, process it and send it to the host spacecraft. If this test is successful it can be concluded that all the subsystems communicate properly.

The second series of tests that should be performed are the mission scenario tests. The purpose of these tests is to validate that the hardware and software can execute the mission under various circumstances. Scenarios should include nominal situations but also contingencies and unexpected but probable events.

The third series of tests that should be performed are the operations readiness tests. The purpose of these tests is to show that the ground segment (software, hardware, mission control, engineers, etc.) can function under a real-time scenario. This test can be seen as a final rehearsal before deployment.

The last test that should be performed are stress tests. Its purpose is to asses the system's robustness to performance variations and fault conditions. The intention of the stress test is to exceed the normal operational limits and determine the stability of the system. This test includes a structural stress test, at what loads does the PICS fail. This test can also be used to validate the structural model.

## 20.3. Model Verification and Validation
### 20.3.1. Thermodynamic Model
#### Verification of the Thermodynamic Model
The thermodynamic model needs to be verified. This is done by comparing the outcome values for a sphere with solar radiation with values from literature [41]. The literature uses a solar flux of 1368 $W/m^2$. This is done for 3 different

[1] End-to-End Testing, `https://www.techopedia.com/definition/7035/end-to-end-test`, retrieved on 16-6-2016

kind of surface areas: white paint, black paint and aluminium. The absorptivity and emissivity for these surface areas are given in Table 20.1. This table also shows the theoretical and the model equilibrium temperature. The white paint has a deviation of 0.1 $^{\circ}C$, the black paint has a deviation of 0.46 $^{\circ}C$ and the aluminium has the largest deviation of 3.61 $^{\circ}C$. The deviations are within margin so with this verification it is concluded that the thermodynamic model is verified.

Table 20.1: Verification values for the thermal model

| | **Absorptivity** [-] | **Emissivity** [-] | **Reference equilibrium temperature** [$^{\circ}C$] | **Model equilibrium temperature** [$^{\circ}C$] |
|---|---|---|---|---|
| White paint | 0.15 | 0.9 | -95 | -95.09 |
| Black paint | 0.9 | 0.85 | 10 | 9.54 |
| Aluminium | 0.15 | 0.05 | 90 | 93.61 |

Figure 20.2 shows how a sphere of different surface finishes reaches equilibrium temperature. These graphs are used to determine the equilibrium temperatures used for the verification.

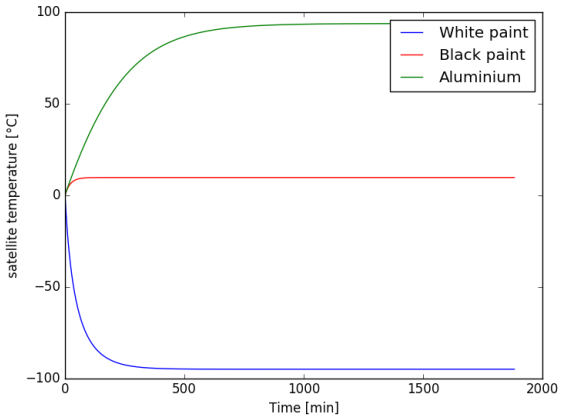


Figure 20.2: Temperature envelope with different surface finishes

**Validation of the Thermodynamic Model**

To validate the thermodynamic model, the parameters of FUNcube are entered into the model explained in Section 14.1 and the simulation result is compared to actual telemetry. This section will go on to give a short introduction to FUNcube and its mission, then the inputs to the model are stated and finally the output of the model is compared to actual telemetry.

FUNcube is a 1U cubesat designed for educational outreach. Its main payloads are a UHF to VHF linear radio transponder and a materials science experiment. It was developed by AMSAT-UK and AMSAT-NL and built at ISIS B.V. in the Netherlands.

70 % of FUNcube's surface are covered by triple-junction GaAs solar panels with an absorptivity of 0.91 and emissivity of 0.90[2]. For the other 30 % the absorptivity and emissivity of anodised aluminium are assumed which are 0.20 and 0.60 respectively[3]. This gives an absorptivity for the whole body of 0.697 and an emissivity of 0.810. A chart of FUNcube telemetry over one orbit was obtained from the FUNcube website[4], see Figure 20.3. From this chart it can be seen that the battery current was about 0.15 $A$ and the voltage approximately 8.5 $V$. Multiplying these gives an internal power dissipation of 1.275 $W$. For modelling FUNcube, an arbitrary starting temperature of 273.15 $K$ is taken. This does not matter however, as only the results of the simulation are used after enough time has passed for it to stabilise.

To obtain the specific heat of the satellite, a weighted average over the different materials is taken. The aluminium structure which is 450 $g$ has a specific heat of 960 $J/(kgK)$ and the 200 $g$ of GaAs solar panels have a specific heat of

[2]Azur Space solar cell data sheet, `http://www.azurspace.com/images/pdfs/HNR_0003429-01-00.pdf`, retrieved on 13-06-2016
[3]Thermo-optical properties, `http://webserver.dmt.upm.es/~isidoro/dat1/Thermooptical.pdf`, retrieved on 13-06-2016
[4]FUNcube whole orbit data, `http://warehouse.funcube.org.uk/wod.html?satelliteId=2`, retrieved on 29-05-2016

330 $J/(kgK)$. For the remaining 350 $g$ which are mostly electronics the specific heat of FR-4 is assumed, i. e. 600 $J/(kgK)$. The electronics consist mostly of silicon with a specific heat of 810 $J/(kgK)$, FR-4 and copper with 400 $J/(kgK)$.[5] The specific heat of FR-4 is taken because it lies right in the middle. This gives an average specific heat of 708 $J/(kgK)$ for the entire FUNcube.

The satellite has an altitude of 630 $km$, an orbital period of 97 minutes and and eclipse time of 32 minutes[6].

With these inputs the simulation was run, the result of which is given in Figure 20.4. The range of attained temperatures is -15.7 and 15.8. Comparing the outcome to temperatures measured on FUNcube given in Figure 20.3 shows that the shape of the curve is about the same and the values reached are also very close. Therefore the thermodynamic model can be considered validated.

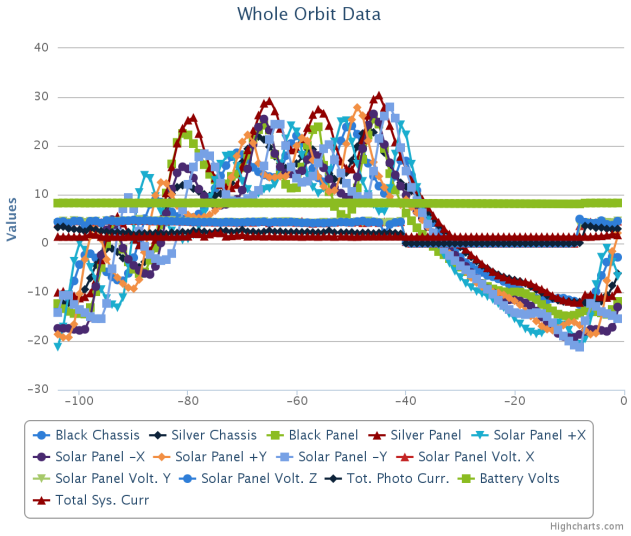


Figure 20.3: Telemetry of FUNcube-1 over the duration of one orbit. Temperatures are in $°C$, currents in $dA$ and voltages in $V$.

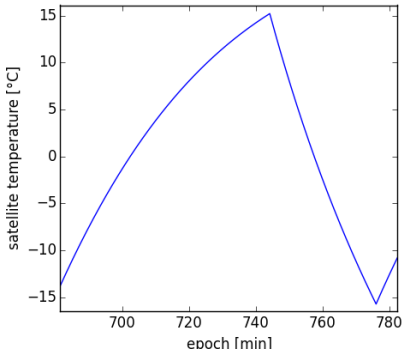


Figure 20.4: Thermal simulation of FUNcube over one orbit after model stabilisation

### 20.3.2. FEM Model of PCBs

This subsection deals with verification and validation of the finite element model.

**Verification of FEM Model**

The FEM analysis tool in CATIA itself is verified because it is a commercial software. Furthermore, all forces as well as the material properties were double-checked.

**Validation Plan for FEM Model**

The FEM model cannot be validated with the resources currently available to group S13. However, validation should be performed in the assembly phase. As soon as the PCBs are delivered, they shall be loaded with dummy parts that have 8.3 times the weight of the actual components. Then the displacements should be measured with a laser measuring device and compared to the displacements predicted by the model. If the measured values come sufficiently close to the predicted values, the FEM model can be considered validated.

## 20.4. Compliance Matrix

The compliance matrix is set up after the final design to see whether the requirements previously set are met. In Table 20.2 the requirements stated before in Chapter 6 are recalled and checked whether the final design complies with them. If they meet the requirement a checkmark is placed and the section where it is discussed will be referred to. The verification method is also specified in the table: I for inspection, T for testing, A for analysis, D for demonstration. If the design does not comply with a requirement a feasibility analysis is performed to check which steps should be taken to make sure the requirement is met.

Table 20.2: Compliance matrix of mission, stakeholder and system requirements, ✓ means it complies, × means it does not

[5] Simplified Transient Model for IC Packages, `http://www.electronics-cooling.com/2002/08/simplified-transient-model-for-ic-packages/`, retrieved on 10-06-2016

[6] FUNcube-1 as an educational tool, `https://funcubetest2.files.wordpress.com/2010/11/funcube-1-as-an-educational-toolc3.pptx`, retrieved on 10-06-2016

| Type | Requirement | Compliance | Verification method | Note |
|---|---|---|---|---|
| **Mission & Stakeholder** | TS-STH-SAR-01 | ✓ | A | |
| | TS-STH-SAR-02 | ✓ | T | |
| | TS-STH-SAR-03 | ✓ | D | |
| | TS-MIS-ORB-03 | × | A, D | Only verifiable after launch |
| | TS-STH-SUS-01-A | ✓ | A | |
| | TS-MIS-IMG-INS-01-B | ✓ | D | |
| | TS-MIS-IMG-PRO-01-B | ✓ | D | |
| | TS-STH-PER-02 | ✓ | A | |
| | TS-STH-PER-03-A | ✓ | I | |
| | TS-STH-PER-05 | × | I | Depends whether the de-orbit device counts towards the payload mass |
| | TS-STH-ENB-01 | ✓ | I | |
| | TS-STH-ENB-02 | ✓ | I | |
| | TS-STH-CST-01 | ✓ | I | |
| | TS-STH-CST-02 | ✓ | I | |
| **System** | TS-SYS-POD-01-B | ✓ | T | Very hard to test on Earth |
| | TS-SYS-POD-04 | ✓ | D | |
| | TS-SYS-POD-05 | ✓ | T | |
| | TS-SYS-POD-07 | ✓ | A, D | Demonstration after release |
| | TS-SYS-POD-09 | ✓ | A, T | |
| | TS-SYS-POD-11 | ✓ | A, T | |
| | TS-SYS-POD-12 | ✓ | A | |
| | TS-SYS-POD-13 | ✓ | T | |
| | TS-SYS-POD-14 | ✓ | T | |
| **Payload** | TS-SYS-POD-PL-01-A | ✓ | D | |
| | TS-SYS-POD-PL-06 | ✓ | T | |
| | TS-SYS-POD-PL-07 | ✓ | T | |
| | TS-SYS-POD-PL-08 | ✓ | D | |
| **Communi-cations** | TS-SYS-POD-COM-01 | ✓ | T | |
| | TS-SYS-POD-COM-02 | ✓ | T | |
| | TS-SYS-POD-COM-03 | ✓ | T | |
| | TS-SYS-POD-COM-04 | ✓ | D | |
| **ADCS** | TS-SYS-POD-ADC-01 | ✓ | T | |
| | TS-SYS-POD-ADC-02 | ✓ | A, T | |
| | TS-SYS-POD-ADC-03 | ✓ | A, T | |
| | TS-SYS-POD-ADC-04 | ✓ | A | |
| | TS-SYS-POD-ADC-05 | ✓ | A | |
| **De-orbit** | TS-SYS-POD-DOD-01-A | × | A, D | Demonstration is done after deployment |
| | TS-SYS-POD-DOD-02 | ✓ | A, D | Demonstration is done after deployment |
| **C&DH** | TS-SYS-POD-CDH-01 | ✓ | D | |
| | TS-SYS-POD-CDH-02 | ✓ | D | |
| | TS-SYS-POD-CDH-03 | ✓ | D | |
| | TS-SYS-POD-CDH-04 | ✓ | D | |
| | TS-SYS-POD-CDH-05 | ✓ | D | |
| | TS-SYS-POD-CDH-06 | ✓ | D | |
| | TS-SYS-POD-CDH-07 | ✓ | D | |
| | TS-SYS-POD-CDH-08 | ✓ | D | |
| | TS-SYS-POD-CDH-09 | ✓ | D | |
| | TS-SYS-POD-CDH-10 | ✓ | D | |
| | TS-SYS-POD-CDH-11 | ✓ | D | |

| | | | | |
|---|---|---|---|---|
| | TS-SYS-POD-CDH-12 | ✓ | D | |
| | TS-SYS-POD-CDH-13 | ✓ | I | |
| | TS-SYS-POD-CDH-14 | ✓ | D | |
| | TS-SYS-POD-CDH-15 | ✓ | D | |
| **Power** | TS-SYS-POD-POW-01-A | ✓ | A, T | |
| | TS-SYS-POD-POW-04-A | ✓ | T | |
| | TS-SYS-POD-POW-05 | ✓ | A, T | |
| | TS-SYS-POD-POW-06 | ✓ | T | |
| | TS-SYS-POD-POW-07 | ✓ | T | |
| | TS-SYS-POD-POW-08 | ✓ | T | |
| | TS-SYS-POD-POW-09 | ✓ | T, D | Demonstration is done after deployment |
| **Thermal control** | TS-SYS-POD-TC-01 | ✓ | A | |
| | TS-SYS-POD-TC-02 | ✓ | A | |
| | TS-SYS-POD-TC-03 | ✓ | A | |
| | TS-SYS-POD-TC-04 | ✓ | A | |
| **Deployment** | TS-SYS-POD-SM-01 | ✓ | A, T | |
| | TS-SYS-POD-SM-02 | ✓ | I | |
| | TS-SYS-POD-SM-03 | ✓ | A, T | |
| | TS-SYS-POD-SM-04 | ✓ | D | |
| | TS-SYS-POD-SM-05 | ✓ | I | |

## 20.5. Feasibility Analysis

As can be seen in Table 20.2 there are a couple of requirements the design does not comply to or that require additional elaboration. **TS-STH-PER-05** Depends on whether the de-orbit device counts towards the payload mass. The de-orbiting device is an important aspect of the mission because it is important to make sure the femto-satellite does not contribute to space debris. This aspect shall be negotiated with the customer to establish the final definition of "payload". **TS-MIS-ORB-03** Deployment in downrange direction is not verifiable during the design process. This requirement can only be verified after deployment from the host spacecraft by analysis of the telemetry received after release. **TS-SYS-POD-COM-03** Communications directly to the ground is not possible on this scale with current technology. When the market expands for smaller components and more technological advancements is present in miniaturisation of components communications directly to the ground might be possible in future iterations. More information can be found in Section 9.2.1 However it is still possible to communicate to the Earth via the host-spacecraft. **TS-SYS-POD-DOD-01-A** With a de-orbit device and balloon of a size specified in Chapter 11 it is not able to de-orbit within 25 years at an altitude of 1000 $km$. Due to time constraints it was not possible to re-evaluate the calculations and introduce an additional iteration step into the design. Additional steps should be taken to check whether it is possible to increase the balloon size so it will meet the requirement without going too much over the mass budget.

# 21

# Performance Analysis

In this chapter the performance analysis of the femto-satellite is presented. This performance analysis will be separated into two categories: hardware performance and mission performance. In the hardware performance section the physical performance of the hardware is documented. In the mission performance the results of the mission will be documented.

## 21.1. Hardware Performance

The hardware performance is separated into ADCS performance and Payload & Communication performance. Both are presented in this section.

### Attitude Control

The attitude determination and control subsystem is able to provide a total torque on the satellite of $1.3 \cdot 10^{-5} Nm$ which is physically limited by the motor torque. [1] Using equation (21.1) it is possible to determine what the time it takes to spin the satellite 180°.[2] Using this equation the slew time for 180° is equal to 168 $s$.

$$\frac{\theta}{2} = \frac{T}{2I}\frac{t^2}{4} \Rightarrow t = \sqrt{\frac{4I\theta}{T}} \tag{21.1}$$

The pointing accuracy of the attitude determination and control system is limited by the accuracy of both the sensors and the actuators. The gyroscope used has an accuracy of 0.007 °/s. [2]. The chip on the ESC produces an output signal with a 10-bit accuracy.[3] This means that when calibrated over the entire range the resolution is $\frac{30\,000}{2^{10}} = 29.29$ $rpm/bit$. Equation (21.2) is a modified conservation of angular momentum equation which relates the resolution in angular velocity of the femto-satellite to the resolution of the ESC.

$$I_{SC} \cdot \Delta\omega_{SC} = I_{wh} \cdot \Delta\omega_{wh} \Rightarrow \Delta\omega_{SC} = \frac{I_{wheel}}{I_{SC}} \cdot \Delta\omega_{wh} \tag{21.2}$$

Using equation (21.2) the angular resolution for the femto-satellite is 0.000084 $rpm$. This is much more accurate than the accuracy of the gyroscope, which is 0.0011 $rpm$. This means that the gyroscope accuracy becomes the leading accuracy. It should be noted that in practice these accuracies will never be reached due to the gyroscope bias and non-linearity effects. Also the camera system will be much less accurate than this, a more detailed analysis will be performed in the next design phase.

### Payload & Communication

The payload is capable of taking 16 $MP$ images which can be transmitted by the communication subsystem at a rate of 54 $Mb/s$. This is more than sufficient to transmit the amount of pictures that are going to be taken by the camera and allows for the transmission of on-board sensor data throughout the satellite lifetime. The images will be stored in a memory cache of 64 $GB$.

In the orbit there are two possible scenarios, depending on the client that uses the femto-satellite on their host. In the first scenario the femto-satellite deploys and will only see one side of the host spacecraft. This allows for in-depth studying of one side, but does not allow for the studying from multiple sides. In the second scenario the femto-satellite will deploy after which the host spacecraft itself will use its ADCS to rotate and 'show' its other sides to the femto-satellite.

## 21.2. Mission Performance

During the satellite lifetime it is able to record 878 photos of the host spacecraft, of which 700 are for inspection purposes and 178 for promotion purposes. The power subsystem is capable of supplying the satellite with sufficient power throughout the entire mission and will ensure that these images can also be transmitted. After the mission is completed the satellite will deploy its de-orbiting device causing it to de-orbit within 10.5 days.

[1] Faulhaber 0308 B Datasheet, `https://fmcc.faulhaber.com/resources/img/EN_0308_B_DFF.PDF`, retrieved on 16-06-2016

[2] Kionix KXG03 Datasheet, `http://kionixfs.kionix.com/en/datasheet/KXG03%20Preliminary%20Specifications%20Rev%200.19.pdf`, retrieved on 13-06-2016

[3] SIL F330 Datasheet, `https://www.silabs.com/Support%20Documents/TechnicalDocs/C8051F33x.pdf`, retrieved on 14-06-2016

## 21.3. Sensitivity Analysis

The sensitivity analysis investigates the sensitivity of the design for a change in system parameters. This will establish a degree of feasibility or flexibility of the final design. The general interactions between subsystems can be seen in the $N^2$ chart, if a change is made it is possible to see which parts in the $N^2$ chart it affects. Please refer to Section 5.1 for the $N^2$ chart. Key mission parameters are: Total mass of the femto-satellite, the $\Delta V$ delivered by the deployment system, the parameters of the host-spacecraft, hibernation time before deployment and the de-orbiting device. The effect of changing these parameters will be elaborated upon in the following sections.

### 21.3.1. Sensitivity Towards Mass

The mass of the femto-satellite has a profound influence on many parameters of the femto-satellite. Significantly increasing the mass on one subsystem for performance increase can lead to an increase of mass for many subsystems. The ADC subsystem depends heavily on the mass of the whole satellite. The momentum wheels need to compensate the disturbance torques during the operational lifetime and by increasing the mass, the disturbance torques will increase as well, which then will lead to larger momentum wheels. The deployment system is designed for a particular value of mass of the femto-satellite. If there are changes these parts will need to be updated as well and can lead to a snowball effect on the total mass. The total mass of the system can still be determined more accurately. The design of the femto-satellite can be made even more detailed by including each sub-component of each part and any element used during the integration of the femto-satellite. These steps will undoubtedly add some additional mass to the system. The safety margins and ranges set for the performance of the spacecraft enable the designers to deal with small variations.

### 21.3.2. Sensitivity Towards Deployment

By varying the $\Delta V$ delivered during deployment the time available for the camera to remain in its operational range will vary; at the same time the duration that the femto-satellite stays within range for communications will change as well. This is elaborated in more detail in Section 7.3. If the $\Delta V$ produced by the deployment system varies from 1 to 1.7 $cm/s$ the duration the femto-satellite stays within communications range varies from 7500 to 17 000 seconds. The number of images taken per second is fixed as seen in Section 8.5. If the time during optimal range for payload is less due to higher $\Delta V$ the total amount of images taken will be reduced. A larger $\Delta V$ will also increase the possible tumble rate after deployment. Analysis has been done and the momentum wheels of the ADCS will be able to cover for the increase of momentum due to the safety margin.

On the other hand if $\Delta V$ is lower than expected the total amount of pictures cannot increase due to constraints set by the communications and power subsystem. This is elaborated in the payload, communications and power chapters. With a lower $\Delta V$ the possible tumble rate after deployment will be lower than designed for, this will not be an issue for the ADC subsystem to manage the de-tumbling before the imaging phase.

### 21.3.3. Sensitivity towards host-spacecraft

The host-spacecraft could have changes in its parameters, for example changes in orbital altitude or size. This will affect the performance of the femto-satellite. Altitude determines the decay rate of the femto-satellite and the distance the femto-satellite drifts from the host spacecraft. Using GMAT the duration the femto-satellite stays within payload working distance and maximum communication distance has been simulated for variations of orbits. This can be seen in Table 21.1. Also the effect of deviations in the ballistic coefficient of the host spacecraft is simulated. This can be seen in Table 21.2. From these tables it is visible that as long as the host spacecraft does not decrease its orbital altitude significantly, there would be no consequences for the operational time limits. The decay rate of the femto-satellite reduces when the orbital altitude is increased, the upper limit is set at 950 $km$ to adhere to the space debris mitigation requirement. Elaboration can be found in Section 11.3.

Table 21.1: Operational limits with different orbital altitudes

| **Orbital altitude** [$km$] | **Duration within camera max distance** [$s$] | **Duration within communications max distance** [$s$] |
|---|---|---|
| 300 | 1660 | 3350 |
| 400 | 810 | 8150 |
| 500 | 709 | 9200 |
| 600 | 697 | 7850 |

### 21.3.4. Sensitivity towards hibernation time

If the hibernation time before deployment is increased significantly the degradation effects on the femto-satellite will increase. The femto-satellite is packed in the deployment system before release and is shielded from many external

Table 21.2: Operational limits with different ballistic coefficient of host-satellite

| **Difference ballistic coefficient of host** [%] | **Duration within camera max distance** [$s$] | **Duration within communications max distance** [$s$] |
|---|---|---|
| +25% | 740 | 15 900 |
| +10% | 740 | 14 850 |
| -10% | 740 | 13 700 |
| -25% | 740 | 13 250 |

effects. The self-discharge of the battery will increase if the time is increased by several years. The safety margin of the battery is 15% and this means that the maximum hibernation time before the safety margin is exceeded is equal to 8 years to perform the same mission. It is however possible to go beyond the limit with the hibernation time but this will affect the amount of pictures taken. In Table 21.3 the degradation of the main battery with increasing hibernation time and the maximum duration the payload can be active is seen. This is taking into account the 2% degradation per year as stated in Section 13.3.4. Until 21 years the amount of inspection images stays the same and afterwards the ratio between inspection and promotion has to be changed. The effect of long hibernation time on the spring within the deployment mechanism is currently unknown. It is recommended in further design to extensively test the performance difference of the spring with varying hibernation time.

Table 21.3: Hibernation time with payload operational duration due to degradation of main battery

| Hibernation time [years] | Degradation of main battery [%] | Maximum payload duration [$s$] |
|---|---|---|
| 10 | 18.3 | 436 |
| 12 | 21.5 | 410 |
| 14 | 24.6 | 386 |
| 16 | 27.6 | 362 |
| 18 | 30.5 | 340 |
| 20 | 33.2 | 318 |
| 22 | 35.9 | 298 |
| 24 | 38.4 | 278 |
| 26 | 40.9 | 259 |
| 28 | 43.2 | 240 |
| 30 | 45.45 | 223 |

### 21.3.5. Sensitivity towards de-orbiting

The decay rate of the femto-satellite depends primarily on the orbital altitude, which is dependant on the host, and the ballistic coefficient. This is elaborated in Section 11.3.1. The de-orbiting device will increase the area of the femto-satellite significantly, however the dimensions of the balloon can be changed. From Section 11.3.1 it is also visible that the de-orbit time will reduce significantly if the balloon is increased in size. The relation between this fact is not linear but in general the de-orbit device will become more efficient if more mass is used to increase its size. Increasing the area will not require additional power for the gas generator since it already can produce more than enough for inflating the device.

# III

# Post-Design Activities & Recommendations

# 22

## Assembly & Integration Plan

After the design of the satellite is finalised a plan needs to be drawn to explain how the spacecraft is assembled and what facilities are used. A diagram of the assembly & integration plan can be seen in Figure 22.1. In sections 22.1 and 22.2 the facilities are elaborated upon and the assembly process is explained.

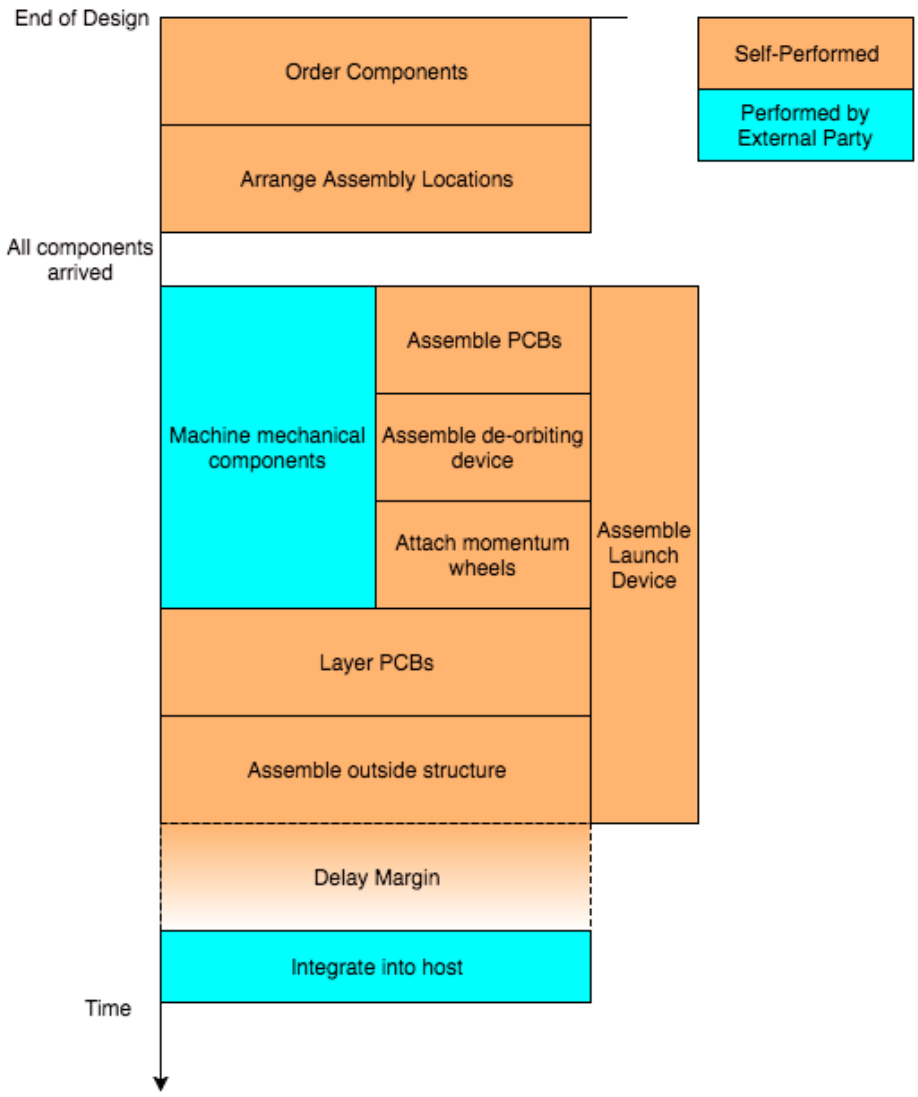


Figure 22.1: Assembly & Integration Plan

## 22.1. Facilities

The spacecraft consists of parts that can be subdivided into three main categories:

1. COTS components
2. Printed Circuit Boards (PCBs)
3. Mechanical components

The assembly and manufacturing will follow a very similar approach to that of other CubeSats. As an example the

assembly and integration of the Delfi N3Xt was studied. [63] The COTS components will need to be ordered from their respective manufacturer and do not require special facilities.

The PCBs must be printed in a circuit printer and will be ordered at an online service company that has these types of machines in-house. PCB assembly will then be performed in a room that has the proper tools and is sufficiently clean. Tools that are required for the assembly include soldering irons, and generic assembly tools to assemble the components.

All of the mechanical components must be machined and processed. The pins that hold the PCBs can be obtained from a manufacturer but the outside structure needs to be machined. This manufacturing needs to be done in a facility that has CNC (Computer Numeric Control) machines to ensure high precision manufacturing. The beryllium reactions wheels that are part of the ADCS (see Chapter 10) will need to be manufactured by personnel that is trained in handling these toxic materials and will need to be manufactured in an enclosed space so that no chips from the material get into the environment and can harm personnel around the manufacturing.

Finally the assembly of both the femto-satellite and the integration into the host spacecraft must be performed in a cleanroom. It is very important that this room has a separate air-conditioning system that makes sure that none of the beryllium will be exposed to the environment. The femto-satellite is integrated into the host spacecraft by tightening the spring of the launch system and then inserting it.

## 22.2. Assembly

The satellite will be assembled in various stages. Below is a step-by-step plan of how the satellite is going to be assembled. After this plan the satellite is assembled and can be placed into the host.

1. **Assembling the PCBs**
   The PCBs will first be assembled by soldering each component into their designated location on the circuit board. Care should be taken of the ball grid components (most of the chips) by making sure that they are solidly attached to the PCB, possibly with the aid of some adhesive to make sure none of the balls will break.
2. **Assembling the individual components**
   The balloon will need to be folded into the de-orbiting device by layering it in a folded shape such that it will fit inside the box. The end of the balloon needs to be attached to the hole in which the gas generator is connected such that it can be inflated.
   Since the motors are already attached on-top of the PCBs the momentum wheels will be attached to the motors in this design step.
   The aluminised Katon is attached to the side, top and bottom panels.
3. **Layering the PCBs**
   The bottom plate is put down and the four corner pins are inserted into it. The PCBs are then layered one by one onto the four pins in the structure, making sure that the intermediary electric connections are installed. In between the layers the batteries are put, making sure that no direct contact is made with the main battery such that it does not start depleting. The switch must be in the disconnected position to achieve this. Lastly the top panel is placed on the pins, finalising the spacecraft interior structure.
4. **Assembling the exterior structure**
   The outside structure is assembled around the PCBs and attached to the top and bottom plates. Care is taken with the payload which protrudes through one of the side panels.

During the assembly of the femto-satellite the deployment system is also assembled. However due to uncertainties in the exact design this assembly plan is not fully worked out and will be worked out in future stages of the development.

# 23

# Operations and Logistics

In this chapter the operations and logistics concept is described. It is crucial to have this concept ready as soon as integration starts. First the operations concept is explained. Then the logistics for manufacturing, transportation, launch and de-orbiting are laid out.

## 23.1. Operations

The operations that will be performed before, during and after the mission of the femto-satellite are depicted in an operational flow block diagram (Figure 23.1).

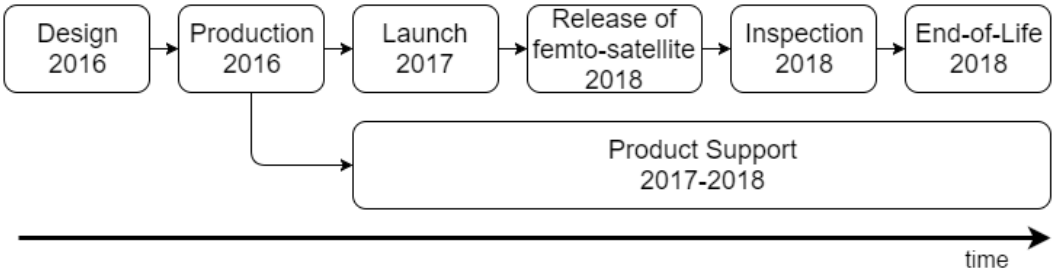


Figure 23.1: Operational flow block diagram

The operations in Figure 23.1 are presented in chronological order starting with the **Design**. After the **Production**, the **Launch, Release of femto-satellite, Inspection** and **End-of-Life** operations are supported by **Product Support**.

Skysat C12 and C13 will be launched in 2017.[1] The design team finds it achievable to design and produce a femto-satellite in 2016. After being launched to space in 2017 the femto-satellite will be offline. In 2018 the femto-satellite will be deployed from the host spacecraft to inspect the host satellite. The choice of 2018 is based on the fact that one wants to know the results from the space test as soon as possible but one also wants to obtain information about impact craters. After deploying, the femto-satellite will operate for three hours and after that the active de-orbit device is deployed. Since the mission also consists of demonstrating the de-orbit device, the end of life is after the satellite is burned up in the atmosphere.

The **Product Support** for the femto-satellite consists of [64]:

- **Manpower and personnel**: The mission is supported by personnel on the ground.
- **Training and training devices**: The personnel should be trained for the usage of programs, documentation and equipment.
- **Technical documentation**: The mission involves the identification, collection, recording, revision, production & distribution of all information & instructions required by operator & maintenance personnel.
- **Facilities**: A control room and antennas support the mission.

During the mission itself the ground station will give the command for releasing the femto-satellite to the host spacecraft. Next, the femto-satellite will operate autonomously during the mission. Finishing the mission with an automated deployment of the active de-orbit device.

The data from the femto-satellite is sent to the ground via the host spacecraft. Therefore no separate ground station needs to be selected for the femto-satellite mission. By not using a separate ground station, the operational costs for the femto-satellite can be kept low [65]. At the ground station the data from the femto-satellite needs to be separated from the data of the host spacecraft itself before it can be analysed.

The personnel on the ground obtains the raw data of the pictures taken during the mission. These pictures need to be processed to obtain a higher resolution picture. This way the impact craters can be seen more precise. This is done with a multi-frame image super-resolution method (SR). Personnel needs to be trained to work with this

[1] Skysat launch,`http://space.skyrocket.de/doc_sdat/skysat-3.htm`09-06-2016

software. Also the hard- and software needs to be available to perform the SR. The raw data needs to be sent to the person that is going to perform the SR and after that, the enhanced pictures need to be sent to experts to identify the impact craters. This information can then be used to improve models of space debris and improve future designs of satellites.

The total personnel needed is as follows: personnel to operate the ground station, personnel to perform the SR and experts to identify the impact craters. The personnel needs training in: operating the ground station and performing the SR. The expert which will be hired for analysing the impact craters needs to be educated in the field of work.

## 23.2. Logistics

### 23.2.1. Manufacturing

The satellite can be integrated at the clean room at Delft University of Technology's faculty of aerospace engineering. It consists of many parts, all of which have to be brought to the integration facility on time and of sufficient quality. COTS components have to be ordered in time, taking into account the delivery time given by the respective manufacturer. Contracts have to be made with suppliers of custom-made components like the momentum wheels to make sure they are delivered in time. As all components are small and hence the storage cost is negligible, it is wise to plan for components to arrive well ahead of time to have some margin in case delivery is delayed.

### 23.2.2. Transportation

The femto-satellite is highly compact with lots of precise equipment. Although the size of it is small, during transportation it still needs to be specially treated. Parts like the camera should be protected due to their fragility. The satellite shall be transported to the manufacturing facility of the host spacecraft. Where the femto-satellite will be integrated into the host spacecraft. A courier service specialised in transporting fragile items will be used to transport the femto-satellite.

### 23.2.3. Launch

During launch the femto-satellite is integrated in the host structure. So during launch the femto-satellite is part of the host spacecraft, so no special attention has to be given to the femto-satellite. When the host spacecraft is in orbit the femto-satellite will stay at its position. The mission of the femto-satellite starts when the ground station gives the command to the host spacecraft to release the femto satellite and the mission of the femto-satellite begins.

### 23.2.4. De-Orbit

The femto-satellite will deploy the active de-orbit mechanism at the end of mission. The moment of activation has to be well calculated to avoid collisions with other spacecrafts during the de-orbiting.

# 24

## Reliability, Availability, Maintainability & Safety

Reliability, availability, maintainability and safety are four important characteristics that will describe how the system will behave within its environment. In this chapter these four aspects will be treated individually and together they will provide an overview of how the femto-satellite will perform in the space environment.

## 24.1. Reliability

Given the short lifetime of the femto-satellite after deployment the reliability will depend greatly on two main pillars: the reliability of the deployment system and the degradation of the femto-satellite.

### 24.1.1. Reliability of the deployment system

The burn wire, electric rod-style actuator and springs can be tested on the ground. The opening of the door of the deployment interface can be tested as well. It should be noted that the zero gravity environment causes uncertainties for the deployment. During the opening of the door the femto-satellite should not move from the plate for an optimal spring release. For that reason, recommendations are stated in Chapter 29 for the detailed design of the deployment interface.

### 24.1.2. Degradation

The femto-satellite will be subject to degradation both while waiting on the host spacecraft and after it is deployed. This degradation is caused by elevated sun exposure and exposure to radiation that is normally not found on the Earth surface. Given that the deployment system has a door shielding the satellite while on the host the influence of radiation will be minimal but should still be taken into account.

The femto-satellite is comprised of various COTS products which are not specifically tested for their operation in a space environment. From past experience it has been determined that electronic COTS components require a reset every few days due to bit errors. This can be improved from a few days to more than a month with error detection and correction software [66]. However since the femto-satellite is going to be turned off during storage in the host and will only be turned on for the short mission lifetime this should not pose a problem.

The structure and thermal subsystem are protected from harmful radiation and impacts during the storage phase of the mission and will only be exposed to the environment during the mission. Micrometeoroid and space debris impacts may alter the absorptivity and emissivity coefficients of the satellite's hull. However, due to the short mission duration these changes are most likely negligible.

The femto-satellite should be vacuum resistant. This means no gas should be present in the materials used that can out-gas. For that reason, extra care should be taken when plastic or electrolytic capacitors are used [1]. If gas bubbles are present in the plastic material the material can become more brittle or even break.

It is expected that mobile phone camera image sensors are applicable for space-bound use. As an example the ST200 star tracker which is a miniaturised star tracker manufactured by Hyperion Technologies[2] uses a camera image sensor similar to the one used on a mobile phone combined with an accurate lens (according to inquiries with Dr. Ir. C. Verhoeven[3]) However, extra care should be taken during manufacturing of the lens to make sure no improper plastic materials are integrated.

On the International Space Station pixel degradation due to particle radiation has occurred at high definition cameras.[4] However, this effect is larger for high-definition cameras than for standard-definition cameras.

In the power system the main battery is physically disconnected from the rest of the system and will not experience losses from electronic components. The battery is subject to self-discharge of less than 2% per year when it is not used[5]. Losses are tolerable if the hibernation time, the time between launch and deployment, is low due to a safety margin.

[1] Outgassing of Engineering Plastics In High-Vacuum Applications, `http://www.boedeker.com/outgas.htm`, retrieved on 11-05-2016

[2] ST200 Star tracker, `http://hyperiontechnologies.nl/wp-content/uploads/2015/07/HTBST-ST200-V1.0_Flyer.pdf`, retrieved on 11-05-2016

[3] Professor TU delft, Analog electronics, applications to satellite communication, contacted on 10-05-2016

[4] The Effects of Radiation on Imagery Sensors in Space, `http://ntrs.nasa.gov/archive/nasa/casi.ntrs.nasa.gov/20070022613.pdf`, retrieved on 11-05-2016

[5] Battery specification, `http://www.vitzrocell.com/sub04/product_list.php?ca_id=40&id=10`, retrieved on 03-06-2016

For the de-orbit device, the cold gas generator is tested to have an operation lifetime of 10 years, which implies a low degradation[6]. The Kapton film used will degrade slowly due to gamma radiation, which mainly decreases the maximum strain and tensile strength and increases dissipation of the material. The dissipation is of bigger impact than the strength properties since there is only a low pressure in the balloon. Ultra violet exposure only reduces the elongation.[7]

## 24.2. Availability

The availability will be subdivided into two categories: availability after launch and general design applicability. The femto-satellite will be fully available to be deployed at any moment after the launch of the SkySat C12 host spacecraft. This implies that at any moment during the mission of the SkySat C12 the ground segment can give the command to deploy, provided that the host spacecraft is leaving eclipse and the system temperature is in order. It should be noted that the inspection pictures are more valuable once the deployment is initiated later in the mission of the host spacecraft since it will have contracted more impact damage to be inspected.

The general design applicability is constrained by two main parameters. The de-orbiting duration and the size of the host spacecraft. According to requirement **TS-STH-SUS-01-A** the femto-satellite must de-orbit within 25 years. The maximum altitude at which this requirement can be satisfied is about 950 $km$. The host spacecraft must have sufficient mass and volume budgets to carry the deployment system. Because this completely depends on what fraction of the host spacecraft's budgets the operator of the SkySat C12 is willing and/or able to reserve no further comments can be made about this.

## 24.3. Maintainability

One can be concise about maintainability of the femto-satellite since once the femto-satellite is in orbit there is no way to perform repairs on the spacecraft, meaning that no maintenance is possible.

## 24.4. Safety

The safety of the design can be subdivided into two categories: manufacturing safety and in-orbit safety. As outlined in Section 7.4 the probability of collision with the host is unlikely due to the high relative drag and the lag of the femto-satellite with respect to the host spacecraft. In addition, in Subsection 19.5.2 it was described that the the low relative velocities largely decrease the impact of an eventual collision. Hence, the risk of collision is deemed moderate, which increases safety though it does not guarantee it.

On the contrary, manufacturing safety is more difficult to quantify. Due to the use of beryllium special care needs to be taken by the people that are assembling the femto-satellite to make sure that none of this toxic material is inhaled or accidentally consumed. The room in which the assembly occurs must be kept clean and staff entrance must be regulated.

[6] The Mirco Cool Gas Generator, `http://www.isispace.nl/brochures/ACQ-CGS-PRM-001%200.15%20nL%20Micro%20CGG%20flyer.pdf`, retrieved 14-6-2016

[7] DuPont Kapton film properties, `http://www.dupont.com/content/dam/dupont/products-and-services/membranes-and-films/polyimde-films/documents/DEC-Kapton-summary-of-properties.pdf`, retrieved 17-6-2016

# 25

## Project Design & Development Logic

## 25.1. Post-DSE Design and Development

After this design phase the femto-satellite is far from complete. In this section the steps after this design phase are presented. These steps can be found in Figure 25.1.

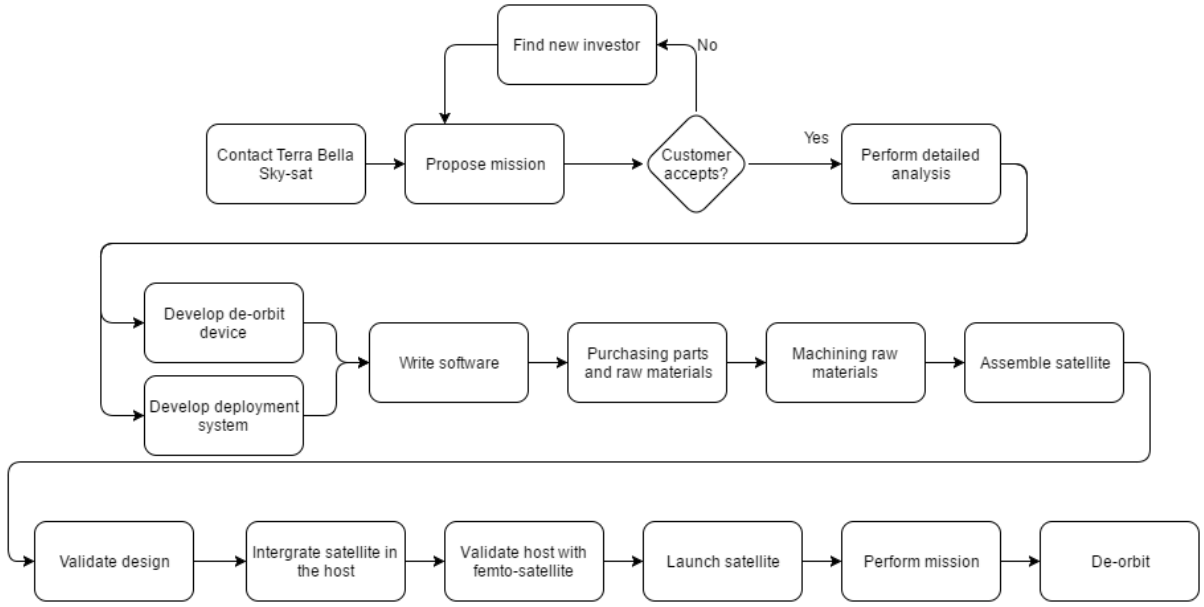


Figure 25.1: Project design & development diagram

The design phases up till now gives a solid foundation for the inspection femto-satellite concept. To demonstrate the potential of the femto-satellite a host satellite needs to be willing to take the femto-satellite with it. So before continuing the design, a host spacecraft needs to be contacted. Since the design is based on the sky-sat program from Terra Bella, this investor will be contacted first. Terra Bella is a Google company with a pioneering mission.[1] Therefore the design team expects Terra Bella to be open for other pioneering concepts. Yet if Terra Bella does not want to provide a host spacecraft for the femto-satellite, a new investor needs to be find. This loop will continue until an investor is found.

The goal of this project is showing the potential of the inspection and promotion femto-satellite. Therefore the provider of a host spacecraft is seen as an investor. When the concept is proven and there is a market for it within the space community, than the companies of the host spacecraft need to pay for having a *PICS* on board.

After insurance of having a host a detailed analysis of the design can be performed. For more information about this analysis is given in the recommendations, Chapter 29.

The SIDD and the deployment system needs to be developed since they are not COTS products. After developing these systems, the software for the whole satellite needs to be developed. Next the parts and the raw material are purchased. The raw material will need machining to create the parts. After machining, the satellite will be assembled. The complete femto-satellite can then be validated. More details about the validation can be found in Chapter 20.

The next step is integrating the femto-satellite in the host spacecraft. Next the host spacecraft and femto-satellite, as a single system, needs to be validated. When everything checked out the whole system can be launched. In space the femto-satellite can perform its mission and this ends with the deployment of the SIDD. Finally the femto-satellite will burn up in the atmosphere.

[1] Terra Bella, `https://terrabella.google.com/`, retrieved on 16-06-2016

## 25.2. Post-DSE Gantt Chart

Together with the project design and development logic, the post-dse gantt chart is also made to give a preliminary schedule for the work after DSE phase.

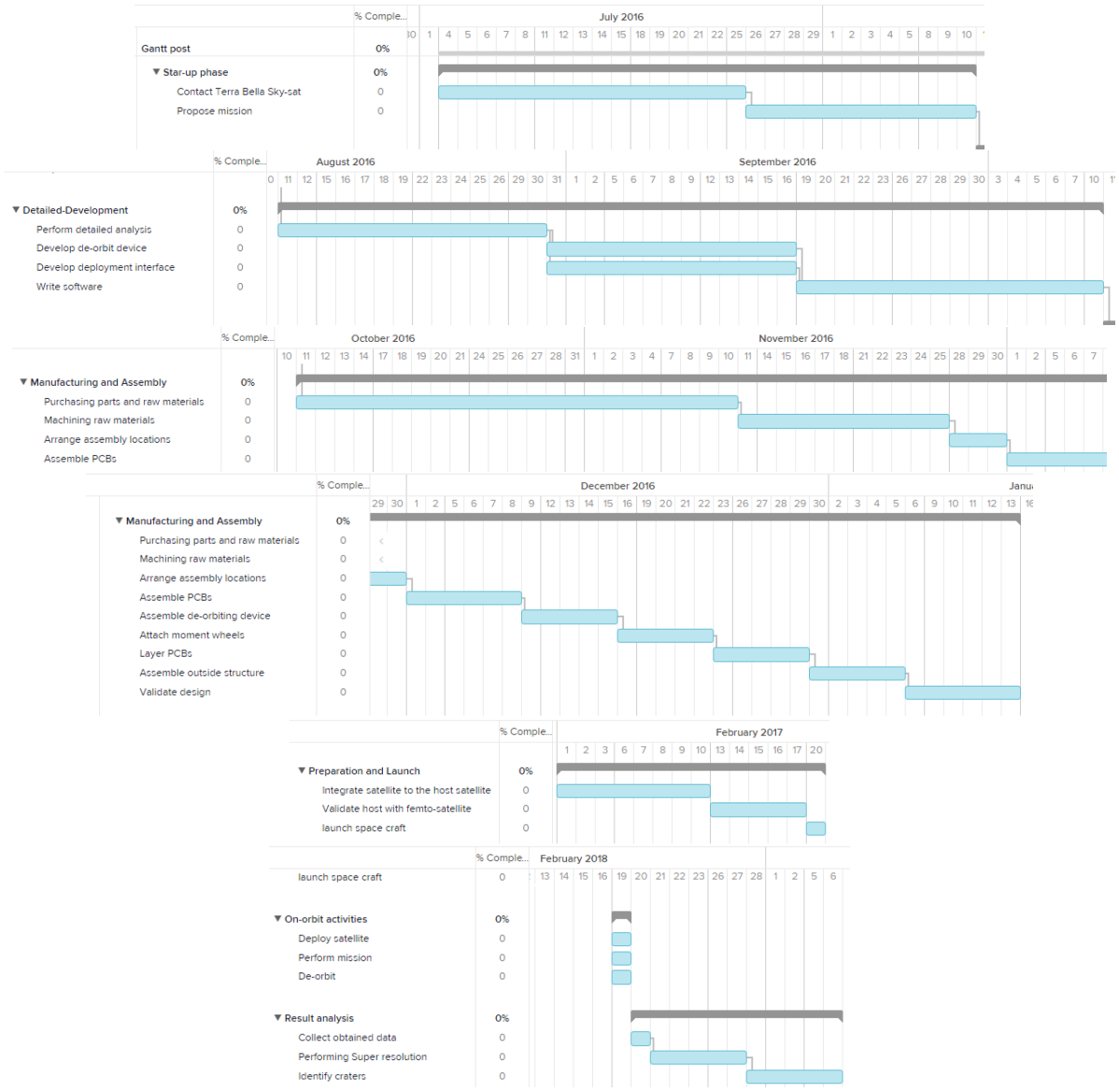


Figure 25.2: Project Gantt chart for post DSE activities

# 26

# Cost Estimation

In order to present a clear business model for the customers, the cost breakdown structure will be presented in this chapter. The life-cycle cost of the satellite, including component, assembly, integration, testing, launch and operations costs will be discussed.

## 26.1. Cost Breakdown Structure

To present a clear view of the whole mission cost, a cost breakdown structure is used. In Figure 26.1, the whole mission cost was divided into several different segments. As can be seen, the cost of building the femto-satellite is only one of the five segments. Development cost, launch and deployment cost, programme level cost, ground equipment and mission support and operation are also included to cover the life-cycle cost of the femto-satellite.

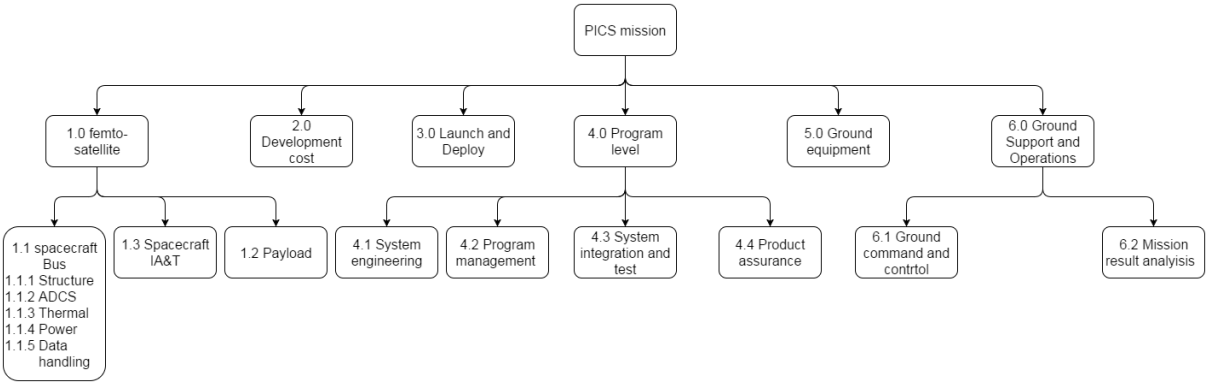


Figure 26.1: Cost breakdown structure

**Femto-Satellite Cost**

The femto-satellite cost consists of three different parts, the femto-satellite bus, the payload and the integration, assembly and testing cost. As the femto-satellite used in this mission has lots of commercial off the shelf components, the calculation of the total product cost is straight-forward. For parts which need to be developed like the de-orbiting system, a rough estimation based on its component prices is made. In Chapter 17, Table 17.3, different subsystem's costs are shown resulting in a total cost of €6805. The payload used in this mission is the camera which has been included in the table. Furthermore the assembly cost is calculated by the following formula [18].

$$COST_{assembly} = 0.l24 \cdot Cost_{spacecraftbus} \tag{26.1}$$

It will result in a cost of 844 Euro for assembly and testing. In the end the femto-satellite will cost €7649 in total.

**Development Cost**

The development cost is an essential part of the total cost. The software used in this femto-satellite can be used for later versions of the satellite too. Based on SMAD [2], the software development cost is determined by the thousands of lines of code and the type of code. The final cost of software development can be calculated by the following equation where $KLOC_{ground}$ is thousands of lines of code for the ground operations system and $KLOC_{flight}$ is thousands of lines of code on the satellite [2].

$$Cost_{software} = 1.67 \cdot (220 \cdot KLOC_{ground} + 435 \cdot KLOC_{flight}) \tag{26.2}$$

The number of lines is estimated based on a quad-copter since a quad-copter is also changing attitude with input sensors and can take images. The number of lines for a quad-copter is 8100[1]. This results in a final cost of €5813. Together with the software, the hardware development cost is also considered. However, for the femto-satellite, most of the components are commercial off the shelf which do not need to be developed by the femto-satellite engineers.

[1] Aeroquad, `http://aeroquad.com/content.php`, retrieved on 17-06-2016

The only exception is de-orbiting system and the deployment interface but the development cost of these systems is already included in the femto-satellite bus cost.

The rest of the development cost can be calculated by the labour time and price. Nine future space engineer participate in this project and have been working on it for 2 months. After the DSE, the more detailed development work can be assumed as another 2 months. By multiplying the average salary of an aerospace engineer[2], one will end up with a final cost of €103305 euro.

In the end, the total development cost is €109118.

**Launch and Deployment Cost**

Besides the femto-satellite production price, the launch cost needs to be analysed. However the femto-satellite will be launched together with the host satellite as an extra function. Also due to the the low mass of the femto-satellite, launch cost is negligible. For these reasons, in the end the launch cost taken as zero. However as a deployment mechanism will be used for the femto-satellite this costs will be taken in as launch costs. As presented in the Table 17.4, the final deploying cost is €2268.

**Programme level cost**

Program level cost is another typical cost which is important in space missions. The cost contractor's cost for systems engineering, programme management, system integration and product assurance are considered here. Based on [18], the program level cost can be estimated as a percentage of spacecraft bus cost. For small satellites, the fraction is 22.9 % of the spacecraft bus cost. This leads to a final value of €1558.

**Ground equipment cost**

The ground facility cost is another important cost in most space missions. The femto-satellite will be operated and supported by the ground station. For this femto-satellite, the ground station is just a control room which is inside of the host satellite ground facility. The communication to ground will be performed through the host satellite, so there will not be any specific ground antenna used for the femto-satellite. With these specifications, the ground facility cost for femto-satellite can be assumed to be zero.

**Mission support and operation cost**

Based on Section 23, the operation cost is divided into two parts: ground command and control cost and mission result analysis cost. As stated in Chapter 23, 2 personnel will be used with one predominantly for command and control and the other one in SR technology and identifying the craters. As stated in [18], contract labour force is €143420 per year per staff. However the operation and result analysis will be less than 2 weeks. By taking the worst case, i. e. two weeks, it will results in a cost of €11032.

## 26.2. Final Mission Cost Estimation

By summing up all the cost for the previous elements, a total mission cost estimation can be made as shown in Table 26.1.

| - | **Price** [€] |
|---|---|
| Femto-satellite cost | 7649 |
| Launch and deploy cost | 2268 |
| Programme level cost | 1558 |
| Ground equipment cost | 0 |
| Mission support and operation cost | 11 032 |
| Development cost | 109 118 |
| **Total mission cost** | **€131625** |

Table 26.1: Total mission cost

## 26.3. Return on Investment

The project started with a budget of €500,000 for the whole mission and €10,000 per satellite. The scope of this mission is to demonstrate new technology with a femto-satellite. So there is no business case where the target is obtaining as much as profit as possible. This concept does create the opportunity to make it a business case and aim

[2]Aerospace engineering average salary, `http://www.payscale.com/research/NL/Industry=Aerospace_Engineering/Salary`, retrieved on 17-06-2016

for profit.

The price of satellites varies from 0.89 to 2020 million Euro[2]. So the additional costs of a femto-satellite on board is smaller than minimum, yet the additional value of the femto-satellite is enormous. For this project the satellite cost is €7,649, which is €2,351 below budget. The total cost is €131,625, which is well within the total budget of €500,000. Assuming that the femto-satellite will weight $100g$ at the end of the design. The price per kilo gram is 1,316,250 €/$Kg$. Which is relative high compared to other satellites since they vary between 10,700 to 296,370 €/$Kg$.

Now the return on investments for a business case is presented. At this moment there are no inspection satellites on the market so this design will have a 100% market share. Also the cost is very low, therefore the PICS program can become an important part of the next generation satellites that are going to be launched. A more detailed business plan is needed, where e.g. companies are interviewed, to determine how many femto-satellites can be sold. Due to large uncertainty of the product not a clear balance can be determined. But the scope of the project is to demonstrate new technology with a femto-satellite. So no detailed profit analysis is needed.

# 27

## Vision on Femto-Satellites

In order to provide a proper vision on femto-satellites it is good to compare the original mission statement with the final result. This comparison will say a lot about the course that the project has run and what difficulties were encountered during the design. The original missions statement was as follows:

*DSE group S13 at the Faculty of Aerospace Engineering at TU Delft will design a femto-satellite to demonstrate its <TBD> space application potential.*

In this very mission statement lies the first problem that had to be tackled by the group. What *is* the purpose of femto-satellites in the current space industry, are they a novel concept, or is there actual value to their existence?

The group was able to come up with 9 concepts for femto-satellite missions that provided actual use, however out of these 9 missions only four were deemed 'technically feasible'. This is mainly restricted by technological development, meaning that should technology get better the number of applications for femto-satellites will increase. This chapter answers the question what would be possible if these technical challenges are solved, either by new technologies or by further development of current technology. First the major drawbacks including workarounds to these drawbacks are given. Subsequently other applications are listed. In the end a future projection on femto-satellites is outlined.

## 27.1. Technological Challenges

During the design of the PICS (Promotion & Inspection Cubic Satellite) four major technological challenges were discovered by the group that limit the technical feasibility and applicability of femto-satellite within the current space industry.

### 27.1.1. Propulsion

In the initial design stages the PICS was specifically designed to operate in close vicinity of a host spacecraft, with a complex orbit around the host spacecraft that would ensure that the femto-satellite would remain close to the host spacecraft. This would result in a much longer mission lifetime and much broader coverage of the host. However, the propulsion system is limited by the performance of the ADCS which will be explained in Section 27.1.3.

### 27.1.2. Communication

Various types of communication have been investigated throughout the project. The conclusion to be drawn from these investigations is that only short range communications are currently feasible for femto-satellites. This will mean that there is always a relay satellite required, causing the mission to become more complex. This problem was circumvented by piggybacking the spacecraft with a host to ensure that this relay satellite is always available.

If the market for femto-satellites grows more research will be performed into smaller communication devices and communication to a ground station may become feasible by utilizing the entire femto-satellite body as an antenna. UHF/VHF transceivers can be used for command and telemetry data and S-band transmitters for larger sized data packages like pictures. This development would make the femto-satellite more independent.

Greater femto-satellite independence would allow for a femto-satellite which can be launched after host-failure via a fail-safe protocol. This would allow engineering teams on the ground to investigate the problems and possibly come up with a solution. The femto-satellite itself can then relay information from the ground to the host spacecraft and possibly return the host to a functioning state through software modifications.

For other mission types, without a host spacecraft, communication to the ground is essential. So to broaden the applicability of the femto-satellite concept smaller transceivers are needed. If these are developed many more of the mission concepts presented in Table 2.1 become feasible.

### 27.1.3. ADCS

During the design of the attitude determination and control system it was discovered that great progress has been made over the past years, mainly due to technological development in the consumer electronics industry and radio-controlled aircraft community.

Many of the inertial measurement units and actuators already exist at the scales required for femto-satellites. The only major components that are currently very hard to find are absolute sensors. Sun sensors, Earth sensors, star sensors, etc. They all start at a mass of about 30 $g$ per sensor, meaning that it is simply not feasible to place them on a

100 *g* satellite. Should these types of technologies develop more it is very possible to design femto-satellites that are just as independent as larger spacecraft are today.

### 27.1.4. Space Debris

In order to guarantee that the amount of space debris does not increase femto-satellites will need an active de-orbiting system. If these are not installed the femto-satellites will become a large problem in the popular orbits, causing the international community to be forced to ban them. This restriction limits application of femto-satellites to orbits where there is still enough aerodynamic resistance to de-orbit, ruling out geostationary orbits.

## 27.2. The Future of Femto-Satellites

In the opinion of DSE group S13 femto-satellites do have a potential in the future, but not in the way it is generally assumed. Very often when people are talking about femto-satellites they start discussing the swarming capabilities of the satellites. An example is a study [67] of the Surrey Space Center, University of Surrey. The problem with swarming satellites however is that (depending on the application) they require a very high amount of inter-satellite communication and very often require high accuracy position determination and/or formation flying. During the mission trade-off it was concluded that swarming without a corrective propulsion system is risky and not sustainable due to the potential of space debris increase.

Instead of swarming the usage of one or a pair femto-satellite(s) has more potential given the current technology. As an example the SunCube [68] developed by the Arizona State University has the application of providing an environment for small experiments. The design proposed in this report focuses on an inspection and promotion mission. The group believes that there is a large gap in the market for these types of satellites since it is not feasible to take large CubeSats on-board of satellites since the trade-off between mass and functionality is not good enough. Femto-satellites however are much lighter and are more feasible to take on-board of a host spacecraft.

The mission of PICS is a test mission to demonstrate the data acquisition of the space debris environment. Group S13 recognises that a single femto-satellite can not gather enough data in order to provide a significant contribution to validating and updating current space debris models. However, if each upcoming SkySat and potential host spacecraft would contain a femto-satellite a much better model of the space debris environment can be formed.

DSE group S13 thinks that the application of taking promotion pictures together with a proper marketing plan can drive the popularity of the space industry for the general public given the significant usage of social media and advertisement these days. Together with the scientific application of the attribution to the mapping of the space debris environment, the usage of femto-satellites is profitable.

# 28

## Conclusion

The assignment of DSE group S13 is to design a femto-satellite for technology demonstration. Technology demonstration is a broad term, and the design team decided to design a femto-satellite with inspection and promotion capabilities. The mission is called PICS (Promotion and Inspection Cubic Satellite). The inspection of the host spacecraft can be used to make better models of space debris of 10-1000 micron size around Earth. The promotion will be used to help the marketing team with promoting their spacecraft to the greater public. For this design the SkySat from Terra Bella is used as host spacecraft.

Long inspection orbits are impossible due to the difference in $A/m$. The femto-satellite's $A/m$ is approximately 4.4 times larger, causing a drift $87m$ per orbit. Adding propulsion to the femto-satellite to compensate for the drift will result in a to heavy design. This leaves no other option than to drop the 1 year lifetime requirement. By injecting the femto-satellite in the direction of the host spacecrafts velocity the lifetime can be maximised to approximately 13000 seconds. There is an amount of uncertainty in the exact orbit of the femto-satellite. The performance of the deployment system after a long hibernation period is uncertain. The density of air at $450km$ is also hard to estimate and can vary with a factor 10.

To speed up the de-orbiting and to broaden the range of possible host spacecraft an active de-orbiting system is mounted on the femto-satellite. This system consists of a gas generator and an inflatable balloon. The balloon has a radius om $0.1m$ and, when deployed, de-orbits the femto-satellite within 11 days from an altitude of $450km$. Such a system has never been used before and shows great potential in terms of sustainability, minimising the chances of additional space debris.

The design consist of a deployment system which will be integrated into the host spacecraft, using a spring system to deploy the femto-satellite outwards. The springs are being compressed with by keeping tension on a wire. When deploying the femto-satellite the wire is heated and burns, ejecting the femto-satellite with a $\Delta V$ of approximately $1.3cm/s$. The visual camera will start with taking pictures 30 seconds after deployment. Then for the next 442 seconds the payload will take a total of 878 pictures. The maximum distance for pictures to be used as inspection is $4.04m$. For promotional purposes this distance is $5.61m$. The camera used on the femto-satellite is the same camera the Samsung S6 mobile phone uses.

Momentum wheels will be used to point the camera to the satellite. The host spacecraft should turn to inspect multiple sides of the host. Due to limitation of the battery the transmitter and camera can not be active at the same time. Therefore after all the pictures are taken, the camera switches of and the communication subsystem becomes active. The communication will send all the data in the next 6250 seconds to the host spacecraft. The host spacecraft will then send the data to the ground station. After sending all the pictures the active de-orbiting device will be activated, causing the femto-satellite to de-orbit within 11 days.

Communication to the ground is not possible, the required transmitters would be too heavy, too large and too power consuming. The femto-satellite sends the pictures to the host spacecraft via a WiFi module. The communication subsystem will send telemetry data to the host as long as the femto-satellite has power and is within communication range of the host. This data will be used to analyse the mission. The host spacecraft also requires a WiFi chip to receive the data from the femto-satellite.

# 29

# Recommendations

In this chapter the recommendations for this project are discussed. The recommendations outline the points of improvement for the astrodynamics, the design of femto-satellite and design of the deployment system. Often due to time constraints these improvements could not have been processed in the current report

## 29.1. Astrodynamics

As discussed in Chapter 7 inspection orbits were not possible due to too high differences in $A/m$. When selecting another host it is important to minimise the difference in $A/m$ making longer trajectories possible. This is a tricky process because $A$ can vary with time on large satellites when keeping their solar panels pointed towards the Sun.

Another thing that needs special attention is the risk of collision. The relative velocities are very small, but a potential customer will never buy the product with a high risk of collision. Although this risk can be mitigated in theory, it is wise to select a host that can perform evasive manoeuvres if necessary.

It is also recommended to carefully evaluate the atmospheric density $\rho$. This value can show great variation up to a factor 10, mainly depending on the solar activity.

## 29.2. Payload

The Samsung S6 camera modules turned out to have the best performance in terms of smallest feature size and working distance. However, during future femto-satellites designs, the state-of-the-art mobile phone camera modules should be investigated. If a mobile phone camera module with an equal or lower mass, power consumption and volume is available, the camera module used on the femto-satellite should be reconsidered. For the inspection pictures it should be noted that a better image resolution does not automatically result in a sharper picture due to the noise (as discussed in Section 8). For that reason, the light sensitivity of the sensor and state-of-the-art post-processing techniques should be considered in the decision which camera type to use.

## 29.3. Communication

The WiFi module is inside the structure and the kapton foil. An analysis needs to be performed to determine the effect of the kapton foil on the signal strength. Since no literature is found to analyse this effect a test needs to be performed. Also the signal strength when sending through the femto-satellite needs to be analysed to determine the effect. With this analysis the communication envelope can be described in more detailed manner.

Also decreasing the size of S-band and UHF/VHF transmitters is needed to be able to communicate directly to the ground. This will lose the dependency of the host spacecraft and gives the ability to inspect the host satellite in case it fails. This helps to determine the cause of failure and will help future design of satellites.

## 29.4. Attitude Determination & Control

There are two things that still need to be determined and are recommended for future research. First of all the flight controller must be designed, due to the simplicity there is a large chance that open-source software can be used to develop the flight controller, however nothing else can be said about this. Secondly, the edge detection algorithm must be developed and optimised to run on the processor selected in the C&DH subsystem. This algorithm must be efficient and fast so that no valuable processing time is lost.

From the performance analysis in Section 21.1 it can be seen that the attitude determination and control subsystem is currently very slow. The characteristics of this system can be optimised by selecting heavier motors and larger momentum wheels which will make the spacecraft much more agile. Doing that would however increase the satellite's mass. So, this remains as an option.

Lastly in the following design stages attention must be paid to the vibrations caused by the motors to make sure that they do not interfere with the sensing capabilities of the IMU.

## 29.5. De-orbit Device

The development of a de-orbit device is a complex process. Therefore it is advised to look into the possibilities of using an off-the-shelf, well tested device for this instead of the proposed theoretical SIDD. In this report the GOLD

is preferred over its counterparts, due to its simplicity and passive nature. However research needs to be done on the application of the device for small satellites like the femto-satellite, which requires funding. Therefore it is recommended to contact the GOLD developer and ask how much funding is required. Further analysis should be performed on the decay rate of the activated de-orbit device, to model for multiple uncertainties in the orbital parameters during the years it is active. Especially the A simulation model needs to be developed to crosscheck the de-orbit trajectory with known operating satellites, to avoid collisions.

## 29.6. Power

Lithium manganese dioxide batteries are currently the highest power density primary batteries that can provide high enough continuous current to power the femto-satellite. If technological advancements in developments of power storage allow producing higher power density batteries, the operational lifetime of the femto-satellite can be increased. This will increase the amount of information gained per mission.

## 29.7. Thermal Analysis

Before production of the satellite, a more detailed thermal analysis with nodes for all major and critical components should be conducted. Furthermore the specific heat capacities of the components should be determined experimentally and this information should be fed back into the thermodynamic analysis.

## 29.8. Deployment system

During the design of the deployment system several concerns were raised. The first issue is manufacturability. Due to the low velocity increment and the resulting low energy storage capacity needed for the spring, the spring force turns out to be extremely low. In order to obtain a reasonable deflection and length for the spring, consequently the spring constant turns out to be very low, driving the coils to a very high number with a pitch of only 1.4 times the wire diameter. Since important spring parameters like the wire diameter and the spring index have been set to their limit values already to obtain a reasonable design these issues raise concerns about the manufacturability. The current dimensions do not appear in the catalogues of any spring manufacturer. Hence, probably dedicated tools will be needed for the manufacturing, which will add to the already high material costs. Therefore, more research should be done into manufacturability.

Another issue is the compression of the spring before deployment. It is yet unknown how this affects the properties of the spring. That is, it could pose a problem if the femto-satellite is stowed for a long time in the deployment system, causing the spring to be continuously compressed for a long time.

The door of the deployment interface should be designed and tested on vibrations caused by the opening of the door. The femto-satellite should not move away from the supporting plate caused by the door opening. After the DSE-phase it is recommended to do a vibrational analysis of the deployment interface structure and determine the expected vibrations during deployment operations before the nichrome wire is burned.

Since the door is opened before deployment and the rails is hard anodised with Teflon impregnation to reduce friction, the $\Delta V$ can be delivered with more accuracy. The friction coefficient can be determined by testing.

The deployment interface structure has a potential of being protective for the femto-satellite in terms of radiation. It is recommended to investigate the possibilities of optimising the deployment system structure by adding radiation protective material and investigate the current radiation protection performance of the materials used.

There exists an uncertainty related to the cutting of the nichrome wire. Since four springs are applied for the deployment two Vectran cables should be released at the same time. In case the two cables are not released at the same time, part of the supporting plate will be pushed forward, creating an asymmetric force which could be fatal for the deployment process. How sensitive the design is to this aspect will remain uncertain until the deployment system is tested. Also the deployment time has not been modelled adequately due to lack of data. Hence, the deployment time should also be measured accurately by testing.

Once all deployment system uncertainties have been identified in terms of velocity increment , it is recommended to model different relative orbits (similar to Figure 7.7) for a the range of possible velocity increments. As shown in the N2-chart (Figure 5.1) a change of velocity increment influences several subsystems. For the payload and communication subsystem this will result in a deviation from the amount of imaging and communication time. Since only a small velocity increment is expected caused by the deployment system uncertainties due to the Teflon impregnation, low spring force and absence of gravity, it is unlikely that this deviation is significant. The smallest feature size of 0.1 $mm$ however may not be reached if the first picture is taken further than 0.39 $m$. The customer can decide to already start imaging closer to the host spacecraft which will return in a smaller coverage of the host spacecraft on the final image.

Lastly, the electric circuit related to the heating of the nichrome wire has not been worked out. It has been simply

stated that the nichrome wire will be attached to the leftmost wall of the deployment interface. However, to obtain an adequate electric circuit the part of the wall between the two ends of the nichrome wire should be electrically insulated. Therefore, either this particular part of the leftmost wall or the entire wall should consist of electrically insulating material.

## 29.9. Structural and Vibrational Analysis

Due to the complexity of both shock analysis and the analysis of small components in the femto-satellite, these findings should be checked by testing. Also all vibrational and structural analysis should be validated by actual testing.

# A

## Trajectory estimation

The orbit of the femto-satellite relative to the host spacecraft depends on many variables. First of all, the applied $\Delta V$ has a great influence. But some orbital parameters like the Right Ascension of the Ascending Node (RAAN), Argument Of Periapsis (AOP) or the True Anomaly (TA) also influence the distance to the host spacecraft. Considering all trajectories is considered to be to time intensive and outside the scope of the DSE. Therefore only various values of $\Delta V$ are considered and the TA is varied from 0 to 90 degrees in steps of 45. The second column gives the time to drift further than $3.8m$ from the host spacecraft. The third column indicates the time to drift outside the communication range of $242m$. The last column gives the minimum distance to the host spacecraft after drifting away.

Table A.1: SMA = 6828 km, ECC = 0.002, INCL = 97 deg, RAAN = 0 deg, AOP = 0 deg, TA = 0 deg

| $\Delta V$ $[cm/s]$ | $t_{3.8}$ $[s]$ | $t_{242}$ $[s]$ | $d_{min}$ $[m]$ |
|---|---|---|---|
| 0 | 1250 | 7500 | - |
| 0.1 | 1550 | 7700 | - |
| 0.5 | 1100 | 8900 | 13.8 |
| 1.0 | 400 | 11 050 | 24.1 |
| 1.3 | 300 | 12 250 | 12.5 |
| 1.5 | 250 | 13 100 | 33.0 |
| 1.7 | 200 | 14 250 | 46.7 |
| 2.0 | 150 | 16 000 | 44.13 |

Table A.2: SMA = 6828 km, ECC = 0.002, INCL = 97 deg, RAAN = 0 deg, AOP = 0 deg, TA = 45 deg

| $\Delta V$ $[cm/s]$ | $t_{3.8}$ $[s]$ | $t_{242}$ $[s]$ | $d_{min}$ $[m]$ |
|---|---|---|---|
| 0 | 1650 | 8000 | - |
| 0.1 | 2200 | 8300 | - |
| 0.5 | 950 | 10 500 | 21.5 |
| 1.0 | 400 | 12 400 | 18.7 |
| 1.3 | 300 | 13 600 | 41.0 |
| 1.5 | 250 | 15 700 | 54.3 |
| 1.7 | 200 | 13 000 | 50.9 |

Table A.3: SMA = 6828 km, ECC = 0.002, INCL = 97 deg, RAAN = 0 deg, AOP = 0 deg, TA = 90 deg

| $\Delta V$ $[cm/s]$ | $t_{3.8}$ $[s]$ | $t_{242}$ $[s]$ | $d_{min}$ $[m]$ |
|---|---|---|---|
| 0 | 2950 | 88 600 | - |
| 0.1 | 2750 | 9200 | - |
| 0.5 | 850 | 11 450 | 25.0 |
| 1.0 | 400 | 13 400 | 14.0 |
| 1.3 | 300 | 16 550 | 53.0 |
| 1.5 | 250 | 17 300 | 42.5 |

# B

## Absolute ADCS Sensors

This appendix contains the old research performed on the absolute ADCS sensors. They were eventually scrapped when the mission was changed and the requirements changed. The absolute sensors to be utilised on the satellite can be separated into two categories: *Orientation* and *Location*. In this section both sensor categories will be treated.

**Orientation**

In order to determine the absolute orientation of the spacecraft some reference points in space will need to be detected. This is often done by finding objects which location are known, like the Sun, the Earth and stars. During the research it was discovered that this is a very problematic sensor to find on the scale that is required by the mission. Most star sensors found weigh more than 20 grams per sensor, meaning it is simply not feasible to use on a femto-satellite. In order to determine orientation an alternative method is required. This alternative is the use of a small camera system with cameras mounted on the face(s) of the satellite in order to detect objects. Then image processing can be used to determine the location of these objects relative to the spacecraft. The proposed method will make use of a set of cameras on the faces of the spacecraft. These cameras can then be used with edge-detection algorithms to determine the location of objects relative to the spacecraft, which will yield the spacecraft orientation. This process will be elaborated upon in Section B. A single sun sensor could be used to determine the orientation of the sun relative to the satellite, this is useful when the concept utilises solar panels since they would have to be pointed towards the sun. The company Elmos has manufactured an integrated solar angle sensor that is able to be utilised as a simple sun sensor, specifications can be seen in Table B.1.[1] However it is not certain that a sun sensor is required since the small camera system could already determine the attitude of the satellite.

Table B.1: Elmos integrated solar angle sensor specifications

| | **Volume** $[mm \times mm \times mm]$ | **Power Usage** $[W]$ | **Resolution** [°] |
|---|---|---|---|
| Elmos E910.86 | $4 \times 4 \times 0.5$ | 0.018 - 0.022 | 2.7 |

**Location**

Location determination of the satellite can be done in a number of ways. If the orbit permits it the use of GPS or another GNSS is a very light-mass and low-power solution to location determination. In Table B.2 two GPS systems are presented that can be used on board of the satellite to determine its location. These systems both have integrated antennas and do not require external components.

Table B.2: Two GPS Systems

| **Manufacturer** | **Product** | **Mass** $[g]$ | **Power**$[W]$ | **Accuracy** $[m]$ |
|---|---|---|---|---|
| OriginGPS | ORG1411[2] | 1.4 | 0.011 | 2.5 |
| uBlox | CAM-M8[3] | 0.5 | 0.087 | 2 |

**Orientation detection using digital camera system**

Possible objects that can be detected are the host spacecraft, the Sun and the Earth. In Figure B.1 the process behind this method can be seen. First edge-detection is used to determine the horizon, then multiple images can be stitched together to improve the readings and finally from these readings the location of Earth can be determined [3]. The host-spacecraft can also be detected and together with the Earth the location of your femto-satellite can be calculated. Research was done into micro-cameras and there are many that can be used on the satellite, however most camera manufacturers don't specify specific camera masses, thus it is currently unknown what the exact camera masses are. One example camera is the *OmniVision OVM 7695-RAEA*[4].itsrelevant specifications can be seen in Table B.3. From

[1] E910.86 datasheet, `http://www.mouser.com/ds/2/594/910_86-224506.pdf`, retrieved on 19-05-2016

[2] origingps,`https://www.origingps.com/wp-content/uploads/2014/11/Nano-Hornet-ORG1411-Datasheet2.pdf`, retrieved on 10-05-2016

[3] u-blox,`https://www.u-blox.com/sites/default/files/CAM-M8_ProductSummary_(UBX-13003595).pdf`, retrieved on 10-05-2016

[4] ovt,`http://www.ovt.com/download_document.php?type=sensor&sensorid=128`, retrieved on 11-05-2016

these specifications it can be seen that the mass per camera is going to be very low. Also with these specifications the accuracy of the system can be calculated.

**Earth detection**

For the detection of the curvature of the Earth a distance of 450 km is assumed. The next calculations can all be calculated using sine, cosine and tangent functions. The distance to the horizon can be calculated to be equal to 2438 $km$ using the Pythagorean Theorem. Now because the diagonal field of view of the camera is equal to 61 degrees the it is possible to calculate the actual area of space each pixel can measure. The highest resolution of 640x480 will be used and knowing the ratio between the horizontal and vertical distance the individual field of views can be calculated which is 48.8 and 36.6 degrees respectively. With these field of views the area one camera captures is calculated and is equal to 2212 km in the horizontal direction and 1612 $km$ in the vertical direction. This particular sensor will have one pixel encompass an area of 3.46 x 3.36 kilometre. Next the curvature of the Earth should be known to be able to calculate the actual orientation of the femto-satellite. Assuming the Earth is a perfect sphere with a radius of 6378 $km$ the circumference will be equal to 40074 $km$. With the distance to the Earth and the radius it is possible to calculate the angle of the curvature that is visible on a camera, which is equal to 22.03 %. With this angle it is also possible to calculate the vertical distance difference between the highest point and the lower one on either side of the sensor boundary. By subtracting the distance obtained by using the previous established angle and cosine rule with the radius of the Earth this distance is equal to 117.6 $km$. The edge-detection algorithm described in the article [3] makes use of 3 scan lines positioned evenly from each other as seen in Figure B.1. By measuring the change of light the curvature of the Earth andits change in time the absolute position can be obtained in combination with the location information obtained from a GPS chip. Because the scan lines are placed on a distance from each other inaccuracy can happen during the imaging. The actual location of the horizon might be one pixel off and this gives at the worst case an rotated picture where the left scan line detects the horizon one pixel higher and the right scan line one pixel lower or vice versa. The algorithm will be robust enough that when errors occur where the curvature changes, and thus also the radius of the Earth, the measurement will be discarded. If the error is a pixel difference the vertical distance between the left or right scan line with respect to the centre scan line will be the same as the distance one pixel bridges. There will be a distance change of 3.46 km added onto the vertical distance between the scan lines, which is equal to 58.8 $km$, and this will give an angle change of 0.162 degrees. This is the same angle change the centre of the Earth will have with respect to the actual position of the centre. The drift of position of Earth's centre will be 18 $km$. Because the orbit of the femto-satellite will be at 450 $km$ above the Earth the actual accuracy this system will provide is equal to 0.15 degrees.

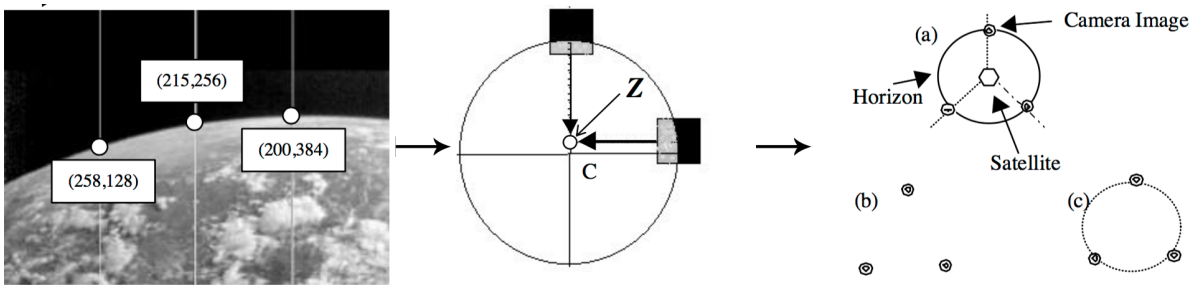


Figure B.1: Using image processing to obtain spacecraft attitude [3]

Table B.3: The OmniVision OVM7695-RAEA camera specifications

| | **Volume** $[mm \times mm \times mm]$ | **Power Usage** $[W]$ | **Image Quality** | **Field of view** $[deg]$ |
|---|---|---|---|---|
| OmniVision OVM7695 | 2.42 x 2.35 x 2.325 | 0.056 | VGA (640x480): 30 fps<br>QVGA (320x240): 60fps<br>QQVGA (160x120): 120fps<br>HF (640x20): 120fps | 61 |

# C

# Propulsion

In this chapter the possible propulsion systems are discussed in depth. First only cold gas propulsion was proposed, now also other other propulsion systems will be evaluated, like ion, Hall effect, electrical propulsion and solid propulsion. **It should be noted that in the final design the propulsion system was removed**, however it is still included for completeness.

## C.1. Selection Propulsion System

Five different propulsion systems are considered, namely cold gas, ion, hall effect, plasma and solid propulsion. As can be seen from Table C.1, cold gas propulsion and solid MEMS based systems are favourable due to their low power usage, so Ion and Hall effect propulsion systems are not favourable. Also cold gas and solid MEMS propulsion systems are simple, do not require ionisation of gasses or liquids and cold gas is well developed compared to the other options. Another option would be a pulsed plasma thruster, however their specific mass is rather high which would yield a higher mass for the same amount of $\Delta V$ delivered as a cold gas propulsion system. Therefore the cold gas propulsion and solid MEMS based systems are favourable over the other three. A closer look into both systems will be taken.

Table C.1: Different considered propulsion systems [2]

| **Type of thruster** | **Power** $[W]$ | **Vacuum** $I_{sp}$ $[s]$ | **Specific mass** $[g/W]$ | **Disadvantages** |
|---|---|---|---|---|
| Cold gas[1] | <1–30 | 50–75 | <1 | Low performance, heavy for given performance |
| Ion[2] | 10> | 2000–6000 | 9.1–25 | Very high power, not well developed |
| Hall effect [69] | 10–40 | 1500–2500 | 6–7 | High power, high development risk |
| (pulsed) Plasma[3] | 1.5> | 1500 | 85–195 | High power |
| Solid [70] | 0.15> | 4–300 | <1 | High ignition power and delay |

## C.2. Cold Gas Propulsion System

Below the proposed cold gas system is discussed, a small design is made to see if the system is viable for the mission and to gather more insight into the system.

### C.2.1. Propulsion system calculations

With the following formulas from the Spacecraft Technology course at the TUDelft the propulsion system can be sized [22]. First Equation (C.1) was used in combination with the chosen propellant (Krypton) giving the maximum specific impulse $I_{sp}$ ($39s$), begin mass $m_0$ of $61.5g$ and the $\Delta V$ needed to determine the mass after usage of all propellant $m_1$. With this the propellant or fuel mass $m_f$ can be determined. Note that $g_0$ is the standard gravity equal to 9.80665 $m/s^2$. Also the exhaust velocity $v_e$ can be determined then with Equation (C.5). With the propellant known the specific heat ratio $\gamma$ can be used to determine the Vandenkerckhove parameter $\Gamma(\gamma)$ with Equation (C.4). Now with different assumed thrust values $F_T$, throat areas $A^*$ and assumed chamber temperatures $T_C$ the chamber pressure $P_C$ can be determined with Equations (C.6) and (C.3). It should be noted that the chamber temperature $T_C$ could be lower or higher depending on the temperature of the spacecraft, this changes the massflow $\dot{m}$, the exit velocity $v_e$, the thrust $F_T$ and the specific impulse $I_{sp}$. In all calculations the exit pressure $P_e$ is assumed to be equal to the ambient pressure $P_a$, which is assumed to be zero Pascals.

So the variable inputs and their ranges are $F_T$ $[0.0001N-1N]$, $\Delta V$ $[0.5m/s-10m/s]$, $A^*$ $[d^* = 0.0001m-0.001m]$ and $T_C$ $[200K-400K]$. Since the system will be a blowdown system with a constant volume tank, the thrust and chamber pressure will decrease when the system is operating. This means that the system needs to be operating longer for the second time it is trying to achieve the same amount of $\Delta V$. The molecular mass of Krypton is $0.084kg/mol$ and the specific heat ratio is 1.68.

$$\Delta V = I_{sp}\ g_0\ ln\frac{m_o}{m_1} \tag{C.1}$$

[1] Cold gas systems, `http://www.lr.tudelft.nl/en/organisation/departments/space-engineering/space-systems-engineering/expertise-areas/space-propulsion/propulsion-options/chemical-rockets/cold-gas/`, retrieved 4-5-2016

[2] BUSEK Ion thrusters, `http://www.busek.com/technologies__ion.htm`, retrieved 4-5-2016

[3] BUSEK Pulsed plasma thrusters, `http://www.busek.com/technologies__ppt.htm`, retrieved 4-5-2016

$$v_e = \sqrt{\frac{2\gamma}{\gamma-1}\frac{R_A}{M_W}T_C\left[1-\left(\frac{P_e}{P_C}\right)^{\frac{\gamma-1}{\gamma}}\right]} = \sqrt{\frac{2\gamma}{\gamma-1}\frac{R_A}{M_W}T_C} \quad \text{when} \quad P_e = 0 \tag{C.2}$$

$$\dot{m} = \frac{P_C A^*}{\sqrt{\frac{R_A}{M_W}T_C}}\Gamma(\gamma) \tag{C.3}$$

$$\Gamma(\gamma) = \sqrt{\gamma}\left(\frac{2}{\gamma+1}\right)^{\frac{\gamma+1}{2(\gamma+1)}} \tag{C.4}$$

$$I_{sp} = \frac{v_e}{g_0} \tag{C.5}$$

$$F_T = \dot{m} v_e \tag{C.6}$$

### C.2.2. Nozzle sizing

The nozzle is a very important component of the propulsion system, it accelerates the propellant to high velocities. The throat area $A^*$ determines together with the chamber pressure $P_C$ the mass flow $\dot{m}$, This means for a fixed thrust $F_T$ the mass flow $\dot{m}$ is fixed as well if a propellant is chosen (and thus the maximum $I_{sp}$, seen from Equations (C.6), (C.5) and (C.3). When the mass flow is fixed a ratio between the throat area and the chamber pressure needs to be found. A too small throat area means a too high chamber pressure increasing the stress in the propellant tank skin. However a too big throat area means a small chamber pressure, but since the amount of propellant is fixed this means a bigger propellant tank is needed. It becomes a trade-off between the maximum stress in the skin of the tank allowed, the manufacturing limits of the smallness of the throat and the volume of the tank.

The smallest nozzles manufactured to date can have throat diameters $d^*$ of $100\mu m$ [70] or even $70\mu m$ [71] with an expansion ratio up to 10:1. Those are made in transparent photo-ceramic material like Pyrex glass with a density of $2230 kg/m^3$ [4] or Borofloat glass with a density of $2220 kg/m^3$ [5]. The length of the nozzle or the thickness of the glass can be as small as $1mm$. This means that if the glass plate is assumed to be maximum of $4cm^2$ it will have a maximum mass of $0.9g$.

For now it seems the best to take the smallest possible throat area to reduce the tank size, as long as the tank maximum skins stress is not exceeded.

### C.2.3. Valve options

The valve of the system makes sure the propellant only leaves the valve at times it is needed, however a valve is a complex mechanism and a lot of different types exist. Types exists that are fail-open and fail closed, for this system a fail-closed valve is needed, this means that if there is a power outage, the valve is closed. Or in other words, the natural condition is closed. This means that power is needed to open the valve, this can be achieved in different ways, although most of them are not suitable for space. Hydraulics and air for example are not feasible, magnets however are preferred since they require no extra pressurised tanks. There also might be a pressure loss over the valve, this means that the tank needs to be smaller to make sure the pressure in the chamber is still the designed value. This is actually preferred since it reduces volume and mass, however it increases the stress in the tank material. For now the pressure loss over the valve is assumed to be a ratio of 3:1 [71]. It should be noted that this pressure loss has a positive effect on the total propulsion system, however a valve of this size might not be able to withstand the pressure difference, so also a pressure ratio of 1:1 should be considered in case no strong enough valve can be designed.

The design of the valve is rather complex, however looking at nominal closed or fail-closed existing micro valves a range of parameters can be obtained, summed up in Table C.2. From this it can be seen that the leakage and power usage differs a lot per valve. The Yang E-H[71] valve seems to be the best one since it has by far the lowest leakage and thus requires less extra propellant to make sure there is enough for the actual manoeuvring. Of course the latter will be determined based on the mission lifetime or delay of the deployment of the femto-satellite. For now the mass will be estimated based on the the geometry and material usage of existing valves. The material mostly used in the valve is Si (100), which has a density of $2330 kg/m^3$, having a thickness of less than $2mm$ and needs to be as wide as the nozzle glass plate of $4cm^2$, giving a maximal estimated mass of $1.9g$. The power usage is $0.3mW$ for the Yang E-H valve.

Table C.2: Ranges of parameters for micro valves

| **Valve name** | **Leakage** $[sccm]$ | **Power** $[W]$ | **Mass** $[g]$ | $N_2$ **leakage** $[g/month]$ | $Kr$ **leakage** $[g/month]$ |
|---|---|---|---|---|---|
| NanoSpace MEMS NC [72] | 0.006 | 3 | 2 | 0.324 | 0.969 |
| Yang E-H [71] | 0.000 005 1 | 0.0003 | N/A | 0.000 276 | 0.000 824 |
| silQflo™ SSV [73] | 500 | 5 | 0.24 | 27 000 | 80 000 |
| Yang HH [74] | 0.03 | 0.01 | N/A | 1.621 | 4.84 |
| Moog Microvalve (MMV) [75] | 0.0001 | 0.7 | 7 | 0.0054 | 0.016 16 |

[4] Material Property Database Pyrex Glass, `http://www.mit.edu/~6.777/matprops/pyrex.htm`, retrieved 12-5-2016

[5] DATA SHEET SCHOTT® BOROFLOAT, `http://psec.uchicago.edu/Papers/Schott_Borofloat.pdf`, retrieved 12-5-2016

### C.2.4. Sizing the tank

Taking into account the pressure loss over the valve and the minimal throat area the tank can be designed. For the design of the tank a safety factor of 4 is taken into account for pressurised vessels [45]. With the ideal gas law (Equation (C.7)) the volume of the tank $V_T$ can be determined, after that assuming a tank thickness $t_T$ of $1mm$ and finding the radius of the tank $r_T$ for its volume (assuming a spherical tank) the maximum stress $\sigma_{max}$ in the material of the tank can be found with Equation (C.8). With the maximum stress $\sigma_{max}$ a material with a higher yield stress $\sigma_Y$ than the found value can be picked and the density $\rho$ of that material can be used to determine the mass of the empty tank $m_T$. For now the Aluminum 2090-T83 alloy is chosen[6] for its low density of $2.590g/cm^3$ and high yield strength of $520MPa$[7]. It is also possible to store the propellant in a cube or rectangular shaped tank, however this is less efficient for the maximum stresses in the tank. A trade-off between the easy manufacturability of the cube or rectangular shaped tank and the more stress efficient spherical tank can be made.

$$PV = nR_AT \tag{C.7}$$

$$\sigma_{max} = \frac{P_C r_T}{2t_T} \tag{C.8}$$

### C.2.5. Cold gas propulsion system configurations

Now that all three main components have been sized a few different cold gas propulsion system configurations can be designed to see how much power, volume and mass it needs. The power is the same since it uses the same Yang E-H valve, which consumes $0.3mW$. In Table C.3 different configurations (femto-satellite total mass $100g$) for the propulsion system are given, all assuming a spherical tank, a throat area $A^*$ of $100\mu m$, valve mass of $1.9g$, nozzle mass of $0.9g$, extra structure mass of $1g$ and the usage of Krypton with a maximum $I_{sp}$ of $39s$. It should be noted that tank volume of less then $4.2cm^3$ indicates a radius of less than $1cm$ which is assumed not to be manufacturable, so all tanks below this value will be discarded. Also the skins stresses given are multiplied by a safety factor of 4 and should stay under the yield stress of Aluminum 2090-T83 which is equal to $520MPa$.

As can be seen all except the top proposed configuration exceed the mid-term mass value, the first row is the only option that is within the mid-term value for the permanently orbiting concept of $7.5g-8.5g$. The contingency margin changed from 30% to 25% for the final design phase [5], this means the propulsion system can now weigh about $8.84g$. Then for now the system with a $\Delta V$ of $5m/s$ is also a configuration that is within this range. Any more $\Delta V$ needed by the mission can not be supplied without exceeding the maximum stress in the skin of the tank, getting heavier than the $8.84g$ or getting a too small tank volume ($<4.18cm^3$), which are all not acceptable.

Table C.3: Cold gas propulsion systems configurations for $\Delta V$ and different $F_T$ needed. Tank skin stress has a safety factor of 4.

| **$\Delta V$** $[m/s]$ | **Thrust** $[N]$ | **Mass** $[g]$ | **Tank volume** $[cm^3]$ | **Tank skin stress** $[MPa]$ | **Notes** |
|---|---|---|---|---|---|
| 4 | 0.37 | 8.5 | 4.2 | 146.2 | Minimum tank size |
| 5 | 0.45 | 8.8 | 4.3 | 179.2 | Minimum tank size |
| 6 | 0.55 | 9.0 | 4.3 | 217.5 | Minimum tank size, Too heavy |
| 10 | 0.9 | 10.0 | 4.3 | 357.2 | Minimum tank size, Too heavy |
| 25 | 1 | 16.2 | 9.5 | 516.3 | Too heavy |
| 50 | 0.7 | 27.7 | 26.2 | 507.3 | Too heavy |

If the risk on rupture of the tank should be made as low as possible, the gas should be stored as a solid in a gas generator. Such a gas generator can not use Krypton, but a $2g$ Nitrogen gas generator exists[8] which could be used instead. This adds about $4g$ to the total propulsion system mass, however such a generator needs to operate for 4 to 10 seconds at 2.2 Ampere and 4.3 Volts [9], which puts high requirements on the power system.

## C.3. MEMS Based Solid Propulsion System

Another option for a propulsion system is a MEMS based solid propulsion system [76–79]. This system consists of up to a few hundred small thrusters to deliver the $\Delta V$. The proposed MEMS based solid propulsion system is derived from a gold-titanium igniter based system [76]. One thruster in vacuum conditions delivers an impulse of $3.52\cdot10^{-5}$ to $2.22\cdot10^{-4}Ns$. For further calculations the lower value for the impulse is used as it is worst case. One thruster is about $3mm$ high, $1.6mm$ wide and $1.6mm$ deep, including the protruding glass part. The mass of a single thruster

[6] http://www.eolss.net/sample-chapters/c05/e6-36-05-03.pdf , `http://www.eolss.net/sample-chapters/c05/e6-36-05-03.pdf`, retrieved 2-6-2016

[7] Aluminum 2090-T83, `http://www.matweb.com/search/DataSheet.aspx?MatGUID=a79a000ba9314c8d90fe75dc76efcc8a`, retrieved 2-6-2016

[8] 0.15 nL N2 Micro-Cool Gas Generator, `http://www.cubesatshop.com/index.php?page=shop.product_details&flypage=flypage.tpl&product_id=120&category_id=21&option=com_virtuemart&Itemid=99`, retrieved 20-5-2016

[9] Interface Control Document 0.15 nL N2 Micro Cool Gas Generator, `http://www.isispace.nl/brochures/ACQ-CGS-RP-001%20Interface%20Control%20Document%200.15%20nL%20N2%20Micro%20Cool%20Gas%20Generator.pdf`, Retrieved on 01-06-2016

is 15.7$mg$ including a fuel mass of 0.8$mg$. The ignition delay is 12.94$s$ and the burn time is 0.8$ms$. To calculate the amount of thrusters needed first the impulse and burn time are used to calculate the average thrust generated by a single thruster, this is done using Equation C.9. A value of 44$mN$ is found. Using Equation C.10, the burn time and the total fuel mass of the solid thruster the average mass flow can be calculated, this is calculated to be 1$g/s$.

$$I = F_{Tavg} \cdot t \quad \text{(C.9)} \qquad m_f = \dot{m} \cdot t \quad \text{(C.10)}$$

With these two values and the $\Delta V$ needed the mass fraction of the system can be calculated via Equation C.13, derived from Equations C.11 and C.12. With the mass fraction $m_0/m_1$ found the amount of fuel needed is found as well, dividing this total fuel mass needed by the mass in each thruster, the total amount of thrusters can be found. In Table C.4 the mass fraction, fuel mass, number of thrusters needed and volume needed for different $\Delta V$ can be found. The thrusters have a footprint of $1.6mm \times 1.6mm = 2.56mm^2$ so for a $\Delta V$ of 0.0567$m/s$ the space needed for these thrusters is about $161 \times 2.56mm^2 = 412mm^2$, which is about $20mm \times 20mm$ or $2cm \times 2cm$, which would easily fit on one side of the femto-satellite.

The theoretical maximum $\Delta V$ that can be acquired via this system would be to fit the whole surface of the femto-satellite with these thrusters, the total area of the femto-satellite is $6 \times 5cm \times 5cm = 150cm^2$ thus about 5859 thrusters could be fit taking into account their footprint. This will be equal to 2.11$m/s$ $\Delta V$. Of course this is not realistic because the whole surface would be filled with micro thrusters.

$$\Delta V = I_{sp}\ g_0\ ln\frac{m_o}{m_1} \quad \text{(C.11)} \qquad I_{sp}\ g_0 = v_e = \frac{F_T}{\dot{m}} \quad \text{(C.12)} \qquad \frac{m_o}{m_1} = e^{\Delta V \frac{\dot{m}}{F_T}} \quad \text{(C.13)}$$

Table C.4: Different amount of thruster needed for a needed $\Delta V$, based on 100$g$ total initial satellite mass.

| **$\Delta V$** [$m/s$] | **Mass fraction** [−] | **Fuel mass** [$g$] | **Number of thrusters** [−] | **Volume** [$cc$] | **Total array mass** [$g$] |
|---|---|---|---|---|---|
| 0.0567 | 1.001 289 5 | 0.1288 | 161 | 1.1 | 2.53 |
| 0.1 | 1.002 275 | 0.2270 | 284 | 1.8 | 4.46 |
| 1 | 1.022 99 | 2.247 | 2809 | 18 | 44.10 |
| 10 | 1.2552 | 20.33 | 25413 | 163 | 398.98 |

For small $\Delta V$ solid propulsion seems a very good option, since it is less complex and uses no pressurised containers, however the power consumption is rather high. It uses 8$V$ for ignition over 12.94$s$ at a rated current of 20$mA$. This means one thruster uses 0.16$W$ for the total ignition process of 12.94$s$. When assuming a battery of 3.6$V$ and 500$mA$ and converting this to roughly 8$V$ and 220$mA$ and assuming no other power consumptions, about 11 thrusters can be ignited at the same time. This means firing all the thrusters will take about 208$s$.

## C.4. Conclusion on Propulsion System

As a conclusion cold gas propulsion can deliver up to a maximum of 5$m/s$ $\Delta V$ and staying within the 8.84$g$ final design phase mass budget. For the MEMS based solid thrusters, a maximum of a little less than 0.2$m/s$ can be reached without exceeding the 8.84$g$. Considering that under certain conditions pressurised containers may be taken on board piggyback missions, the maximum $\Delta V$ of 5$m/s$ can be reached with a cold gas propulsion system for this mission. However since the mission in iteration 0 would need more $\Delta V$ than the propulsion systems could provide the propulsion system was removed. No costs and temperature ranges have been computed since the subsystem was removed from the final design.

# D

## Rechargeable power solution

This chapter contains the steps leading to the selecting of the current design. This includes the research into other types of power generation. Due to the limited size of the design the options for power generation is limited. Radioisotope Thermoelectic Generators and nuclear reactors are not applicable due to mass and volume constaints and the lifespan is too low to optimally make use of them[1] [2].

## D.1. Rechargeable Power Solution

Independent power generation has been investigated. The means of power generation shall be done by having solar cells and harvesting the energy of the Sun. The output power is calculated based on the standard value of solar irradiance of 1365.4 $W/m^2$ and shall be scaled with the size of the solar panel.[80] The available power can be calculated using Equation (D.1). [81] 2 options are drafted for a mission that might requires solar panels for independent power generation. Each solar panel is designed to be a square panel of 5 by 5 centimetre to minimise complexity when storing them before deploying. Option one, as seen in Figure D.1, is to have 4 solar panels at an angle of 45 deg pointing inwards with two at opposite side of the satellite. In the figure the satellite bus is pictured as yellow and the side with solar cells is in blue. This option would be a passive method of charging the batteries. On average one solar panel would be facing the sun where the incidence angle would vary between 45 degrees on one panel and 45 degrees on two panels. If the most efficient solar cell is used with the power output would be between 797 - 1593 $mW$. Taking into account the shadow period of an orbit at 450 $km$ altitude which can be calculated using Equation (D.2) to (D.5) the average power output would be between 490 - 982 $mW$.[3] Table D.1 shows the ratio and period of shadow and sunlight at specific orbit altitude which highlights the available time per orbit the satellite has for charging the battery.

Option two, as seen in Figure D.2, is to have all 4 solar panels facing one side of the satellite. This option would include a separate charging cycle where all 4 solar panels are facing the sun. When each solar panel is 25 $cm^2$ the total area would be 100 $cm^2$. When using the Advanced Quadruple Junction solar cells from SolAero listed in Table D.2 the maximum amount of power generated would be 4506 $mW$, provided that the ADCS would be able to keep the solar panels pointed towards the sun. If a 5 degree pointing offset is assumed for the worst case scenario the output would be reduced by cosine 5 degree which is 0.4 %. The power generation would drop to 4489 $mW$. Whenever the batteries are running low on energy the spacecraft would orientate itself and the solar panels towards the sun and keep them at the same attitude until the batteries are charged again. The pointing accuracy needed to keep pointing to the sun is 180 degrees over half an orbit, this is equal to 1.1 $\cdot 10^{-3} rad/s$.

Option two would require 4 solar panels and would have a mass of 4.9 $g$. For this option a deployment mechanism would have to be developed. This should keep the solar panels stored during launch and only deploy after the satellite is switched on. The performance degradation of multi-junction solar panels over a year is less than 0.5%, which is low enough that it won't affect the power production significantly[2]. The pointing inaccuracy will be a larger factor.

Figure D.1: Orientation of solar panels on the satellite with option 1

[1] RTG on previous satellites, `https://solarsystem.nasa.gov/rps/rtg.cfm`, retrieved on 10-06-2016

[2] Nuclear reactor on previous satellites, `http://www.world-nuclear.org/information-library/non-power-nuclear-applications/transport/nuclear-reactors-for-space.aspx`, retrieved on 10-06-2016

[3] Shadow orbit analysis ,`http://design.ae.utexas.edu/mission_planning/mission_resources/orbital_mechanics/Orbit_Shadow_Analysis.pdf`, retrieved on 13-05-2016

Figure D.2: Orientation of solar panels on the satellite with option 2

$$P_{sa} = S_{in} \cdot A_s \cdot \eta_s \cdot I_d \cdot L_d cos(\theta_{incidence}) \quad \text{(D.1)}$$

$$sin(\theta) = \frac{R_E}{r} \quad \text{(D.2)} \qquad f_{shadow} = \frac{\theta_{shadow}}{\pi} \quad \text{(D.3)} \qquad T_{orbit} = 2\pi\sqrt{\frac{r^3}{\mu}} \quad \text{(D.4)} \qquad t_{shadow} = f_{shadow} T_{orbit} \quad \text{(D.5)}$$

Table D.1: Orbit parameters with eclipse period

| **Orbit altitude** $[km]$ | **Orbit duration** $[min]$ | **Shadow fraction** $[-]$ | **Shadow period** $[min]$ | **Orbit in sunlight** $[min]$ |
|---|---|---|---|---|
| 450 | 93.58 | 0.384 | 35.92 | 57.67 |

Table D.2: Solar panel selection

| **Manufacturer** | **Model** | **Efficiency** [%] | **Voltage** $[V]$ | **Output** power $[mW/cm^2]$ | **Density** $[mg/cm^2]$ | **Absorptivity** |
|---|---|---|---|---|---|---|
| SolAero | Advanced Quadruple Junction [11] | 33 | 2.82 | 45.06 | 49 | 0.81 |

Table D.3: Rechargeable battery selection

| **Model** | **Nominal voltage** $[V]$ | **Nominal capacity** $[mAh]$ | **Continuous current** $[mA]$ | **Charge current** $[C]$ | **Mass** $[g]$ | **Dimensions** $[mm]$ | **Power density** $[mWh/g]$ | **Temperature range** $[°C]$ |
|---|---|---|---|---|---|---|---|---|
| GMB652535 [4] | 3.7 | 500 | 500 | 0.5 – 1 | 10 | 36 x 25.5 x 6.7 | 185.0 | 0 – +45 |
| GMB1007090096 [5] | 3.7 | 850 | 850 | 0.2 – 1 | 17 | 49 x 30.5 x 6 | 185.0 | 0 – +45 |
| NCA463436A [6] | 3.6 | 720 | 720 | 0.7 – 1 | 12.4 | 35.5 x 34.3 x 4.6 | 209.0 | 10 – +45 |
| NCA752836A [7] | 3.6 | 1010 | 1010 | 0.7 – 1 | 16.7 | 35.9 x 27.9 x 7.8 | 217.7 | 10 – +45 |

### D.1.1. Power plan

Both options can not connect the output of the solar panels directly to the battery since the voltage is not equal. The output of the solar panels is equal to 2.82 $V$ and depending on the surface area the current produces will be changing [8]. A battery monitor will be used to continuously know the capacity of the battery system and able to tell the board computer the state of the battery [9]. If option one is chosen the voltage needs to be increased to 4.2 for charging of the lithium ion batteries, this is specified in the manufacturers specifications. In order to do this a converter is needed, this is performed with a buck-boost converter. A conversion between 2.8V to 4.2V can be done with an efficiency of 95% [10]. The mass of the converter has been estimated by taking the volume of the component and assuming it is made of pure silicon, this will give a mass of 0.02 grams each. This means that the current output will drop to 180 - 360 $mA$. Only the first three batteries are capable to be charged with this amount of current. A smaller battery will charge faster but will also discharge faster depending on the power consumption of the whole system. When

[4] GMB652535 datasheet, `http://www.powerstream.com/lip/GMB652535.pdf`, retrieved on 12-05-2016
[5] GMB1007090096 datasheet, `http://www.powerstream.com/lip/GM063048.pdf`, retrieved on 12-05-2016
[6] NCA463436A datasheet, `http://industrial.panasonic.com/kr/products/batteries/secondary-batteries/lithium-ion/prismatic-type/NCA463436A`, retrieved on 1-06-2016
[7] NCA752836A datasheet, `http://industrial.panasonic.com/ww/products/batteries/secondary-batteries/lithium-ion/prismatic-type/NCA752836A`, retrieved on 1-06-2016
[9] Smart battery monitor, `https://datasheets.maximintegrated.com/en/ds/DS2745.pdf`, retrieved on 2-06-2016
[10] Buck-boost specifications, `http://www.linear.com/product/LTC3533`, retrieved on 30-05-2016

charging with a current of 1C, equal to the nominal capacity, for one hour the capacity of the battery would be equal to 80% of its total. For maximum capacity the charging time should be extended by another 2 hours [11]. This means that a power plan needs to be established to optimise the available power. For option one it is possible to shut down all other subsystem to only focus on charging the battery for the first charge cycle. This means that the first several orbits are used for mainly charging the battery to full. Afterwards the solar panels can sustain a power consumption of at at least 180 $mA$ on 3.6 $V$. When the consumption increases the battery will be used and in case the battery runs low, subsystems will be shut down for a charging cycle.
For option two the output power is considered when the panels are facing the sun under a maximum offset of 5 degrees. This is equal to 4489 $mW$. Using a buck-boost converter to increase the output voltage to 4.2 $V$ and accounting for efficiency the output current is equal to 1015 $mA$. In this case the battery NCA752836A, seen in Table D.3, can be used since the charge current would be equal. During one orbit the spacecraft should orientate the solar panels towards the sun and during a sunlight period of 57.67 minutes the battery is able to be charged till 80%[11]. During normal operations the solar panels should not charge the battery since the current produced is not enough to properly charge this battery.
Some subsystems that require power have components that require different input voltage. This can be solved by having power regulators in form of buck-boost converters to regulate the voltages across the bus. Shunt dissipators are used to make sure the overflow power, or in case of option 2 power when not in a charging cycle, is dissipated instead of forced into the system. This will be regulated by having a direct-energy-transfer system as power regulation. This is advantageous compared with a peak-power-tracking system because it does not consume power on its own and is therefore extremely efficient. The total parts and mass of the DET system is lower. [18]

## D.2. Power Solution Selection

A trade-off can be made between the two major options for the power subsystem. Trade-off criteria can be set up for the selection of the power subsystem type. Since the mission concept has an operational lifespan of 2 orbits which is equal to 187 minutes or 3.1 hours it will influence how the trade-off is interpreted. More emphasis is placed on the power availability in a shorter duration than over a range of days.

**Power availability** This is mainly measured in the amount of power that can be made available per orbit. The higher the value the better it is for the system as a whole since the mission life is short.
**Cost** The cost is measured in how much the system will cost to implement. Because the lifespan is low it is generally better to keep the cost low for the whole spacecraft.
**Complexity** The higher the complexity of the system, the more risk it will bring with it. To reduce the amount of failure modes it is preferable that the power subsystem is less complex.

Table D.4: Power solution trade-off

| Type | Power availability | Cost | Complexity |
|---|---|---|---|
| Passive rechargeable | Low | High | High |
| Active rechargeable | Medium | High | very high |
| non rechargeable | High | Low | Low |

The biggest difference between choosing them is the operational lifespan of the spacecraft. The benefits of having a rechargeable power solution is that the power consumption of your system is important, but not to an extend that it will heavily influence your operational lifespan, less than with a non-rechargeable solution. The drawback is that the whole system will become slightly more complicated due to the solar panels and their interactions with the structure and power storage. The non-rechargeable solution is only possible to maintain for a lifespan of several hours but will come with more simplicity since it will only depend on the capacity of the battery. From this small trade-off it is clear that a non-rechargeable power solution is more favourable. This will be the chosen design for the power subsystem. Matching the power budget it is possible to select a suitable battery for this specific mission.

[11] Charging of lithium ion battery, `http://batteryuniversity.com/learn/article/charging_lithium_ion_batteries`, retrieved on 30-05-2016
[11] Solar cell datasheet5, `http://solaerotech.com/wp-content/uploads/2015/04/IMM4J-CIC-Datasheet.pdf`, retrieved on 12-05-2016

# Bibliography


[1] Woffinden, D. C., *On-orbit satellite inspection: navigation and $\Delta v$ analysis*, Ph.D. thesis, Massachusetts Institute of Technology, 2004.

[2] Larson, W. J. and Wertz, J. R., *Space Mission Analysis and Design*, Microcosm, 1999.

[3] Meller, D., "Digital CMOS Cameras for Attitude Determination," *14 AIAA/USU Conference on Small Satellites*, 2001.

[4] Doncaster, B. and Shulman, J., "Nano/Microsatellite Market Forecast," 2016.

[5] Colijn, R. M., Geng, M., Mollinga, J., Rikken, R. P., Schoemaker, B. G. T., Schreiber, L., Trees, V. J. H., Wang, B., and Wolfs, R. H. H., "Midterm Report," Tech. rep., Delft University of Technology, 2016.

[6] R.M. Colijn and M. Geng, J. Mollinga and R.P. Rikken and B.G.T. Schoemaker and L. Schreiber and V.J.H. Trees and B. Wang and R.H.H. Wolfs, "Baseline Report DSE S13," Tech. rep., Delft University of Technology, 2016.

[7] Jacobovits, A., "AeroAstro's Escort – A Microsatellite for On-Orbit Inspection of Space Assets," *$17^{th}$ Annual AIAA/USU Conference on Small Satellites*, 2003, pp. 1–9.

[8] See, T., Allbrooks, M., Atkinson, D., Simon, C., and Zolensky, M., "Meteroid and Debris Impact Features Documented on the Long Duration Exposure Facility," Tech. rep., Lyndon B. Johnson Space Center, 1990.

[9] Love, S. G., Brownlee, D. E., King, N. L., and Hörz, F., "Morphology of meteoroid and debris impact craters formed in soft metal targets on the LDEF satellite," *International Journal of Impact Engineering*, Vol. 16, 1995.

[10] Aceti, R., Drolshagen, G., McDonnell, J., and Stevenson, T., "Micrometeoroids and Space Debris - The Eureca Post-Flight Analysis," *ESA Bulletin Nr. 80*, 1994.

[11] Moussi, A., Drolshagen, G., McDonnell, J. A. M., Mandeville, J. C., and Kearsley, A., "Results of Impact Analysis on HST Service Mission 3B Solar Arrays," *Proceedings of the 4th European Conference on Space Debris*, 2005, pp. 207–214.

[12] Arceti, R., Drolshagen, G., McDonnell, J. A. M., and Stevenson, T., "Micrometeoroids and space debris-the Eureca post-flight analysis." *ESA bulletin*, Vol. 80, 1994, pp. 21–26.

[13] Smirnov, N. N., *Space Debris, Hazard Evaluation and Mitigation*, Taylor & Francis Ltd, 2001.

[14] U.S. Government, "Orbital Debris Mitigation Standard Practices," 1997.

[15] Azzarelli, T., "International Regulations for Nano/Pico Satellites," ITU Seminar, 14-16 April 2014, Cyprus, Ofcom Space and Science, Spectrum Policy Group.

[16] Belward, A. S. and Skøien, J. O., "Who launched what, when and why; trends in global land-cover observation capacity from civilian earth observation satellites," *ISPRS Journal of Photogrammetry and Remote Sensing*, Vol. 103, 2015, pp. 115–128.

[17] World Commission on Environment and Development, *Our common future*, Oxford University Press, 1987.

[18] Wertz, J. R., Everett, D. F., and Puschell, J., *Space Mission Engineering: The New SMAD*, Microcosm, 2011.

[19] Harris, D. T., Sakiestewa, D., Robledo, R. F., and Wittent, M., "Short-Term Exposure To Jp-8 Jet Fuel Results in Longterm Immunotoxicity," *Toxicol Ind Health September*, Vol. vol. 13 no. 5, 1997, pp. 559–570.

[20] Leaderer, B. P., "Air Pollutant Emissions from Kerosene Space Heaters," *Science*, Vol. Vol. 218, Issue 4577, 1982, pp. 1113–1115.

[21] Frimer, C., Oliveira, G. B., Tonet, J. H., and Sánches, S. M., "LI-ION BATTERY BREAKTHROUGH FOR SUSTAINABILITY, DURABILITY AND AFFORDABILITY," Tech. rep., Department of Chemical Engineering, Lund University, 2015.

[22] Gill, E., LaRocca, G., and Verhagen, W., "Systems Engineering and Aerospace Design," Lecture slides, AE3211-I, Delft University of Technology, 2015.

[23] Huber, T. E., *Mission Design Processes*, NASA Goddard Space Flight Center, 2000.

[24] Bate, R. R., Mueller, D. D., and White, J. E., *Fundamentals of astrodynamics*, Courier Corporation, 1971.

[25] Hughes, S. P., Qureshi, R. H., Cooley, D. S., Parker, J. J., and Grubb, T. G., "Verification and Validation of the General Mission Analysis Tool (GMAT)," *Proceedings of the AIAA/AAS Astrodynamics Specialist Conference*, 2014, pp. 1–32.

[26] Cook, D. G., *Solar Radiation Pressure Modeling Issues for High Altitude Satellites*, Master's thesis, Air Force Institute of Technology, Department of the Airforce Air University, 2001.

[27] Gill, E., Sundaramoorthy, P., Bouwmeester, J., and Sanders, B., "Formation Flying to Enhance the QB50 Space Network," *Small Satellite Systems and Services Symposium (4S), Funchal, Portugal, 31 May – 4 June 2010*, 2010, pp. 1–15.

[28] Gießelmann, J., *Development of an Active Magnetic Attitude Determination and Control System for Picosatellites on highly inclined circular Low Earth Orbits*, Master's thesis, RMIT University, 2006.

[29] Giancoli, D. C., *Physics for Scientists and Engineers, Volume 2*, Pearson Education, 2008.

[30] de Man, D., *Fotograferen met een Nikon D7000*, Pearson Education Benelux, 2011.

[31] Smith, W., *Modern Optical Engineering*, McGraw-Hill, 2000.

[32] Gravdahl, J. T., Eida, E., Skavhaug, A., Fauske, K. M., Svartveit, K., and Indergaard, F. M., "Three axis attitude determination and control system for a pico-satellite: Design and implementation," *54th International Astronautical Congress of the International Astronautical Federation, the International Academy of Astronautics, and the International Institute of Space Law*, Norwegian University of Science and Technology, 2003, pp. 1–12.

[33] Moen, J. I., "FYS3610 - Space Physics - Chapter 2 - The Earth's Permanent Magnetic Field," 2004.

[34] Grilli, R., Watts, J. F., Baker, M. A., and Dunn, B., "Localized Corrosion on 2219 Aluminium Alloy Coated with a Titatium Based Coversion Coating," *Surface and Interface Analysis*, Vol. 42, 2010.

[35] Snider, R. E., *Attitude Control of a Satellite Simulator Using Reaction Wheels and a PID Controller*, Master's thesis, Air Force Institude of Technology Ohio, 2010.

[36] Hoyt, R. and Forward, R., "The Terminator Tether™: Autonomous deorbit of LEO spacecraft for space debris mitigation," 2000.

[37] Nock, K. T., Aaron, K. M., and McKnight, D., "Removing Orbital Debris with Less Risk," *Journal of spacecraft and rockets*, Vol. 50, 2013, pp. 365–379.

[38] Nock, K. T., Gates, K. L., Aaron, K. M., and McRonald, A. D., "Gossamer Orbit Lowering Device (GOLD) for Safe and Efficient De-orbit," *AIAA/AAS 2010 Astrodynamics Specialist Conference*, 2010, pp. 1–11.

[39] Harknessa, P., McRobba, M., Lützkendorfb, P., Milligana, R., Feeneya, A., and Clarkc, C., "Development status of AEOLDOS – A deorbit module for small satellites," *Advances in Space Research*, Vol. 54, 2014, pp. 82–91.

[40] Maessen, D., "iDod, Development of a generic inflatable de-orbit device for CubeSats," Tech. Rep. IAC-07-A6.3.06, Delft University of Technology, 2007.

[41] Zandbergen, B., "AE1222-II: Aerospace Design & Systems Engineering Elements I," Lecture slides, AE1222-II, Delft University of Technology, 2013.

[42] Fischer, U., Gomeringer, R., Heinzler, M., Kilgus, R., Näher, F., Oesterle, S., Paetzold, H., and Stephan, A., *Tabellenbuch Metall*, Europa-Lehrmittel, 2011.

[43] Behrens, V., *Group VIII Advanced Materials and Technologies: Powder Metallurgy Data. Refractory, Hard and Intermetallic Materials 2A1*, Beiss, P. Landolt-Börnstein, 2003.

[44] Du, T., Xu, B., Wu, M., Liu, G., and Ouyang, C., "Insight into the Vibrational and Thermodynamic Properties of Layered Lithium Transition-Metal Oxides LiMO2 (M = Co, Ni, Mn): A First-Principles Study," *The Journal of Physical Chemistry*, Vol. 120, 2016, pp. 5876–5882.

[45] Fortescue, P., Swinerd, G., and Stark, J., *Spacecraft Systems Engineering, Fourth Edition*, Wiley, 2011.

[46] Gardiner, J., "Suitability of Nickel Chromium Wire Cutters as Deployable Release Mechanisms on CubeSats in Low Earth Orbit," *Physics Capstone Project, Paper 24*, 2015.

[47] Huang, W., *Shape Memory Alloys and their Application to Actuators for Deployable Structures*, Master's thesis, University of Cambridge, Department of Engineering, 03 1998.

[48] Thurn, A., "A Nichrome Burn Wire Release Mechanism for CubeSats," *41st Aerospace Mechanisms Symposium*, 2012.

[49] Hibbeler, R. C. and Yap, K. B., *Mechanics for Engineers: Dynamics*, Pearson, 2013.

[50] Budynas, R. and Nisbett, J., *Shigley's Mechanical Engineering Design, Tenth Edition*, McGraw-Hill Education, 2015.

[51] Megson, T., *Aircraft Structures for Engineering Students*, Butterworth-Heinemann, 2012.

[52] Conley, P. L., *Space Vehicle Mechanisms, Elements of Successful Design*, J. Wiley & Sons, 1998.

[53] Garrett, H. and Whittlesey, A., "Guide to Mitigating Spacecraft Charging Effects," *JPL Space Science and Technology Series*, 2011.

[54] de Rooij, A., "Corrosion in Space," *Encyclopedia of Aerospace Engineering*, 2010.

[55] Kleiman, J. and Tennyson, R., "Protection of Materials and Structures from the Low Earth Orbit Space Environment," *Proceedings of ICPMSE-3, Third International Space Conference, held in Toronto, Canada*, 1996.

[56] Inc, S. S. W., "Spring Materials," 2015, Size and Strength Values, Issue 9a.

[57] Kim, J., "CINEMA Production Document 10005 – P-POD Compliance and Integration," 2011.

[58] Inman, D. J., *Engineering Vibrations, Third Edition*, Pearson Education, 2009.

[59] Kosmotras, *Space Launch System DNEPR, user's guide*, November 2001, Issue 2.

[60] Arianespace, *Soyuz, at the Guiana Space Centre, User's Manual*, March 2012, Issue 2.

[61] Arianespace, *Ariane 5, User's Manual*, July 2011, Issue 5, Revision 1.

[62] Gill, E. and Hoevenaars, T., "Verification and Validation for the Attitude and Orbit Control System," 2015, Lecture slides AE3211-I.

[63] G.F. Brouwer, W.J. Ubbels, A. V. F. t. H., "ASSEMBLY, INTEGRATION AND TESTING OF THE DELFI-C3 NANOSATELLITE," *59th International Astronautical Congress*, 2008.

[64] Curran, R. and Verhagen, W., "Concurrent Engineering & Design for Lifecycle," 2010-2011, Lecture slides AE3211-I.

[65] Miau, J. J. and Holdaway, R., *Reducing the Cost of Spacecraft Ground Systems and Operations*, Kluwer Academic Publishers, 2000.

[66] Shirvani, P., Oh, N., McCluskey, E., Wood, D., Lovellette, M., and Wood, K., "Software-Implemented Hardware Fault Tolerance Experiments COTS in Space," *Dependable Systems and Networks - DSN 2000*, 2000, pp. 1–2.

[67] D.J. Barnhart, U., "A Low-Cost Femtosatellite To Enable Distributed Space Missions," 2007, United Kingdom.

[68] M. Martinez, A. Warren, A. C. J. T., "SunCube FemtoSat Design Specifications (SFDS)," 2016.

[69] Ito, T., Gascon, N., Crawford, W. S., and Cappelli, M. A., "Experimental Characterization of a Micro-Hall Thruster," *Journal of propulsion and power*, Vol. 23 No. 5, 2007, pp. 1068–1074.

[70] Helvajian, H., *microengineering aerospace systems*, The Aerospace Corporation, 1999.

[71] Louwerse, M. C., *Cold Gas Micro Propulsion*, Master's thesis, University of Twente, Enschede, The Netherlands, 2009.

[72] Nanospace, *MEMS Flow Control Vavles*, March 2011, Brochure.

[73] DunAn Microstaq, I., "Product Datasheet: silQflo™ Silicon Servo Valve," Revision 1.001, Datasheet.

[74] X.Yang, Hölke, A., and Schmidt, M., "An electrostatic, on/off MEMS valve for gas fuel delivery of a microengine," *Journal of micromechanical systems*, Vol. 13, 2002, pp. 660–668.

[75] Muellera, J., Yanga, E., Greena, A., V. Whitea, I. C., and Reinicke', R., "Design and Fabrication of MEMS-Based Micropropulsion Devices at JPL," *SPIE, Reliability, Testing, and Characterization of MEMS/MOEMS*, Vol. 4558, 2001, pp. 58–71.

[76] Zhanga, K., Choua, S., Angb, S., and Tangc, X., "A MEMS-based solid propellant microthruster with Au/Ti igniter," *Sensors and Actuators A: Physical*, Vol. 122, 2005, pp. 113–123.

[77] Zhang, K. L., Chou, S. K., and Ang, S. S., "Development of a solid propellant microthruster with chamber and nozzle etched on a wafer surface," *Journal of Micromechanics and Microengineering*, Vol. 14, 2004, pp. 785–792.

[78] Leea, J. and Kimb, T., "MEMS solid propellant thruster array with micro membrane igniter," *Sensors and Actuators A: Physical*, Vol. 190, 2013, pp. 52–60.

[79] Larangot, B., ConÈdÈra, V., Dubreuil, P., Conto, T. D., and C.Rossi, "Solid Propellant MicroThruster : an alternative propulsion device for nanosatellite," LAAS-CNRS, 7 avenue du colonel Roche, 31077 Toulouse cedex 4, France.

[80] Kopp, G. and Lean, J. L., "A new, lower value of total solar irradiance: Evidence and climate significance," *Geophysical Research Letters*, 2010.

[81] Cervone, A., "Ae2230-II Propulsion & Power," Lecture slides, Electrical Power Systems lecture 9, Delft University of Technology, 2015.